Phosphorus in marine sediments during the last 150,000 years: exploring relationships between continental weathering, productivity, and climate

The Joides Resolution

Ph.D thesis presented by
Federica Tamburini

Université de Neuchâtel
Facultés des Sciences
Institut de Géologie

December 2001

Thesis Jury:

Prof. Karl B. Föllmi (Neuchâtel)	*Director*
Dr. Thierry Adatte (Neuchâtel)	*Examinator*
Dr. Sylvain Huon (Paris)	*Examinator*
Prof. Judith A. McKenzie (Zürich)	*Examinator*
Dr. Caroline P. Slomp (Utrecht)	*Examinator*
Dr. Philipp Steinmann (Neuchâtel)	*Examinator*

IMPRIMATUR POUR LA THESE

Phosphorus in marine sediments during the last 150'000 years: exploring relations between continental weathering, productivity and climate

de Mme Federica Tamburini

UNIVERSITE DE NEUCHATEL

FACULTE DES SCIENCES

La Faculté des sciences de l'Université de Neuchâtel sur le rapport des membres du jury,

Mme C. Slomp (Utrecht NL),
MM. K. Föllmi (directeur de thèse), T. Adatte,
P. Steinmann, J. McKenzie (Zürich) et
S. Huon (Paris)

autorise l'impression de la présente thèse.

Neuchâtel, le 8 janvier 2002

Le doyen:

F. Zwahlen

Every man who is high up loves
to think that he has done it all himself;
and the wife smiles, and lets it go at that.

Sir James M. Barrie
(Peter Pan's dad; 1860-1937)

The thesis you hold in your hands is the result of my Ph.D. research work. Before plunging inside, I would like to invite you to read these few lines.
During the last four years I have crossed paths with many people, and now it is time to acknownoledge them for everything they have done. Few minutes spent together even talking about nonsense, a short walk, their irony and kindness, all this has helped me in being in high spirits and in keeping on with my work. Thanking each of them would take a long long time. All these persons know what they have done for me and I know they know I know (Io so che tu sai che io so... an old italian movie).

I would like to dedicate this thesis to my parents, Alfio (Dad) and Cesarina (Mom). Without them, their support, help, understanding, and love I would not be who I am.

A special thank to Karl, my advisor. He has supported and, probably some times, tolerated me. I am not sure he really loves the conclusions of my thesis, but he is great in accepting them as they are.

I would also thank the members of the thesis jury (Judy McKenzie, Caroline Slomp, Thierry Adatte, Philipp Steinmann, Sylvain Huon) to have taken a bit of their time to read and review my work.

ODP (for providing samples, of course)
Thierry and Philipp (pour toutes les fois que vous m'avez écoutée)
Judy (I will never thank her enough)
Laurent (tu m'as supportée pendant cette dernière période. Merci avec tout mon coeur)
Stefano (now nitrogen stable isotopes have no more secrets to me!)
Crisogono, Daniel, and Silvia (they made my time in Zürich unforgettable)
Julia and Pierre, Rachel and K'spar, Nat and Baba, Sévérine, Marina, Sabine B., Claire et Ronnie (bonne chance), Bas and all the other students in Neuchâtel (je n'oublierai jamais ces quatre années ensemble)
Sabine and Elisabeth (MERCI !!!)
Eric Verrecchia (la "référence" en statistiques)
Hilary, André, Khaoula, Yvann, José and Sébastien (your help has been really important)
Kate, Matt, Peter, John, Steve, Eve and the whole Leg 184 scientific and technical party (I have wonderful memories of those two months of hard work)
M. Tissot (la "référence" Mac)
Lia (I wish you were here...)
The Vanderkluysen Clan and Gil (your support has been significant to me)
Bruna, Elena, Sabrina, Simona and Simona (grazie per essere mie amiche)
My family in Italy (un abbraccio enorme)
Forese Wezel (for his view of science and research)

THANK YOU
GRAZIE
MERCI

Federica

CONTENTS

Training on board of the Joides Resolution (1999).

Contents

Phosphorus in marine sediments during the last 150,000 years: exploring relationships between continental weathering, productivity, and climate

οὐδὲν γὰρ χρῆμα γίνεται οὐδὲ
ἀπόλλυται, ἀλλ᾽ ἀπὸ ἐόντων
χρημάτων συμμίσγεταί τε καὶ διακρίνεται.
καὶ οὕτως ἄν ὀρθῶς καλοῖεν τό
τε γίνεθαι συμμίσγεσθαι
καὶ τὸ ἀπόλλυσθαι διακρίνεσθαι

Anaxagoras of Clazomenae (500 - 428 B.C.)

Wrongly do the Greeks suppose that aught begins or ceases to be; for nothing comes into being or is destroyed; but all is an aggregation or secretion of pre-existing things; so that all becoming might more correctly be called becoming mixed, and all corruption, becoming separate.

Anaxagoras, 500 - 428 B.C.

Nothing is lost, nothing is created, everything is transformed.

Antoine-Laurent de Lavoisier , 1743-1794

Abstract

Phosphorus is an essential element for life and its delivery to the biosphere is primarily controlled by continental weathering. These two aspects render phosphorus a critical element for biogeochemical and paleoclimatic studies. In the last decades, several studies have addressed phosphorus geochemistry and its record in marine sediments. Some of these forwarded hypotheses of feedback mechanisms between the supply of phosphorus to the ocean, productivity and climate, through the "nutrient-CO_2" connection. But many fundamental aspects of the coupled carbon and phosphorus cycles have been poorly understood. Little is known about the cycling of this biophile element, its fate once transferred into the ocean and into the sediment, and how it is trasferred during rapid and extreme climate changes. Understanding the feedback mechanisms in the Pleistocene and Holocene period, a time of rapid glacial-interglacial shifts, is critical, yet phosphorus-carbon-climate relationships have been poorly investigated in recent paleoclimatic studies for this time period.

In this research project marine sedimentary records of the last 120-150,000 years from nine locations (Peru and Oman margins, Northeastern and North Atlantic, South China Sea, Ontong Java plateau, Japan Sea) have been analyzed by means of a geochemical (i.e. phosphorus geochemistry, nitrogen stable isotopes, organic matter characterization) and mineralogical (i.e. bulk and clay mineralogy by XRD, granulometry) approach. Phosphorus phases, detected employing a sequential extraction technique (SEDEX), have been used to decipher the relationships between the phosphorus record, continental weathering, and climate, and to assess the relative importance of global and local processes on the distribution of phosphorus in sediments during the last glacial-interglacial cycle.

Phosphorus is usually partitioned between inorganic and organic phases in sediments; both forms have been detected at all locations. Detrital phosphorus generally varies in proportion to the continental sediment supply. Authigenic P, present at all sites, is the most important sink of reactive and formerly bioavailable phosphorus, and comprises on average between 35 and 78% of the total phosphorus content. The distribution of phosphorus between the reactive forms (i.e. Fe-bound, authigenic and organic-bound phosphorus) is generally controlled by the environmental conditions in the bottom waters and in the uppermost part of the sediment column. These in turn may be linked to larger scale phenomena (e.g. oceanic circulation and climate). The study of phosphorus geochemistry in sediments deposited during Heinrich events shows that the concentrations of phosphorus in each phase vary in response to rapidly changing processes. Oceanic circulation, water column ventilation, and the organic carbon flux to the sea floor may rapidly

change and alter diagenetic conditions in the uppermost section of the sediment column. As the reactive phosphorus cycle is redox sensitive, the distribution of the phases in the sediments is affected by these changes.

Concentrations of reactive and total phosphorus are comparable between locations, and fluctuate on average between 0.3 and 0.65 mg/g of sediment, regardless of the geographic, oceanographic and environmental setting. Only two sites, the Oman and the Peru margin, characterized by upwelling and high productivity rates, exhibit higher phosphorus concentrations (1.2 and 2.5 mg/g on average, respectively). Neither organic carbon flux to the sediments, or the initial supply of phosphorus, or the sedimentation rates seem to be the controlling factor.

Phosphorus mass accumulation rates (MAR) are clearly controlled by sedimentation rates, and vary depending on local conditions. Lower values are found in the North Atlantic sediments, where MAR are about 0.9 mg/m^2·ky, while ODP site 1144 (South China Sea) shows the highest MAR (a mean of 40 mg/m^2·ky), which are comparable to those of phosphogenic sites (e.g. the Peru margin). There is no meaningful distinction between glacial and interglacial reactive phosphorus MAR averages. The analysis of standardized reactive P MAR points to a relationship between reactive P MAR variability and the precessional cycle. This would imply that low latitude climate (e.g. monsoonal climate) controls phosphorus delivery, through continental weathering, and diagenetic transformation and final burial, through changes in oceanic circulation.

Proxies such as nitrogen stable isotopes and total organic carbon, as well as the relation between standardized reactive P and TOC MAR, indicate that regenerated dissolved phosphorus is lost from the sediments, mainly during periods characterized by high organic carbon flux to the sediments and oxygen-depleted bottom and pore water conditions. This phenomenon is particularly evident during glacial periods, and may have significant consequences with regard to the carbon cycle and climate change, notably during periods already characterized by high biological export. Standardized MAR indicate that periods of high organic matter productivity clearly correlate with the decreasing burial rate of reactive P.

Les Grecs ne pensent pas correctement au sujet de la création et de la destruction; car aucune chose ne se crée ni ne se détruit, mais à partir de "fluides-qualités" préexistants se produisent des mélanges, qui se différencient à nouveau. D'après cela, ils nommeraient correctement la création "mélange" et la destruction "différenciation".

Anaxagore, 500 – 428 av. J.-C.

Rien ne se crée, rien ne se perd, tout se transforme.

Antoine-Laurent de Lavoisier , 1743-1794

Résumé

Le phosphore est un élément essentiel pour tout organisme. Parce que son apport à la biosphère est garanti exclusivement par le transport des produits d'altération, le phosphore est considéré comme un élément clé pour les études biogéochimiques et paléoclimatologiques.

Pendant les dernières décennies, plusieurs études ont approfondi les connaissances sur la géochimie du phosphore, et sur son enregistrement dans les sédiments marins. Les résultats de ces études indiquent l'existence d'un possible lien entre l'apport du phosphore à l'océan, la productivité marine et le climat, par l'intermédiaire de la connexion entre les nutriments et le dioxyde de carbone (CO_2). Malgré tout cela, il existe encore plusieurs aspects fondamentaux des cycles du carbone et du phosphore qui ont été peu explorés.

Le cycle du phosphore dans les sédiments marins, ainsi que ses réponses aux changements climatiques rapides ne sont pas si bien connus. La période géologique du Quaternaire est très importante pour les études paléoclimatologiques, car elle est caractérisée par des changements entre périodes glaciaires et interglaciaires. La compréhension des phénomènes de rétroaction entre le phosphore et le climat pendant cette période est essentielle, mais peu étudiée.

Cette recherche se propose d'analyser par des méthodes minéralogiques (analyses par XRD de la roche totale et des argiles, granulométrie) et géochimiques (détermination des phases du phosphore, isotopes stables de l’azote et caracterization de la matière organique) les sédiments prélevés en différents endroits dans les océans (marges du Pérou et d’Oman, Atlantique nord et du nord-est, Mer de Chine méridionale et du Japon, plateau d’Ontong Java). Les phases du phosphore, mesurées par une méthode d'extraction séquentielle (SEDEX), ont été comparées à l'enregistrement d'autres paramètres. Cela dans le but de mieux comprendre les relations entre le phosphore, l'érosion continentale et le climat, et d'établir l'impact des facteurs locaux et globaux sur la distribution du phosphore dans les sédiments pendant le dernier cycle glaciaire-interglaciaire.

On trouve du phosphore organique et inorganique dans les sédiments marins de touts les sites étudiés. Le phosphore détritique varie en fonction de l'apport de matériel détritique du continent. Le phosphore authigénique représente le dépôt le plus important du phosphore réactif et représente en moyenne entre 35 et 78 % du phosphore total. La distribution du phosphore entre les différentes formes réactives (lié au fer, authigenique, lié à la matière organique) est contrôlée par les conditions environnementales dans les eaux profondes et dans les premiers centimètres des sédiments. Ces conditions sont elles-mêmes liées à des phénomènes de plus large ampleur, comme la circulation océanique et le climat. L'étude du phosphore dans les sédiments déposés pendant les événements d’Heinrich montre que les concentrations de chaque phase du phosphore répondent

à des changements rapides. La circulation océanique, la ventilation de la colonne d'eau et le flux de matière organique peuvent changer rapidement et modifier les conditions de diagenèse dans les sédiments. Parce que le phosphore est sensible aux conditions d'oxydation et de réduction dans les sédiments (conditions redox), il est par conséquent influencé par ces phénomènes à large échelle.

Les concentrations du phosphore réactif et total sont comparables entre les différents endroits et fluctuent entre 0.3 et 0.65 mg/g, indépendamment des conditions géographiques, océanographiques et environnementales. Seuls deux sites, dans la marge du Pérou et dans la marge d'Oman, tous deux caractérisés par la remontée d'eaux profondes et par des taux de productivité élevés, montrent des concentrations plus élevées (1.2 et 2.5 mg/g respectivement). Donc, les concentrations du phosphore ne semblent pas contrôlées ni par le flux de matière organique, ni par l'apport initial du phosphore, ni par le taux de sédimentation.

Les taux d'accumulation du phosphore sont clairement contrôlés par les taux de sédimentation et varient selon les conditions locales. Les valeurs les plus faibles ont étés enregistrées dans les sédiments de l'Atlantique nord (0.9 mg/m^2·ky), tandis que les taux d'accumulation les plus importants ont étés trouvés en Mer de Chine (40 mg/m^2·ky). Il n'y a pas de différences significatives entre les moyennes enregistrées pendant les périodes glaciaires et interglaciaires. L'analyse de valeurs centrées et réduites des taux d'accumulation indique qu'il pourrait exister une liaison entre la variabilité des taux d'accumulation du phosphore et le cycle de précession. Cela impliquerait que à basse latitude, le climat de type mousson, contrôle l'apport du phosphore par l'érosion continentale, et règle les transformations diagénétiques et l'enfouissement final par son emprise sur la circulation océanique. Certains paramètres chimiques, comme les isotopes de l'azote et le contenu en carbone organique, et les relations entre les valeurs centrées et réduites des taux d'accumulation du phosphore réactif et du carbone organique, suggèrent que le phosphore régénéré et dissous dans les sédiments, peut s'enfuir de nouveau dans la colonne d'eau. Cela s'observe surtout pendant les périodes caractérisées par des flux importants de matière organique et par des conditions pauvres en oxygène dans les eaux profondes. Ce phénomène est particulièrement évident pendant les périodes glaciaires, et pourrait avoir des conséquences importantes sur le cycle du carbone et sur le climat, spécialement pendant les périodes déjà caractérisées par une forte productivité. L'analyse des taux d'accumulation centrés et réduits indique, en effet, que les intervalles de haute productivité sont correlés aux faibles taux d’enfouissement de phosphore réactif.

Del nascere e del morire i Greci non hanno una giusta concezione, perché nessuna cosa nasce né muore, ma da cose esistenti ogni cosa si compone e si separa. E così dovrebbero propriamente chiamare il nascere comporsi, il morire separarsi.

Anassagora, 500 - 428 a.C.

Nella natura niente si crea, niente si perde, tutto si trasforma.

Antoine-Laurent de Lavoisier , 1743-1794

Riassunto

Il fosforo è un elemento essenziale per la vita. Dal momento che l'erosione continentale e la degradazione meteorica delle rocce controllano l'apporto di fosforo alla biosfera, molti ricercatori considerano il fosforo come un elemento chiave per le ricerche paleoclimatiche e biogeochimiche. Negli ultimi decenni, diversi studi hanno indagato il comportamento geochimico del fosforo e il suo segnale nei sedimenti marini. Alcune di queste ricerche hanno evidenziato l'esistenza di un meccanismo di *feedback* tra l'apporto di fosforo all'oceano, la produttività marina e il clima, per mezzo della connessione tra nutrienti e anidride carbonica (CO_2). Molti aspetti rilevanti del ciclo del fosforo e del carbonio sono ancora poco chiari; tra questi, in particolare, le modalità di riciclo del fosforo nell'oceano e nei sedimenti, e la sua risposta ai cambiamenti repentini ed estremi del clima. Il Pleistocene e l'Olocene sono caratterizzati dal susseguirsi di periodi glaciali e interglaciali: l'esplorazione dei meccanismi di *feedback* tra il carbonio, il fosforo e il clima durante questo intervallo, pur essendo di fondamentale importanza, è stata finora oggetto di pochi studi.

Questo progetto di ricerca si propone di analizzare, attraverso un approccio geochimico (studio delle fasi del fosforo, degli isotopi stabili dell'azoto, della materia organica) e mineralogico (studio per diffractometria del sedimento totale e delle argille, granulometria), i sedimenti marini depositatisi durante l'ultimo ciclo glaciale-interglaciale e provenienti da nove diverse località (margine del Perù e dell'Oman, Oceano Atlantico settentrionale e nord-orientale, Mare della China, Mar del Giappone, plateau d'Ontong Java). L'utilizzo di un particolare metodo di laboratorio (estrazione in sequenza, SEDEX) ha permesso di differenziare quattro forme di fosforo, che poi sono state rapportate ad altri parametri. Lo scopo di questa ricerca è di comprendere le relazioni tra il segnale del fosforo registrato nei sedimenti, l'erosione continentale e il clima, e di valutare l'impatto di fattori locali e globali sulla distribuzione del fosforo durante l'ultimo periodo glaciale-interglaciale.

Il fosforo conservato nei sedimenti può essere associato a fasi organiche e inorganiche, entrambe rilevate in tutte le località prese in considerazione. Il fosforo detritico generalmente varia in relazione all'apporto di materiale eroso dal continente; il fosforo autigenico, che è stato rilevato in tutte le località e rappresenta la forma reattiva di deposito più importante, è presente in percentuali che variano dal 35 al 78% del totale. La distribuzione del fosforo tra le sue forme reattive (legato agli ossidi e idrossidi di ferro, autigenico e legato alla materia organica) è normalmente controllata dalle condizioni ambientali che caratterizzano le acque profonde e la parte superiore dei sedimenti.

Tali condizioni sono poi connesse a fenomeni di larga portata, come la circolazione oceanica e il clima. Lo studio del comportamento geochimico del fosforo nei sedimenti depositatisi durante gli *Heinrich events* mostra che la proporzione relativa di ogni fase del fosforo risponde a processi che mutano molto velocemente. La circolazione oceanica, l'ossigenazione della colonna d'acqua e il flusso di materia organica verso i fondali marini possono cambiare alquanto rapidamente e modificare i parametri che regolano l'autigenesi. Visto che il fosforo è sensibile a tali parametri, la sua distribuzione nei sedimenti ne è influenzata.

Le concentrazioni del fosforo reattivo e totale rilevate nelle singole località sono simili, in media tra 0.3 e 0.65 mg/g, a dispetto della diversità delle condizioni geografiche, oceanografiche e ambientali. Solo i siti del margine del Perù e dell'Oman, entrambi caratterizzati da alta produttività, mostrano concentrazioni di fosforo considerevolmente più alte (1.2 e 2.5 mg/g rispettivamente). Sembra che il flusso di materia organica, l’apporto iniziale di fosforo e le velocità di sedimentazione non influenzino le concentrazioni finali di fosforo nei sedimenti.

Le velocità di accumulo del fosforo sono chiaramente controllate dalle velocità di sedimentazione e variano da una località all'altra. I valori più bassi sono stati trovati nei sedimenti dell'Atlantico settentrionale (0.9 mg/m^2·ky), mentre i sedimenti del Mare della China meridionale sono caratterizzati dai valori più elevati (circa 40 mg/m^2·ky), simili a quelli riscontrati in località fosfogeniche, come il margine del Perù, dove si formano depositi di fosforo economicamente importanti. Non c'è alcuna differenza sostanziale tra i valori medi calcolati per i periodi glaciali e per quelli interglaciali. L'analisi dei valori normalizzati delle velocità di accumulo del fosforo reattivo indica l'esistenza di una possibile connessione tra l'accumulo del fosforo nei sedimenti e il ciclo di precessione. Questa ipotesi, se vera, implicherebbe che a basse latitudini, il clima di tipo monsonico controlla l'apporto di fosforo agli oceani attraverso la degradazione meteorica e regola le trasformazioni diagenetiche del fosforo attraverso la sua influenza sulla circolazione oceanica.

Parametri come gli isotopi dell'azoto e la quantità di carbonio organico, così come la relazione tra i valori normalizzati delle velocità di accumulo del fosforo reattivo e del carbonio organico, indicano che parte del fosforo che viene dissolto e che è presente nei sedimenti si diffonde nuovamente nelle acque sovrastanti, specialmente durante periodi di elevato flusso di materia organica e di ridotto contenuto di ossigeno nelle acque profonde e nelle acque interstiziali. Questo fenomeno è particolarmente evidente durante i periodi glaciali e potrebbe avere un impatto importante sul ciclo del carbonio e sul clima, specialmente durante fasi già caratterizzate da una rilevante produttività biologica. I valori normalizzati dei tassi di accumulazione evidenziano una chiara correlazione tra produttività abbondante e basso accumulo di fosforo reattivo.

Die Worte Entstehen und Vergehen gebrauchen die Griechen nicht richtig. Denn kein Ding entsteht oder vergeht (in eigentlichem Sinne), sondern aus (schon) vorhandenen Dingen findet eine Mischung wie andererseits eine Trennung statt. Und so dürften sie wohl mit Recht das Entstehen als ein Sich-Mischen und das Vergehen als ein Sich-Trennen (von Stoffen) bezeichnen.

Anaxagoras, 500 - 428 B.C.

In dieser Welt wird nichts erschaffen und nichts verloren, sondern alles verwandelt.

Antoine-Laurent de Lavoisier , 1743-1794

Zusammenfassung

Phosphor ist ein lebenswichtiges Element. Da sein Eintrag in die Biosphäre primär durch kontinentale Verwitterung kontrolliert wird, wird Phosphor auch als Schlüsselelement für biogeochemische und paläoklimatische Studien angesehen. Während der letzten Dekaden wurden verschiedene Studien zur Geochemie des Phosphors und seiner Aufzeichnung in marinen Sedimenten verfasst. Einzelne davon verfolgten die Hypothese von Rückkoppelungsmechanismen zwischen Phosphorzufuhr in den Ozean, Produktivität und Klima, durch die "Nährstoff-CO_2"-Beziehung. Viele fundamentale Aspekte von gekoppelten Phosphor-Kohlenstoff-Kreisläufen jedoch wurden kaum erforscht. Wenig ist bekannt über den Kreislauf dieses biophilen Elementes, über sein Schicksal im Meerwasser und im Sediment und über sein Verhalten während schnellen und extremen Klimawandeln. Die Beziehungen von Phosphor, Kohlenstoff und Klima wurden in jüngeren paläoklimatischen Studien kaum behandelt. Ziel dieser Arbeit ist das Verstehen von Rückkopplungsmechanismen in der Epoche des Pleistozäns und Holozäns, einer Zeitspanne schneller Glazial-Interglazial Wechsel. Das vorliegende Forschungsprojekt untersucht marine Sedimentkerne von neun Lokalitäten (Küstengewässer vor Peru und Oman, Nordost- und Nordatlantik, Südchinasee, Ontong Java Plateau, Japansee) mittels geochemischer und mineralogischer Methoden.

Verschiedene Phasen von Phosphor, gemessen unter Anwendung einer sequentiellen Extraktionstechnik (SEDEX), wurden mit anderen Parametern korreliert, um Beziehungen zwischen dem Phosphorarchiv, kontinentaler Verwitterung und Klima zu entschlüsseln, und um die relative Wichtigkeit von globalen und lokalen Prozessen in Bezug auf die Verteilung von Phosphor in Sedimenten während dem letzten Glazial-Interglazial Zyklus aufzuzeigen.

Phosphor erscheint in anorganischen und organischen Phasen im Sediment. Beide Formen wurden in allen Lokalitäten festgestellt. Detritischer Phosphor ändert generell proportional zu der kontinentalen Sedimentzufuhr. Authigener Phosphor war an allen Lokalitäten vorhanden und ist die wichtigste Senke für reaktiven Phosphor, der ursprünglich biologisch brauchbar war, und macht im Durchschnitt zwischen 35 und 78 % vom totalen Phosphor aus. Die Verteilung von Phosphor zwischen den reaktiven Formen (z.B. Fe-gebundener, authigener und organisch gebundener Phosphor) wird normalerweise durch die Umweltbedingungen in den basalen Wasserschichten und in den obersten Teilen der Sedimentsäule kontrolliert. Diese wiederum können mit Phänomenen grösseren Massstabs (z.B. ozeanische Zirkulation und Klima) zusammenhängen. Die Untersuchung der Phosphorgeochemie in Sedimenten, die während Heinrich-Ereignissen abgelagert wurden, zeigt, dass die schnell ändernden Prozesse zu einer Änderung der Phosphorkonzentrationen in allen Phasen führen. Meereszirkulation, Zirkulation in der

Wassersäule und der Flux von organischem Kohlenstoff zum Ozeanboden können sich schnell verändern. Sie beeinflussen dabei zusätzlich die diagenetischen Bedingungen im obersten Teil der Sedimentsäule. Da der reaktive Phosphor redox-empfindlich ist, wird die Verteilung der Phasen im Sediment durch die oben genannten Änderungen beeinflusst. Konzentrationen von reaktivem und totalem Phosphor sind sehr ähnlich in den verschiedenen Lokalitäten und variieren im Durchschnitt zwischen 0.3 und 0.65 mg/g Sediment, unabhängig von den geographischen und ozeanographischen Gegebenheiten, sowie den Umweltbedingungen. Nur zwei Stellen, die Küstengewässer vor Oman und Peru, die durch Auftrieb und hohe Produktivität charakterisiert sind, zeigen höhere Phosphorkonzentrationen im Sediment (1.2 resp. 2.5 mg/g im Durchschnitt). Weder der Flux organischen Kohlenstoff ins Sediment, noch die ursprüngliche Phosphorzufuhr, noch die Sedimentationsrate ist der kontrollierende Faktor.

Phosphor Massenakkumulationsraten (MAR) sind klar kontrolliert durch die Sedimentationsraten und variieren abhängig von lokalen Bedingungen. Tiefere Werte wurden in nordatlantischen Sedimenten gefunden, wo MAR-Werte um 0.9 mg/m^2·ky sind, während ODP site 1144 (Südchinasee) die höchsten MAR-Werte zeigt (im Durchschnitt 40 mg/m^2·ky), welche mit denjenigen der phosphogenen Stellen (z.B. Küstengewässer vor Peru) vergleichbar sind. Es gibt keine signifikanten Unterschiede zwischen glazialen und interglazialen Durchschnitten von reaktiven Phosphor-MAR. Die statistische Analyse reaktiver Phosphor-MAR weist in Richtung einer möglichen Beziehung zwischen der Änderung reaktiver Phosphor-MAR und der durch die Präzession verursachten Schwankungen der Sonneneinstrahlung. Dies würde bedeuten, dass das Klima niederer geographischer Breiten (z.B. das Monsun-Klima) einerseits den Phosphoreintrag durch kontinentale Verwitterung beeinflussen würde, andererseits die diagenetische Umwandlung und Fixierung im Sediment durch Änderungen in der ozeanischen Zirkulation. Parameter wie die stabilen Isotope von Stickstoff und totalem organischem Kohlenstoff (TOC) sowie der Beziehung zwischen normiertem reaktivem Phosphor und TOC MAR weisen darauf hin, dass regenerierter gelöster Phosphor aus dem Sediment verloren geht - hauptsächlich während Zeiten mit hohem Flux von organischem Kohlenstoff ins Sediment und mit sauerstoffarmen Bedingungen in Boden- und Porenwässern. Dieses Phänomen ist insbesonders deutlich während glazialen Perioden und hat möglicherweise wichtige Konsequenzen in Bezug auf Kohlenstoffkreislauf und Klimaänderung, vor allem während Zeiten mit bereits erhöhter Sedimentation organischem Material. Normierte MAR implizieren, dass Zeiten mit hoher Produktivität von organischem Material klar mit abnehmendem Rückalt von reaktivem Phosphor im Sediment korrelieren.

CHAPTER 1

From left to right: Anchun Li, Peter Clift, Federica Tamburini and Wolfgang Kuhnt (day shift in the sedimentology lab, Leg 184, 1999).

Introduction

Since the 19th century, when earth scientists discovered indications of past climate changes on the continents (Lyell, 1877; Croll, 1883; Agassiz and Carozzi, 1967), paleoclimatology has become an important discipline. A multitude of factors influences climate which, through feedback mechanisms, interacts and regulates them (Fig. 1). Then, after the discovery of lowered CO_2 levels in the atmosphere during the last glacial period (Neftel et al., 1982), researchers have perceived the importance of the carbon cycle and its interaction with climate (Broecker, 1982; Broecker and Peng, 1992; Siegenthaler and Sarmiento, 1993; Cerling, 1997).

Continental weathering and primary productivity influence CO_2 concentration in the atmosphere. CO_2 is pumped from the atmosphere during the alteration of silicate minerals on the continent. Moreover, the products of physical and chemical weathering of rocks and soils, once transported to the oceans by rivers and winds, provide dissolved elements (e.g. macro- and micronutrients) that are used by primary producers in the upper photic zone. Through photosynthesis and consequent burial of organic matter in the marine sediments, CO_2 is again sequestered from the atmosphere.

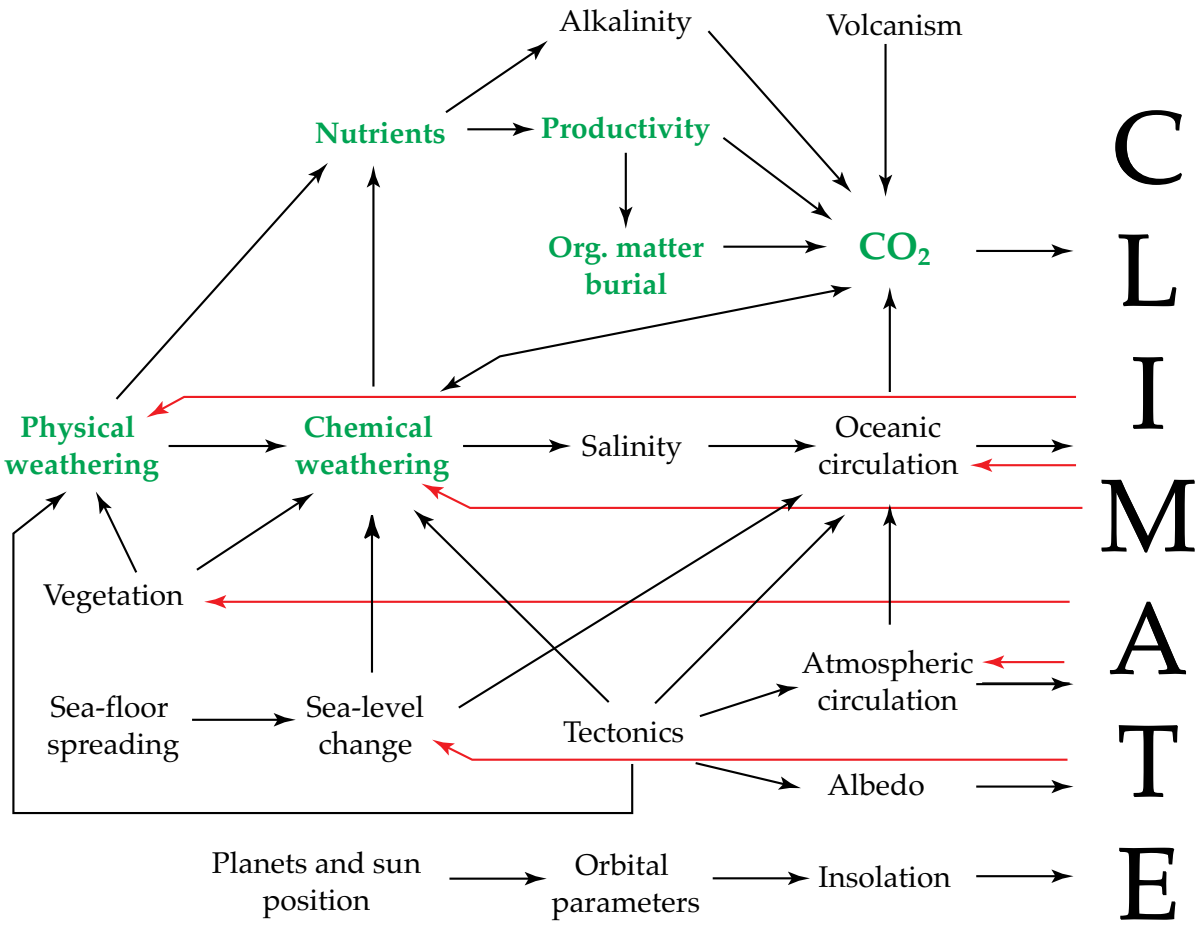

Fig. 1: Schematic representation of the different processes influencing the climate system. Red arrows indicate feedback responses of climate. Weathering, nutrient supply to the ocean, productivity and organic matter burial (in green) are the processes investigated by this study.

Several hypotheses on the relationship between CO_2, weathering and climate have been forwarded (e.g. Raymo, 1994; Filippelli, 1997), but many aspects such as nutrient budget, productivity and rate of continental weathering during glacial periods, remain poorly constrained.

The element phosphorus

Phosphorus (P) is an essential element for all living organisms and is believed to control primary productivity in the oceans, especially on "geological" time scales (Broecker, 1982; Delaney, 1998; Tyrrell, 1999). As phosphorus lacks an important atmospheric phase and major input from hydrothermal activity, its delivery to the oceans is mainly ruled by continental weathering and transport by rivers and winds (Fig. 2; Froelich et al., 1982). The importance of the "nutrient-CO_2" connection in controlling climate changes (Broecker, 1982), has therefore persuaded many researchers of the existence of a feedback mechanism between phosphorus delivery to the ocean, productivity and climate change. Phosphorus has thus been proposed as an ideal geochemical proxy to link continental weathering and productivity on geological timescales (e.g. Föllmi, 1995; Filippelli, 1997). On the other hand, the biophile character of phosphorus and its strong affinity to iron oxyhydroxides greatly influence P geochemistry and cycling in the sediments. The result is that the ultimate removal of P in the sediments does not exactly mirror the delivery of P from the continent (Berger et al., 1989; Berner et al., 1993; Delaney, 1998).

P cycle in marine sediments

Dissolved and particulate phosphorus enters the ocean via rivers and/or wind transport, in two forms: detrital P, associated to igneous and metamorphic P-bearing minerals, and reactive (e.g. bio-available) P. Recent

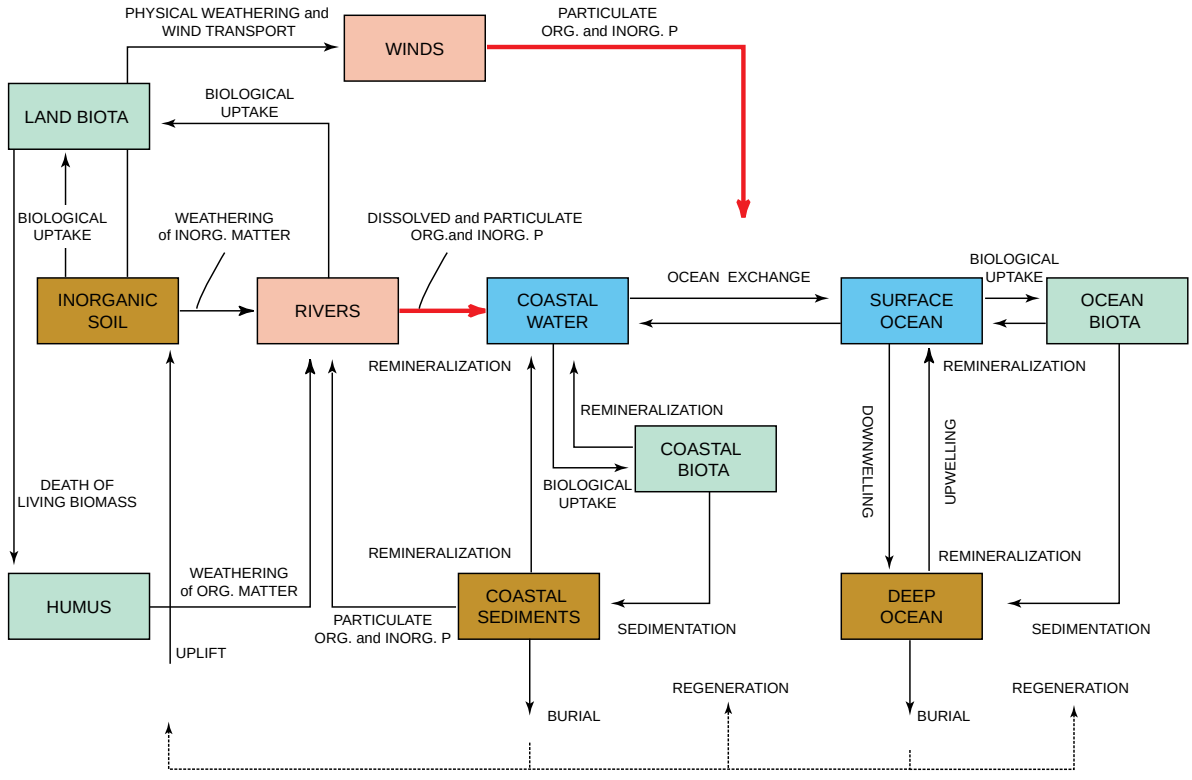

Fig. 2: Schematic representation of the phosphorus cycle (after Mackenzie et al., 1993)

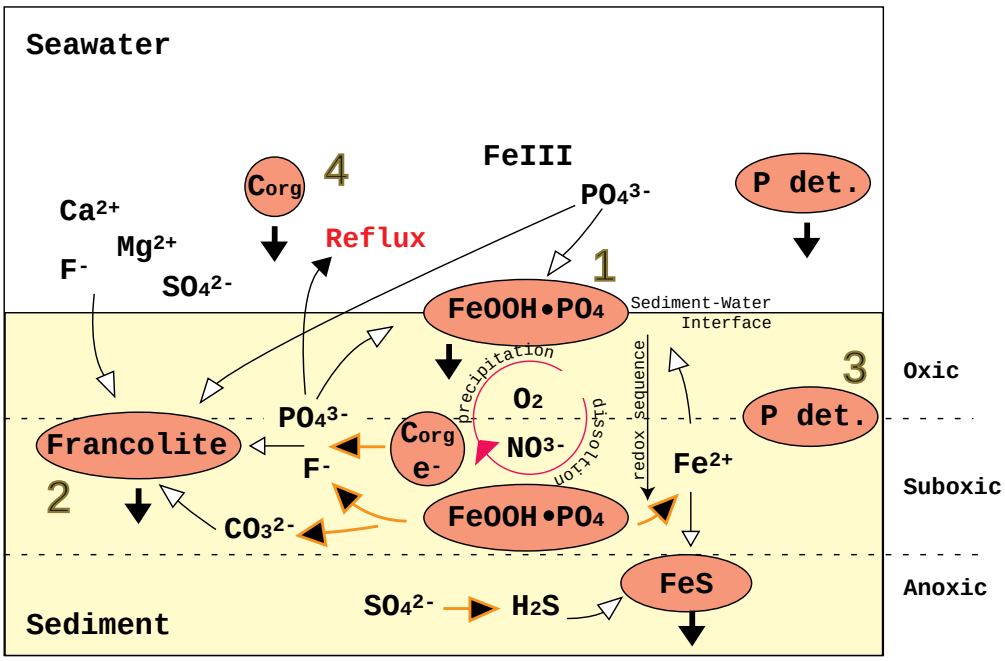

Fig. 3: Phosphorus cycle in marine sediments. P det. is detrital phosphorus. Francolite is a P-bearing authigenic mineral (after Jarvis et al., 1994).

studies have shown that also particulate P contributes to the oceanic pool of reactive P (e.g. Berner and Rao, 1994). Reactive P is removed from the water column in association with organic matter, iron and manganese oxyhydroxides, and, to a lesser extent, with fish debris (Filippelli and Delaney, 1996; Delaney, 1998). Hydrothermal removal of P is considered as not significant (Delaney, 1998). The first tens of centimeters of the sediment column may be considered as a biogeochemical laboratory, where reactive phosphorus undergoes several transformations, the rates and extent of which depending on environmental and diagenetic conditions (Fig. 3). Organic matter is the main carrier of reactive P to the sediments. During organic matter degradation, reactive P is partially regenerated and returns to a dissolved form (Ruttenberg and Gõni, 1997). Studies of elemental ratios of organic matter indicate that organically bound P is preferentially regenerated with respect to organic carbon, especially under oxygen-depleted bottom waters conditions (Anderson and Sarmiento, 1994; Ingall and Jahnke, 1994; Colman and Holland, 2000).

Iron and manganese oxyhydroxides supply another important temporary and sometimes permanent sink of dissolved phosphorus (Jarvis et al., 1994; Slomp et al., 1996). Once in the suboxic section, the iron and manganese oxyhydroxides are dissolved and phosphates, again released in a dissolved form, may diffuse upward in sediments, be sequestrated again onto oxyhydroxides in the oxic portion of the sediments or diffuse into the overlying waters (Fig. 3). The depth of the redox boundary and the redox conditions are determined by sedimentation rates, organic carbon flux, ventilation of bottom waters, bioirrigation and bioturbation among others (Colman and Holland, 2000), and control the evolution and the extent of this process. Fish debris, mainly composed of hydroxyapatite, a mineral highly soluble in sea water, constitutes a minor supply of reactive P to the sediments (Krajewski et al., 1994). Only in limited settings, such as the Peru and the Oman margins, fish debris may significantly contribute to the overall pool of reactive P (Suess, 1981; Schenau et al., 2000).

The most important sedimentary sink for

reactive P in the oceans is provided by authigenic apatite, mainly carbonate-fluorapatite (CFA), whose formation is not only limited to restricted environments along the continental margins (e.g. upwelling areas), but is more widespread (Delaney, 1998). The sedimentary conditions leading to CFA precipitation are still not completely understood, and have been the subject of extensive studies (for a comprehensive review, see Glenn, 1990; Jarvis et al., 1994; Delaney, 1998). Both phosphate and fluoride concentrations in the pore waters, as well as carbonate alkalinity and oxygen levels are the most important factors influencing the redistribution of P and the amount of CFA precipitation in the sediments (Jarvis et al., 1994).

Given the complexity of the phosphorus geochemistry in marine sediments, a better understanding of phosphorus distribution in marine sediments, both under different oceanographic and environmental conditions, as well as through time is essential.

In the last 20 years several studies have focused on the different aspects of the phosphorus cycle. Phosphorus distribution and mass accumulation rates have been investigated in different settings, such as in continental margins (Lucotte and D'Anglejan, 1988; Ruttenberg and Berner, 1993; Ruttenberg and Gõni, 1997; Slomp, 1997), and deep-sea sediments (Moody et al., 1988; Filippelli and Delaney, 1996); phosphorus geochemistry in marine sediments has been studied in connection with other geochemical tracers (e.g. rare earth elements, stable oxygen and carbon isotopes; Jarvis et al., 1994); some researchers have proposed overviews of phosphorus records in the oceans (e.g. Baturin, 1988) and have tried to find global trends in phosphorus accumulation rates and to link them to climate changes (e.g. Föllmi, 1995).

Table 1: Name, location and other characteristics for the studied sites. References at the end of *Annex B* .

Site	Water depth	Localition	Sed. Rates	Lithology	Environment
ODP 108-658	2263 m	**Eastern Tropical Atlantic**	14.7 cm/k.y.	Nannofossil ooze Cyclic variations	Lower to upper bathyal Under an upwelling cell High productivity
ODP 112-680	252.2 m	**Peru Continental Margin**	6.3-52.3 cm/k.y.	Foraminifer-diatom mud Phosphatic nodules High organic matter	Outer shelf/upper bathyal Under an upwelling cell Oxygen minimum zone
ODP 117-724	592.8 m	**Oman Margin**	3.5-15 cm/k.y.	Dark clay with terrigenous material	Upper slope of a basin Under an upwelling cell Oxygen minimum zone
ODP 128-798	900.1 m	**Japan Sea**	12-13.8 cm/k.y.	Clay and silty clay with siliciclastic material Laminated sequences Volcanic ash layers	Upper-middle bathyal Epicontinental sea
ODP 130-806	2520.7 m	**Ontong-Java Plateau**	2.2 cm/k.y.	Foraminifer nannofossil ooze Clayey silt to sandy clayey silt	Upper bathyal Above the present lysocline
ODP 151-907	1800.8 m	**North Atlantic Artic Gateways I**	2 cm/k.y.	Biogenic calcareous material Silt, clay and mud	Upper bathyal Low productivity
ODP 184-1143	2772 m	**South China Sea**	10 cm/k.y.	Clay and nannofossil ooze mixed sediments	Depression inside a carbonate platform
ODP 184-1144	2037 m	**South China Sea**	100 cm /k.y.	Bioturbated clay and nannofossil ooze High organic matter Iron sulfides and pyrite	Sediment drift Upper slope
SU 90-09	3375 m	**North Atlantic**	4-10 cm/k.y.	Detrital material and foraminifer ooze	Southern limit of polar water during glacial, IRD belt

Fig. 4: World map with the location of the investigated sites. Results from ODP sites 724 (Oman margin), 1143 and 1144 (South China Sea), and core SU 90-09 (North Atlantic) will be detailed in Chapters 2 to 5 (sites in yellow). The results from the other ODP sites (in purple) will be discussed in the last chapter (Chapter 6).

Rationale and outline of this research thesis

In spite of the number of studies addressing phosphorus geochemistry records in ancient and modern sediments, little work has been done on Pleistocene and Holocene sediments. As the climate system experienced important shifts during the last 140,000 years (the last glacial-interglacial cycle), this time period may be considered as ideal for paleoclimatic studies. Moreover, the large amount of available material and the possibility of high-resolution studies stress the relevance of investigating this geological interval.

This research thesis focuses on phosphorus record in marine sediments spanning the last glacial-interglacial cycle. This study aims at 1) having a better insight on feedback mechanisms between continental weathering, marine productivity, the carbon cycle, and climate change; 2) quantifying P mass accumulation rates (MAR) over the last glacial-interglacial period in order to identify the link between weathering and P supply to the ocean; 3) determining the existing links between P phases distribution and oceanographic and climatic variations; and 4) looking for a "global P signal" in the ocean. In order to answer these questions, sediments recovered from different oceanographic settings during ODP (Ocean Drilling Program) cruises have been requested and analyzed (Table 1 and Fig. 4). The time resolution, for most of the sites, ranges between 2 and 5 ky.

Phosphorus determination is the key element of this research. As phosphorus geochemistry in marine sediments is rather complex, the determination of phosphates by standard methods, such as XRD and/or XRF, would have not given enough information and would have not allowed the distinction between different phosphorus phases. Moreover, the generally low concentrations of phosphate-bearing phases in most sediments would have been below the detection limits, at least for XRD measurements. In 1976, Aspila proposed an analytic technique permitting to separate inorganic and organic forms of phosphorus in marine sediments. Later on, sequential extraction techniques, previously applied to soils and to lake and river sediments (Lucotte and D'Anglejan, 1985), have been modified and optimized for marine sediments (Ruttenberg, 1992; Anderson and Delaney, 2000). I have used this sequential extraction method, called SEDEX, which allows to differentiate four “phosphorus sedimentary reservoirs” (Ruttenberg, 1992; see *Annex A* for a detailed outline of the method).

Moreover, given the complexity of the climate system, the diversity of the studied environments and the variations in productivity, continental input and oceanographic conditions between glacial and interglacial stages, I have employed a multiproxy approach which combines, besides P phases determination, bulk and clay mineralogy (by XRD), nitrogen stable isotopes analysis, and organic matter characterization (by Rock-Eval).

Bulk sediment XRD results have been then used to constrain detrital flux rates and to infer variations in continental material input related to changes in climatic conditions. Clay minerals are generally considered as a proxy for climate and weathering regime on the continent, for diagenesis, for the origin of the sediments, and their temporal variations may record changes in these parameters (e.g. Chamley, 1989; Chamley, 1997; Weaver, 1989). Nitrogen stable isotopic analysis of the bulk sediments is an essential tool for paleoproductivity studies as they may give information about nutrient utilization in the surface waters, and the occurrence of nitrogen fixation and of denitrification (e.g. Farrell et al., 1995). Besides providing estimates of the organic carbon content in sediments, Rock-Eval parameters (i.e. the Oxygen and Hydrogen Indexes, approximations of the oxygen and hydrogen contents of the organic matter, respectively) may be used to constrain the nature and origin of the organic matter and the

degree of degradation (e.g. Espitalié et al., 1986).

All the measurements were performed in Neuchâtel, except for nitrogen stable isotopic studies, which were carried out at the ETH in Zürich, in collaboration with S.M. Bernasconi.

Chapter 2 addresses the sedimentary history of the Oman margin during the last glacial-interglacial cycle. The Oman margin is at the centre of an important upwelling zone and it is under the influence of the Indian monsoon. The location of ODP Site 724 close to the oxygen minimum zone (OMZ), which is known to oscillate in response to monsoonal variability, makes the site ideal to study phosphorus geochemistry and its responses to oxygen levels variations, productivity, and climate change.

In the course of my thesis project, I have had the opportunity to sail as a sedimentologist on an ODP cruise (Leg 184: South China Sea, February-April 1999). Two new sites (ODP Sites 1143 and 1144) were then added to the list of the locations to be investigated, and the results of this study are presented in *Chapter 3*. As for the Oman margin, phosphorus geochemistry has been used in concert with the other sedimentary and geochemical proxies in order to better understand the evolution of the South China Sea climate and oceanography during the last 140,000 years.

Recently discovered in North Atlantic sediments and then correlated in records from all over the globe, Heinrich layers record episodes of fast and dramatic iceberg discharges, down to relatively low latitudes (Ruddiman, 1977; Heinrich, 1988). These short events, spanning few thousand of years, deeply influenced oceanic circulation and bottom water conditions. Sediments from core SU 90-09 (North Atlantic), sampled at high resolution, were provided by S. Huon (Université Pierre et Marie Curie, Paris, France), and analyzed for phosphorus phases. The results are detailed in *Chapter 4*. The phosphorus record shows rapid variations, and gives indications of enhanced detrital supply and of important regeneration of reactive phosphorus during Heinrich events.

During Leg 184 in the South China Sea, distinct sedimentary features, called "green clay layers", were recognized. It was difficult to obtain a clear and complete understanding of the nature and genesis of these layers on board. Given the possible diagenetic origin of the layers, I proposed to perform a more detailed investigation. Along with the extraction and determination of phosphorus phases, clay and bulk mineralogy, granulometry, and XRF analyses were carried out on selected samples. The outcomes of these analyses and the interpretations on the nature of the green clay layers are reported in *Chapter 5*.

During Leg 184, I have also collected sediments samples from the “squeezed cakes” used to collect pore water. I have performed phosphorus phases extraction on those sediments, in order to compare the variations in sedimentary phosphorus phases to phosphates in pore water. The results are reported in *Annex B*, along with the results from all the investigated sites.

Chapter 6 is thought as an overview of the phosphorus geochemistry and the mineralogical records from the other five investigated locations (North Eastern Atlantic, Peru margin, Japan Sea, Ontong-Java Plateau and North Atlantic Gateways, see Fig. 4). This chapter also includes some general considerations, which take into account all the studied sites, and the final conclusions of the thesis. Here, I have tried to draw a comprehensive picture of the phosphorus record in the oceans, to connect it to large-scale phenomena, such as climate and continental weathering, and, finally, to understand the impact of variations of the phosphorus cycle in marine sediments on the carbon cycle and on climate itself. Far from being definitive, I consider these conclusions as the starting point for my future research.

REFERENCES

Agassiz, L. and Carozzi, A.V. (Editors), 1967. Studies on glaciers preceded by the Discourse of Neuchatel, 213 pp.

Anderson, L.A. and Sarmiento, J.L., 1994. Redfield ratios of remineralization determined by nutrient data analysis. Global Biogeochemical Cycles, 8(1): 65-80.

Anderson, L.D. and Delaney, M.L., 2000. Sequential extraction and analysis of phosphorus in marine sediments: Streamlining of the SEDEX procedure. Limnol. Oceanogr., 45(2): 509-515.

Aspila, K.I., Agemian, H. and Chau, A.S.Y., 1976. A semi-automated method for the determination of inorganic, organic and total phosphate in sediments. Analyst, 101: 187-197.

Baturin, G.N., 1988. Disseminated phosphorus in oceanic sediments - a review. Marine Geology, 84: 95-104.

Berger, W.H., Smetacek, V.S. and Wefer, G. (Editors), 1989. Productivity of the ocean; present and past. Dahlem workshop on Productivity of the ocean; present and past, 44: 471.

Berner, R.A. and Rao, J.-L., 1994. Phosphorus in sediments of the Amazon river and estuary: implications for the global flux of phosphorus to the sea. Geochimica et Cosmochimica Acta, 58(10): 2333-2339.

Berner, R.A., Ruttenberg, K.C., Ingall, E.D. and Rao, J.-L., 1993. The nature of phosphorus burial in modern marine sediments. In: R. Wollast, F.T. Mackenzie and L. Chou (Editors), Intaractions of C, N, P and S biogeochemical Cycles and global change. NATO ASI Series. Springer-Verlag, Berlin, pp. 365-378.

Broecker, W.S., 1982. Ocean chemistry during glacial time. Geochimica et Cosmochimica Acta, 46: 1689-1705.

Broecker, W.S. and Peng, T.-H., 1992. Interhemispheric transport of carbon dioxide by ocean circulation. Nature, 356(587-593).

Cerling, T.E., 1997. Late Cenozoic vegetation change, atmospheric CO_2 and tectonics. In: W.F. Ruddiman (Editor), Tectonic uplift and climate change. Plenum, New York, pp. 313-327.

Chamley, H., 1989. Clay sedimentology. Springler-Verlag.

Chamley, H., 1997. Clay mineral sedimentation in the ocean. In: H. Paquet and N. Clauer (Editors), Soils and sediments, Mineralogy and Geochemistry. Springer-Verlag, Berlin: 269-302.

Colman, A.S. and Holland, H.D., 2000. The global diagenetic flux of phosphorus from marine sediments to the oceans: redox sensitivity and the control of atmospheric oxygen levels. In: C.R. Glenn, L. Prevot-Lucas and J. Lucas (Editors), Marine authigenesis: from global to microbial. SEPM: 53-75.

Croll, J., 1883. On some controverted points in geological climatology. American Journal of Science, 26: 249-271.

Delaney, M.L., 1998. Phosphorus accumulation in marine sediments and the oceanic phosphorus cycle. Global Biogeochemical Cycles, 12(4): 563-572.

Espitalié, J., G. Deroo, and F. Marquis, 1986. La pyrolyse Rock-Eval et ses applications - III partie. Rev. Inst. Fr. Pet., 41 (1): 73-89.

Farrell, J.W., T.F. Pedersen, S.E. Calvert, and B. Nielsen, 1995. Glacial-interglacial changes in nutrient utilization in the equatorial Pacific Ocean. Nature, 377: 514-517.

Filippelli, G.M., 1997. Intensification of the Asian monsoon and a chemical weathering event in the late Miocene-early Pliocene; implications for the late Neogene climate change. Geology, 25(1): 27-30.

Filippelli, G.M. and Delaney, M.L., 1996. Phosphorus geochemistry of equatorial Pacific sediments. Geochimica et Cosmochimica Acta, 60(9): 1479-1495.

Föllmi, K.B., 1995. 160 m.y. record of marine sedimentary phosphorus burial: coupling of climate and continental weathering under greenhouse and icehouse conditions. Geology, 23(6): 859-862.

Froelich, P.N., Bender, M.L., Luedtke, N.A., Heath, G.R. and DeVries, T., 1982. The marine phosphorus cycle. American Journal of Science, 282(4): 474-511.

Glenn, C.R., 1990. Pore water, petrologic and stable carbon isotopic data bearing on the origin of modern Peru margin phosphorites and associated authigenic phases. In: S.R. Riggs, Burnett, W. C. (Editors), Neogene to modern phosphorites. Phosphate deposits of the world. Cambridge Unviversity Press, New York, NY, USA, pp. 46-61.

Heinrich, H., 1988. Origin and consequences of cyclic ice rafting in the Northeast Atlantic Ocean during

the past 130,000 years. Quaternary Res., 29: 142-152.

Ingall, E. and Jahnke, R., 1994. Evidence for enhanced phosphorus regeneration from marine sediments overlain by oxygen depleted waters. Geochimica et Cosmochimica Acta, 58(11): 2571-275.

Jarvis, I., Burnett, W.C., Nathan, Y., Almbaydin, F.S.M., Attia, A.K.M., Castro, L.N., Flicoteaux, R., Hilmy, M.E., Husain, V., Qutawnah, A.A., Serjani, A. and Zanin, Y.N., 1994. Phosphorite geochemistry: state-of-art and environmental concerns. Eclogae geol. Helv., 87(3): 643-700.

Krajewski, K.P., Van Cappellen, P., Trichet, J., Kuhn, O., Lucas, J., Martin-Algarra, A., Prévot, L., Tewari, V.C., Gaspar, L., Knight, R.I. and Lamboy, M., 1994. Biological processes and apatite formation in sedimentary environments. Eclogae Geol. Helv., 87(3): 701-745.

Lucotte, M. and D'Anglejan, B., 1985. A comparision of several methods for the determination of iron hydroxides and associated orthophospates in estuarine particulate matter. Chemical Geology, 48: 257-264.

Lucotte, M. and D'Anglejan, B., 1988. Processes controlling phospate adsorption by iron hydroxides in estuaries. Chemical Geology, 67: 75-83.

Lyell, C., 1877. Principles of geology: pp. 546.

Mackenzie, F.T., Ver, L.M., Sabine, C., Lane, M. and Lerman, A., 1993. C, N, P, S global biogeochemical cycles and modeling of global change. In: R. Wollast, F.T. Mackenzie and L. Chou (Editors), Interactions of C, N, P and S biogeochemical Cycles and global change. NATO ASI Series. Springer-Verlag, Berlin: 1-61

Moody, J.B., Chaboudy, L.R. and Worsley, T.R., 1988. Pacific pelagic phosphorus accumulation during the last 10 m.y. Paleoceanography, 3: 113-136.

Neftel, A., Oeschger, H., Schwander, J., Stauffer, B. and Zumbrunn, R., 1982. Ice core sample measurements give atmospheric CO_2 content during the past 40,000 yr. Nature, 295(5846): 220-223.

Raymo, M.E., 1994. The Himalayas, organic carbon burial and climate in the Miocene. Paleoceanography, 9(3): 399-404.

Ruddiman, W.F., 1977. Late Quaternary deposition of ice-rafted sand in the subpolar North Atlantic (lat. 40° to 65°N). Geol. Soc. Am. Bull., 88: 1813-1827.

Ruttenberg, K.C., 1992. Development of a sequential extraction method for different forms of phosphorus in marine sediments. Limnology Oceanography, 37(7): 1460-1482.

Ruttenberg, K.C. and Berner, R.A., 1993. Authigenic apatite formation and burial in sediments from non-upwelling, continental margin environments. Geochimica et Cosmochimica Acta, 57: 991-1007.

Ruttenberg, K.C. and Gõni, M.A., 1997. Phosphorus distribution, C:N:P ratios, and δ^{13}Coc in artic, temperate, and tropical coastal sediments: tools for characterizing bulk sedimentary organic matter. Marine Geology, 139: 123-145.

Schenau, S.J., Slomp, C.P. and De Lange, G.J., 2000. Phosphogenesis and active phosphorite formation in sediments from the Arabian Sea oxygen minimum zone. Marine Geology, 169(1-2): 1-20.

Siegenthaler, U. and Sarmiento, J.L., 1993. Atmospheric carbon dioxide and the ocean. Nature, 365: 119-125.

Slomp, C.P., 1997. Early diagenesis of phosphorus in continental margin sediments. Ph.D. Thesis, Den Burg, Texel, The Netherlands, 178 pp.

Slomp, C.P., Van der Gaast, S.J. and Van Raaphorst, W., 1996. Phosphorus binding by poorly crystalline iron oxides in North Sea sediments. Marine Chemistry, 52: 55-73.

Suess, E., 1981. Phosphate regeneration from sediments of the Peru continental margin by dissolution of fish debris. Geochimica et Cosmochimica Acta, 45(4): 577-588.

Tyrrell, T., 1999. The relative influences of nitrogen and phosphorus on oceanic primary production. Nature, 400: 525-531.

Weaver, C.E., 1989. Clays, Muds, and Shales. Elsevier: pp. 819.

CHAPTER 2


"Marginal Behaviour"
MARGIN
MINES
MOUNTAINS
MONSOONS
MILANKOVITCH
ODP
COLOMBO
LEG 117
MAURITIUS
MOST MUD
SEDCO/BP 471
SEPTEMBER-OCTOBER, 1987

*Sedimentary phosphorus record from the Oman margin: new evidence of high productivity during glacial periods**

ABSTRACT

The northern region of the Arabian sea is one of the biologically most productive regions of the world oceans, with present productivity rates varying between 200 and 2,500 mgC/m^2·day [Madhupratap et al., 1996]. This is related to the influence of southwesterly summer monsoons which cause vigorous upwelling along the Oman margin. Upwelling ceases during northeasterly winter monsoon activty; productivity rates, however, remain relatively high (about 800 mgC/m^2·day), related to deep-water mixing [Madhupratap et al., 1996].

The goal of this study is to verify if during the last glacial period – a period in which winter monsoon conditions prevailed – productivity rates were similarly high. With an analysis of phosphorus phases, stable nitrogen isotopes, organic matter content, and bulk mineralogy of the upper 10 m of the cores of ODP Hole 724C (corresponding to the last 140,000 years, sample resolution is ca. 5 kyr), we provide new evidence of high productivity during this last glacial period, especially during isotopic stages 4, 3 and 2. This was probably related to the combined effect of increased eolian input of iron-containing dust, due to enhanced dryness on the adjacent continent, and the regeneration and diffusion of dissolved phosphorus from the sediments to the water column, due to variations in the position and intensity of the Oxygen Minimum Zone (OMZ), which are in turn related to changes in circulation patterns along the Oman margin.

These findings suggest that there is no one-to-one relationship between summer monsoon activity, upwelling, and productivity, and that a redefinition of the role of upwelling in monsoon regions in controlling productivity and organic carbon burial on glacial-interglacial timescales is necessary.

INTRODUCTION

Since 1982, with the discovery of low levels of atmospheric CO_2 during the Last Glacial Maximum (LGM) [Neftel et al., 1982; Barnola et al., 1987; Petit et al., 1999], great attention has been paid to the global carbon cycle, and to its effects and feedback mechanisms on global climate [Heinze et al., 1991; Raymo, 1994; Goddéris and François, 1995]. Despite the number of studies aiming at unravelling the complexity of climate system and finding the ultimate controlling mechanisms [Broecker and Peng, 1992; Siegenthaler and Sarmiento, 1993; Haug and Tiedemann, 1998], many aspects of the carbon cycle and its interaction with climate still need to be resolved: for example the influence of changes in continental weathering as a source of nutrients to the sea [Föllmi, 1995; France-Lanord and Derry, 1997], the glacial nutrient inventory in the ocean [Ganeshram et al., 1995], and the impact of productivity on the carbon cycle during glacials [Raymo, 1994].

Modern and ancient upwelling regions have been shown to have an impact on the carbon cycle, due to delivery of nutrients to surface waters, enhancing primary productivity rates, and eventually the export production of organic carbon (CO_2 biological pump) [Raymo, 1994; Delaney, 1998]. Estimates of global primary production indicate that the contribution of upwelling regions amounts to 4.8 Gt C/year, representing 67% of new total production [Chavez and Toggweiler, 1995]. New production supplied by monsoon-related upwelling regions (1.5% of world's ocean surface) represents about 5.5% (0.4 Gt C/year) of global primary production.

* This chapter by Federica Tamburini, Karl B. Föllmi, Thierry Adatte, Stefano M. Bernasconi and Philipp Steinmann has been submitted for publication in *Paleoceanography*.

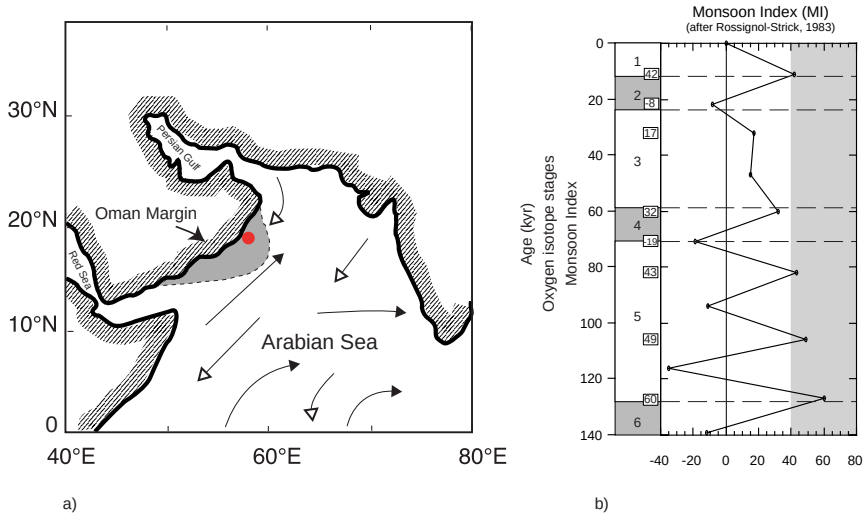

Fig. 1: a) ODP Site 724 location in the Oman margin (•). The Oman margin upwelling area is marked in light gray and arrows show wind directions during summer (solid) and winter (open) monsoon. b) Monsoon index (MI) as calculated in *Rossignol-Strick* (1983). MI higher than 41 (light gray areay) correspond to wet phases and heavy african monsoon (summer).

The Oman margin

The Oman margin is located south of the Arabian peninsula and constitutes the northwestern side of the Arabian Sea (Fig. 1). Intermediate waters along the Oman margin are mainly formed by the outflow of warm, O_2-depleted and nutrient-rich waters from the Red Sea, while contributions from the Persian Gulf mostly influence shallower waters (< 300 m). The extent of these outflows is controlled by monsoon intensity, with winter-summer changes in wind direction affecting the amount of nutrients (P and N) exported to the Indian Ocean [Bethoux, 1988].

The Arabian region is influenced by the Indian Ocean Monsoon, which is characterized by a seasonal reversal of the winds, coupled with an alternation of dry and wet conditions on the mainland [Webster et al., 1998]. Strong southwesterly winds blow during summer (May through October), bringing rain and moisture over the continent, while weak northeasterly winds promote dry conditions during winter (November through April; Fig. 1a). The main driving forces of monsoon circulation are the differential heating of land and water masses and the tropospheric transfer of latent heat in onshore direction [Hastenrath and Greischar, 1993]. Differential heating causes the formation of low and high atmospheric pressure cells on the Tibetan Plateau and the Indian Ocean, respectively. Latent heat, collected over the Southern subtropical Indian Ocean and released during precipitation on the Asian Plateau, modulates the intensity of summer monsoon circulation. Factors controlling the onset and variability of the monsoon system are still debated [Ruddiman et al., 1989], but on millennial time scales, insolation and changes in solar radiation are thought to be one of the principal driving forces [Rossignol-Strick, 1983; Prell, 1984b; Prell and Kutzbach, 1992].

During summer monsoon, wind-induced offshore Ekman transport of surface waters causes strong upwelling along the coasts of Somalia and Oman. Along the Oman margin, in response to the injection of nutrients from below the thermocline, modern primary productivity in surface waters averages >500 mgC/m^2·day between May and October, but drops to about 150 mgC/m^2·day during the rest of the year (according to Prell and Niitsuma, 1989, but see below). The stratification of the water masses, the sluggish circulation and the decomposition of organic matter produce an

Oxygen Minimum Zone (OMZ) between 200 and 1200 m, with O_2 concentrations below 0.2 ml/l [Prell and Niitsuma, 1989]. Consequently, denitrification is an active process both in the water column and in the sediments above 1200 m [Altabet et al., 1999]. Moreover, as in other active upwelling systems (e.g. Peru margin; Burnett, 1990), the input of dissolved reactive phosphorus from degradation of organic matter and dissolution of fish debris, leads to the active formation of phosphorite deposits [Schenau et al., 2000].

During winter monsoon, winds reverse and northeasterlies blow from the continent to the ocean, resulting in onshore Ekman transport, which stops upwelling activity. This situation is assumed to be dominating during glacial periods, which are, thus, characterized by stronger northeasterly monsoons, weak southwesterlies and overall reduced upwelling.

A number of paleoclimatic records indicates a stronger summer monsoon in correspondance to higher monsoon index maxima (MI, as described in Rossignol-Strick, 1983), mainly present during interglacial stages 5 and 1 (Prell and Kutzbach, 1987; Fig. 1b). Most studies on the Arabian monsoon area claim, indeed, that upwelling and, linked to that, high productivity were almost exclusively active during full interglacial periods (stages 5 and 1), when southwestern monsoon winds were strongest and induced important Ekman transport of surficial waters [Prell, 1984a; Webster et al., 1998; Altabet et al., 1999].

Summer monsoon-induced upwelling, however, may not be the only factor promoting high productivity along the coasts of the Arabian Sea. Reconstructed SST (Sea Surface Temperature) and organic carbon content variations do not correlate with other monsoon proxies, such as *Globigerina bulloides* percentages [Prell and Kutzbach, 1987; Prell et al., 1992], monsoon index [Rossignol-Strick, 1983], or pollen records. Moreover, recent observations of plankton variability in the northeastern Arabian Sea during the year [Madhupratap et al., 1996], indicate the occurrence of relatively high productivity, with maxima of 807 $mgC/m^2 \cdot day$, during winter (December-February), contradicting the above mentioned estimates [Prell and Niitsuma, 1989]. These apparent contradictions have already been interpreted as evidence for regional mechanisms other than monsoon and wind strength that controlled nutrient supply and productivity during glacial times [Zahn and Pedersen, 1991].

Madhupratap and co-authors (1996) found that the enhanced dryness, generated by winter winds blowing from the mainland over the Oman coasts, induces evaporation, increased salinity, cooling of surficial waters and consequent sinking. This winter deep water mixing down to 800 m [Reichart et al., 1998], is responsible for upwelling and can concur in sustaining primary production during winter and, possibly, glacial periods.

Along with these processes, major changes in oceanic circulation linked to glacio-eustatism, took place at glacial-interglacial transitions, as is indicated by important discrepancies between the glacial isotopic signature of benthic foraminifers and mean ocean values [Zahn and Pedersen, 1991]. The glacial lowered sea level may have reduced or even completely closed off the connection with the Red Sea, allowing Southern Ocean waters to flow northward [Kallel et al., 1988]. These modifications in the hydrography of the region may likely have produced considerable changes in nutrients and oxygen budget of intermediate waters, thereby affecting productivity.

Sedimentary records from the Oman margin and the Arabian Sea have been extensively studied during the last 20 years: stable isotopes [Zahn and Pedersen, 1991; Altabet et al., 1999], mineralogy [Krissek and Clemens, 1991], organic matter [Bertrand et al., 1991], planktonic and benthic foraminifers [Prell et al., 1992], major and minor elements have been analyzed [Shimmield and Mowbray, 1991; Weedon and Shimmield, 1991]. Time

series analyses to detect the presence of Milankovitch cyclicity [Prell, 1984a] and factor analysis have been performed, to characterize the Oman upwelling system and understand monsoon activity and its connection to global climate.

Here we present a multi-proxy study on sediments from ODP Site 724 along the Oman margin. We have analyzed mineralogy, organic matter, nitrogen stable isotopes and characterized different phosphorus forms in the sediments. We concentrate on nutrient variations during the last glacial cycle, in trying to decipher the role of the monsoon and its charges on productivity, and to search for mechanisms other than monsoon enhancing productivity at glacial-interglacial time scales in this area.

Hole 724C

The data presented here are from ODP Leg 117, Hole 724C (Oman Margin, Fig. 1). This work is part of a more extensive investigation studying phosphorus variations during the last 140,000 years and their relation to climatic changes in different oceanographic settings. Site 724 was chosen because of its location in the Oman upwelling area and the availability of an oxygen isotope stratigraphy of the sedimentary sequence, on which the age model is based [Zahn and Pedersen, 1991].

Hole 724C (Oman Margin, 18°27.713' N, 57°47.147' E, 592.8 m water depth) was sampled from 0 to 10.27 mbsf, at a time resolution of about 5 kyr, yielding a total of 26 samples. This interval represents the top of lithologic Unit I, whose sediments consist of dark calcareous clayey silt, moderately bioturbated throughout, with abundant amounts of well-preserved nannofossils and foraminifers. The sedimentation rates for the studied sequence are relatively low and range between 4 and 17 cm/kyr. No evidence of redeposition and/or winnowing was detected [Prell and Niitsuma, 1989].

Phosphorus and nitrogen

Phosphorus and nitrogen are essential nutrients in the marine environment [Froelich et al., 1982; Codispoti, 1989; Tyrrell, 1999]. Along with other geochemical indicators, such as $\delta^{13}C_{org}$ [Ruttenberg and Goni, 1997], Ge/Si and Cd/Ca [Froelich et al., 1992; Rickaby and Elderfield, 1999], phosphates and $\delta^{15}N$ have been extensively used as proxies for nutrient utilization and their temporal variations have been related to changes in productivity, oceanic circulation and climate on glacial-interglacial timescales [Farrell et al., 1995; Falkowski et al., 1998].

Phosphorus (P) is a primary nutrient and often considered as limiting productivity, particularly in marginal seas [Broecker, 1982; Delaney, 1998]. Due to its role in controlling productivity, it plays an important function in the biogeochemical cycle of carbon and other biophile elements. Thus, variations in the distribution of phosphorus in the ocean and in its burial rates may have important implications on feedback mechanisms between climate and carbon and phosphorus cycles over glacial-interglacial periods [Broecker, 1982].

The phosphorus cycle (Fig. 2) is relatively simple due to the lack of an important gaseous phase in the atmosphere and of a consistent output from volcanic and hydrothermal activity [Delaney, 1998]. The only source of "new" P to the ocean is weathering of rocks and soils [Froelich et al., 1982]. Several models have been developed to explain the relationship between P weathering and changes in climate on glacial-interglacial scales [Föllmi, 1995], but these interactions are still not well understood.

Once phosphorus enters the ocean, it reaches the sediments as a non-reactive detrital phase and a bioavailable phase. Reactive P is removed from the water column in association with organic matter, iron and manganese oxides and hydroxides, and as fish debris

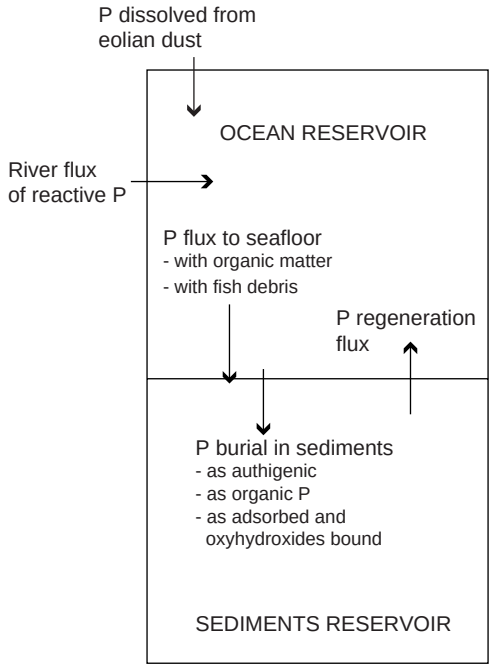

Fig. 2: Schematic representation of reactive phosphorus (P) fluxes into the ocean (modified after *Delaney*, 1998). Input and removal of dissolved reactive P by hydrothermal processes are not included. Redistribution of reactive P in sediments is controlled by diagenetic processes.

[Föllmi, 1996; Delaney, 1998]. Generally, organic matter is the main carrier of reactive P to the sediment. In the upper part of the sediment column, P is partly regenerated during organic matter degradation by benthic microbial activity [Ruttenberg and Gõni, 1997], desorption from Fe- and Mn oxides [Jarvis et al., 1994], and dissolution of fish debris [Schenau et al., 2000]. Depending on the physical and chemical conditions in the uppermost sediment (pH, alkalinity, redox conditions), the dissolved P is re-adsorbed by iron oxides, re-enters the water column or precipitates as authigenic apatite (CFA or carbonate-fluorapatite; Krajewski et al., 1994). Although Fe-, organic-bound and authigenic P represent the three long-term sedimentary sinks of reactive P, authigenic apatite is the most important phase because it represents in average more than 50% of total reactive P. Moreover, its formation is not only limited to coastal upwelling areas, where phosphogenesis is an active process (e.g. Peru shelf; Glenn et al., 1994), but is more widespread (i.e. deep sea sediments, non-upwelling continental margins; Ruttenberg and Berner, 1993; Delaney, 1998). The sedimentary conditions leading to CFA precipitation are still not completely understood, and have been the subject of extensive studies (for a comprehensive review, see Glenn et al., 1994; Jarvis et al., 1994; Föllmi, 1996). Among the factors influencing the redistribution of P and the extension of CFA precipitation in the sediments, phosphate and fluoride concentration in the pore water, carbonate alkalinity and redox conditions are the most important [Jarvis et al., 1994; Van Cappellen and Ingall, 1996].

Due to all diagenetic processes which influence the regeneration and redistribution of reactive P in the uppermost sediments, the final phosphorus signature in marine sediments cannot be considered as a direct indicator of phosphorus input fluxes to the sediments: Broecker and Peng [1982] calculated that 99% of the reactive phosphorus reaching the sea floor is redissolved and either reincorporated in the water column and/or precipitated in association with (hydro)oxides or authigenic forms.

The isotopic signature of nitrogen in marine sediment is influenced mainly by three processes: the degree of nitrate utilization by primary producers, denitrification occurring in oxygen-depleted bottom waters and nitrogen fixation by planktonic cyanobacteria [Altabet and Francois, 1994]. An inverse relation between the (NO_3^-) concentration in the surface water and the $\delta^{15}N$ of the sediment has been observed. During biological utilization, phytoplankton preferentially uptakes the lighter isotope ^{14}N, leaving the residual nitrate progressively enriched in ^{15}N. If the supply of NO_3^- is lower than its consumption, surface waters nitrates and the produced OM (organic matter) will be progressively enriched in the heavier isotope [Altabet and Francois, 1994].

Denitrification, which reduces NO_3^- to N_2 and enriches the remaining NO_3^- in ^{15}N, occurs in oxygen-depleted sediments and bottom waters, where bacteria utilize nitrates, instead of oxygen, to oxidize organic matter [Altabet et al., 1995; Farrell et al., 1995]. Denitrification has an important feedback on the total budget of nitrate available for production, because available fixed nitrogen is reduced to N_2 and consequently lost and removed from the oceans.

In oligotrophic regions (i.e. tropical and subtropical Atlantic, Pacific Ocean, Indian Ocean, cfr. Capone et al. 1997), especially if nitrogen-limited, nitrogen gas (N_2) is fixed by planktonic cyanobacteria, such as *Trichodesmium* [Capone et al., 1997]. The newly fixed nitrogen has a low $\delta^{15}N$ composition close to the isotopic signature of air (~ 0‰) and it consequentially contributes to the low nitrogen isotopic ratio of the newly produced biomass.

METHODS

All samples, of approximately 10 cc each, were oven-dried at 50°C and divided in subsamples. All analyses were performed at the GEA laboratory of the Geological Institute in Neuchâtel, except for ICP- AES and nitrogen stable isotope analyses.

5 g of dried sediment were ground to obtain a homogeneous powder with particle sizes <40 µm. An aliquot of this powder was pressed (20 bars) in a powder holder to determine bulk sediment mineralogy by XRD (SCINTAG XRD 2000 Diffractometer) based on a semi-quantitative estimation, and using external standards [Kübler, 1987]. The relative error of the bulk rock mineralogy is about 5% (RSD).

The characterization of organic matter was performed on about 100 mg of dried and ground sediment, with a Rock-Eval 6, and using a standard whole rock pyrolysis method [Espitalié et al., 1986; Lafargue et al., 1996].

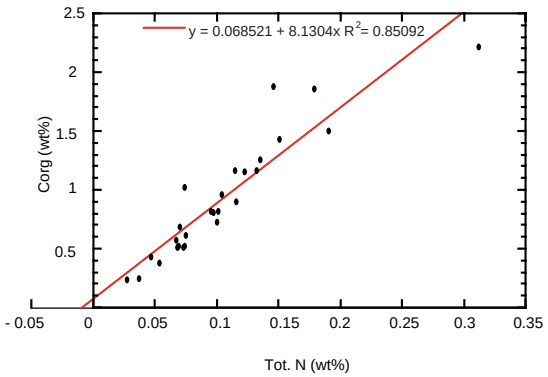

Fig. 3: Correlation between C_{org} (wt%) and Tot. N (wt%) from Site 724. The intercept of the regression line on the x axis when $C_{org} = 0$ is negative (y = 0, x = 0.008).

Nitrogen contents and stable isotopic analyses of the bulk sediment were performed at the Stable Isotope Laboratory, ETH-Zentrum, Zürich, using a Carlo Erba CNS2500 CHN Elemental Analyzer coupled with a FISONS OPTIMA mass spectrometer. Mean errors, calculated as the relative standard deviations on measurements are about 0.15‰. All data are reported in the conventional δ notation with respect to atmospheric nitrogen (AIR‰). A variable quantity of dried sediment (27-54 mg), depending on total nitrogen content, was weighted directly on tin cups, that were introduced in the Elemental Analyzer. Sample replicates have been analyzed to assess the validity of the data.

Total nitrogen is here considered as representing the organic nitrogen fraction. To justify this assumption, our data were plotted on a TOC wt% vs. Tot. N wt% diagram (Fig. 3). The x-intercept of the calculated regression line has a negative value, indicating that when organic matter is lacking in the sediments, no significant inorganic component of nitrogen is present [Hedges et al., 1988]. Tests carried out on several samples treated with HCl at differents concentrations (10 and 30%), show that acidification and decarbonation have a strong and somehow unpredictable effect on nitrogen isotopes. Nitrogen isotopic signal of those samples shows a change ranging between 0.02

Table 1

Step name	Treatments	P component isolated
Iron-bound P	10 ml CBD solution (6hr) (0.22 M sodium citrate, 0.11 M sodium bicarbonate 0.13 M sodium dithionite) 10 ml 1M MgCl2 (2hr) 10 ml H2O (2hr)	Exchangeable or loosely sorbed P Reducible or reactive iron-bound P
Authigenic P	10 ml 1M Na-acetate buffered to pH 4 with acetic acid (5hr) 10 ml 1M MgCl2 (2hr) 10 ml 1M MgCl2 (2hr) 10 ml H2O (2hr)	Carbonate fluorapatite (CFA) biogenic hydroxyapatite
Detrital P	10 ml 1N HCl (16 hr)	Detrital fluorapatite-bound P
Organic P	1 ml 50% (w/v) MgNO3, dry in low oven, ash at 500°C (2 hr) 10 ml 1N HCl (24 hr)	Organically-bound P

Table 1: Sequential extraction technique applied for phosphorus phases determination [*Ruttenberg*, 1992; *Anderson and Delaney*, 2000].

and 4.4 ‰, with no apparent relation to the strenght of the acid. Moreover, recent studies [Lohse et al., 2000] have brought new information about the effect of acidification on nitrogenous compounds in sediments: the use of sulphuric acid seems to attack part of the organic matter, resulting in the loss of up to 50% of N_{tot} [Lohse et al., 2000], which may consequentely change the nitrogen isotopic values of the residual sediments. Nitrogen isotopes from Site 724 were already analyzed by Muzuka et al. (1991), who used 30% HCl to remove carbonates from the sediments, washed the residue to remove the salts, and analyzed nitrogen isotopes on the carbonate-free residue [Muzuka et al., 1991]. Based on our experience, we believe that acidification biases the $\delta^{15}N$ of the residue sediment and this may explain the major differences between the values presented in this study and those reported by Muzuka et al. (1991).

The distribution of different phosphorus phases in bulk sediment was determined using a 4-step sequential extraction technique, adapted from the SEDEX method, developed by Ruttenberg (1992) and modified by Anderson et al. (2000). This method utilizes progressive dissolution of solid phases in four steps to extract P associated with well defined sedimentary components: iron and manganese oxi-hydroxides, authigenic minerals, detrital material and organic matter (Table 1). During the first step of this extraction, because of the reduction of Fe by dithionite and subsequent complexation by citrate, we are able to separate also ferric Fe, referred as $Fe_{(CBD)}$ (see Table 1).

Grain-size, quantity of sediment and solutions, reaction time and shaking speed have been optimized for marine sediments [Ruttenberg, 1992; Filippelli and Delaney, 1996]. For all the steps other than the iron-bound P, the ascorbic acid molybdate blue technique was employed to develop colour [Eaton et al., 1995]. A Perkin-Elmer UV/Vis spectrophotometer Lambda 10 with a 5-cm quartz cell was used to determine absorbances and P concentrations. All samples were diluted 10:1 for determination.

The impossibility of detecting iron-bound P concentration by spectrophotometer stems from the use of the citrate-dithionite complex (see Table 1), which interferes with the molybdate-phosphorus compound; therefore, concentrations of the iron-bound P phase and $Fe_{(CBD)}$ were determined using an OPTIMA 3000 Perkin Elmer ICP-AES, at the "Laboratoire des eaux et de l'environnement" in Peseux, Switzerland.

Reagent blanks, standards and consistency standards were used to perform calibration curves for each step and check analytical reproducibility over time. Typical mean errors for each phase were calculated as the relative standard deviation of the consistency standards and ranged from 2-7% for authigenic P, 3-5% for detrital P, 2-5% for organic P, and 3-6% for iron-bound P. The concentrations of all the analyzed samples are at least 7 times higher than the detection limit, defined as three times the standard deviation of a reagent blank.

RESULTS AND DISCUSSION

Mineralogy

Calcite, phyllosilicates, quartz, and dolomite contents are shown in Fig. 4. Detrital silicates, calculated as the sum of quartz, phyllosilicates, plagioclase and K-feldspar, account on average for 30% (around 40% during glacial periods), of the sediments of the Oman core (Fig. 4; K-feldspar and plagioclase never exceed 5% of the detritic fraction and are not shown). This relatively high percentage compared to other sites drilled during Leg 117, is probably due to the proximity of the coast. Because of its higher abundance and mass accumulation rates (MAR; Fig. 4 and 5) during generally arid periods (glacial stages 4 and 2, and stage 3), and due to the absence of major rivers, the detrital material is considered as predominantly eolian with only minor fluvial contributions from the mainland.

During interglacial stage 5, both quartz and phyllosilicates show lower abundances (8% and 7% in average respectively) than during glacial stage 2 and stage 3 (15% and 9%). Prominent peaks are present at the end of stage 4 and during stage 2. Despite the similarity between general trends, the correlation between quartz and phyllosilicates is poor (r=0.48), probably due to a different source of the material and/or to differentiation during transport.

Dolomite shows the same trend as other detrital indices, with an increase to an average of about 9% during stages 4-2. The correlation with phyllosilicates is rather good (r=0.64). The origin of dolomite is eolian, and its source area is the Northern Arabian Peninsula and Oman, where Permo-Triassic dolomitic series extensively outcrop and where the deposition of sebkha dolomites is an active process [Krissek and Clemens, 1991; Sirocko, 1993].

The Oman margin sediments are characterized by high percentages (average of 40%) of mostly biogenic calcite (foraminifers and nannofossils are well preserved in the upper part of the sedimentary sequence; Prell and Niitsuma, 1989), which mimics the general profile of the $\delta^{18}O$ record. Values are higher during interglacial stages 5 and 1, with peaks of about 50% at 90 kyr and 60% at 8 kyr (Fig. 4). The calcite record shows an upward-decreasing trend starting at about 90 kyr, and reaches a minimum of about 30% at the top of stage 2. Calcite MAR are, conversely, higher between stage 4 and 2, showing an important resemblance with detrital silicates MAR and implying that possibly a proportion of calcite is of detrital origin. Sirocko (1989) found, in fact, that a variable percentage, between 20 and 40%, of total calcite in sediments from the Oman margin is of detrital origin [Sirocko, 1989]. Moreover, the presence of considerable amounts of detrital dolomite (up to 14%, Fig. 4) may support this assumption. Though aware of this complication, we have not calculated the proportion of detrital to total calcite in the

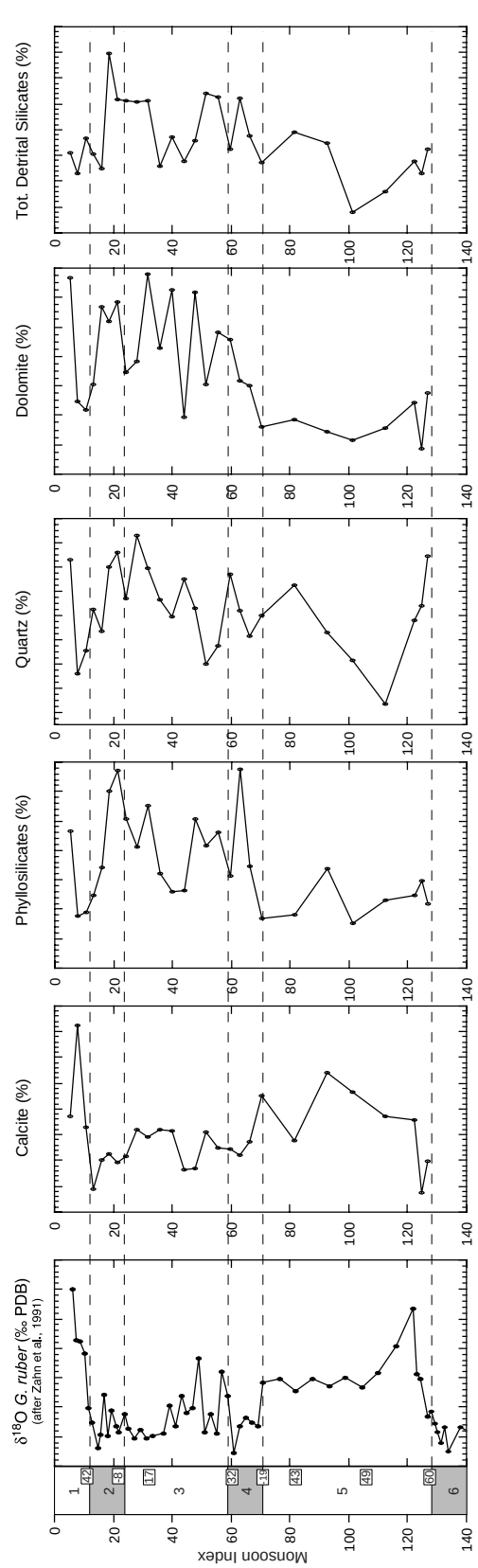

Fig. 4 (top): $\delta^{18}O$ data of *G. ruber* from Site 724 (after *Zahn et al.*, 1991). Percentages of calcite, phyllosilicates, quartz, dolomite, and total detrital silicates. Total detrital silicates percentage is calculated as the sum of quartz, phyllosicates, plagioclase and K-feldspar. Horizontal lines represent the boundaries between isotopic stages.

Fig. 5 (bottom): Bulk sedimentation rates (cm/kyr) from Site 724 (after *Zahn et al.*, 1991); C_{org}, calcite, total detrital silicates, $Fe_{(CBD)}$, P_{reac} and detrital P mass accumulation rates from Site 724. Horizontal lines as in Fig. 4.

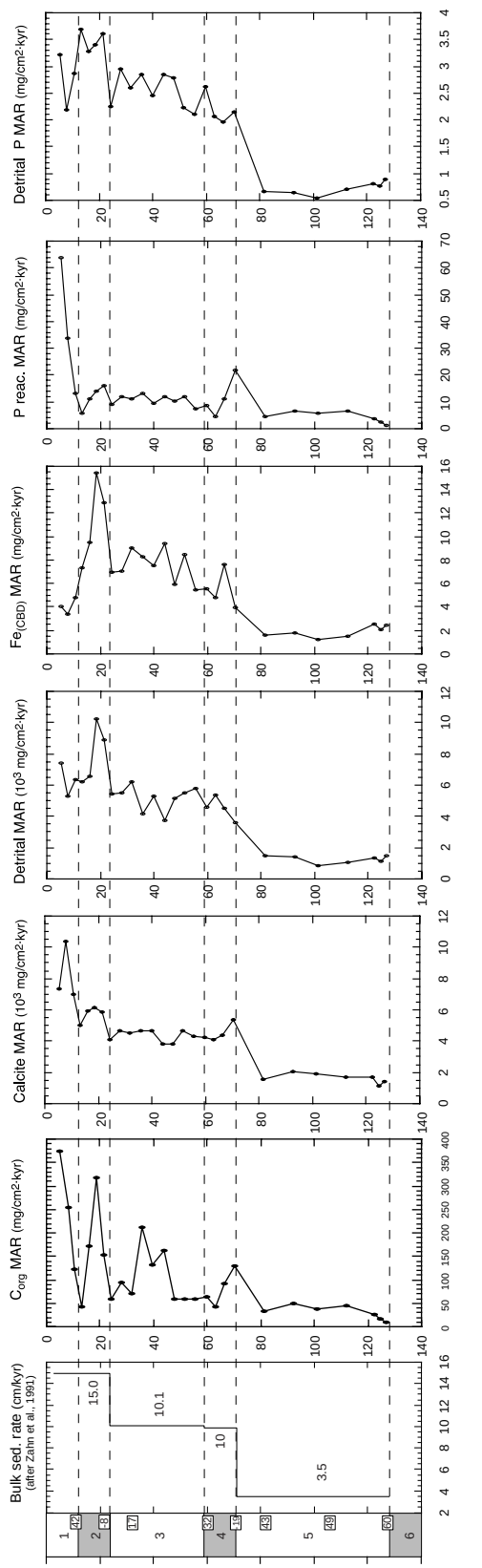

studied samples because of the few data available from cores close to Site 724 [Sirocko, 1989].

Detrital MAR (Fig. 5) are low during interglacial 5 and show a 4-fold increase during glacial stages 4 and 2 and stage 3. The most prominent peak is observed during glacial stage 2, where it reaches about 104 $mg/cm^2 \cdot kyr$. This observation confirms the correlation between land-derived and eolian-transported dust MAR with aridity [Krissek and Clemens, 1992], implying maximum dust transport during glacial times. The low correlation of almost all the detrital indices with the $\delta^{18}O$ seems to exclude the influence of glacio-eustatic variations, and the consequent exposition of the platform sediments, with redeposition of detrital material during sea-level glacial lows.

Phosphorus

Phosphorus phases represent only a small fraction of the total sediment (about 0.1%), but relative variations between the phases are important. Reactive phosphorus, the formerly biologically available phase, is calculated as the arithmetic sum of Fe-bound, authigenic and organic-bound phosphorus. Authigenic phosphorus represents the most abundant form, on average 75% of total phosphorus, while detrital and Fe-bound phosphorus represent only 18% and 5% respectively (see Table 2 and Fig. 6). The occurrence of phosphatic nodules in sediments from Site 724 in intervals older than the studied sequence [Rao and Lamboy, 1994], was recorded and confirmed by XRD analysis. Pore water phosphate levels at Site 724 C were variable and, in the sampled interval, low (about 4 μmol PO_4/l). This was interpreted as an indication of apatite precipitation [Prell and Niitsuma, 1989].

The three reactive phases, Fe-bound, authigenic and organic-bound P, significantly increase after stage 2 and during the Holocene. High concentrations of the authigenic P in the upper part of the core may be explained by the presence of an authigenic-precursor mineral, representing the first step of apatite (CFA) precipitation [Krajewski et al., 1994]. This is consistent with the assumption that CFA or the precursor mineral precipitation is promoted under slightly dysaerobic bottom water conditions, which are currently present along the Oman margin (O_2 about 0.2 ml/l ; Prell and Niitsuma, 1989).

Fe-bound P shows a poor correlation with $Fe_{(CBD)}$ and concentrations lower than 0.05 mg P/g, except in stage 1, when it shows values up to 0.2 mg P/g. Ferric iron ($Fe_{(CBD)}$) follows the overall trend of detrital indices (r= 0.62 with detrital P), with a two-fold increase during stage 3 and glacial stage 2 compared to interglacial stages. Highest values are on the order of 0.8 mg Fe/g. The relatively strong relation with detrital indices may reflect the eolian origin of iron.

Lack of correlation between $Fe_{(CBD)}$ and

Table 2

	Fe-bound P mg P/g sed.	Authigenic P mg P/g sed.	Detrital P mg P/g sed.	Organic-bound P mg P/g sed.
Mean Interglacial value	0.0719	1.3668	0.1761	0.0415
Mean Glacial value	0.0523	0.8462	0.2134	0.0284
Min value	0.0410	0.2750	0.1290	0.0130
Average	0.0596	1.0390	0.2000	0.0330
Max value	0.1826	3.5820	0.2580	0.1500

Table 2: Mean concentrations of phosphorus phases from Site 724, Oman margin.

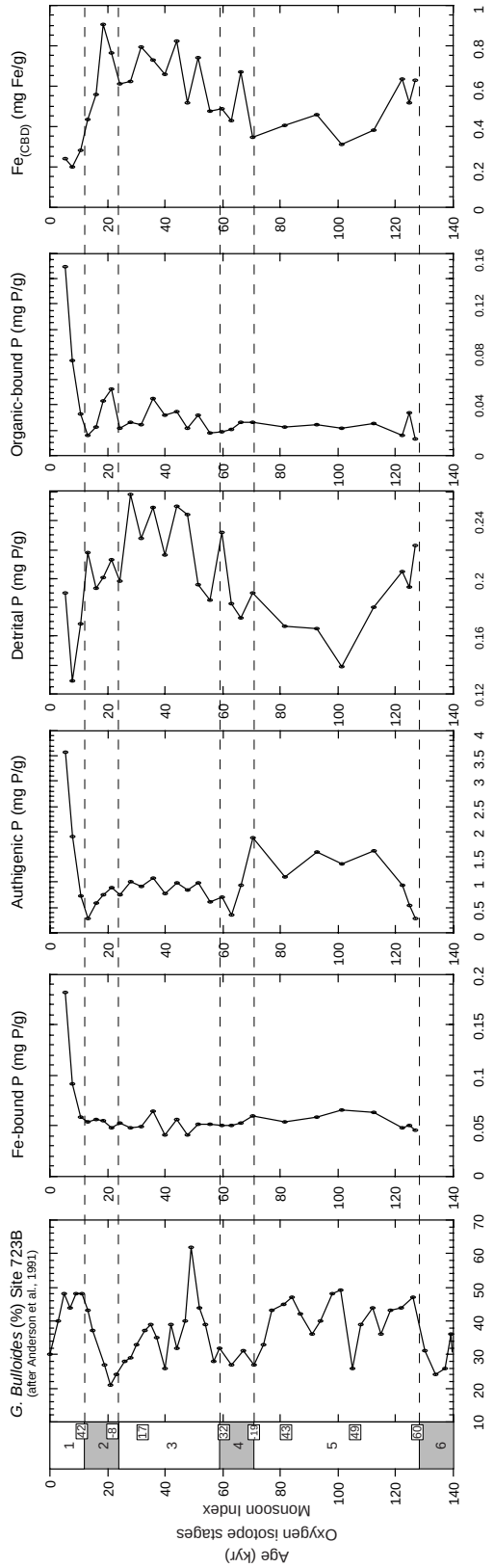

Fig. 6 (top): Percentage of *G. bulloides* from Site 723 (after *Anderson et al.*, 1991); concentrations of Fe-bound P, authigenic P, detrital P , organic-buond P and $Fe_{(CBD)}$ from Site 724. The different phases are defined in the text. Horizontal lines as in Fig. 4.
Fig. 7 (bottom): C_{org}/P_{org}, C_{org}/P_{reac}, C_{org}/N, and $Fe/P_{(CBD)}$ molar ratios, as defined in the text. Horizontal lines as in Fig. 4.

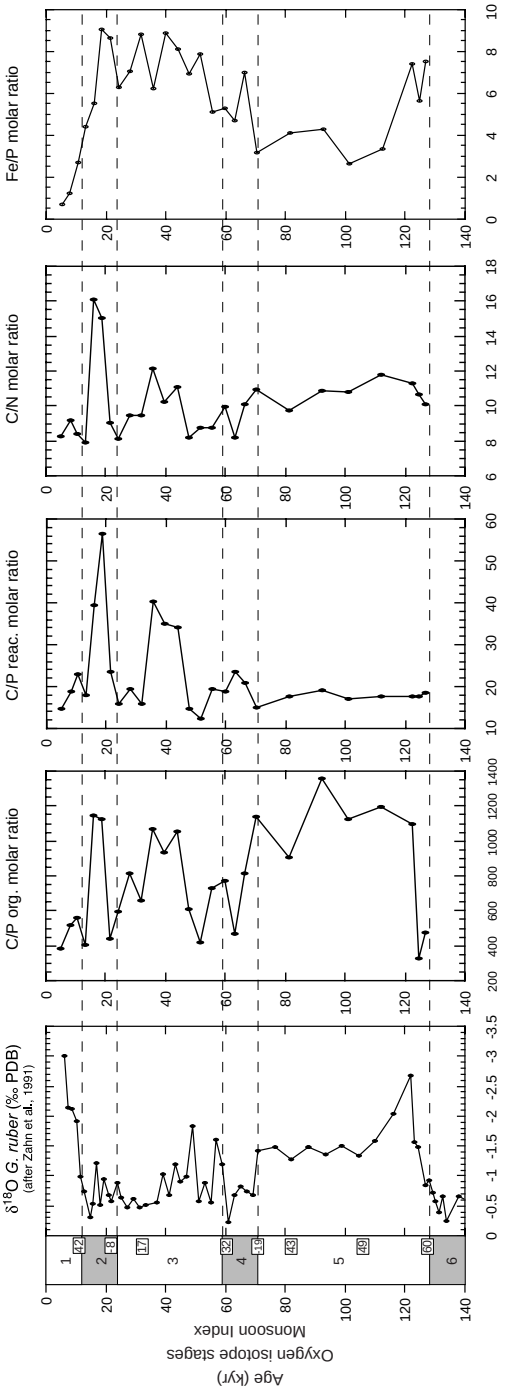

Fe-bound P (r= 0.46) may be due to low sedimentation rates and desorption of P from Fe- and Mn-hydroxides once buried in the reduced zone of the sediments. The development of suboxic to anoxic conditions in the upper part of the sediments, in relation to extensive degradation of organic matter, can, in fact, reduce the thickness or even remove the oxidized sediment layer and, thus, inhibit the adsorption of phosphorus by Fe-oxides [Glenn, 1990; Slomp et al., 1996]. This is confirmed by the $Fe/P_{(CBD)}$ molar ratio ($Fe_{(CBD)}$/Fe-bound P), showing low values during stage 5, ranging between 2 and 4, and higher values, averaging 7, during stage 3 and at the base of stage 2 (Fig. 7). The $Fe/P_{(CBD)}$ molar ratio can be considered as an indicator of oxygenation at the water/sediment interface, and such high values are characteristics of oxygen-depleted conditions and partial desorption of reactive P from iron hydroxides [Lucotte and D'Anglejan, 1988].

Authigenic phosphorus, which shows a remarkable correlation with the oxygen stable isotope and carbonate records (r=0.79 and 0.60 respectively), shows higher values during interglacial stages than during glacials. From average values of about 1.5 mg P/g during stage 5, it decreases to 0.3 mg P/g during stages 4 and 2, and averages 1 mg P/g during stage 3 (Table 2 and Fig. 6).

Detrital P is correlated to quartz (r=0.65 and 0.67 during glacial times), with peaks during stages 4-2 of about 2.5 mg P/g and minima during interglacial stages 5 and 1. Again, the lack of a strong correlation with other detrital indices such as phyllosilicates (r=0.33), may indicate an alternate source for these detrital components. Detrital P MAR show the same trend of detrital silicates MAR, with higher values during stages 4-2, reaching maxima of about 3.5 mg/cm^2·kyr during glacial stage 2 (Fig. 5).

Organic-bound P exhibits extremely low values, around 0.02 mg P/g, along the entire sequence and a sharp and pronounced increase at the beginning of stage 1. Higher variability is noticed during stage 3, and a more prominent spike, with values up to 0.05 mg P/g, is present at the beginning of stage 2.

Reactive phosphorus MAR show a singular trend, compared to other proxies: values generally range between 10 and 15 mg/cm^2·kyr, and they show no particular increasing trend due to higher sedimentation rates (Fig. 5). Besides the Holocene increase of all the reactive phases of phosphorus, only two significant peaks are documented, at 70 kyr and at 20 kyr, both at the beginning of glacial periods. Otherwise it seems that reactive P fluxes to the sediments were fairly constant throughout the investigated period.

$Fe_{(CBD)}$ MAR match the detrital MAR trend, with higher values during stages 4-2, and show a significant increase between 70 kyr and 20 kyr, where they reach values of 15 mg/cm^2·kyr.

Organic matter

Immature marine organic matter is the primary component of organic material present at Site 724. This is suggested by the Tmax (Tmax=420°C in average) and the hydrogen index (HI) values. HI values are generally higher than 150 mg HC/g total organic carbon (TOC), with few points above 400 mg HC/g TOC (Fig. 8a). These data are in agreement with previous analyses [Bertrand et al., 1991]. When Rock Eval analyses are performed on bulk sediments, as in this case, low values of HI could indicate a strong mineral matrix effect [Espitalié et al., 1986]. The occurrence of a rock-matrix effect and the uniform origin of the organic matter are corroborated by the S_2 vs. C_{org} graph (Fig. 8b). The regression line in a S_2 vs. C_{org} diagram should have a 0 intercept, if no mineral matrix is present, while a negative y-axis intercept generally indicates adsorption by minerals, with clays representing the main agent of adsorption [Langford and Blanc-Valleron, 1990]. As shown in Fig.

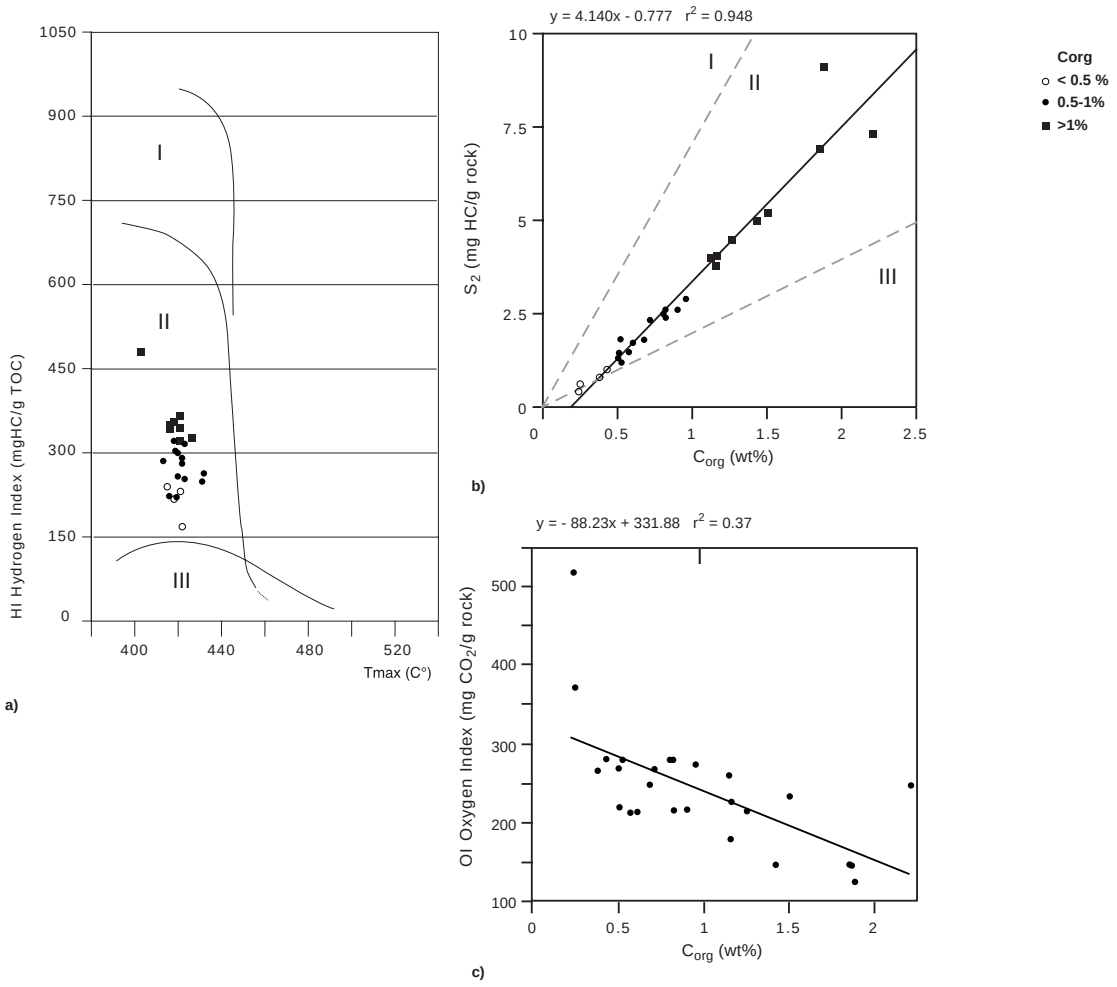

Fig. 8: a) HI vs. Tmax diagram. All the points, representing samples from Site 724, fall in type II kerogen field (marine organic matter); b) S_2 vs. C_{org} diagram of data from Site 724. Boundaries between the three fields are defined as in *Langford et al.*, 1990. Samples falling close to type I kerogen field and with low C_{org} content are most likely influenced by matrix effect. The slope of the regression line and the high degree of correlation confirm the marine origin of the organic matter; c) C_{org} vs. OI diagram. Samples with high organic matter content present low OI values, indicating enhanced preservation due to deposition in suboxic-anoxic environment.

8b, when S_2=0, C_{org} equals 0.188 wt%. The samples, linearly distributed, show a high correlation (r^2=0.95), indicating a coherent group. If the regression line is shifted towards the origin to eliminate the rock matrix effect [Langford and Blanc-Valleron, 1990], all the sample fall in the type II kerogen field, confirming the marine origin of the organic matter, with an average HI of 414, as given by the slope of the regression line.

Average value of organic carbon from Site 724 is about 0.8 wt% (Fig. 9), but the record exhibits large oscillations, especially during the last 60 kyr, with values up to 2 wt%. Higher organic carbon concentrations and accumulation rates are recorded during stage 3 and during glacial stage 2, with two major peaks between 30 and 45 kyr and at 20 kyr, during the LGM. High organic matter contents are also present in the Holocene part of the sequence.

Organic carbon MAR show a high flux of organic matter during stage 3 and during glacial stage 2, while the lowest fluxes are recorded during interglacial 5. It is unclear if this trend is a real feature or represents the effect of higher glacial sedimentation rates (Fig. 5) and consequent better preservation [Canfield, 1993]. This relation was already observed by Murray and Prell (1991) for Site 722 on the

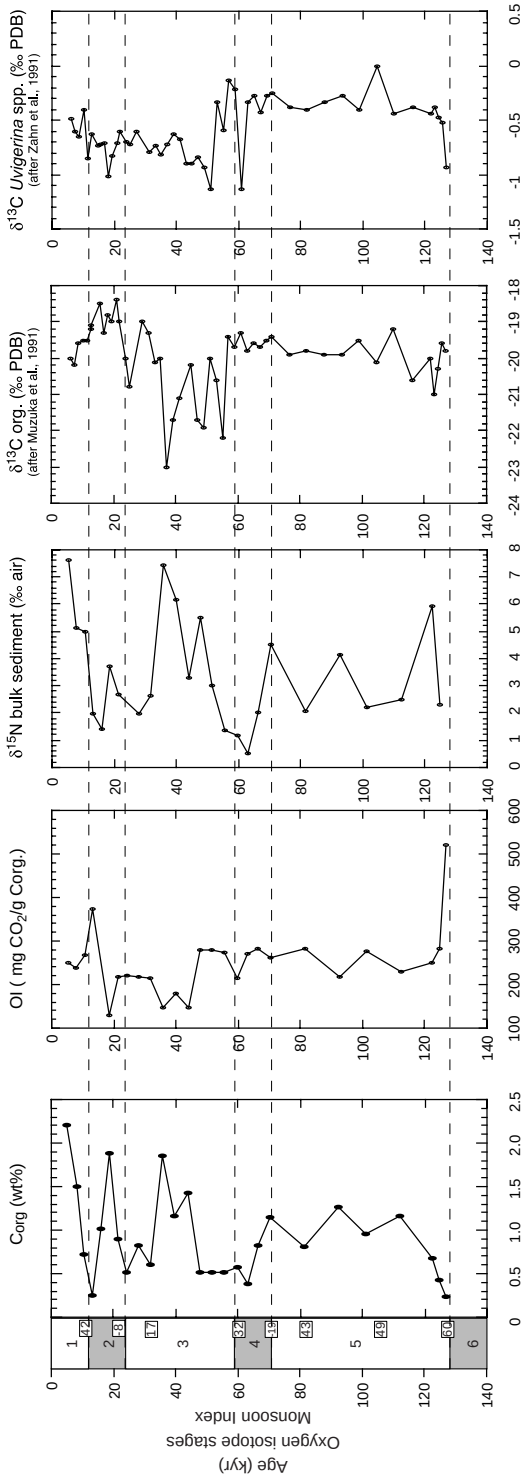

Fig. 9: Concentration of C_{org} from Site 724. HI and OI diagrams, as determined by Rock Eval analysis; $\delta^{15}N$ of bulk sediment from Site 724; $\delta^{13}C_{org}$ (after *Muzuka et al.*, 1991) and $\delta^{13}C$ *Uvigerina* spp. (after *Zahn et al.*, 19919) from Site 724. Horizontal lines as in Fig. 4.

Owen Ridge, but, despite their attempt of removing the possible effect of sedimentation rate, they found that greater fluxes of organic material were still related to glacial or low-monsoon index periods [Murray and Prell, 1991]. Moreover, enhanced organic matter burial during glacials (see peaks at 20 and at around 40 kyr, Fig. 5) correlates with low $\delta^{13}C$ *Uvigerina* spp. values (Fig.9), an endobenthic foraminifer, whose low carbon isotopic signature indicates higher supply and oxidation of organic matter in the sediments [Zahn et al., 1986].

$\delta^{15}N$ of the sediments shows a fairly good correlation (r=0.62) with the organic carbon content: values are low during glacial stage 4 and the upper part of stage 2, with the lowest value of 1.2 ‰ reached during stage 4; the two most prominent peaks are recorded during stage 3 ($\delta^{15}N$=7.4‰), and at the top of the sequence, during the Holocene ($\delta^{15}N$=7.6‰).

As previously mentioned in the methodology chapter, nitrogen isotopes from Site 724 were already analyzed by Muzuka et al. (1991). Major discrepancies in trend between their data and the data presented here are most likely due to different methodology and sample preparation. As described above, we measured $\delta^{15}N$ on bulk sediments to avoid any effect of acidification on the results.

Although the trend, as well as maxima and minima of nitrogen isotopes of Site 724 sediments are in agreement with other records from the area, $\delta^{15}N$ values from this study are generally lower than the values observed in nearby sites in the Oman region [Altabet et al., 1999]. It is not clear why the magnitude of the signal (~ 6‰) is higher than the one observed by Altabet (1999).

These low values are difficult to interpret: one explication could be the influence of terrestrial organic matter, but evidences from other proxies (e.g. $\delta^{13}C_{org}$, HI, C_{org}/N ratio, Fig. 7 and 9) seem to exclude this possibility. Light interglacial $\delta^{15}N$ values have been already observed in sediments from other

regions, i.e. the Cariaco Basin [Haug et al., 1998], and have been related to nitrogen fixation by cyanobacteria. Though nitrogen fixation in the Indian Ocean and in the Red Sea is an established phenomenon [Bethoux, 1988; Capone et al., 1997], we observe a high degree of correlation between the $\delta^{15}N$ values and the organic matter content, which indicates that high $\delta^{15}N$ during stage 3 are likely to be caused by denitrification. Values ranging between 3 and 6‰, as in interglacial 5 and glacial stages 4 and 2 (Fig. 9), are characteristic of a well-oxygenated water column, with reduced denitrification and intensity of the OMZ [Ganeshram et al., 1995]. It is possible, however, that the initial isotopic signature of the organic matter, determined by processes like nitrogen fixation, could have influenced the final ratio.

C_{org}/P_{org} and C_{org}/N elemental ratios are higher than the expected Redfield ratios for marine OM. They show an increasing trend towards the bottom of the record, indicating a strong depletion of P and a minor preferential loss of N during organic matter degradation (Fig. 7). Again, these values could be explained by a larger input of terrestrial organic matter, but, as mentioned before, this is not supported by other data. Moreover, the lack of a positive correlation between light $\delta^{15}N$ and $\delta^{13}C_{org}$ data (interpolated from Muzuka et al. 1991; Fig. 9) does not support this assumption.

Relatively high elemental ratios in organic matter are thus considered as indicating degraded organic material. The presence of high concentrations of degraded organic matter in the Oman margin sediments was interpreted by Pedersen et al. (1992) as suggestive of winnowing processes [Pedersen et al., 1992]. One evidence against this hypothesis is given by the anti-correlation between the C_{org} wt% and the oxygen index (OI). The water/sediment interface was mostly oxic to dysaerobic, favouring the degradation of the organic material, with some anoxic episodes. Higher organic matter contents, in fact, coincide with lower OI (Fig. 8c and 9), implying deposition and enhanced preservation in a suboxic-anoxic environment [Kenig et al., 1994].

Organic matter is normally considered as the principal carrier of phosphorus to the sediment, and, once degraded, constitutes the major source of dissolved reactive phosphorus of the pore water. If this was the case, the elemental ratio between C_{org} and reactive P (C_{org}/P_{reac}) in Oman sediments should partially explain the deviation of the C_{org}/P_{org} from the Redfield ratio assumed for marine organic matter (106:1). The C_{org}/P_{reac} ratio shows values averaging 20, indicating that reactive phosphorus exceeds organic carbon on the base of a normal marine Redfield ratio by a factor of 5, for most samples, except for the intervals between 50 and 30 kyr and at 20 kyr, where values between 40 and 60 are observed (Fig. 7). These two peaks could be explained by either a reduced phosphorus input to the system, or an increased C preservation in the sediments relative to P, or a reduced phosphorus retention in the sediments, as the result of hampering conditions (oxygen levels, alkalinity, pH, pore water - bottom water concentration gradient, etc.). During stage 3, the co-occurrence of high $\delta^{15}N$ and $Fe/P_{(CBD)}$ values with the peak in the C_{org}/P_{reac} ratio (Fig. 7 and 9), indicates low oxygen content of the bottom waters, which likely inhibited the precipitation of authigenic P and prompted the release of dissolved phosphorus to the water column. During stage 2, $\delta^{15}N$ and $Fe/P_{(CBD)}$ (Fig. 7 and 9) give more ambiguous information about oxygen levels in the bottom waters, but relatively uniform P_{reac} MAR (Fig. 5) indicate that the flux of reactive P to the sediments was more or less unchanged. The peak in the C_{org}/P_{reac} ratio at 20 kyr may be the result of a gradient-induced rediffusion of dissolved P back to the water column (see "Implications").

Although part of the original organic carbon has also been oxidized and lost, it is clear from C_{org}/P_{reac} ratio (Fig. 7) that an alternative

source of dissolved reactive phosphorus needs to be considered. This assumption is true especially if we assume that a bigger proportion of organic-bound P than organic carbon has been regenerated during benthic respiration of organic matter [Ingall and Jahnke, 1994]. Schenau (2000) has demonstrated that fish debris dissolution constitutes an additional and important source of dissolved reactive phosphorus for modern sediments of the Oman margin.

IMPLICATIONS

The results obtained from the multiproxy study of sediments from the Oman margin have brought new information on the paleoceanographic and upwelling history of this region during the last 140,000 years. Three different situations emerge as the response to changed monsoon strength, sea-level, and oceanic circulation (Fig. 10).

During full interglacial periods (i.e. lower part of stage 5, Fig. 10a), characterized by high sea level stands and strong summer monsoon activity, as expected during high insolation index periods, the Oman margin showed high biological production rates, connected to increased upwelling intensity. *G. bulloides* % (upwelling indicator) and carbonate content are high, but low organic matter accumulation rates seem to indicate that productivity and/or preservation were not enhanced compared to glacial periods. The main source of nutrients was the upwelling of cold and nutrient-rich waters from below the thermocline. The input of intermediate waters from the Red Sea contributed to maintain high nutrient levels. Dissolved reactive phosphorus, along with other nutrients, was regenerated in the water column and in the uppermost part of the sediments and upwelled to the surface water, enhancing productivity.

Oxygen levels were low, as expected in high productivity regions and with the presence of an OMZ, but they did not create extreme anoxic conditions and denitrification did presumably not take place, as indicated by $\delta^{15}N$ values. One plausible explication is that the increased and intense upwelling could have brought oxygen-rich waters from below the OMZ to shallower depths, decreasing therefore its intensity (see $Fe/P_{(CBD)}$ ratio, Fig. 7). Extensive oxidation of organic matter (as indicated by C_{org}/P_{org} and OI, Fig. 7 and 9) and dissolution of fish debris regenerated high quantities of dissolved P that, in such an oxic-suboxic environment, could in part precipitate as authigenic P. Low $\delta^{15}N$ during interglacial 5 could also indicate effective nitrogen fixation by cyanobacteria.

Low detrital contents of the sediments during stage 5 are interpreted as the result of prevailing humid conditions on the mainland [Burns et al., 1998]. The ITCZ (Intertropical Convergence Zone) was, in fact, located inside the Arabian peninsula and northwesterly winds could not reach the investigated site. It is questionable if the increased humidity could have developed a coastal riverine system, enhancing nutrient and dissolved phosphorus input directly from the mainland. But during warm interglacials a continental input of nutrient to the ocean is not likely to have occurred. There is no evidence of any kind of terrestrial contribution to the organic pool, and proxies, such as the HI index (Fig. 8), indicate an autochthonous origin of the organic matter.

During glacials and low monsoon index periods (stages 4-2) the ITCZ shifted southward and arid conditions prevailed on land, promoting eolian uptake of material (Fig. 10 b and c). Northwesterlies, now blowing more southwardly, along with persistent and stronger northeasterlies contributed to high detrital input from the continent, as indicated by all the detrital indices. General glacial/arid conditions can be assumed also for stage 3, as confirmed by the lack of speleothems development in Oman [Burns et al., 1998].

Despite their increased strength, winter

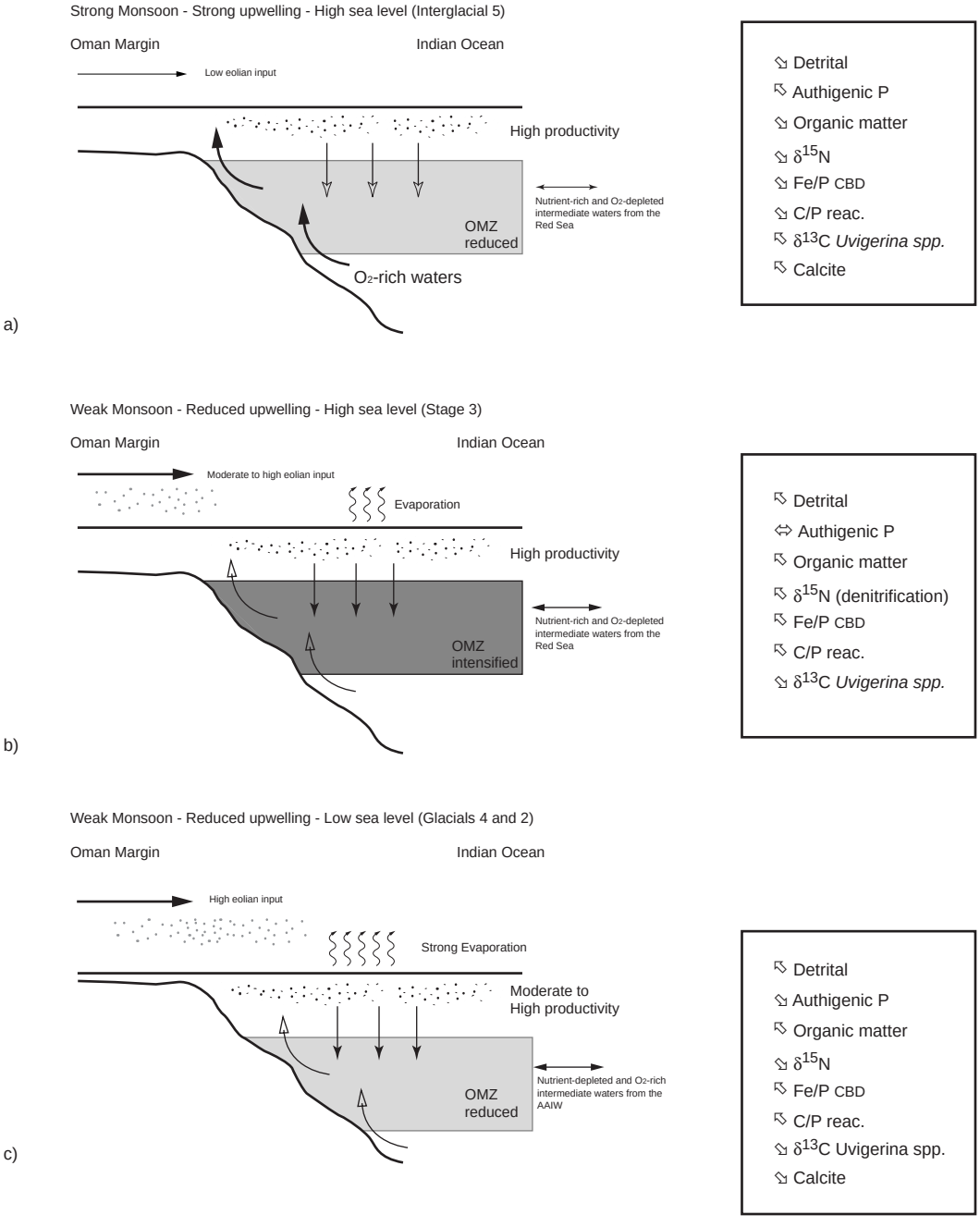

Fig. 10: Schematic representations of the oceanographic and climatic situation during the last 140,000 years along the Oman margin. Three different operational modes are hypothesized. See text for explication.

monsoons were too weak to produce any substantial upwelling [Madhupratap et al., 1996]. But several proxies, such as organic matter, nitrogen stable isotopes (this study) and $\delta^{13}C$ *Uvigerina* spp. (Fig. 9) [Zahn and Pedersen, 1991] clearly point out that productivity and burial of organic matter were high, especially during stage 3. Madhupratap and co-authors (1996) found evidence that high productivity and high nutrient content in the Arabian Sea are present throughout the year, so even during winter monsoon activity. Winter monsoon dryness has been called as the factor causing high nutrient content; in fact, during winter time, cool and dry air, brought by the northeasterlies, enhances evaporation leading to cooling

of surface waters. So, despite unfavourable conditions for upwelling, sinking of cooler and denser surface waters provokes an upward flux of deep and nutrient-rich waters.

Stage 3 is characterized by a low monsoon index [Rossignol-Strick, 1983], and reduced summer monsoon-induced upwelling. A high sea-level fostered the input of oxygen-depleted intermediate waters from the Red Sea and the increased and more persistent winter monsoons introduced high amounts of detrital material and micro-nutrients, such as iron (Fig. 4 and 5); along with the above mentioned evaporation-induced mixing process, the input of eolian material maintained high nutrients levels along the Oman margin (Fig. 10b).

Weaker upwelling produced a more severe stratification of the water column and, along with persistent high productivity, enhanced the intensity of the OMZ. Suboxic to anoxic conditions led to high organic matter accumulation and preservation, as indicated by C_{org} MAR and OI (Fig. 5 and 9). Nitrogen isotopes are highest and show strong correlation with organic matter, an indication of denitrification and consequent loss of nitrates from the system. Degradation of organic matter regenerated high amounts of dissolved reactive phosphorus. However, the extension of the OMZ during stage 3 and the consequent oxygen demand probably provoked unfavourable conditions to authigenic P precipitation, as indicated by low values of authigenic P, and high $Fe/P_{(CBD)}$ and C_{org}/P_{reac} ratios (Fig. 6 and 7). A diagenetic model developed for phosphorus cycling [Slomp et al., 1996] and applied to results from box cores from the Oman margin [Schenau et al., 2000] confirms that without bioturbation and in intense oxygen-depleted waters, reactive phosphorus is easily regenerated at the water-sediment interface and can re-enter the water column [Ingall and Jahnke, 1994].

During glacial stages 4 and 2, persistent arid conditions on the continent [Burns et al., 1998] allowed for high eolian input of detrital material and iron-containing dust, and induced the glacial vertical mixing of the water column (see above). Glacial lowering of sea level reduced or even cut off the contribution from the Persian Gulf and the Red Sea, allowing waters from remote sources, possibly AAIW (Antartic Intermediate Water) [Kallel et al., 1988], to spread northward (Fig. 10c).

As deduced from the isotopic analysis of benthic foraminifers [Kallel et al., 1988; Zahn and Pedersen, 1991], these waters were characterized by low nutrients content and high oxygen, that could have reduced the intensity of the glacial OMZ. Glacial mass accumulation rates of organic carbon were high, especially during stage 2, but despite favourable conditions to authigenic P precipitation, peaks in both C_{org}/P_{org} and C_{org}/P_{reac} clearly indicate a loss of dissolved and regenerated reactive P from the sediments to the water column (Fig. 7). The presence of intermediate nutrient-depleted waters could, in fact, have induced a gradient between nutrient-rich pore waters and the bottom waters, provoking a flux of dissolved P to the water column [Sundby et al., 1992].

This implies that during glacial periods P release from the sediments was enhanced and regenerated P, along with nutrients and micronutrients introduced from the mainland, could have sustained high rates of productivity.

CONCLUSIONS

This multiproxy approach to the study of Site 724 allows for the explanation of different aspects of the climatic and oceanographic history of the Oman margin since interglacial 5.

During the last 140,000 years, the Oman margin was characterized by an extremely complex situation, where regional and global processes were coupled and interacted. Changes in monsoon intensity, due to glacial-interglacial variations in insolation strength, did combine with different oceanic circulation

modes, imposed by glacio-eustatic changes in sea level, and both controlled sedimentation, nutrients distribution and primary production (Fig. 10).

Along with the other used proxies, the study of the different P phases stored in the Oman sediments brought important elements, because their variations are the product not only of modified inputs, but also of changes in physical and chemical conditions at the sea bottom, produced by changes in productivity, oceanic circulation and glacio-eustatism. During the last 140,000 years the overall flux of P to the Oman margin sediments seemed not to have changed significantly; despite this, its redistribution and regeneration, both controlled by changed conditions in the sediments, have certainly played an important role in sustaining productivity.

During full interglacial stages (stages 5 and 1), with strong summer monsoon inducing intense upwelling, productivity was sustained by the contribution of renewed nutrients from below the thermocline. Preservation was not enhanced because of persisting oxic or slightly suboxic conditions at the water-sediment interface. P was preferentially regenerated during respiration of OM, and could partially precipitate as CFA. During low summer monsoon index periods (stages 4-2), P was regenerated and rediffused to the water column, because of suboxic and periodically anaerobic conditions in the bottom waters which prevent the precipitation of authigenic minerals (stage 3), and/or because of a nutrient gradient between bottom and pore waters (stages 4 and 2). Deep vertical mixing helped in providing the renewed nutrients to the euphotic zone, sustaining productivity.

From this study, productivity along the Oman margin emerges to be a quasi-persistent phenomenon throughout the year and across glacial and interglacial stages, and seems to be controlled both by summer monsoon-induced upwelling and winter monsoon-induced deep vertical mixing. This has certainly important implications on the local and global carbon budget, especially on glacial-interglacial timescales.

The hypothesis of high productivity along the Oman margin, a monsoon-controlled region, also during glacial periods could redefine, if confirmed by further studies, the role of monsoon regions in controlling and enhancing carbon dioxide drawdown from the atmosphere into the ocean and in maintaining low CO_2 concentration during glacials.

Acknowledgements. We thank Sébastien Reiser and José Richard for their help in the laboratory. Special thanks to Hilary Paul for her help in processing samples for $\delta^{15}N$ analysis.

REFERENCES

Altabet, M.A., and R. Francois, Sedimentary nitrogen isotopic ratio as a recorder for surface ocean nitrogen utilization, Global Biogeochemical Cycles, 8 (1), 103-116, 1994.

Altabet, M.A., R. Francois, D.W. Murray, and W.L. Prell, Climate-related variations in denitrification in the Arabian Sea from sediment $^{15}N/^{14}N$ ratios, Nature, 373, 506-509, 1995.

Altabet, M.A., D.W. Murray, and W.L. Prell, Climatically linked oscillations in Arabian Sea denitrification over the past 1 m.y.: implications for the marine N cycle, Paleoceanography, 14 (6), 732-743, 1999.

Anderson, D.M., and W.L. Prell, Coastal upwelling gradient during the Late Pleistocene, in *Proceedings of the Ocean Drilling Program, Scientific Results*, edited by W.L. Prell, Niitsuma, N., et al., pp. 265-273, 1991.

Anderson, L.D., and M.L. Delaney, Sequential extraction and analysis of phosphorus in marine sediments: Streamlining of the SEDEX procedure, Limnol. Oceanogr., 45 (2), 509-515, 2000.

Barnola, J.M., D. Raynaud, Y.S. Korotkevich, and C. Lorius, Vostok ice core provides 160,000-year record of atmospheric CO_2, Nature, 329 (6138), 408-414, 1987.

Bertrand, P., E. Lallier-Verges, and H. Grall, Organic petrology of Neogene sediments from North Indian Ocean (Leg 117): amount, type, and preservation of organic matter, in *Proceedings of the Ocean Drilling Program, Scientific Results*, Vol. 117, edited by W. Prell., L., Niitsuma, N., et al., pp. 587-594, 1991.

Bethoux, J.P., Red Sea Geochemical Budgets and Exchanges with the Indian Ocean, Marine Chemistry, 24, 83-92, 1988.

Broecker, W.S., Ocean chemistry during glacial time, Geochimica et Cosmochimica Acta, 46, 1689-1705, 1982.

Broecker, W.S., and T.-H. Peng, Tracers in the Sea, Lamont-Doherty Geological Observatory, Palisades, N.Y., 1982.

Broecker, W.S., and T.-H. Peng, Interhemispheric transport of carbon dioxide by ocean circulation, Nature, 356 (587-593), 1992.

Burnett, W.C., Phosphorite growth and sediment dynamics in the Modern Peru shelf upwelling system, in *Neogene to modern phosphorites*, edited by S.R. Riggs, Burnett, W.C., pp. 62-72, Cambridge Unviversity Press, New York, NY, USA, 1990.

Burns, S.J., A. Matter, N. Frank, and A. Mangini, Speleothem-based paleoclimate record from northern Oman, Geology, 26 (6), 499-502, 1998.

Canfield, E.D., Organic matter oxydation in marine sediments, in *Interactions of C, N, P and S biogeochemical Cycles and Global Change*, edited by R. Wollast, MacKenzie, F. T., Chou, L., Springer-Verlag, Berlin, 1993.

Capone, D.G., J.P. Zehr, H.W. Paerl, B. Bergman, and E.J. Carpenter, *Trichodesmium*, a globally significant marine cyanobacteria, Science, 276, 1221-1229, 1997.

Chavez, F.P., and J.R. Toggweiler, Physical Estimates of Global New Production: the upwelling contribution, in *Upwelling in the Ocean: Modern processes and Ancient records*, edited by C.P. Summerhayes, Emeis, K.-C., Angel, M.V., Smith, R.L., Zeitzschel, B., pp. 313-320, 1995.

Codispoti, L.A., Phosphorus vs. nitrogen limitation of new and export production, in *Productivity on the Ocean: Present and Past*, edited by W.H. Berger, et al., pp. 377-394, John Wiley, New York, 1989.

Delaney, M.L., Phosphorus accumulation in marine sediments and the oceanic phosphorus cycle, Global Biogeochemical Cycles, 12 (4), 563-572, 1998.

Eaton, A.D., L.S. Clesceri, and A.E. Greenberg, Standard methods for the examination of water and wastewater, 1995.

Espitalié, J., G. Deroo, and F. Marquis, La pyrolyse Rock-Eval et ses applications - III partie, Rev. Inst. Fr. Pet., 41 (1), 73-89, 1986.

Falkowski, P.G., R.T. Barber, and V. Smetacek, Biogeochemical controls and feedbacks on ocean primary productivity, Science, 281 (5374), 200-206, 1998.

Farrell, J.W., T.F. Pedersen, S.E. Calvert, and B. Nielsen, Glacial-interglacial changes in nutrient utilization in the equatorial Pacific Ocean, Nature, 377, 514-517, 1995.

Filippelli, G.M., and M.L. Delaney, Phosphorus geochemistry of equatorial Pacific sediments, Geochimica et Cosmochimica Acta, 60 (9), 1479-1495, 1996.

Föllmi, K.B., 160 m.y. record of marine sedimentary phosphorus burial: coupling of climate and continental weathering under greenhouse and icehouse conditions, Geology, 23 (6), 859-862, 1995.

Föllmi, K.B., The phosphorus cycle, phosphogenesis and marine phosphate-rich deposits, Earth-Science Reviews, 40, 55-124, 1996.

France-Lanord, C., and L.A. Derry, Organic carbon burial forcing of the carbon cycle from Himalayan erosion, Nature, 390, 65-67, 1997.

Froelich, P.N., M.L. Bender, N.A. Luedtke, G.R. Heath, and T. DeVries, The marine phosphorus cycle, American Journal of Science, 282 (4), 474-511, 1982.

Froelich, P.N., V. Blanc, R.A. Mortlock, S.N. Chillrud, W. Dunstan, A. Udomikit, and T.-H. Peng, River fluxes of dissolved silica to the ocean were higher during glacials: Ge/Si in diatoms, rivers, and oceans, Paleoceanography, 7 (6), 739-767, 1992.

Ganeshram, R.S., T.F. Pedersen, S.E. Calvert, and J.W. Murray, Large change in oceanic nutrient inventories from glacial to interglacial periods, Nature, 376, 755-758, 1995.

Glenn, C.G., K.B. Föllmi, S.R. Riggs, G.N. Baturin, K.A. Grimm, J. Trappe, A.M. Abed, C. Galli-Olivier, R.E. Garrison, A.V. Ilyin, C. Jehl., V. Rohrlich, R.M.Y. Sadaqah, M. Schidlowski, R.E. Sheldon, and H. Siegmund, Phosphorus and phosphorites: sedimentol-

ogy and environments of formation, Eclogae geol. Helv., 87 (3), 747-788, 1994.

Glenn, C.R., Pore water, petrologic and stable carbon isotopic data bearing on the origin of modern Peru margin phosphorites and associated authigenic phases, in *Neogene to modern phosphorites*, edited by S.R. Riggs, Burnett, W.C., pp. 46-61, Cambridge Unviversity Press, New York, NY, USA, 1990.

Goddéris, Y., and L.M. François, The Cenozoic evolution of the strontium and carbon cycles: relative importance of continental erosion and mantle exchanges, Chemical Geology, 126, 169-190, 1995.

Hastenrath, S., and L. Greischar, The monsoonal heat budget of the hydrosphere-atmosphere system in the Indian Ocean sector, Journ. of Geophys. Research, 98 (C4), 6869-6881, 1993.

Haug, G.H., T.F. Pedersen, D.M. Sigman, S.E. Calvert, B. Nielsen, and L.C. Peterson, Glacial/interglacial variations in production and nitrogen fixation in the Cariaco Basin during the last 580 kyr, Paleoceanography, 13 (5), 427-432, 1998.

Haug, G.H., and R. Tiedemann, Effect of the formation of the Isthmus of Panama on Atlantic Ocean thermohaline circulation, Nature, 393, 673-676, 1998.

Hedges, J.I., W.A. Clark, and G.L. Cowie, Organic matter sources to the water column and surficial sediments of a marine bay, Limnol. Oceanogr., 33, 1116-1136, 1988.

Heinze, C., E. Maier-Reimer, and K. Winn, Glacial pCO_2 reduction by the world ocean: experiments with the Hamburg Carbon Cycle model, Paleoceanography, 6 (4), 395-430, 1991.

Ingall, E., and R. Jahnke, Evidence for enhanced phosphorus regeneration from marine sediments overlain by oxygen depleted waters, Geochimica et Cosmochimica Acta, 58 (11), 2571-275, 1994.

Jarvis, I., W.C. Burnett, Y. Nathan, F.S.M. Almbaydin, A.K.M. Attia, L.N. Castro, R. Flicoteaux, M.E. Hilmy, V. Husain, A.A. Qutawnah, A. Serjani, and Y.N. Zanin, Phosphorite geochemistry: state-of-art and environmental concerns, Eclogae geol. Helv., 87 (3), 643-700, 1994.

Kallel, N., L.D. Labeyrie, A. Juillet-Leclerc, and J.-C. Duplessy, A deep hydrological front between intermediate and deep-water masses in the glacial Indian Ocean, Nature, 333, 651-655, 1988.

Kenig, F., B.N. Popp, J.M. Hayes, and R. Summons, An isotopic biogeochemical study of the Oxford Clay formation, Jurassic, UK, Journal of the Geological Society of London, 151, 139-152, 1994.

Krajewski, K.P., P. Van Cappellen, J. Trichet, O. Kuhn, J. Lucas, A. Martin-Algarra, L. Prévot, V.C. Tewari, L. Gaspar, R.I. Knight, and M. Lamboy, Biological processes and apatite formation in sedimentary environments, Eclogae Geol. Helv., 87 (3), 701-745, 1994.

Krissek, L.A., and S.C. Clemens, Mineralogic variations in a Pleistocene high-resolution eolian record from the Owen Ridge, western Arabian Sea (Site 722): implications for sediment source conditions and monsoon history, in *Proceedings of the Ocean Drilling Program, Scientific Results,*Vol. 117, edited by W.L. Prell., Niitsuma, N., et al., pp. 197-211, 1991.

Krissek, L.A., and S.C. Clemens, Evidence for aridity-driven dust flux to the northwest Arabian Sea and for decoupling of the dust and upwelling system, in *Upwelling systems: evolution since the early Miocene*, edited by C.P. Summerhayes, Prell, W. L., Emeis, K. C., pp. 359-378, The Geological Society, London, 1992.

Kübler, B., Dosage quantitatif des minéraux maieurs des roches sédimentaires par diffraction X, Cahier de l'Institut de Géologie de Neuchâtel, Série ADX, 1987.

Lafargue, E., J. Espitalié, F. Marquis, and D. Pillot, Rock Eval 6 applications in hydrocarbon exploration, production and in soil contamination studies, Latin American Congress on Organic Geochemistry, Cancun, 1996.

Langford, F.F., and M.-M. Blanc-Valleron, Interpreting Rock-Eval Pyrolysis data using graphs of Pyrolizable Hydrocarbons vs. Total Organic Carbon, AAPG, 74 (6), 799-804, 1990.

Lohse, L., R.T. Kloosterhuis, H.C. de Stigter, W. Helder, W. van Raaphorst, and T.C.E. van Weering, Carbonate removal by acidification causes loss of nitrogenous compounds in continental margin sediments, Marine Chemistry, 69, 193-201, 2000.

Lucotte, M., and B. D'Anglejan, Processes controlling phospate adsorption by iron hydroxides in estuaries, Chemical Geology, 67, 75-83, 1988.

Madhupratap, M., S. Prasanna Kumar, P.M.A. Bhattathiri, M. Dileep Kumar, S. Raghukumar, K.K.C. Nair, and N. Ramaiah, Mechanism of the biological

response to winter cooling in the northeastern Arabian Sea, Nature, 384, 549-552, 1996.

Murray, D.W., and W.L. Prell, Pliocene to Pleistocene variations in calcium carbonate, organic carbon, and opal on the Owen Ridge, northern Arabian sea, in *Proceedings of the Ocean Drilling Program, Scientific Results*, Vol. 117, edited by W.L. Prell., Niitsuma, N., et al., pp. 343-363, 1991.

Muzuka, A.N.N., S.A. Macko, and T.F. Pedersen, Stable carbon and nitrogen isotope compositions of organic matter from Sites 724 and 725, Oman Margin, in *Proceedings of the Ocean drilling Program, Scientif ic Results*, Vol. 117, edited by W.L. Prell, Niitsuma, N. et al., pp. 571-586, 1991.

Neftel, A., H. Oeschger, J. Schwander, B. Stauffer, and R. Zumbrunn, Ice core sample measurements give atmospheric CO_2 content during the past 40,000 yr, Nature, 295 (5846), 220-223, 1982.

Pedersen, T.F., G.B. Shimmield, and N.B. Price, Lack of enhanced preservation of organic matter in sediments under the oxygen minimum on the Oman margin, Geochimica et Cosmochimica Acta, 56, 545-551, 1992.

Petit, J.R., J. Jopuzel, D. Raynaud, N.I. Barkov, J.-M. Barnola, I. Basile, M. Benders, J. Chappellaz, M. Davis, G. Delaygue, M. Delmotte, V.M. Kotlyakov, M. Legrand, V.Y. Lipenkov, C. Lorius, L. Pépin, C. Ritz, E. Saltzman, and M. Stievenard, Climate and atmospheric history of the past 420,000 years from the Vostok ice core, Antartica, Nature, 399, 429-436, 1999.

Prell, W.L., Monsoonal climate of the Arabian Sea during late Quaternary: a response to changing solar radiation, in *Milankovitch and Climate*, edited by A.L. Berger, Imbrie, J., Hays, J., Kukla, G., Saltzman, B., pp. 349-366, D. Ridel, Hingham, 1984a.

Prell, W.L., Variation of monsoonal upwelling: a response to changing solar radiation, in *Climate processes and climate sensitivity*, edited by J. Hansen, Takahashi, T., pp. 48-57, Amer. Geophys. Union, 1984b.

Prell, W.L., and J.E. Kutzbach, Monsoon Variability over the past 150,000 years, Journal of Geophys. Research, 92 (D7), 8411-8425, 1987.

Prell, W.L., and J.E. Kutzbach, Sensitivity of the Indian monsoon to forcing parameters and implications for its evolution, Nature, 360, 647-652, 1992.

Prell, W.L., D.W. Murray, S.C. Clemens, and D.M. Anderson, Evolution and Variability of the Indian Ocean Summer Monsoon: Evidence from the Western Arabian Sea Drilling Program, in *The Indian Ocean: A synthesis of results from the Ocean Drilling Program*, edited by R.A. Duncan, pp. 447-469, Amer. Geophys. Union, Washington D.C., 1992.

Prell, W.L., and N. Niitsuma, Proc. ODP, Init. Repts., Vol. 117, Ocean Drilling Program, College Station, TX, 1989.

Rao, V.P., and M. Lamboy, Phosphorites from the Oman margin, ODP Leg 117, Oceanologica Acta, 18 (3), 289-307, 1994.

Raymo, M.E., The Himalayas, organic carbon burial and climate in the Miocene, Paleoceanography, 9 (3), 399-404, 1994.

Reichart, G.J., L.J. Lourens, and W.J. Zachariasse, Temporal variability in the northern Arabian Sea Oxygen Minimum Zone (OMZ) during the last 225,000 years., Paleoceanography, 13 (6), 607-621, 1998.

Rickaby, R.E.M., and H. Elderfield, Planktonic foraminiferal Cd/Ca: paleonutrients or paleotemperature, Paleoceanography, 14, 293-303, 1999.

Rossignol-Strick, M., African Monoons, an immediate climate response to orbital insolation, Nature, 304, 46-49, 1983.

Ruddiman, W.F., W.L. Prell, and M.E. Raymo, Late Cenozoic uplift in Southern Asia and the American West: rationale for general circulation modeling experiments, Journ. of Geophys. Research, 94 (D15), 379-391, 1989.

Ruttenberg, K.C., Development of a sequential extraction method for different forms of phosphorus in marine sediments, Limnology Oceanography, 37 (7), 1460-1482, 1992.

Ruttenberg, K.C., and R.A. Berner, Authigenic apatite formation and burial in sediments from non-upwelling, continental margin environments, Geochimica et Cosmochimica Acta, 57, 991-1007, 1993.

Ruttenberg, K.C., and M.A. Goni, Phosphorus distribution, C:N:P ratios, and $\delta^{13}C_{oc}$ in artic, temperate, and tropical coastal sediments: tools for characterizing bulk sedimentary organic matter, Marine Geology, 139, 123-145, 1997.

Schenau, S.J., C.P. Slomp, and G.J. De Lange,

Phosphogenesis and active phosphorite formation in sediments from the Arabian Sea oxygen minimum zone, Marine Geology, 169 (1-2), 1-20, 2000.

Shimmield, G.B., and S.R. Mowbray, The inorganic geochemical record of the Northwest Arabian Sea: a history of productivity variation over the last 400 k.y. from Sites 722 and 724, in *Proceedings of the Ocean Drilling Program, Scientific Results*, Vol. 117, edited by W.L. Prell., Niitsuma, N., et al., pp. 409-429, 1991.

Siegenthaler, U., and J.L. Sarmiento, Atmospheric carbon dioxide and the ocean, Nature, 365, 119-125, 1993.

Sirocko, F., Accumulation of eolian sediments in the northern Indian Ocean; record of the climatic history of Arabia and India, Ph.D. thesis, Christian-Albrechts-Universität, Kiel, Germany, 1989.

Sirocko, F., Sarnthein, M., Erlenkeuser, H., Lange, H., Arnold, M., Duplessy, J.C., Century-scale events in monsoonal climate over the past 24,000 years, Nature, 364, 322-324, 1993.

Slomp, C.P., E.H.G. Epping, W. Helder, and W. van Raaphorst, A key role of iron-bound phosphorus in authigenic apatite formation in North Atlantic continental platform sediments, Journal of Marine Research, 54, 1179-1205, 1996.

Sundby, B., C. Gobeil, N. Silverberg, and A. Mucci, The phosphorus cycle in coastal marine sediments, Limnology and Oceanography, 37 (6), 1129-1145, 1992.

Tyrrell, T., The relative influences of nitrogen and phosphorus on oceanic primary production, Nature, 400, 525-531, 1999.

Van Cappellen, P., and E.D. Ingall, Redox stabilization of the atmosphere and oceans by phosphorus-limited marine productivity, Science, 271, 493-496, 1996.

Webster, P.J., V.O. Magana, T.N. Palmer, J. Shukla, R.A. Tomas, M. Yanai, and T. Yasunari, Monsoons: processes, predictability, and the prospects for prediction, Journ. of Geophys. Research, 103 (C7), 14451-14510, 1998.

Weedon, G.P., and G.B. Shimmield, Late Pleistocene upwelling and productivity variations in the Northwest Indian Ocean deduced from spectral analyses of geochemical data from Sites 722 and 724, in *Proceedings of the Ocean Drilling Program, Scientific Results*, Vol. 117, edited by W.L. Prell., Niitsuma, N., et al., pp. 431-443, 1991.

Zahn, R., and T.F. Pedersen, Late Pleistocene evolution of surface and mid-depth hydrography at the Oman margin: planktonic and benthic isotope records at Site 724, in *Proceedings of the Ocean Drilling Program, Scientific Results*, Vol. 117, edited by W.L. Prell., Niitsuma, N., et al., pp. 291-308, 1991.

Zahn, R., K. Winn, and M. Sarnthein, Benthic foraminiferal $\delta^{13}C$ and accumulation rates of organic carbon: *Uvigerina Peregrina* group and *Cibicidoides Wuellerstorfi*, Paleoceanography, 1 (1), 27-42, 1986.

CHAPTER 3

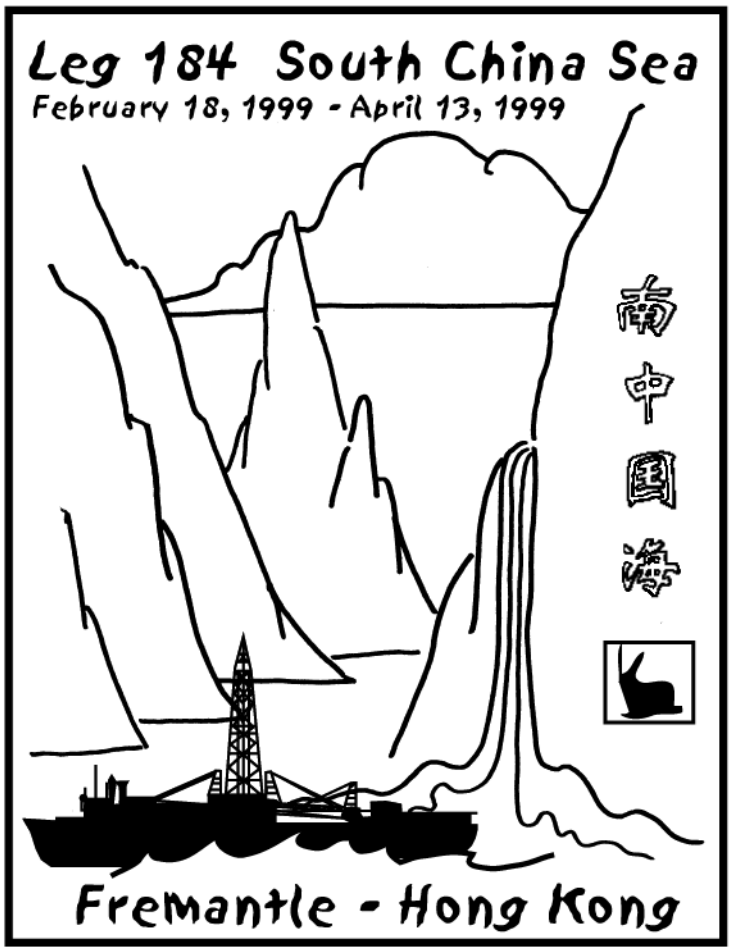
Leg 184 South China Sea
February 18, 1999 - April 13, 1999
南中國海
Fremantle - Hong Kong

*Mineralogy and geochemistry of ODP Sites 1143 and 1144, South China Sea. Investigating the history of East Asian monsoon and climate during the last glacial interglacial period (0-140,000 years).**

ABSTRACT

Monsoon climate is an important component of the global climatic system. A comprehensive understanding of its variability over glacial-interglacial time scales as well as of its effects on the continent and in the ocean is required in order to decipher links between climate, continental weathering and productivity. A detailed multiproxy study, including bulk and clay mineralogy, granulometry, phosphorus geochemistry (SEDEX extraction), organic matter characterization and nitrogen stable isotopes, has been carried out on samples from ODP Sites 1143 and 1144 (Leg 184, South China Sea), covering the past 140,000 years. We have reconstructed the complex sedimentation and climatic history of the region during the last glacial interglacial cycle, when sea level variations, linked to the formation and melting of ice caps, interacted with monsoon variability. During interglacial periods and high sea level, summer monsoon was strongest, and the surrounding continent and islands was characterized by humid and warm climate. Clay minerals bear signals of chemical weathering during this period. High calcite and reactive phosphorus MAR indicate high productivity, especially in the southern region of the South China Sea basin. During glacial intervals, strong winter monsoon and low sea level significantly influenced the hydrography and the configuration of the basin, as inferred by mineralogical and granulometry data. Drop in sea level during glacial stages resulted in reworking of sediments from the exposed Sunda shelf on the south and changes in source sediments on the northern region, while higher detrital input was the outcome of enhanced eolian input from the continent, as indicated by detrital MAR. Physical weathering on the mainland of China and chemical weathering on Indonesia and tropical islands, as deduced from clay minerals variations, confirm that warm and humid conditions were still preserved in tropical areas during glacials. Reduced circulation during glacial periods possibly induced active remobilization of nutrients, such as phosphorus, from the sediments. The rediffusion of bio-available phosphorus in the water column could have helped in maintaining high primary productivity, along with enhanced input of nutrients, such as iron, from land. Despite the low time resolution of this study, we have proofs of intense and short lasting cold periods, both during glacial and interglacial stages, which correlate with loess records in China and marine climatic records in the North Atlantic, confirming a teleconnection between low and high latitude climate variability.

KEYWORDS

South China Sea, Pleistocene-Holocene Climate, Monsoon, Continent-Ocean Interaction, Mineralogy, Phosphorus Geochemistry.

1. INTRODUCTION

The South China Sea (SCS), with a total area of $3.5 \cdot 10^6$ km^2, represents one of the largest marginal basins in the Pacific region. The climate of the SCS and the surrounding areas is presently influenced by the East Asian monsoon. Its location at the interface of the Pacific and Indian oceans and Asia makes the SCS basin ideal to record past climatic changes. The SCS is sensitive to changes in East Asian monsoon intensity and duration, to

* This chapter by Federica Tamburini, Thierry Adatte, Karl B. Föllmi, Stefano M. Bernasconi and Philipp Steinmann has been submitted for publication in *Marine Geology* (East Asian Monsoon special volume).

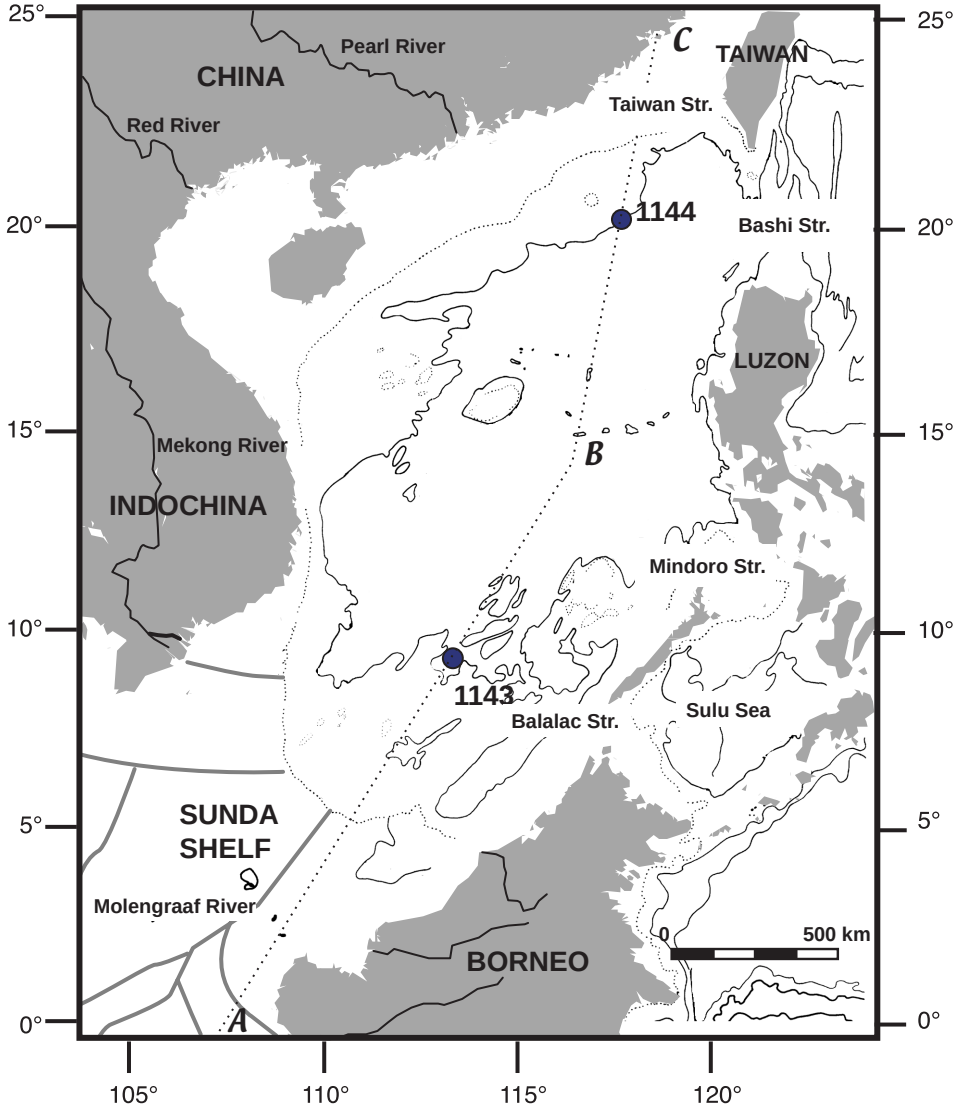

Fig. 1: Map of the South China Sea (SCS) and location of ODP Sites 1143 and 1144. Thin dotted and solid lines are isobaths of 200 and 2000 m. The 200 m isobath represents the limit between the continental shelf and the slope. Thick dotted line (ABC) is the track of the bathymetric profile used in the schematic models of figures 13 and 15.

changes in detrital (river/eolian) input from the continent, as well as to variations in atmospheric and oceanic circulation and exchanges with the open ocean (Wang et al., 2000). Moreover, because of its geographic position, the SCS is a location highly suitable to study and reconstruct relations between continental weathering, productivity and climate, as the basin receives detrital fluxes from three of the largest rivers in the world (Mekong river in the south, Red and Pearl river in the North, Fig. 1). Despite the number of studies on marine sediments (for a comprehensive review see Wang and Wang, 1990 and An, 2000), many aspects of monsoon climate, such as the Cenozoic evolution of the monsoon, and its teleconnections with climate evolution during the Neogene on millennial and sub-millennial time scales, need to be clarified.

The primary objective of ODP Leg 184 was to recover cores from the South China Sea (Wang et al., 2000), to obtain records of the climatic and paleoceanographic history of this area. Here we present the results of a multi-proxy investigation aiming at i) deciphering changes in the sedimentation history of the SCS related to variations in monsoon regime, ii) examining patterns and gradients in detrital

material distribution and nutrient concentration between the northern and the southern region of the SCS, and, finally, iii) having a better insight on connections between monsoon and climate variations, continental weathering and productivity, during the last glacial-interglacial cycle (140,000 years). Bulk and clay mineralogy, organic matter analyses, granulometry, nitrogen stable isotopes analyses, and determination of sedimentary forms of phosphorus have been performed. The investigated samples are from ODP Leg 184 Sites 1143 and 1144, situated on the southern and on the northern regions of the SCS, respectively (Fig. 1).

1.1. East Asian Monsoon

The Asian monsoon is a major component of the climate system, both on a regional and on a global scale. An important teleconnection between the Asian monsoon and high-latitude climate is confirmed by the comparison and correlation between low- (e.g. SCS, Arabian Sea) and high-latitude records (e.g. GRIP; An, 2000; Sirocko et al., 1996; Wang and Oba, 1998). Monsoon circulation results from the heating capacity contrast between land and ocean. This situation linked to the annual cycle in received solar energy, produces extreme seasonality in wind direction, rainfall and temperature patterns on the Asian continent (Webster, 1987). During summer, the formation of a low pressure cell on the Tibetan plateau contrasts with a high pressure cell on the ocean, causing southwesterly winds to blow from the sea to the continent. These winds bring along moisture which provokes heavy rains and promotes a humid and warm climate on land. During winter time the low pressure cell is located on the Pacific ocean and northeasterly winds blow from the interior of the continent, which is characterized by cold and dry conditions, to the ocean (Fig. 2). The East Asian Monsoon is characterized by strong summer and winter monsoonal circulation, unlike the Indian Monsoon, which shows strong summer and weak winter monsoonal circulation (Huang et al., 1997).

1.2. Area description and sites location

The SCS is a semi-enclosed continental sea, (Fig. 1), connected to the East China Sea through the Taiwan strait, the Pacific Ocean through the Bashi strait, the Sulu Sea through the Mindoro, the Java Sea through the Gasper and Karimata straits, and to the Indian Ocean through the Malacca strait (Fig. 1).

Sea surface circulation is controlled by monsoon activity: during summer, subtropical waters are advected into the SCS through the southern straits, flow northward along the Vietnamese and the Chinese coasts, following an anticyclonic pattern, and exit the SCS through the Taiwan strait (Fig. 2b). This pattern is reversed during winter time, with colder and more saline waters entering the SCS from the north, and establishing a cyclonic circulation (Fig. 2a). The surface circulation causes a strong N-S gradient in sea surface temperature (SST) during winter (21° C at north, 27° C at south), which is smaller during summer (28°C at north, 29° C at south) (Huang et al., 1997). According to Wang and Wang (1990) glacial periods are characterized by a marked temperature seasonality, as much as 9-10°C, while the difference between summer and winter temperatures during interglacials and interstadials amounts to 4-6°C. Seasonal upwelling cells, promoted by summer monsoon activity, are observed along the SE coast of Vietnam and the NW coast of the Philippines (Fig. 2); their activity might cease or diminish during glacial periods, in relation to weakened SW monsoons (Wang et al., 1999).

During glacial sea level low stands, a wide portion of the continental platform surrounding the SCS emerged, changing the hydrography of the basin (Fig. 1). Because of the shallow depth of most of the sills, only the Bashi

a)

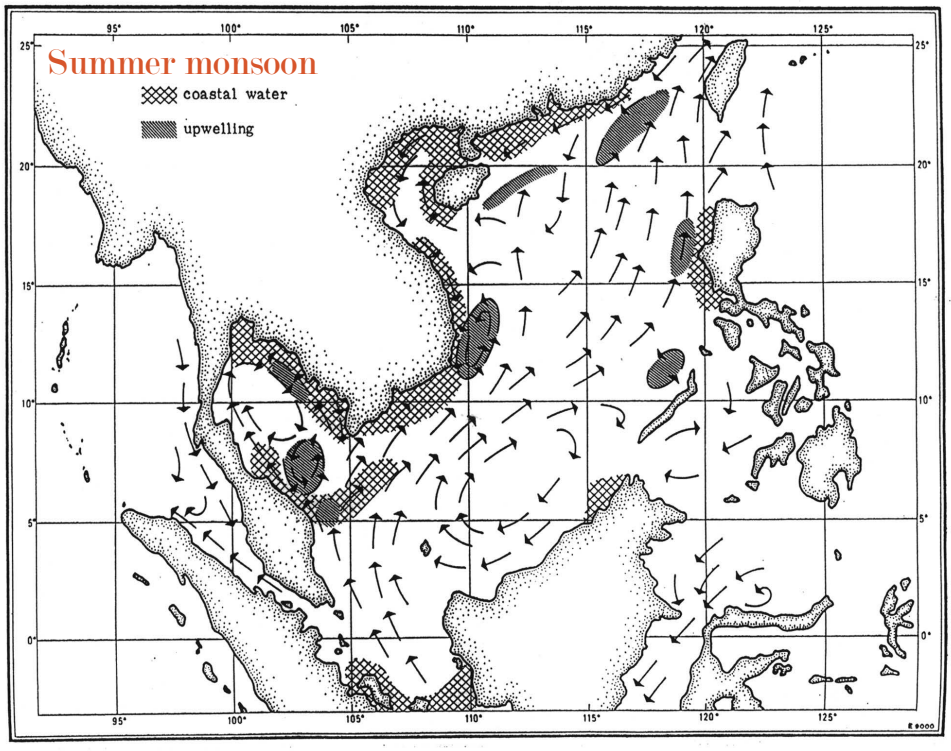

b)

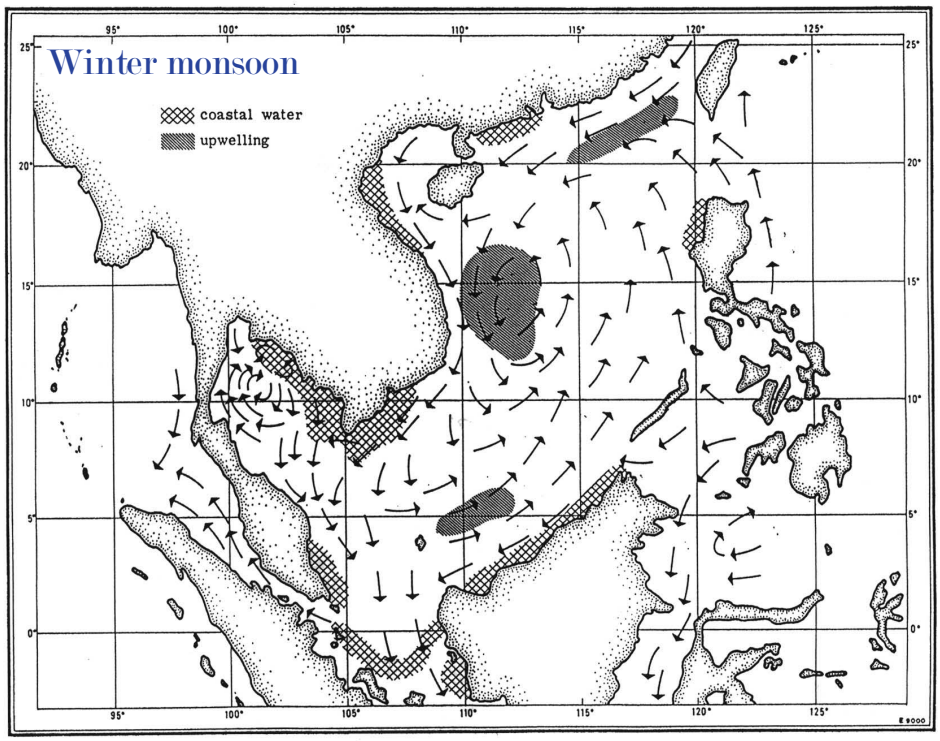

Fig. 2: Oceanic circulation and areas of upwelling during a) summer and b) winter monsoon seasons in the SCS.

strait (2500 water depth) between Taiwan and Luzon remained open during glacial periods, allowing only the inflow of temperate waters from the Pacific Ocean (Wang and Wang, 1990). The southern area of the SCS was presumably more affected by these glacio-eustatic changes, as the emergence of the Sunda shelf closed the straits connecting the SCS

with the Indian Ocean and a fluvial system (Molengraaf river) developed on the emerged platform sediments (Pelejero et al., 1999). Accumulation rates of organic carbon indicate that primary productivity was high during glacial periods compared to Holocene levels, as high nutrient levels were most likely maintained by the enhanced input of material from the continent and from the exposed shelf (Schönfeld and Kudrass, 1993; Wang et al., 1999). The reduced circulation and the increased accumulation of organic material may have prompted oxygen depletion of intermediate and bottom waters (Wang et al., 1999). During glacials, the interior of the Asian continent experienced cold and dry conditions, as is testified by loess accumulation and pollen data (An, 2000), while the southern islands were indeed characterized by a tropical to sub-tropical climate (Wang et al., 1999).

Site 1143 (9°21.72'N, 113°17.11'E, 2777 meters water depth) is located within a depression on the carbonate platform on the southern continental shelf of the SCS, south of the Vietnamese upwelling region and close to the Mekong river estuary and the Sunda shelf. It is situated inside the Western Pacific Warm Pool, a region of relatively high and stable sea surface temperature (SST). Sediments consist of bioturbated green and gray clay mixed with nannofossil ooze, which indicate hemipelagic and pelagic conditions.

Site 1144 (20°3.18'N, 117°25.14'E, 2037 meters water depth) is located on a sediment drift on the northern continental margin of the SCS, SE of Hong Kong and of the Pearl river mouth. Recovered sediments are homogenized by bioturbation, consist of hemipelagic clay mixed with quartz silt and nannofossil ooze, characterized by high organic matter content and black spots of iron sulfides. This site shows an extremely high sedimentation rate (80 cm/k.y. for the last 1 Ma), allowing to obtain a high resolution record of paleomonsoon history. Its location close to the Pearl river mouth and to the Taiwan strait records variations in both eolian and river inputs (Wang et al., 1999), and changes in the origin of water masses. Comparison between the mineralogy and geochemistry from these two sites provides information on N-S gradients in nutrients and productivity. It also reveals differences in sedimentation patterns and weathering on the continent between the northern and the southern part of the SCS.

2. METHODS

A total of 132 samples were taken from Sites 1143 and 1144 (61 and 71 respectively), leading to a time resolution averaging 2.5 k.y. for Site 1143 and 2 k.y. for Site 1144. The stratigraphy of the two cores was inferred by interpolation of the age model as determined by isotopic stratigraphy provided by J. Tian and P. Wang for Site 1143 and by C. Bühring and M. Sarnthein for Site 1144 (in Marine Geology special volume on East Asian Monsoon, referred from now on as MG). Based on the isotopic stratigraphy, the sedimentation record at Site 1143 of the investigated interval is continuous, while a hiatus, covering an interval of about 9 k.y., between stages 5.5 and 5.4, has been indentified at Site 1144 (Bühring, MG).

Analyses were performed at the GEA laboratory of the Geological Institute in Neuchâtel, except for ICP- AES and nitrogen stable isotope analyses, which were performed at the "State Environmental Laboratory" in Neuchâtel and at the ETH in Zürich, respectively. All samples were oven-dried at 50°C and divided in subsamples. Five grams of dried sediment were ground to obtain a homogeneous powder with particle sizes <40 μm. Clay mineral analyses were based on methods by Kübler (1987). An aliquot of the sample was mixed with de-ionized water (pH 7-8) and agitated. The carbonate fraction was removed by the addition of HCl 10% (1.25 N) at room temperature. The insoluble residue was washed and centrifuged (5-6 times) until a

Table 1

Step name	Treatments	P component isolated	Errors *a*	Detection limits *b*
Iron-bound P	10 ml CBD solution (6hr) (0.22 M sodium citrate, 0.11 M sodium bicarbonate 0.13 M sodium dithionite) 10 ml 1M MgCl2 (2hr) 10 ml H2O (2hr)	Exchangeable or loosely sorbed P Reducible or reactive iron-bound P	3-6%	0.03
Authigenic P	10 ml 1M Na-acetate buffered to pH 4 with acetic acid (5hr) 10 ml 1M MgCl2 (2hr) 10 ml 1M MgCl2 (2hr) 10 ml H2O (2hr)	Carbonate fluorapatite (CFA) biogenic hydroxyapatite	2-7%	0.025
Detrital P	10 ml 1N HCl (16 hr)	Detrital fluorapatite-bound P	3-5%	0.003
Organic P	1 ml 50% (w/v) MgNO3, dry in low oven, ash at 500°C (2 hr) 10 ml 1N HCl (24 hr)	Organic-bound P	2-5%	0.004

Table 1: Sequential extraction technique applied for phosphorus phases determination (Ruttenberg, 1992; Anderson and Delaney, 2000).
a) Typical mean errors for each phase were calculated as the relative standard deviation of the consistency standards.
b) Detection limits for each phase were calculated as three time the standard deviation of blank measurements.

neutral suspension was obtained (pH 7-8). Separation of different grain size fractions (< 2μm and 2-16 μm) was obtained by the timed settling method based on Stokes law. XRD analyses of oriented clay samples were made after air drying at room temperature and ethylene-glycol solvated conditions. Clay minerals for each fraction are given in relative percent abundance. Content in smectite, measured on the fraction < 2μm treated with glycol, is estimated by using the method of Moore and Reynolds (1989). The relative error does not exceed 10%. The geochemical composition and nature of micas and chlorites is determined using ternary diagrams with relative percentages of selected diffraction peaks, as proposed by Rey and Kübler (1983) and Oinuma et al., (1972). The other aliquot was pressed (20 bars) in a powder holder to determine bulk sediment mineralogy by XRD (SCINTAG XRD 2000 Diffractometer) based on a semi-quantitative estimation, and using external standards (Kübler, 1987). The relative error of the bulk rock mineralogy is about 5% (RSD). Granulometry analyses were performed on the insoluble, carbonate-free residues prepared for the clay mineralogy analyses using a Granulometry Laser Oriel CIS. The relative error is 10%. We performed a physical grain size separation on selected carbonate-free samples, using a Retsch Ultra-Sonic Sieving Apparatus, which allows to distinguish between 5 granulometry classes (>60, 35, 20, 10 and 5 μm). The different aliquots of sediments were then visually analyzed with an Environmental Scanning Electron Microscope (ESEM) at the Institute of Microtechnology of the University of Neuchâtel.

The characterization of organic matter was performed on about 100 mg of dried and ground sediment, with a Rock-Eval 6, and using a standard whole rock pyrolysis method (Espitalié et al., 1986; Lafargue et al., 1996). Nitrogen contents and stable isotopic analyses of the bulk sediment were performed using a Carlo Erba CNS2500 CHN Elemental Analyzer coupled with a FISONS OPTIMA mass spectrometer. Mean errors, calculated as relative standard deviations on measurements are about 0.15‰. All data are reported in the δ

notation with respect to atmospheric nitrogen (AIR‰). Total nitrogen is here considered as representing the organic nitrogen fraction. Our tests showed that acidification to remove carbonate and preconcentrate organic matter has a strong and somehow unpredictable impact on the isotopic nitrogen signature, therefore no acidification was performed on the samples.

The distribution of sedimentary phosphorus phases was determined using a 4-step sequential extraction technique, adapted from the SEDEX method (Anderson and Delaney, 2000; Ruttenberg, 1992). This method utilizes a progressive dissolution of solid phases to extract phosphorus (P) associated with well defined sedimentary components: iron and manganese oxi-hydroxides, authigenic apatite, detrital apatite and organic matter (Table 1). For all the steps other than the iron-bound P, the ascorbic acid molybdate blue technique was employed (Eaton et al., 1995). A Perkin-Elmer UV/Vis spectrophotometer Lambda 10 with a 4-cm quartz cell was used to determine absorbance of the developed color at 810 nm and to calculate P concentrations. Concentrations of the iron-bound P phase and ferric Fe were determined using an OPTIMA 3000 Perkin Elmer ICP-AES. Reagent blanks, standards and consistency standards were used to perform calibration curves for each step and check analytical reproducibility over time.

3. RESULTS

3.1. Bulk sediment mineralogy

Generally, detrital silicate minerals (quartz, phyllosilicates, K-feldspar and plagioclase) are present in higher percentages in the northern (32% in average) than in the southern site (22% in average). Calcite shows high values in Site 1143 (up to 25% of total bulk sediments), while calcite at Site 1144 is not higher than 10% (Fig. 3).

Site 1143 shows high phyllosilicate contents, up to 45 % of total detrital silicates, while quartz represents only 25% of the detrital silicate fraction. Quartz and phyllosilicates show quite a similar trend, with minima at the beginning of Marine Isotopic Stages (MIS) 5 and 1, and higher values during stages 3 and 2. K-feldspar shows no significant changes between glacial and interglacial periods. Plagioclase shares the same peaks and minima of quartz, but its trend diverges at the beginning of stage 3, with plagioclase tending to lower values. In contrast to other minerals, calcite at Site 1143 shows important changes between glacial and interglacial values. Maxima are observed at the beginning of stage 5 (30% at 120 ka) and stage 1 (25%), while values almost reaching 0% are characteristic of stages 4 and to a lesser extent, of stage 2.

Quartz is the most abundant mineral in sediments from Site 1144, with concentrations reaching about 50% of total detrital silicates. Two marked minima are present at the beginning of stages 5 and 1, and are paralleled by phyllosilicates and at the base of stage 5, by plagioclase and calcite. Generally higher values in quartz are found during glacial or interstadial periods, with peaks of up to 25%. Phyllosilicates follow the same pattern as quartz during stages 6 and 5, but diverge at the beginning of stage 4, when phyllosilicates drop and remain constant at low values till stage 1. Quartz and plagioclase, on the other hand, start to increase and reach their maximum values between 35 and 30 ka. As for Site 1143, K-feldspar displays rather stable values, except for a maximum at 60 ka. Calcite is generally less than 9%, and mirrors the detrital minerals pattern, suggesting a detrital origin. The most remarkable features are a minimum during stage 5.2 and a maximum at the end of stage 2.

The presence of "iron sulfides" (Wang et al., 2000) and of pyrite was detected at Site 1144 already during onboard description and is presumably due to the generally high content in organic matter. The XRD analyses of the bulk sediments and ESEM images reveal

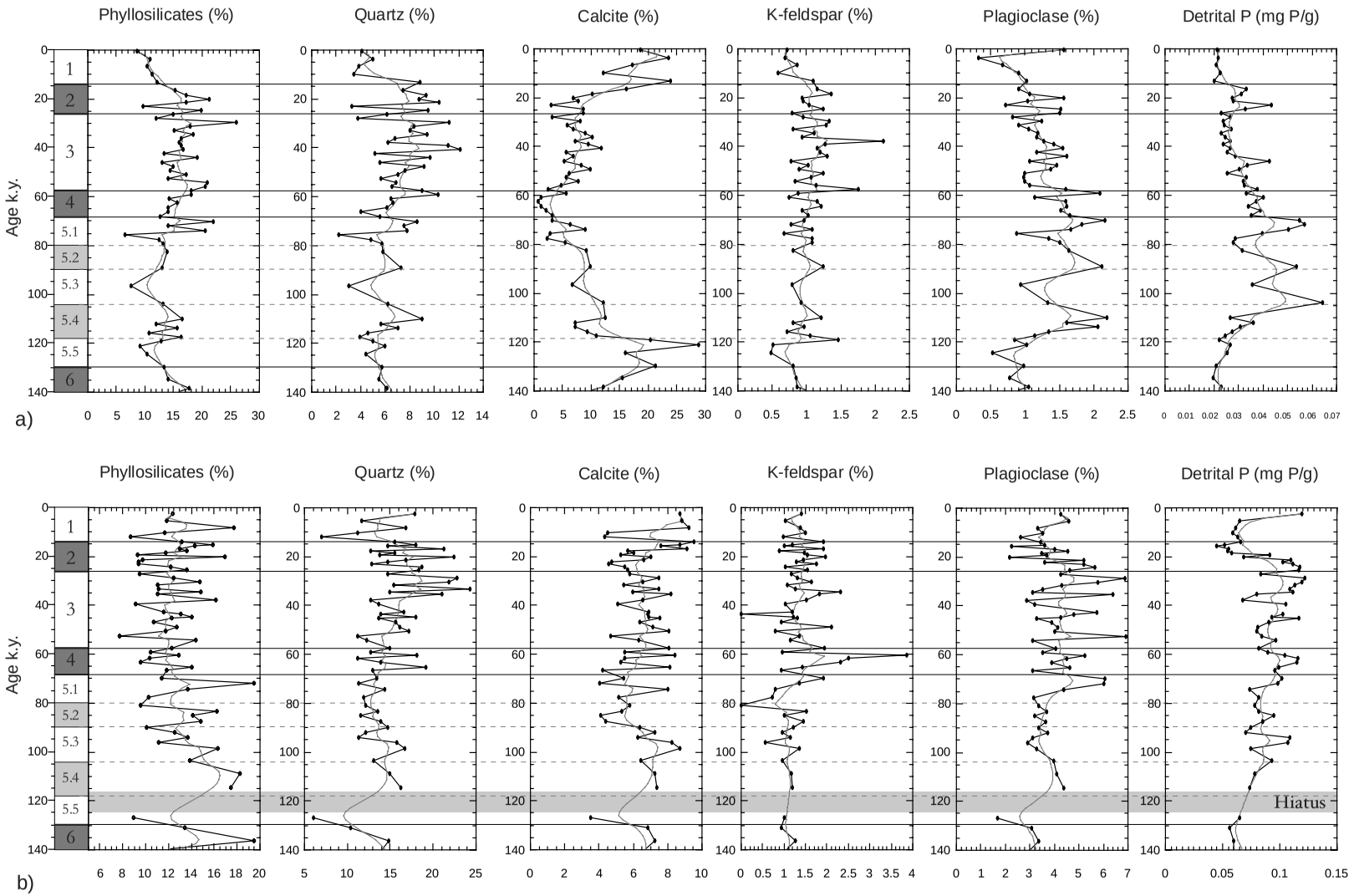

Fig. 3: Percent phyllosicates, quartz, calcite, K-feldspar and plagioclase and concentration of detrital P of bulk sediment from a) Site 1143 and b) Site 1144. In each graph, the thin gray line represents the smoothed curve, calculated using a geometric weight applied to the point and ± 10% of the data range. Age is in k.y. Marine isotopic stages (MIS) are labeled on the left of the graphs. Glacial stages are represented in dark gray, interstadials in light gray and interglacials in white. The gray bar crossing Site 1144 records represents the hiatus between 120 and 126 ka recognized using isotopic stratigraphy (Bühring, MG).

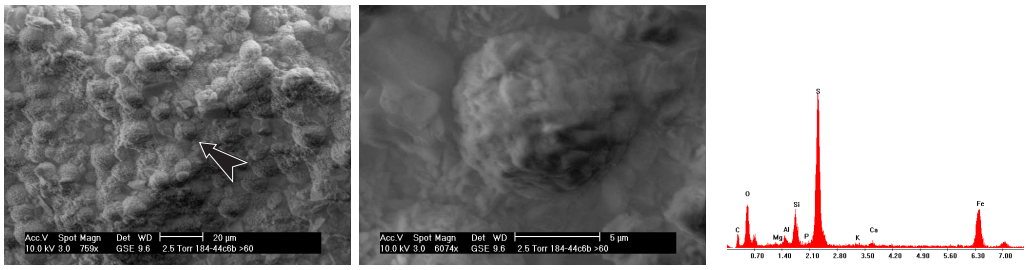

a) b) c)

Fig. 4: ESEM pictures of a) authigenic pyrite "stick", longer than 80 µm, covered by framboidal crystals. The arrow indicates the nodule magnified in b). c) results of the qualitative EDX chemical analysis on the nodule. Sample 184-1144C-1H-5 (98-100 cm), fraction >60 µm.

the presence of authigenic pyrite (Fig. 4), though at very low percentages (average=0.11% for the entire studied sequence). A peak in pyrite is located right at the top of stage 2, where pyrite reaches values around 0.6%. This peak coincides with a minimum in ferric Fe and in magnetic susceptibility (Laj and Solheid, MG).

Mass Accumulation Rates (MAR) are calculated as the product of the concentration in mg/g of sediment, the dry bulk density, as recorded onboard during Leg 184, and sedimentation rates, estimated by oxygen isotope stratigraphy. Site 1143 detrital silicate MAR show a clear glacial-interglacial change, with higher values during MIS 3 and 2, and at the end of stage 5, and minima at the beginning of MIS 5 and 1. Calcite MAR show a minimum during stage 4 and a maximum during stage 5.5, which is reflected also in reactive P MAR (Fig. 5). MAR of all indices at Site 1144 generally show high variability, due to strong changes in sedimentation rates during the studied interval, but especially during glacial stages (Bühring, MG). MAR are generally higher during MISs 4-2, and at the boundary between stage 5.3 and 5.2. The boundary between stage 2 and 1 is marked by a significant drop in sedimentation rates, which dominates the different MAR records, except for ferric Fe MAR and detrital P (Fig. 5).

3.2. Clay mineralogy

Illite is the most abundant clay mineral at Site 1143, representing in average 45 % and 60% of the <2 and 2-16 µm fractions, respectively, and displays quite constant percentages throughout the investigated section (Fig. 6). Higher values of illite in the 2-16 µm fraction are observed during MISs 3 and 2, and in the <2 µm fraction at the lower boundaries of glacials. Illite and chlorite of the 2-16 µm fraction are inversely correlated. Chlorite is quite abundant, averaging 15% and 25% of the <2 and 2-16 µm fractions, respectively. No important changes are observed for chlorite in the <2 µm fraction. Chlorite in the 2-16 µm fraction decreases from the upper part of MIS 4, with the average shifting from 32% to about 23% of MISs 3 and 2, and reaches its lowest values at around 40 ka (about 10%). Kaolinite abundance (2-16 µm fraction) is rather constant throughout the core, with values averaging 15%. No significant variations related to glacial-interglacial variability are observed, and highest percentages are recorded during MISs 3 and 2, at about 40 ka (28%), 20 ka (26%), and 10 ka (29%). The <2 µm kaolinite content decreases right after stage 6 to the low values characterizing stage 5. Its record shows an increasing trend starting at the beginning of stage 4 and reaching the highest values during MIS 3, at around 40 ka (25%). High values are also recorded in the Holocene section of the core. Smectite presents a quite scattered pat-

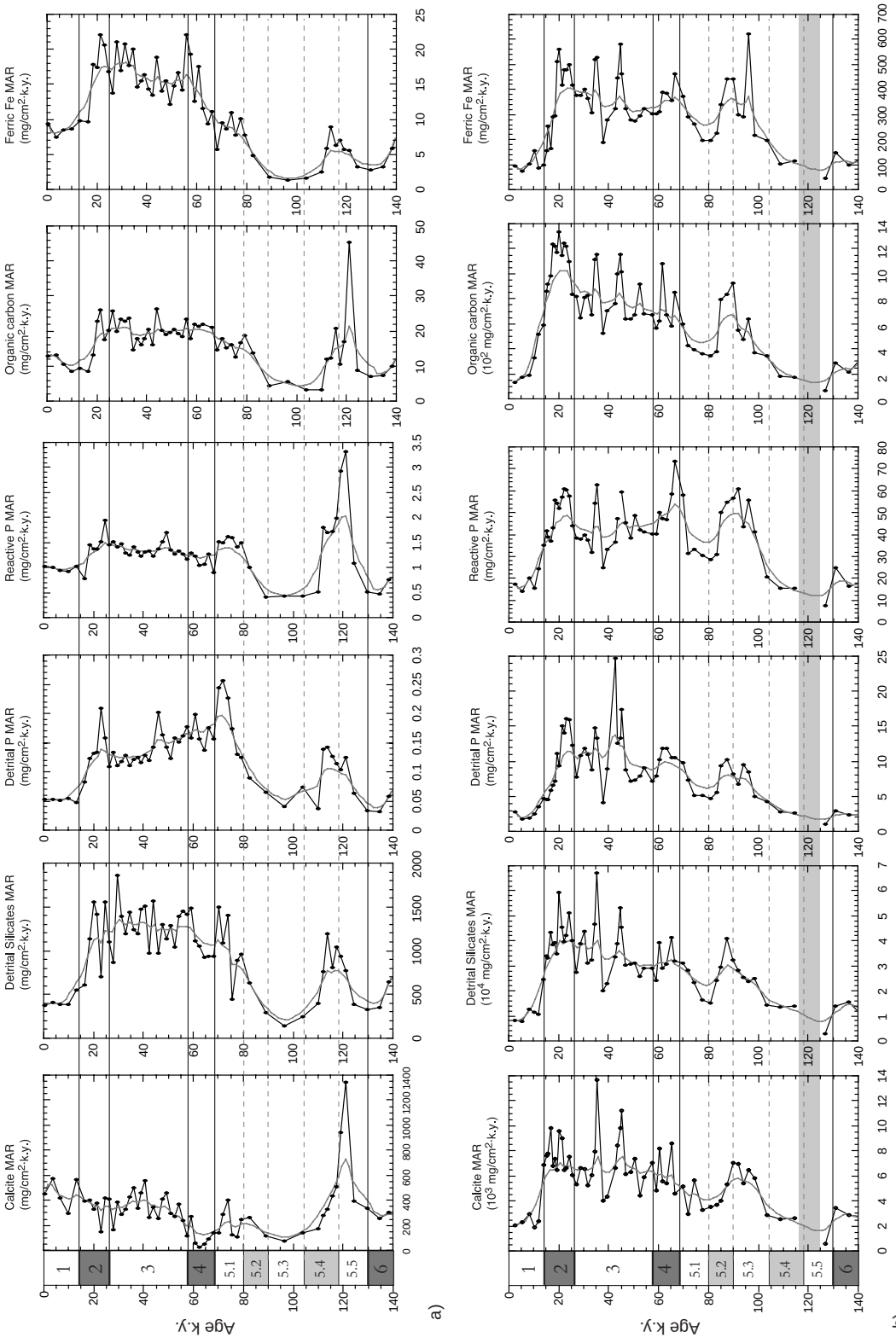

Fig. 5: Mass accumulation rates (MAR) of calcite, detrital silicates, detrital P, reactive P, organic carbon and ferric Fe from a) Site 1143 and b) Site 1144. Age and MIS as in figure 3. MAR were calculated using the concentration of the different indices as determined by XRD (calcite and detrital silicates), by SEDEX extraction (ferric Fe, detrital and reactive P) and Rock Eval analysis (organic carbon). Dry bulk density determined onboard and sedimentation rates as inferred from isotopic stratigraphy (Tian, MG; Bühring, MG), were used. Detrital silicates represent the sum of quartz, phyllosilicates, plagioclase and K-feldspar. Reactive P is the sum of Fe-bound, authigenic and organic-bound P (see text for details).

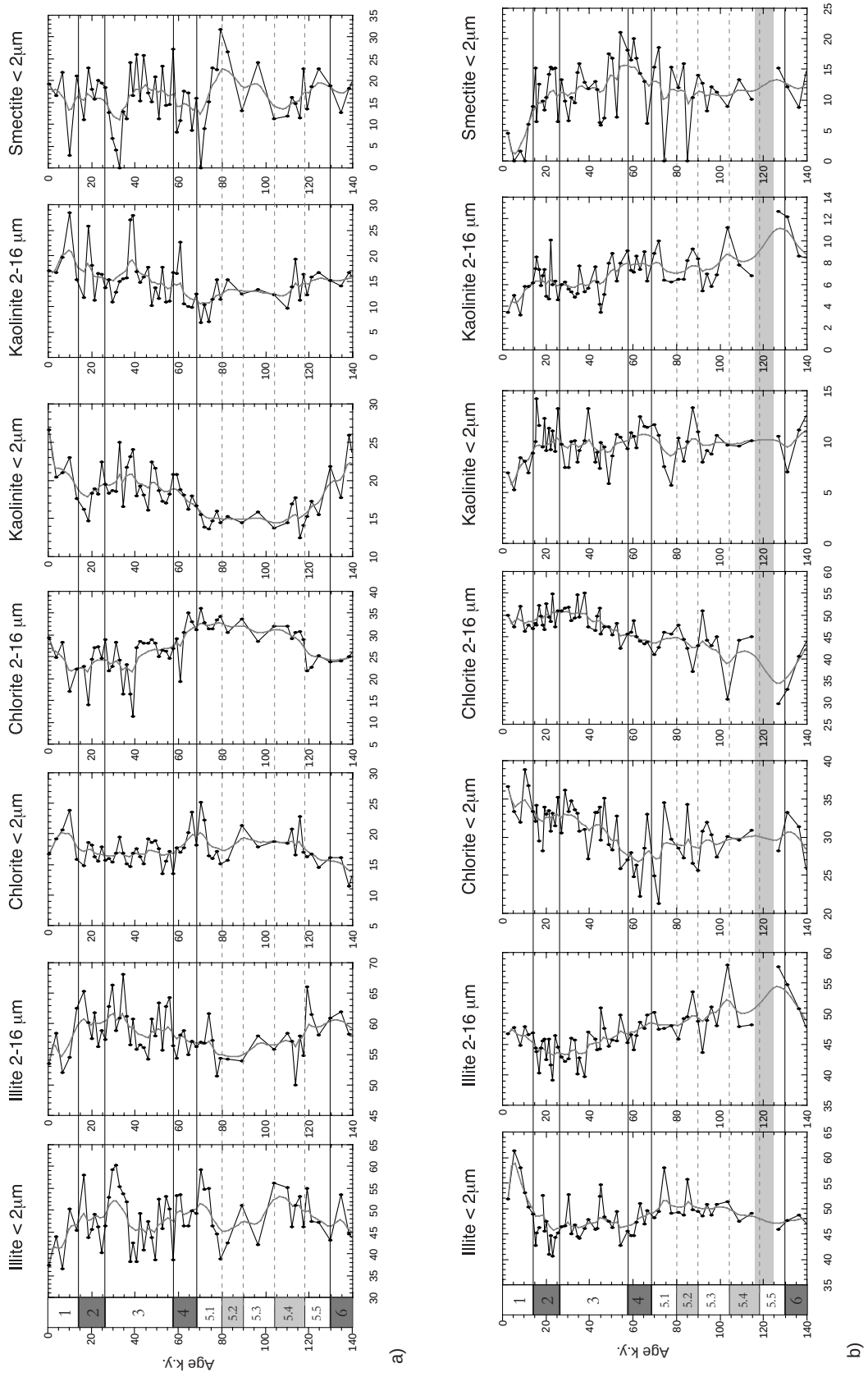

Fig. 6: Relative percentages of illite, chlorite, kaolinite (fractions 2-16 and <2 µm) and smectite (fraction <2 µm) from a) Site 1143 and b) Site 1144. Age and MIS as in figure 3

tern: high values, up to 25-30% are recorded during MIS 5, and the base of stages 3 and 2. Generally, smectite and illite are anticorrelated.

A different picture is present at Site 1144, where chlorite and illite represent the most abundant clay minerals of the 2-16 μm and <2 μm fractions, averaging 45% and 50%, respectively (Fig. 6). Kaolinite and illite (2-16 μm fraction) correlate throughout the whole section and, from the base of stage 5, they both show a decreasing trend, reaching their lowest values at the top of stage 3. Chlorite (clay fraction <2 μm) shows nearly invariable values during stage 5 and starts increasing at the base of stage 3. A minimum in chlorite (2-16 μm fraction) characterizes stage 5.5. Afterward, chlorite increases and reached its highest values at stage 3-2 boundary (55%). Smectite represents in average 15% of clays constituting the <2 μm fraction, and values close to 0% are recorded at 85 ka, at 75 ka, and during the Holocene.

No changes in the composition of micas and chlorites are observed between glacial and interglacial samples and between the two sites. The < 2 μm fraction is mainly constituted by illite-phengite micas, while the coarser fraction composition is shifted toward the muscovite pole (Fig. 7). Chlorites are enriched in iron concentrated in the silicate layers. Most of

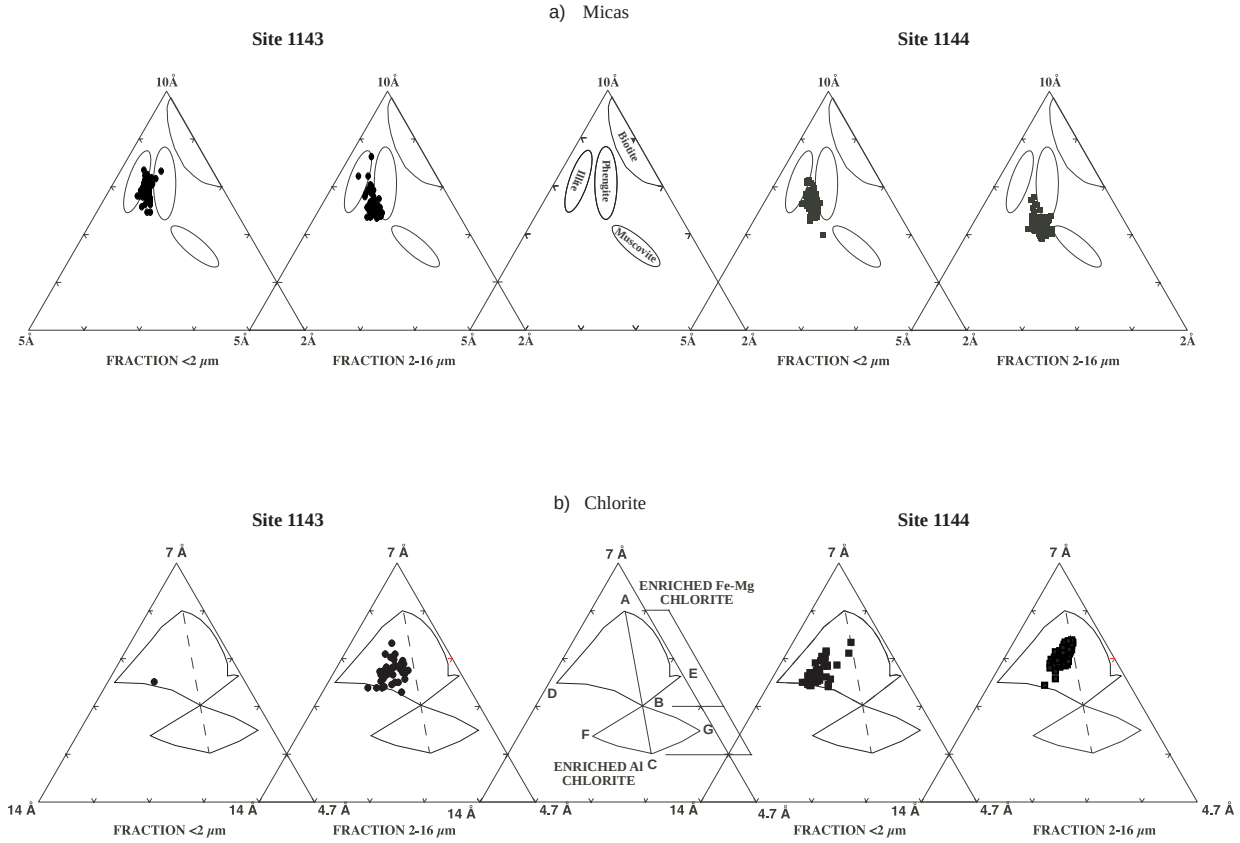

Fig. 7: Ternary diagrams used to determine the geochemical composition and nature of a) micas and b) chlorites. The relative percentages of selected diffraction peaks was used and plotted in a ternary diagram, as proposed by Rey and Kübler (1983) for micas and by Oinuma et al., (1972) for chlorites. Samples from Site 1143 are represented by solid circles, while samples from Site 1144 by solid square symbols. b) Chlorites falling in fields ABD and ABE are characterized by Fe excess in silicate and hydroxyl layers, respectively. Chlorites falling in fields BCG and BCF are characterized by Al excess in silicate and hydroxyl layers, respectively. Most of the analyzed samples, mainly from Site 1143, fall outside the fields, and are shifted toward the 14 Å pole of the diagram. They are therefore not represented here. This shift is due to the relatively high content of smectite in the fine fraction (<2 μm) whose 001 peak at 14 Å get confused to the 14 Å peak of chlorite. Moreover, highly Fe-enriched chlorites are generally characterized by weak 14 and 4.7 Å peaks (Moore and Reynolds, 1997).

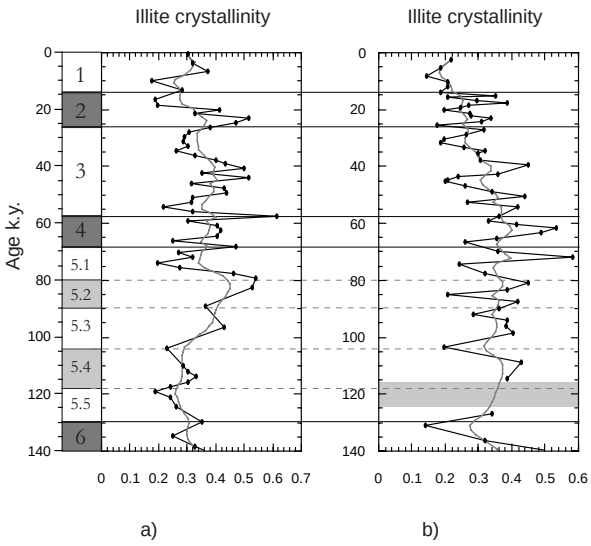

Fig. 8: Illite crystallinity from a) Site 1143 and b) Site 1144. Age and MIS as for figure 3. On average, values at Site 1144 are lower than at Site 1143 (0.32 and 0.34, respectively), indicating that illite is relatively less weathered at the northern site.

the samples of the finer fraction, especially from Site 1143, are situated outside the ABD area and they are not plotted (Fig. 7). This is probably an artifact due to the high content of smectite in sediments and to the presence of extremely Fe-rich chlorite, whose difractogram is normally characterized by weak or nearly undetectable 001 and 003 (14 and 4.7 Å) peaks (Moore and Reynolds, 1997).

Illite crystallinity in sediments not affected by strong burial, can be considered as a proxy indicating the degree of alteration (hydrolysis) of clay minerals. This parameter is calculated using the width of the illite peak at 10 Å, measured at half of the length of the peak itself (Chamley, 1989; Kübler, 1984). Generally, high values of illite cristallinity indicate highly degraded illites, which have been subjected to chemical weathering and transport, while low values characterized relatively unaltered illites. Despite the scattering character of the records, illite crystallinity from both sites exhibits comparable values (averaging 0.3) and similar trends, increasing toward stage 4 and then decreasing, reaching values of about 0.2, similar to stage 5.5 values, in the Holocene (Fig. 8).

3.3. Granulometry

Granulometry records from Sites 1143 and 1144 display important differences as the result of the different position and distance of the two sites from the coastline (Fig. 1 and 9). Fine material with particles <6 μm is more abundant at Site 1143 (more distal) than at Site 1144. This is shown also by the median (in volume) of the grains, averaging 3 μm for Site 1143 and 4.6 μm for Site 1144. Clay contents are higher during interglacials and interstadials at Site 1143, with maxima, higher than 90% during stages 5.5, 5.2, at the boundary between 5.1 and 4, during stage 3, at around 40 ka, and at the base of the Holocene (Fig. 9). Low values are observed during MISs 6, 4 and 2, when coarser material is up to more than 50%.

In a Koopmann diagram (Koopmann, 1981), which defines three types of sediments, fluvial, eolian and winnowed (Fig. 9) most of the samples at Site 1143 fall in the eolian and fluvial sediment fields. Eolian deposits are present throughout the sequence, but are more frequent during glacial stages. Fluvial sediments, characterized by less sorted material, are observed during interglacial stages 5.5, 5.1 and 1, but also during glacial periods (Fig. 9).

The sediments are generally coarser at Site 1144, with clays constituting in average 70% of the carbonate-free sediment. Visual inspection at the ESEM of selected samples showed that detrital material (quartz, phyllosilicates and to a lesser extent plagioclases) is mainly concentrated in the <20 μm fraction. Clays are abundant during stages 5 and 2 and at the base of stage 3. Silt and coarser sediments are present in high amounts during stage 4, at the top of stage 3 and during the Holocene (Fig. 9). In the Koopmann diagram, most of the samples fall in the field of winnowed sediments, while eolian deposits are scarce. At both sites, samples of the eolian field generally correspond to samples with higher median grain size. Despite the uncertainties due to stratigraphy,

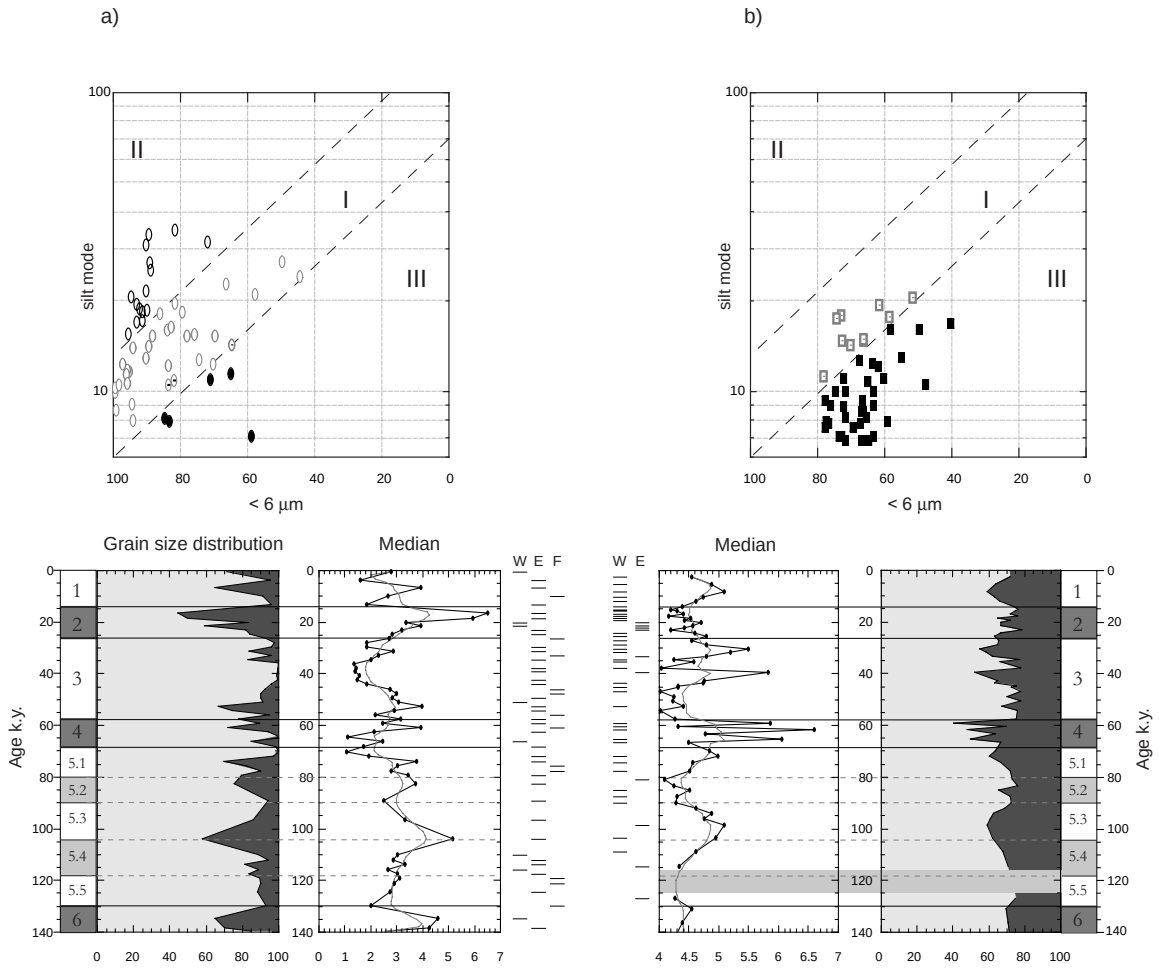

Fig. 9: Koopmann's diagram, grain size distribution and median grain size for a) Site 1143 and b) Site 1144. In a Koopmann's diagram, percentages of the fraction <6 μm and values of the silt mode (6-63 μm fraction) are plotted. The three fields indicate I= eolian (E), II= fluvial (F) and III= winnowed (W) sediments. The nature of the sediments as determined using the Koopmann's diagram, is also reported on the side of the median grain size graphs. In the grain size distribution graphs, the <6 μm fraction is represented in light gray, while the 6-63 μm fraction is dark gray. Sediments at Site 1143 are clearly finer than at Site 1144, most likely as the result of a more distal location.

correspondence of peaks in median grain size between the sites is observed (Fig. 9 and Table 2).

3.4. Sediment Geochemistry: sedimentary P and iron

Total phosphorus (P) concentrations are about 1 mg P/g sediment at Site 1144 and not higher than 0.5 mgP/g at Site 1143. Authigenic P and the Fe-bound P are the most abundant phases at both sites (see Table 3), representing together more than 60% of total P. The authigenic fraction is the most abundant at Site 1143, but the iron- and the organic-bound fractions are present in considerable amounts, and important variations are observed in relative abundance (Fig. 10). Detrital P represents in average only 9% of total P, with highest values during middle MIS 5 (up to 0.06 mgP/g, Fig. 3) and shows a positive correlation with plagioclase and, to a lesser extent, with quartz. Authigenic P, generally a carbonate-fluorapatite mineral (CFA), correlates with calcite, with high amounts occurring at the beginning of stage 5; after 110 ka, authigenic P decreases in concentration until it reaches a minimum of 0.05 mgP/g at about 40 ka. Iron-bound P occurs in amounts around 0.1 mgP/g and at the beginning of stage 3, it starts to increase till it

Table 2

ODP 184-1143			ODP 184-1144			Luochan Section	Notes
mcd	Age k.y.	Median grain size	Depth mcd	Age k.y.	Median grain size	Age k.y.	
0.32	6.76	3.95	3.8424	8.1	5.09		
0.77	16.35	6.5	14.043	16.82	4.4	15	1
0.92	18.32	5.95	16.974	18.44	4.52		
1.22	21.54	3.92	20.393	20.42	4.7	21.5	1
1.67	26.37	2.72	29	25.37	4.79	25.5-27.5	1
2.12	31.16	2.86	34.751	30.23	5.5	33.5-35	1
2.72	37.62	1.44	41.678	35.28	4.58		
			45.302	39.51	5.82	42-43.5	1
4.27	52.62	3.96	61.004	52.73	4.4	49.5-50.5	1
			67.449	59.19	5.86	58.5	1
4.87	60.67	3.94	70.204	61.73	6.59	61.5	1
			74.089	65.21	6.06	63.5-64	1
						66.5-67.5	1
6.07	75.69	3.78	80.598	72.01	4.98	69-71	2
6.52	82.34	3.74	89.899	85.02	4.51	81.3-84	2
			102.85	98.47	5.08	99.5-102	2
6.97	103.73	5.15					
7.42	113.84	3.3				113.5-115	2
7.87	119.24	3.13				119-121.6	2

Table 2: Depth (mcd) and age (k.y.) of peaks in median grain size from Sites 1143 and 1144 compared to age of peaks in quartz abundance (fraction >40 μm) from the Luochan Loess section.
1: Data from Porter and An (1995); 2: Data from An and Porter (1997)

Table 3

	Fe-bound P %	*Authigenic P* %	*Detrital P* %	*Organic-bound P* %
Site 184-1143	29	34	9	28
Site 184-1144	31	38	16	15

Table 3: Relative percentages of the different sedimentary phases of phosphorus.

reaches the maximum value of 0.22 mgP/g at around 14 ka. Organic-bound P shows a downward decrease, probably associated with diagenesis and organic matter degradation. Slightly higher values are observed during MISs 4-2, followed by a decrease at the top of stage 2, and correlating to higher clay percentages (see discussion below, Figs. 9 and 10).

Authigenic P in sediments from Site 1144 averages 0.22 mgP/g representing 38% of total phosphorus. Higher values are recorded during stages 4, 2 and at the end of stage 1. The steep increase at the top of the core can probably be linked to nuclei formation of a precursor mineral of CFA, related to relatively high PO_4^{3-} pore water concentrations (see Site 1144 Inorganic Geochemistry chapter in Wang et al., 2000). Iron-bound P, the second most abundant P species at Site 1144, shows significant variations, with peaks during MISs 5.3, 4 and 1. Organic-bound P occurs in quantities comparable to Site 1143. Detrital P, which averages 0.7 mgP/g, occurs in slightly higher amounts during stage 3 and at the beginning of stage 2, and as for Site 1143, it shows a positive correlation with plagioclase (Fig. 3).

Ferric iron is present at relatively high amounts in both cores (in average 3 mg/g). At

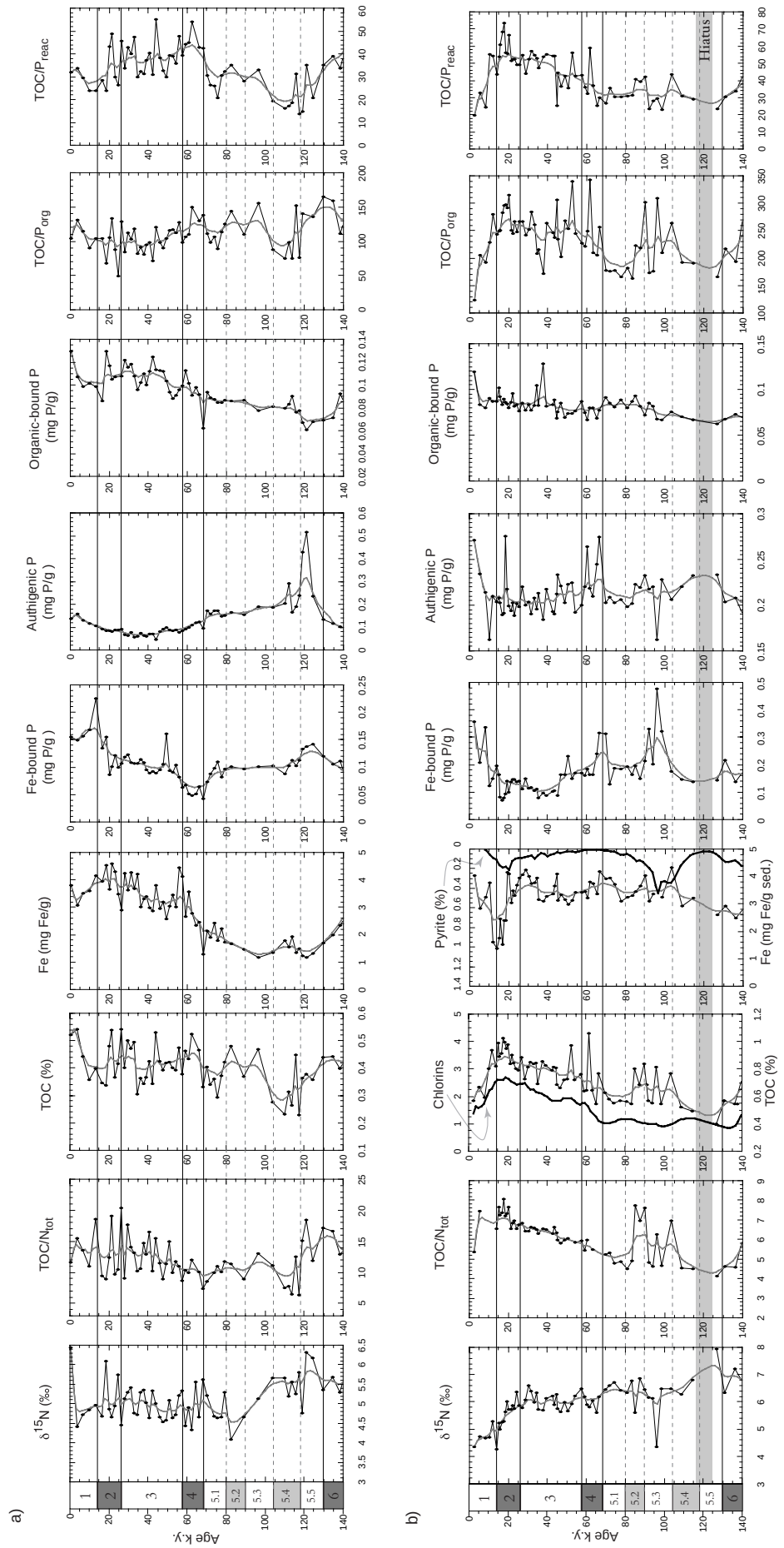

Fig. 10. Nitrogen isotope record, organic matter percentage, Fe concentration, Fe-bound, authigenic and organic-bound phosphorus concentrations and TOC/N_{tot}, TOC/P_{org} and TOC/P_{reac} molar ratios from a) Site 1143 and b) Site 1144. Age and MIS as in figure 3. For Site 1144, chlorins measured onboard are plotted against TOC %. Chlorins concentrations are given as relative abundance per gram dry weight (see Explanatory Notes in Wang et al, 2000). The smoothed record of pyrite percentages, determined by XRD, is plotted against ferric Fe. Raw data are not shown.

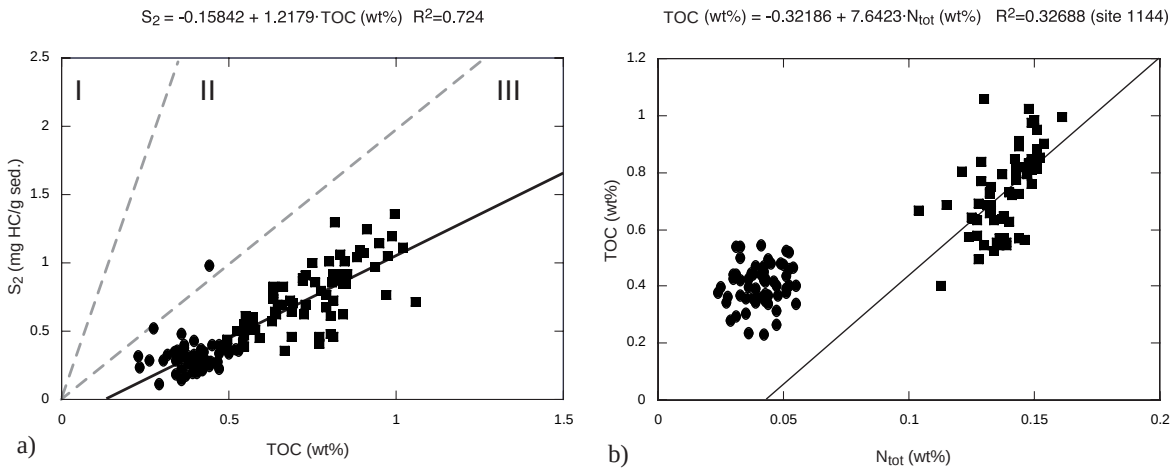

Fig. 11: a) TOC % vs. S_2 values from Rock Eval analysis. All samples fall in field III, indicating organic matter of continental origin. The correlation between the samples is significant. S_2 values from Rock Eval should be taken with caution because of the low TOC content of the sample and the possible absorption of organic matter on clay minerals. b) N_{tot} % vs. TOC % data from Sites 1143 and 1144. Linear fitting for samples from Site 1143 (solid circles) yielded an extremely low correlation (not shown). The positive intercept of the x-axis for Site 1144 indicates that inorganic nitrogen is present, most likely adsorbed onto clay minerals. Samples from Sites 1143 and 1144 are represented by solid circle and solid square symbols, respectively.

Site 1143 Fe shows an upward increase from the minimum at the base of stage 5 to highest values during MISs 3 and 2 (about 4 mg/g). At Site 1144 Fe concentrations are stable with only a minimum at the transition between stage 2 and 1, which correlates with a minimum in magnetic susceptibility and to a pyrite-enriched interval.

Generally, higher MAR of reactive P are observed during glacial periods in both sites, but a maximum is recorded at the beginning of stage 5 at Site 1143, correlating to peaks in calcite and organic carbon MAR (Fig. 5). As for other indices MAR, reactive P MAR at Site 1144 display a pronounced maximum at around 90 ka. Detrital P and Fe MAR are typically high during glacial periods in both sites and show low accumulations during stage 5 and the Holocene. At Site 1144 Fe, detrital and reactive P MAR start decreasing before the end of stage 2, at around 20 ka (Fig. 5).

3.5. Organic matter and $\delta^{15}N$

Organic carbon at Site 1143 is low, between 0.2 and 0.5 %. Prominent minima in the TOC curve are found during interstadial 5.4 and at the top of stage 2. This latter is associated to a minimum in organic-bound P. Total organic carbon (TOC) at Site 1144 correlates with chlorins concentrations, considered as reflecting marine productivity (Higginson, MG; Fig. 10). The correlation between chlorins, measured on board (Wang et al., 2000), and TOC is not significant (r^2=0.48), but both records display a similar trend, with high values during stages 4-2 and a decrease starting at around 20 ka, which mimics detrital indices variations. The records do not correlate during MIS 5. Organic matter MAR are similar to MAR of the other indices, showing highest values during glacial stages 4-2. A pronounced peak is observed at Site 1143 during stage 5.5, which correlates to the maximum in calcite MAR (Fig. 5).

The graph in Fig. 11a represents S_2 and TOC parameters from the Rock Eval. As TOC % are quite low, above all for Site 1143, values should be taken with caution, but all sam-

ples fall in type III kerogen field, which defines terrestrial organic material (Langford and Blanc-Valleron, 1990). The negative y axis intercept of the regression line calculated for all samples indicates adsorption by a mineral matrix, presumably clays (Langford and Blanc-Valleron, 1990). The samples, linearly distributed, display a significant correlation coefficient (r^2=0.73), pointing at a coherent group in terms of origin/source. Analysis of variance performed on HI values, which represent the S_2/TOC ratio and in average the slope of the regression curve of the S_2 vs. TOC graph, confirms that all samples belong to the same population. The TOC/organic phosphorus (TOC/P_{org}) ratio at Site 1143 is close to Redfield values (~ 106) for not-degraded phytoplankton material, while is higher at Site 1144, especially at around 100-90 ka, during stages 2-4 and at the beginning of the Holocene (Fig. 10).

$\delta^{15}N$ values from Site 1143 correlate with calcite, with generally high values during interglacials and low values during glacial periods (Figs. 3 and 10). The record shows slightly higher values during stage 5.5 and 5.4, where it averages 5.5 ‰, and decreases to its lowest values during stage 5.2. The record shows quite stable and invariable values all through stages 4-2. At Site 1144, $\delta^{15}N$ presents more constant values, averaging 6 ‰. From around 20 ka to the top of the interval, the nitrogen isotope signature decreases to 4 ‰ (Fig. 10).

TOC/total nitrogen (TOC/N_{tot}) molar ratio averages 11 for Site 1143 and 6 for Site 1144. Values at Site 1143 are quite high (up to 20) during stages 6, 5.5, 2 and the beginning of the Holocene, while at Site 1144 highest values (up to 8) are observed during stages 5.3 and 5.2, stage 2 and the Holocene. Values for Site 1143 situate between Redfield ratios for marine and terrestrial organic matter.

4. DISCUSSION

4.1. Detrital material: key to weathering and oceanic circulation

Clay distribution in recent sediments from the SCS is controlled by provenance. Chen (1978) recognized 7 different provinces, where the relative amount of clay minerals is determined by the mixing of clays coming from two main sources: the Asian continent, characterized by high contents of illite and chlorite, and the southern tropical islands, which, due to more humid and warm conditions, are characterized by important amounts of kaolinite and smectite. Latitudinal climatic zonation as well as differences in source rocks

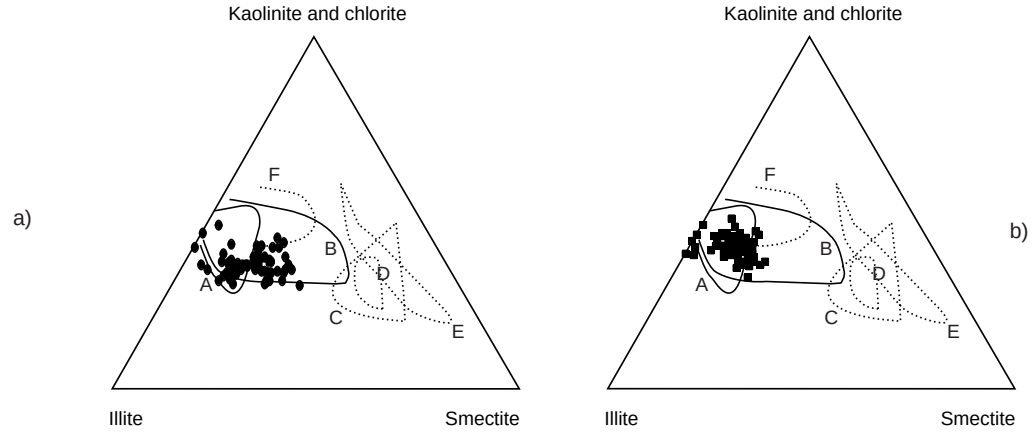

Fig. 12: Triangular diagrams representing different clay provinces in the SCS, based on relative abundance of illite, smectite and kaolinite-chlorite. A = northern continental shelf and Taiwan strait; B = central SCS, Bashi strait, NW Philippine Sea. Other provinces as defined in Chen (1978). Samples from Sites 1143 and 1144 are represented by solid circle and solid square symbols, respectively. See text for discussion.

determine this distinction (Chen, 1978). Generally, clay distribution at Sites 1143 and 1144 corresponds well to this pattern, with the northern site presenting higher amounts of micas and chlorite, while the southern site is richer in kaolinite and to a lesser extent in smectite (Fig. 12). Relative variations of clay in time may, thus, be interpreted as resulting from changes in monsoonal regime, which affected weathering on the Asian continent, and in sources, due to changes in oceanographic conditions.

Site 1143 is considered to belong to a transitional area (Chen, 1978), where sediments from the northern Asian continent and from the Mekong, whose mineral and clay composition is akin to the northern one, are mixed to clays coming from the tropical islands. Relatively high amounts of smectite are probably related to the alteration of volcanic rocks on the surrounding islands and/or to preferential settling (more distal; Chamley, 1989; Chen, 1978). Due to differences in shape and in size, illite and kaolinite normally tend to deposit on the external platform, while smectite is transported further offshore in deeper environments (Adatte and Rumley, 1989). This assumption is also in agreement with relative low amounts of kaolinite and to a lesser extent of micas during stage 5 compared to glacial periods. Kaolinite and illite from the coarser fraction were presumably trapped on the Sunda shelf during high sea level (Fig. 13), while finer clays could have been carried along longer distances. High values of kaolinite at Site 1143 during glacial periods may therefore have multiple explanations: they can be the result of 1) increased chemical weathering on the southern islands; 2) reworking of older sediments from the shelf, or 3) increased eolian input. The illite/kaolinite ratio at Site 1143 (Fig. 14), calculated on the 2-16 μm fraction and considered as an indicator of weathering regime (Chamley, 1989), decreased during glacial periods (stages 4-2), pointing at enhanced chemical weathering. This is in agreement with the assumption of the persistence of tropical climatic conditions (warm and humid) on the southern islands of the SCS during glacial periods (Fig. 15; Wang et al., 1999), but we can not exclude the influence of the other factors discussed above on the glacial distribution of clays. High values of chlorite at Site 1143, especially during stage 5, are compatible with a continental source.

Quartz, iron and other detrital minerals are higher during glacial periods, supporting the hypothesis of enhanced eolian input from the continent and of reworking of shelf sediments. MAR of detrital material indicate increased accumulation during glacials, which is compatible with high input from the continent. Changes in granulometry at Site 1143 are most likely related to the same causes: the more proximal location of Site 1143 during glacial sea low stands and the establishment of a large drainage system as well as increased winter monsoon strength could provide coarser material to deep basins. Eolian contribution to the site is active also during interglacial stage 5, possibly during short lasting cold periods, when winter monsoon was stronger. Also high clay contents observed during stage 3 are probably related to eolian deposits, as indicated by the Koopmann's classification. As glacial times in the tropical regions of the SCS are characterized by humid and warm conditions as well as interglacials, fluvial material contribution to Site 1143 is observed throughout the studied interval (Figs. 9, 14 and 15).

Detrital P and plagioclase at Site 1143, are also influenced by volcanic input: the peak located at 75-70 ka most likely corresponds to the remaining of volcanic ash layer produced by the Toba eruption. Unaltered volcanic glass were found at Site 1143, Hole A, but not in Holes B and C (Bühring et al., 2000; Wang et al., 2000), which were sampled for this study. Relatively high contents of detrital phosphorus are compatible with the rhyolitic nature of the Toba tephra and the overall mineralogical composition of the interval well corresponds

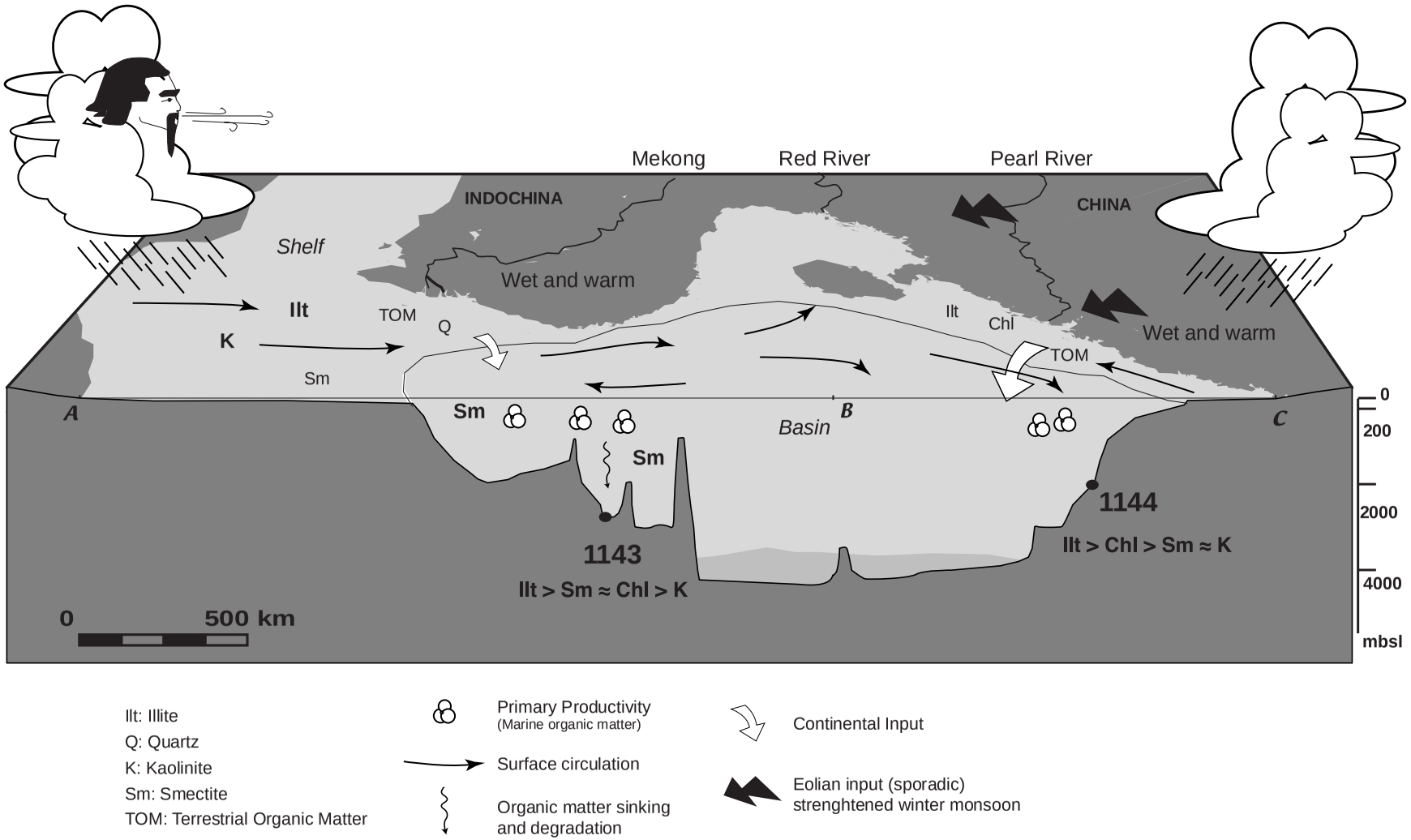

Fig. 13: Schematic model of the oceanographic, climatic and sedimentological situation of the SCS characterizing interglacial periods, during the last 140,000 years. Interglacial conditions are considered as denoted by strong summer monsoon activity and high sea level. See text and legend for details.

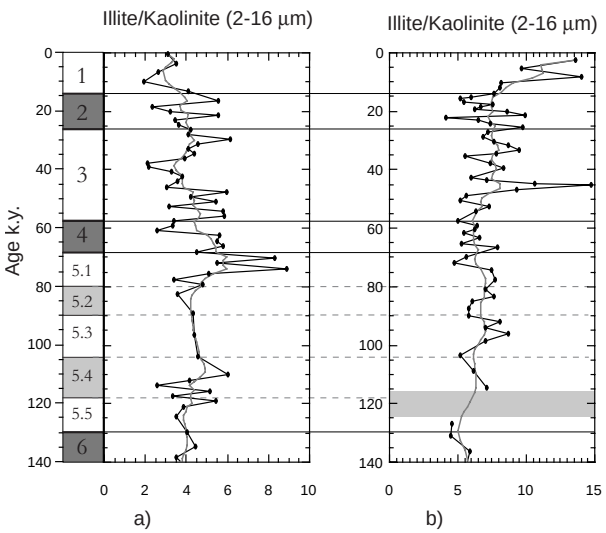

Fig. 14: Illite/kaolinite ratio for a) Site 1143 and b) Site 1144. The ratio between these two clay minerals may be regarded as an indicator of the relative strength of chemical (low ratio) and physical (high ratio) weathering. Age and MIS as in figure 3.

to the composition of the Toba ashes (Beauregard et al., 1998; Middlemost, 1985).

Clay minerals at Site 1144 reflect a continental source, micas and chlorite being the main constituents of clays at this site. During stage 5 and high sea level, Pearl river input and current transport from the East China Sea (ECS) through the open Taiwan strait (Chen, 1978) were the main vectors responsible of clay and mineral distribution at the northern site (Fig. 13). High amounts of kaolinite could testify to enhanced wetness on the Asian continent and important chemical weathering during interglacial 5. During glacial stages 4-2 the situation at Site 1144 is reversed compared to Site 1143: low amounts of kaolinite and micas are paralleled by increased quantities of chlorites. We prefer to explain these features invoking both changes in climatic conditions and weathering regime on the continent and changes in ocean circulation. During glacials, the Asian continent underwent dry and cold climate, which strongly reduced chemical weathering and hydrolysis, and hampered the formation of kaolinite. This is also shown by decreasing values of illite crystallinity, a proxy of chemical alteration (Fig. 8). Because the nature and probably the source of illite to both sites is most likely the same (Fig. 7), it is not surprising that illite crystallinity shows the same trend (Fig. 8). As aridity is expected to intensify during glacials on the continent, as indicated by many proxies, we should then expect also illite contents to increase at Site 1144, which is not the case. The closing of the Taiwan strait probably interrupted the input of material from the ECS shelf, whose sediments are rich in illite. The connection between the SCS and the Pacific ocean during glacials was only provided by the Bashi strait, between Luzon and Taiwan. Kolla et al. (1980) reported surface sediments east of the coast of Luzon rich in chlorite but relatively depleted in illite, compared to Asian continent sediments. This enrichment in chlorite is probably related to the presence of chloritic schistose rocks on the island (Kolla et al., 1980). Oceanic circulation during glacials could have prompted the transport of chlorite-enriched sediments from Luzon into the SCS (Fig. 15). Arid conditions on the Asian continent during glacials are also confirmed by the illite/kaolinite ratio at Site 1144 (Fig. 14), which increased during stages 4-2, indicating the predominance of physical weathering.

Coarser granulometry at Site 1144 than at Site 1143 is the expression of a more proximal location. Despite the fact that Site 1144 is probably a site of focused sedimentation, as testified by extremely high sedimentation rates (Wang et al., 2000), and that most of the deposits are originated by winnowing and transport on nearby sites, episodes of strengthened eolian input are recorded by higher percentages of silt material and variations in the median grain size, observed throughout the studied interval. Peaks in median at Site 1144 correlate within error with peaks at Site 1143 (Table 2). Despite the low time resolution of our study, we observe a remarkable correspondence between the high values in the median grain size at both sites and peaks in quartz median diameter measured in the Luochan

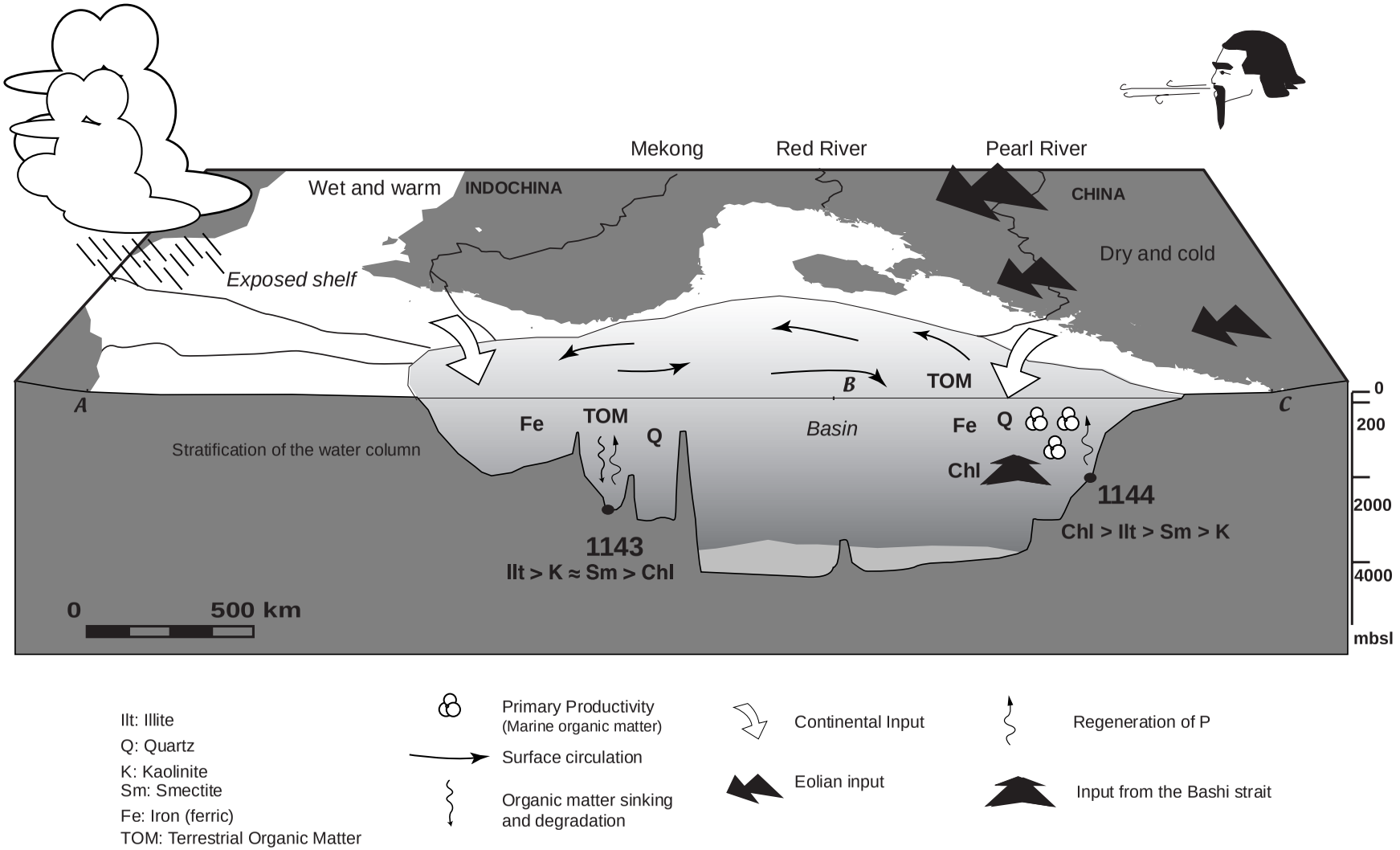

Fig. 15: Schematic model of the oceanographic, climatic and sedimentological situation of the SCS characterizing glacial periods, during the last 140,000 years. Glacial conditions are considered as denoted by strong winter monsoon activity and low sea level. Most of the continental shelf surrounding the SCS is exposed. See text and legend for details.

loess succession (Table 2; An and Porter, 1997; Porter and An, 1995). Porter and An (1995 and 1997) interpreted these features as representing periods of increased winter monsoon intensity and loess development also during interglacial periods, and they correlated them to cold events recorded in the North Atlantic region. MAR of detrital material at Site 1144 are highly dependent on sedimentation rates, but peaks are mainly observed during stages 4-2 and all of them correspond to peaks in median grain size, most likely related to enhanced eolian transport from the continent. On the other hand, coarser material at around 9 ka could be the evidence of early Holocene strengthened summer monsoon, which implies increased rainfall and consequent high fluvial input (Wang et al., 1999).

4.2. Organic matter and nutrients: key to productivity and sedimentation

As indicated by Rock-Eval data and TOC/N_{tot}, organic material at Sites 1143 and 1144 is composed by a mixture of terrestrial and degraded marine organic matter. TOC/P_{org} ratios at Site 1143 are close to the Redfield value (about 106) characteristic of marine phytoplankton (Fig. 10). This is in contradiction with the Rock Eval data indicating degraded organic matter constituted by a mixture of terrestrial and marine material, which should imply relatively high TOC/P_{org} ratios (> 300). High organic P relative to organic carbon has been observed in different marine environments, especially in settings characterized by fine-grained sediments, as it is the case for Site 1143. Good correlation of organic-bound P and clays suggests sorption of organic P onto clay mineral surfaces and this may prevent remineralization of phosphorus and preferentially preserve it compared to organic carbon (Ruttenberg and Gõni, 1997). TOC/P_{org} ratios at Site 1144, on the other side, reach higher values, especially at around 100 ka and during stages 4-2. These higher ratios may reflect a mixture of terrestrial and marine organic matter with enhanced input of terrestrial material during glacial periods and arid spells during interglacials.

Degradation of organic material is normally considered as the main source of reactive P to pore waters and sediments. Dissolved P is then redistributed to different sedimentary phases or regenerated and diffused back in the water column, depending on bottom water conditions (Jarvis et al., 1994). The ratio between organic C and reactive P (sum of Fe-bound, authigenic and organic-bound P) in sediments may give indications about the presence of alternate sources of dissolved P and/or of enhanced regeneration. Generally, low TOC/P_{reac} ratios from Sites 1143 and 1144 indicate an excess of reactive P compared to organic carbon, pointing to the presence of another source of reactive P, such as river discharge and/or dissolution of fish debris, as it is the case for sediments in Oman margin (Schenau et al., 2000). Higher values, even though lower than Redfield ratios, may indicate periods characterized by less intense precipitation and/or conservation of reactive phosphorus relative to organic carbon. Relatively high values for TOC/P_{reac} are observed during glacial stages 4-2 at both sites. This may be explained either by reduced input of P to the SCS, or enhanced regeneration and loss to the water column, due for instance to oxygen depletion in bottom waters. High reactive P MAR during glacial periods, as well as other detrital indices MAR, all indicate increased glacial continental contribution to sedimentation (Fig. 5). These results reasonably exclude the hypothesis of a decreased glacial P input, suggesting, therefore, that reactive P was preferentially regenerated and recycled back to the water column, probably in relation to oxygen depleted conditions of bottom waters (Wang et al., 1999), which hampered the precipitation of the reactive phases (Ingall and Jahnke, 1994). This conclusion agrees with a scenario characterized by glacial

reduced circulation and increased oxygen deficiency in intermediate and bottom waters, and applies to both sites. In fact, during glacial periods, Site 1144 is characterized by extremely high sedimentation rates (up to 2 m/k.y., Bühring, MG) and the consistent input of detrital material as well as organic matter, as testified by TOC MAR, could have fostered or reinforced already existent dysaerobic conditions. The glacial situation in the southern region of the SCS is characterized by a tropical climate, with enhanced precipitation and the establishment of a large fluvial system. The enhanced input of fresh water, as is also corroborated by the reconstruction of sea surface salinity (SSS) values using foraminifera (Wang et al., 1999 and references therein), may have triggered periodic stratification of the water column and consequent oxygen depletion.

Upwelling is known to occur along the Vietnamese coast during summer monsoon periods, and evidence of the same phenomenon during interglacial times exists: high percentages of calcite are observed at Site 1143 at the boundaries between stages 6-5 and 2-1, and persist all through stage 5.5 and the Holocene. Calcite MAR are high during stage 5.5, while relatively low values during glacial stages possibly imply diminished marine productivity due to weakened upwelling. Carbon isotopic data on foraminifera collected in cores from the southern SCS agree with our assumption, based on carbonate MAR, of high productivity during stage 5.5 (Wang et al., 1999).

High nutrients levels during glacials and deglaciation, as resulting from strengthened input of material from the continent (see MAR of Fe and detrital minerals) along with recycling from organic matter degradation (dissolved P), could have sustained high primary production at the northern site. This scenario has already been suggested by Wang et al. (1999), who used $\delta^{13}C$ of foraminifera to reconstruct fertility of surface and subsurface waters. Despite the fact that TOC at Site 1144 is a mixture of marine and terrestrial organic matter, the similarity in trend between TOC concentration and chlorins concentrations, may indicate high productivity during glacial and arid periods, where the two records display the highest values and highest similarity. In fact, high input of terrestrial organic matter would imply high nutrients from the land, which is consistent with the indications given by detrital proxies.

Recent studies on nitrate concentrations in SCS surface waters (for a review, see Kienast, 2000) indicate that nitrates are completely consumed by primary producers and that the SCS is consequently a nitrate-limited environment. Therefore, sedimentary $\delta^{15}N$ variability could be the expression of changes in circulation, of contribution of terrigenous organic material, fluctuation in oxygen content in the water column, and/or nitrogen fixation (Higginson, MG). One major concern while studying nitrogen isotopes from clay-rich environments, is to assess the influence of inorganic nitrogen on the isotopic signature of the bulk sediment. To estimate this influence, data from both sites were plotted on a TOC wt% vs. N_{tot} wt% diagram (Fig. 11b) (Hedges et al., 1988). We have performed statistical analysis on the distribution of the residuals (difference between each data point and its estimate) in order to use the correlation for data from Site 1144. The residuals show a normal distribution, so despite the low correlation coefficient (r^2=0.327 for Site 1144), we can confidently use the linear fit. The positive x-axis intercept for 1144 samples indicates that inorganic nitrogen, most likely sorbed on clay minerals, may account for at least 30% of the total nitrogen pool of these sediments. Sediments at this site are rich in clays whose main constituent of the fraction <2 μm is illite (Fig. 6). It is known that illites can easily incorporate ammonium (NH_4^+) at the place of K^+ in interlayer exchange sites. A recent study on Arctic sediments shows that the nitrogen

isotopic signature of inorganic nitrogen bound in clay minerals is lower than the one of organic nitrogen, and that most likely it bears a signal formed on land (Schubert and Calvert, 2001). If the isotopic signal of sediments from Site 1144 were influenced by adsorption of inorganic nitrogen, low values of $\delta^{15}N$ should correspond to low values of the TOC/N_{tot} ratio, which is not the case (Fig. 10). In fact, $\delta^{15}N$ and TOC/Ntot ratios are anti-correlated throughout stages 4-2 (r^2=0.47), as the low values in nitrogen isotopes observed during glacial stage 2 and the Holocene coincide to high values of the TOC/N_{tot} molar ratios, which presumably indicate a more important contribution of terrestrial organic material. We still lack a clear understanding of the isotopic differences between organic and inorganic nitrogen, but seen the relation between $\delta^{15}N$ and TOC/N_{tot}, we consider nitrogen isotopes of bulk sediment as mainly reflecting the isotopic signature of both marine and terrestrial organic material, despite the presence of inorganic nitrogen.

$\delta^{15}N$ values indicate that higher input of terrestrial organic material at Site 1144 started probably before the boundary between stages 2 and 1, and continued throughout the Holocene, where nitrogen isotopes are lowest. This is probably the result of the flooding of the shelf, the consequent reworking of terrestrial organic matter, and the increased rainfall on the Asian continent, related to the reinforced summer monsoon. Nitrogen isotopes are almost invariable at Site 1143. The shift at stage 5.3, leading to slightly low values of glacial stages 4-2 correlates to the increase of both TOC and detrital concentrations and MAR. This shift in $\delta^{15}N$ values may record 1) an increased contribution of terrestrial organic matter, 2) nitrogen fixation, due to complete utilization of nitrate if other nutrients are present (see phosphorus regeneration during the same period as discussed above), or 3) reduced fractionation by phytoplankton caused by high nitrate levels in surface waters. The somehow higher TOC/N_{tot} molar ratios characterizing this interval point to the first hypothesis as the most plausible explanation. In any case, the augmented input of material from land and the exposed shelf could also have risen nutrient levels in surface water during glacials (Fig. 15).

Generally, TOC/N_{tot} ratios of sediments from Sites 1143 and 1144 averages 6 and 11, respectively. The low correlation between TOC and total N at both sites (r^2=0.019 for Site 1143 and r^2=0.327 for Site 1144, Fig. 11b) implies, again, that organic matter is constituted by a variable mixture of a terrestrial and a marine end-member. The difference in the TOC/N_{tot} ratios between the two sites is in agreement with the finding that sediments from Site 1144 bear an important percentage of inorganic nitrogen, possibly related to its closer position to the continent and to higher detrital input.

The distribution of Fe-bound P is controlled mainly by redox conditions in the sediments, by variations in sedimentation rates, and the degree of crystallization of the Fe-oxides (Slomp, 1997; Sundby et al., 1986; Van Cappellen and Ingall, 1994). The lack of correlation observed at Site 1143 between ferric iron and Fe-bound P (r^2 = 0.0221) may be due to the presence of better crystallized detrital iron-oxides (Schulz and Zabel, 2000; Slomp et al., 1996): dissolved P is adsorbed in small concentrations on the surface of Fe oxide-bearing minerals and it is released under reducing conditions, while a large part of well crystallized Fe-oxides is preserved. The upward increase of Fe-bound P may be the result of a larger amount of amorphous, diagenetically formed Fe-oxides compared to glacial periods, when Fe-oxides were provided by eolian and river input from the continent. The situation is far more complex at Site 1144, where the high sedimentation rates and the sediments rich in organic matter may have promoted oxygen depletion in the sediments, reducing the adsorbing capacity of Fe-oxides.

The most prominent peaks in Fe-bound P concentrations are strongly related to peaks in sedimentation rates, as it is the case for the interval at around 100 ka and during stage 4. High sedimentation rates may fasten the burial of sediments and P adsorbed on Fe-oxides may have been preserved.

The ferric Fe record at Site 1144 presents a well-defined minimum at stages 2-1 boundary, already below the zone of sulfate reduction (see Inorganic Geochemistry chapter, Site 1144 in Wang et al., 2000), which corresponds to a maximum in authigenic pyrite (Fig. 10) and to a minimum in magnetic susceptibility (Laj and Solheid, MG). At the base of this minimum, where pyrite percentages are higher, Fe-bound P is low, possibly recording important changes in sedimentation. Post-depositional enrichments of Fe sulfides, such as authigenic pyrite, have been observed in different sedimentary environments, i.e. the Amazon deep-sea fan (Kasten et al., 1998). The process responsible of this phenomenon is believed to be the installation of a nonsteady-state diagenetic regime, where the redox boundary remains fixed at a certain fixed depth for a long time, promoting the precipitation of authigenic minerals. Kasten and co-authors recognized the significant drop in sedimentation rates and in organic carbon accumulation characterizing the transition between stage 2 and the Holocene as the controlling factor (Kasten et al., 1998). As it is observed also for Site 1144 in the SCS, the boundary between stage 2 and 1 is marked by a 4-fold decrease in sedimentation rates (Bühring, MG), which easily explains the observed feature. The decreased sedimentation rate, as inferred both by isotopic stratigraphy and sedimentary geochemistry at Site 1144, may indicate that sea level started rising already during the last interval of stage 2. Tropical sea level records south of 35°N clearly indicate that sea level changes after the Last Glacial Maximum may have began as early as 18 ka (Winkler and Wang, 1993). Moreover, Wang and co-authors (1999), studying two cores situated on the northern margin of the SCS in a close location to Site 1144, observed that clay content started to increase at around 18 ka and they interpreted this feature as the signal of the onset of summer monsoon and more important fluvial input. The enhanced input of terrestrial organic matter at Site 1144, as interpreted using nitrogen isotopes, may in fact indicate reworking of terrestrial material deposited on the exposed shelf within glacial times, during the flooding of the shelf itself.

5. CONCLUSIONS

The multiproxy study of sediments from ODP Sites 1143 and 1144 provides information on the evolution of sedimentation and climate in the SCS area during the last glacial-interglacial cycle. The complex interplay of monsoonal climate, which controls river and eolian input as well as current circulation, sea level variations, linked to global climate changes, and the different location of the sites in respect to the continent drives the distribution of sediments, of nutrients and organic matter in the SCS.

1) Interglacial periods are characterized by high sea level which permitted the connection of the SCS both with the Indian and the Pacific oceans. Sediments were derived from the Asian continent, the tropical islands surrounding the SCS, and the ECS, brought in by the inflow through the Taiwan strait. The circulation in the SCS was controlled by wind direction and by the overturn between summer and winter monsoons. High productivity was fostered by the presence of upwelling cells in the southern region of the SCS and by fluvial input of nutrients. Short arid and cold periods, characterized by enhanced eolian input, were common and possibly correlated to a more global climatic variability.

2) During glacial stages, sea level was about 120 m lower than during interglacial periods, changing in a drastic way the config-

uration of the basin. Most of the connections with the open ocean were shut down, oceanographic circulation changed, and the wide Sunda shelf was exposed and drained by a large fluvial system. Sediments previously deposited on the shelf were presumably reworked and deposited in deeper areas, and the changed current system brought into the sites sediments from other sources than the interglacial ones. Arid conditions on the Asian continent promoted the development of loess deposition and physical weathering, and the strengthened winter monsoon brought high amounts of detrital material and nutrients to the SCS. Reduced circulation caused by the closing of most of the connections with the open ocean, and stratification of the water column in the southern SCS, due to increased humidity on the tropical islands and associated intensified river discharge, fostered oxygen depletion in intermediate and bottom waters. These conditions hampered diagenetic deposition of dissolved reactive phosphorus, which was released from the sediments and re-diffused to the water column, where it helped in sustaining primary production.

3) The transition between stages 2 and 1 was marked by a severe drop in sedimentation rates, and, within the error given by isotopic stratigraphy uncertainty, the sea level started to rise as early as 18 ka. The Holocene was characterized by the re-establishment of humid conditions all over the Asian continent and of open circulation and connection with the Indian and the Pacific oceans. As for the interglacial stage 5, arid and cold periods, related to short intensification of the winter monsoon and to cold global episodes, sporadically affected the SCS area during the Holocene. The good correlation between terrestrial and marine records from the Southeast Asian region and records from the North Atlantic corroborates the existence and extent of a teleconnection between low and high latitudes.

Besides providing new mineralogical and geochemical data and a careful reconstruction of the history of sedimentation and climate during the last glacial-interglacial cycle, this study brings new evidences from the SCS region of the link between climate, continental weathering and productivity, which operated mainly during glacial periods. Similar multi-proxy studies of sediments from the SCS at higher time resolution are now needed to asses the importance and the extent of these processes and of the related feedback mechanisms, and the connection (leads and lags) with other climate forcing factors (atmosphere and ocean circulation, Milankovitch cycles).

Aknowledgements. The authors would like to express their gratitude to the captain, the crew and the technical staff of ODP Leg 184, for their precious help and assistance. F.T. thanks Juan Tian, Pinxian Wang, Christian Bürhing and Michael Sarnthein for kindly providing the isotopic stratigraphy for sites 1143 and 1144. The authors gratefully thank J. Richard, K. Hamila and H. Paul for preparation of samples and help in laboratory work. This study was supported by the University of Neuchâtel, Switzerland.

REFERENCES

Adatte, T. and Rumley, G., 1989. Sedimentology and mineralogy of Valanginian and Hauterivian in the stratotypic region (Jura mountains, Switzerland). In: J. Wiedmann (Editor), Cretaceous of the Western Tethys. Proc. 3rd Int. Cretaceous Symp., 1987, Tübingen, Germany, pp. 329-351.

An, Z.S., 2000. The history and variability of the East Asian paleomonsoon climate. Quaternary Science Review, 19: 171-187.

An, Z.S. and Porter, S.C., 1997. Millennial-scale climatic oscillations during the last interglaciation in central China. Geology, 25(7): 603-607.

Anderson, L.D. and Delaney, M.L., 2000. Sequential extraction and analysis of phosphorus in marine sediments: Streamlining of the SEDEX procedure. Limnol. Oceanogr., 45(2): 509-515.

Beauregard, J.L., Carey, S., Sigurdsson, H., Mandeville, C. and Guichard, F., 1998. Correlating marine tephra layers to Krakatau volcano and the Toba caldera, Indonesia, AGU spring meeting, Boston, pp. 359.

Bühring, C., Sarnthein, M. and Party, L.S.S., 2000. Toba ash layers in the South China Sea: evidence of contrasting wind directions during eruption ca 74 ka. Geology, 28(3): 275-278.

Chamley, H., 1989. Clay sedimentology. Springler-Verlag.

Chen, P.-Y., 1978. Minerals in bottom sediments of the South China Sea. Geol. Soc. of Amer. Bull., 89: 211-222.

Eaton, A.D., Clesceri, L.S. and Greenberg, A.E. (Editors), 1995. Standard methods for the examination of water and wastewater.

Espitalié, J., Deroo, G. and Marquis, F., 1986. La pyrolyse Rock-Eval et ses applications - III partie. Rev. Inst. Fr. Pet., 41(1): 73-89.

Hedges, J.I., Clark, W.A. and Cowie, G.L., 1988. Organic matter sources to the water column and surficial sediments of a marine bay. Limnol. Oceanogr., 33: 1116-1136.

Huang, C.-Y., Liew, P.-M., Zhao, M., Chang, T.-C., Kuo, C.-M., Chen, M.-T., Wang, C.-H. and Zheng, L.-F., 1997. Deep sea and lake records of the Southeast Asian paleomonsoons for the last 25 thousand years. Earth and Planetary Science Letters, 146: 59-72.

Ingall, E. and Jahnke, R., 1994. Evidence for enhanced phosphorus regeneration from marine sediments overlain by oxygen depleted waters. Geochimica et Cosmochimica Acta, 58(11): 2571-275.

Jarvis, I., Burnett, W.C., Nathan, Y., Almbaydin, F.S.M., Attia, A.K.M., Castro, L.N., Flicoteaux, R., Hilmy, M.E., Husain, V., Qutawnah, A.A., Serjani, A. and Zanin, Y.N., 1994. Phosphorite geochemistry: state-of-art and environmental concerns. Eclogae geol. Helv., 87(3): 643-700.

Kasten, S., Freudenthal, T., Gingele, F.X. and Schulz, H.D., 1998. Simultaneous formation of iron-rich layers at different redox boundaries in sediments of the Amazon deep-sea fan. Geochimica et Cosmochimica Acta, 62(13): 2253-2264.

Kienast, M., 2000. Unchanged nitrogen isotopic composition of organic matter in the South China Sea during the last climatic cycle: Global implications. Paleoceanography, 15(2): 244-253.

Kolla, V., Nadler, L. and Bonatti, E., 1980. Clay mineral distributions in surface sediments of the Philippine Sea. Oceanologica Acta, 3(2): 245-250.

Koopmann, B., 1981. Saharan dust deposition in the subtropical Atlantic during the last 25,000 years. 'Meteor' Forschungsergeb, C 5: 23.54.

Kübler, B., 1984. Les indicateurs des transformations physiques et chimiques dans la diagenèse. Temperature et calorimetrie., Thermométrie et barométrie géologique. Société Française de Minéralogie et de Cristallographie, Paris, pp. 489-596.

Kübler, B., 1987. Dosage quantitatif des minéraux majeurs des roches sédimentaires par diffraction X. Cahier de l'Institut de Géologie de Neuchâtel, Série ADX.

Lafargue, E., Espitalié, J., Marquis, F. and Pillot, D., 1996. Rock Eval 6 applications in hydrocarbon exploration, production and in soil contamination studies, Latin American Congress on Organic Geochemistry, Cancun.

Langford, F.F. and Blanc-Valleron, M.-M., 1990. Interpreting Rock-Eval Pyrolysis data using graphs of Pyrolizable Hydrocarbons vs. Total Organic Carbon. AAPG, 74(6): 799-804.

Middlemost, E.A.K., 1985. Magmas and magmatic rocks. An introduction to igneous petrology. Longman, London, 266 pp.

Moore, D.M. and Reynolds, R.C.J., 1997. X-Ray diffraction and the identification and analysis of clay minerals. Oxford University Press.

Oinuma, K., Shimoda, S. and Sudo, T., 1972. Triangular diagrams of surveying chemical composition of chlorites. J. Tokyo Univ., 15: 1-13.

Pelejero, C., Kienast, M., Wang, L. and Grimalt, J.O., 1999. The flooding of Sundaland during the last deglaciation: imprints in hemipelagic sediments from the southern South China Sea. Earth and Planetary Science Letters, 171: 661-671.

Porter, S.C. and An, Z., 1995. Correlation between climate events in the North Atlantic and China during the last glaciation. Nature, 375: 305-308.

Rey, M. and Kübler, B., 1983. Identification des micas des séries sédimentaires par diffraction X, à partir de la série harmonique (001) des préparation orientées. Bull. suisse de minéralogie et pétrographie, 63: 13-36.

Ruttenberg, K.C., 1992. Development of a sequential extraction method for different forms of phosphorus in marine sediments. Limnology Oceanography, 37(7): 1460-1482.

Ruttenberg, K.C. and Gõni, M.A., 1997. Phosphorus distribution, C:N:P ratios, and δ^{13}Coc in artic, temper-

ate, and tropical coastal sediments: tools for characterizing bulk sedimentary organic matter. Marine Geology, 139: 123-145.

Schenau, S.J., Slomp, C.P. and De Lange, G.J., 2000. Phosphogenesis and active phosphorite formation in sediments from the Arabian Sea oxygen minimum zone. Marine Geology, 169(1-2): 1-20.

Schönfeld, J. and Kudrass, H.-R., 1993. Hemipelagic sediment accumulation rates in the South China Sea related to late quaternary sea-level changes. Quaternary research, 40: 368-379.

Schubert, C.J. and Calvert, S.E., 2001. Nitrogen and carbon isotopic composition of marine and terrestrial organic matter in Arctic Ocean sediments: implications for nutrient utilization and organic matter composition. Deep-Sea Research I, 48: 789-810.

Schulz, H.D. and Zabel, M., 2000. Marine Geochemistry. Springer-Verlag, Berlin, 455 pp.

Sirocko, F., Garbe-Schönberg, D., McIntyre, A. and Molfino, B., 1996. Teleconnections between the subtropical monsoons and high-latitudes climates during the last deglaciation. Science, 272: 526-529.

Slomp, C.P., 1997. Early diagenesis of phosphorus in continental margin sediments, Ph.D. Thesis, Den Burg, Texel, The Netherlands, 178 pp.

Slomp, C.P., Epping, E.H.G., Helder, W. and van Raaphorst, W., 1996. A key role of iron-bound phosphorus in authigenic apatite formation in North Atlantic continental platform sediments. Journal of Marine Research, 54: 1179-1205.

Sundby, B., Anderson, L.G., Hall, P.O.J., Iverfeldt, A., Van der Loeff, M.M.R. and Westerlund, S.F.G., 1986. The effect of oxygen on release and uptake of cobalt, manganese, iron and phosphate at the sediment-water interface. Geochimica et Cosmochimica Acta, 50: 1281-1288.

Van Cappellen, P. and Ingall, E.D., 1994. Benthic phosphorus regeneration, net primary production, and ocean anoxia: a model of the coupled marine biogeochemical cycles and phosphorus. Paleoceanography, 9(5): 677-698.

Wang, L. and Oba, T., 1998. Tele-connections between East Asian Monsoon and the High-latitude climate: A Comparison between the GISP 2 Ice Core record and the High resolution Marine records from the Japan and the South China Sea. The Quaternary Research, 37(3): 211-219.

Wang, L., Sarnthein, M., Erlenkeuser, H., Grimalt, J., Grootes, P., Heilig, S., Ivanova, E., Kienast, M. and Pflaumann, U., 1999. East Asian Monsoon climate during the Late Pleistocene: high-resolution sediment records from the South China Sea. Marine Geology, 156: 245-284.

Wang, L. and Wang, P., 1990. Late Quaternary Paleoceanography of the South China Sea: glacial-interglacial contrasts in an enclosed basin. Paleoceanography, 5(1): 77-90.

Wang, P. et al., 2000. Proc. ODP, Init. Repts., Vol. 184. Ocean Drilling Program, College Station, TX.

Webster, P.J., 1987. The elementary monsoon. In: J. Fien, stephens, P. (Editor), Monsoon. Wiley, New York, pp. 3-32.

Winkler, M.G. and Wang, P.W., 1993. The Late-Quaternary Vegetation and Climate of China. In: H.E.J. Wright et al. (Editors), Global climate since the Last Glacial Maximum. University of Minnesota Press, pp. 221-261.

CHAPTER 4

Carrying cores on the catwalk of the Joides Resolution (1999)

*Dysaerobic conditions during Heinrich events 4 and 5: evidence from phosphorus distribution in core SU 90-09, North Atlantic Ocean**

ABSTRACT

Dissolved reactive phosphorus undergoes diagenetic transformation once transferred into marine sediments. The degree of regeneration and redistribution of phosphorus depends on early diagenetic and environmental conditions, which may be linked to larger scale phenomena, such as bottom water circulation, water column ventilation and organic carbon flux. Phosphorus phases of the <50 μm fraction of deep sea sediments from core SU 90-09 (North Atlantic, 43°31'N – 30°24'W, 3375 m.b.s.l.) have been analyzed using a sequential extraction technique (SEDEX method), in order to reconstruct phosphorus geochemistry during Heinrich events 4 and 5. The comparison with Holocene samples indicates that post-deposition diagenetic transformation has not affected phosphorus distribution in the deeper part of the sediments. Total and reactive phosphorus average 0.4 ± 0.04 mg/g and 0.3 ± 0.05 mg/g, respectively, and are comparable to values found in analogue deep-sea environments in the North Atlantic. Detrital phosphorus, the phase linked to igneous and metamorphic derived material, sharply increases during Heinrich events and covaries with the ice-rafted debris (IRD) record, whereas authigenic and Fe-bound phosphorus phases, both influenced by redox conditions, decrease or even disappear. These findings suggest that during Heinrich layers deposition, environmental parameters hampered the precipitation of these phases. Large fresh water discharges in relation to iceberg surges may have provoked a temporary stratification of the water column. Accordingly, dysaerobic bottom water conditions may have fostered the loss of dissolved phosphorus from the sediments to the water column, in a direct and rapid response to the changed conditions. Decreasing trends in organic matter elemental ratios (TOC/P_{org}) and Rock-Eval oxygen index values, along with the presence of partly authigenic dolomite and ankerite within Heinrich layers, also support this assumption.

1. INTRODUCTION

During the last glaciation (marine isotope stages 2-4), six episodes of enhanced ice-rafted debris (IRD) supply produced the so-called Heinrich layers (HLs; HEINRICH, 1988; BROECKER et al., 1992; ANDREWS, 1998). These layers, found across the North Atlantic down to 40°N in the area called IRD belt (RUDDIMAN, 1977), contrast sharply with ambient glacial sedimentation. They are characterized by the sequential deposition of high amounts of lithogenic material, which originated both from European and Canadian soil and rock sources (GROUSSET et al., 2000), high detrital carbonate contents (BOND et al., 1992), low amounts of foraminiferal tests (HEINRICH, 1988; BROECKER et al., 1992) and high supply of organic matter derived from terrestrial sources (e.g. ROSELL-MELÉ et al., 1997; HUON et al., in press). There is convincing evidence that HL deposition was accompanied by the formation of a fresh water lid (BOND et al., 1992), which possibly stopped or strongly reduced North Atlantic deep water formation and thermohaline circulation (BROECKER, 1994; PAILLARD and LABEYRIE, 1994; MASLIN et al., 1995; VIDAL et al., 1997; ZAHN et al., 1997). The signature of Heinrich events has been not only found in North Atlantic sediments (i.e. Arabian and South China sea; SCHULZ et al.,

* This chapter by Federica Tamburini, Sylvain Huon, Philipp Steinmann, Francis E. Grousset, Thierry Adatte and Karl B. Föllmi has been submitted for publication in *Geochimica et Cosmochimica Acta.*

1998; WANG et al., 1999), but also in terrestrial records (i.e. GRIMM et al., 1993; LOWELL et al., 1995; BENSON et al., 1996; SANCHEZ-GÕNI et al., 2000) and has been correlated with the Greenland ice core isotope record (BOND et al., 1993), pointing to possible tele-connections between high and low latitudes climate at short time scales.

The present study addresses the geochemical signature of Heinrich events 4 and 5 (at about 35 and 45 ka, respectively), as expressed in their marine phosphorus records. Phosphorus (P) is an essential nutrient, limiting oceanic productivity on geological time scale (TYRRELL, 1999). Being involved in biological processes and having a strong affinity to iron- and manganese oxides and hydroxides, the P cycle in marine sediments is rather complex and controlled by environmental conditions (for a comprehensive review see in JARVIS et al., 1994; KRAJEWSKI et al., 1994; FÖLLMI, 1996; DELANEY, 1998). Regenerated dissolved and reactive (biologically available) P is potentially redistributed to different sedimentary phases or rediffused into the water column, depending on chemical and physical parameters, such as alkalinity, dissolved oxygen levels, fluoride and phosphorus concentrations in pore waters, nature of sediments, and bio-irrigation (KRAJEWSKI et al., 1994; VAN CAPPELLEN and INGALL, 1994; SLOMP, 1997; COLMAN and HOLLAND, 2000). Being influenced by parameters which may change quite rapidly, P phase concentrations in sediments are expected to fluctuate at a comparable rate. Thus, a clear understanding of P geochemistry in the marine environment during and between Heinrich events may contribute to a better interpretation of the bottom water environment (oxic/suboxic conditions), water column dynamics, and circulation. In that sense, constraints on the redistribution and recycling of P during the deposition of HLs are consequential as phosphate concentrations in bottom waters, inferred from Cd/Ca and $\delta^{13}C$ measurements on benthic foraminifers, are widely used to assess changes in oceanic circulation (e.g. shut-off of the thermohaline circulation and northward penetration of nutrient-rich waters from the South Atlantic Ocean; BERTRAM et al., 1995; MARCHAL et al., 1999). The determination of the extent of recycling of dissolved phosphorus from sediments and its

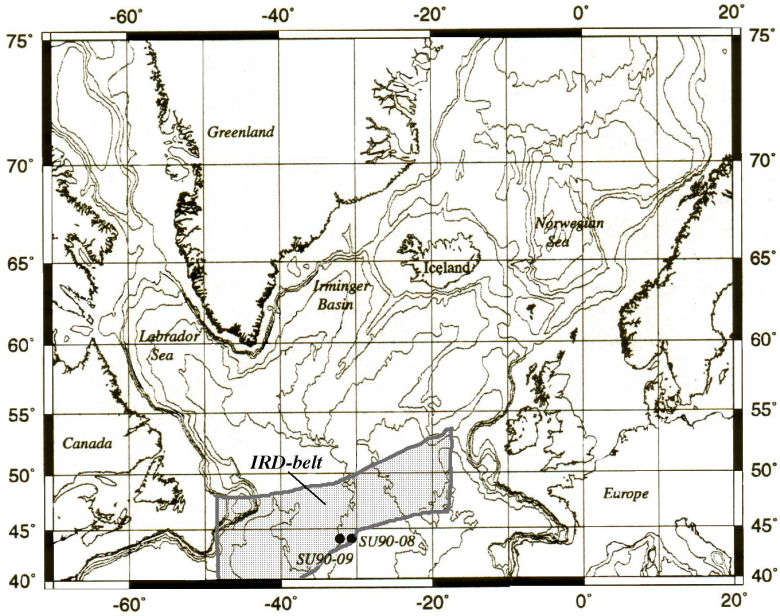

Fig. 1: Location of core SU 90-09 in the central North Atlantic. The map was obtained through the Aquarius Geomar Online Map Creation (http://www.aquarius.geomar.de/omc). The gray area represents the "Ruddiman ice-rafted detritus belt" (RUDDIMAN, 1977).

Table 1: Phosphorus sequential extraction technique (SEDEX; Ruttenberg, 1992).

Step name	Treatments	P component isolated *a*	Errors *b*	Detection limits *c*
Iron-bound P *d*	10 ml CBD solution (6hr) (0.22 M sodium citrate, 0.11 M sodium bicarbonate 0.13 M sodium dithionite) 10 ml 1M MgCl2 (2hr) 10 ml H2O (2hr)	Exchangeable or loosely sorbed P Reducible or reactive iron-bound P **PLUS Ferric Fe**	3-6%	0.03
Authigenic P *e*	10 ml 1M Na-acetate buffered to pH 4 with acetic acid (5hr) 10 ml 1M MgCl2 (2hr) 10 ml 1M MgCl2 (2hr) 10 ml H2O (2hr)	Carbonate fluorapatite (CFA) biogenic hydroxyapatite	2-7%	0.025
Detrital P *e*	10 ml 1N HCl (16 hr)	Detrital fluorapatite-bound P	3-5%	0.003
Organic P *e*	1 ml 50% (w/v) MgNO3, dry in low oven, ash at 500°C (2 hr) 10 ml 1N HCl (24 hr)	Organic-bound P	2-5%	0.004

a: Concentrations of all phases are expressed in mg/g of sediment.
b: Errors for each phase determination are considered as the rel. standard deviation calculated on replicate analyses of consistency standards.
c: Detection limits are considered as 3 * rel. standard deviation calculated on replicate analyses of blank solutions.
d: Iron-bound phosphorus and ferric Fe concentrations were measured using an ICP-AES.
e: The other phases were measured using a spectrophotometer. Sample solutions were diluted in distilled water and a color developping agent was added to the solution, following the ascorbic acid method for phosphates (Eaton et al., 1995).

contribution to the total phosphate concentration in bottom waters during Heinrich events may, therefore, help in future biogeochemical and oceanographic modelling.

The aim of this study is to provide a high resolution record of fine-sized (<50 μm) P compounds in marine sediments from a North Atlantic deep-sea core (including HL_4 and HL_5), using a sequential P extraction procedure in order to: 1) estimate the contribution of detrital P during the phases of enhanced ice-rafting detritus supply; 2) determine the influence of this supply on reactive P redistribution in sediments; and 3) discuss some of the factors controlling bottom water conditions during Heinrich events using P sedimentary cycling as a proxy for oxic vs. anoxic conditions.

2. MATERIAL AND METHODS

Sediment samples were recovered from piston core SU90-09 (43°05'N - 31°05'W, 3375 mbsl), located in the central North Atlantic on the western side of the Mid-Atlantic Ridge (Fig. 1; GROUSSET et al., 2001; HUON et al., in press). Stratigraphic correlation with reference core SU90-08 (43°31'N–30°24'W) and downcore position of HL_1-HL_5 were performed using AMS ^{14}C ages on *Neogloboquadrina pachyderma* sin. shells, coarse lithic grains (>150 μm) counts under the binocular, low-field magnetic susceptibility and grey-scale reflectance records, following the methods described in (GROUSSET et al., 1993; CORTIJO et al., 1995; GROUSSET et al., 2001).

Our study focuses on fine size fraction (<50 μm) of 83 samples recovered within and between HL_4 and HL_5. Samples were taken from 130 cm to 200 cm core depth at 1 cm interval between HLs, and at 0.5 cm within HL_4 and HL_5 that were identified at core depths 144.0 - 153.5 cm and 187.0 - 193.5 cm, respectively (HUON et al., in press). Thirteen samples between 10 and 30 cm, representing Holocene (post glacial) sediments, were also analyzed in order to better constrain the possible overprint of diagenesis on P. The <50 μm size fraction of sediments was used because it has been shown that fine-grained fractions also record enhanced ice-rafting supply

(HUON and RUCH, 1992; JANTSCHIK and HUON, 1992; HUON and JANTSCHIK, 1993). Morerover, the high lithic supply contained in coarse-sized fractions may reduce the analytical precision of organic matter concentration measurements, limiting the reliability of direct comparison with ambient sediments that bear low amounts of IRD (HUON et al., in press).

Phosphorus (P) was extracted from the <50 μm size fraction of the sediment samples using the SEDEX method, a sequential extraction technique (RUTTENBERG, 1992; FILIPPELLI and DELANEY, 1996; ANDERSON and DELANEY, 2000). Fe-bound, authigenic, detrital and organic-bound P represent the four extracted P phases which are linked to different sedimentary sinks (see Table 1 for details, errors and detection limits of the method). Fe-bound and organic-bound P correspond to P linked to Fe and Mn oxi-hydroxides, and to organic matter, respectively. Carbonate-fluorapatite (CFA), a neo-formed P-bearing mineral, is the principal component of authigenic P. Detrital P, represented by metamorphic and igneous-derived apatite and P-bearing minerals, is considered non reactive, as it does not interfer with the biological cycle and it is not involved in the redox cycle (RUTTENBERG, 1992). Ferric Fe has been extracted during the first step of the SEDEX method (for details on the methodology, see Table 1 and SLOMP et al., 1996).

The approximate values of organic-bound hydrogen (in terms of hydrogen index, HI, mg HC/g TOC) and organic-bound oxygen (in terms of oxygen index, OI, mg CO_2/g sed.) were calculated by Rock-Eval pyrolysis (ESPITALIÉ et al., 1986). Because our samples are rich in carbonate minerals (i.e. calcite and dolomite), but have very low total organic carbon (TOC) contents (less than 0.5 %), the measured values could be potentially biased. The reason is that some of the CO_2 produced from carbonate decomposition during pyrolysis at relatively low temperature overlaps with the CO_2 originating from organic matter. In our samples this phenomenon leads to a systematic overestimation of OI, and to an underestimation of TOC and HI. We evaluated these effects by analyzing a subset of de-carbonated (1 M HCl) samples, which were selected both from ambient glacial and HLs sediments. The OI and HI values calculated before and after carbonate removal are well and linearly correlated (r^2 = 0.946 and 0.785 for OI and HI, respectively), and the carbonate-free samples reveal the same trends as the untreated samples (i.e. higher HI and lower OI within HLs compared to ambient glacial sediments). We, therefore, corrected the values obtained for bulk samples, using the linear correlations of OI and HI in carbonate-free vs. untreated samples. Even though the so-obtained absolute values are less accurate, the relative trends are still reliable and allow us to compare them with other organic matter proxies, such as $\delta^{13}C$, obtained on carbonate-free (<50 μm)

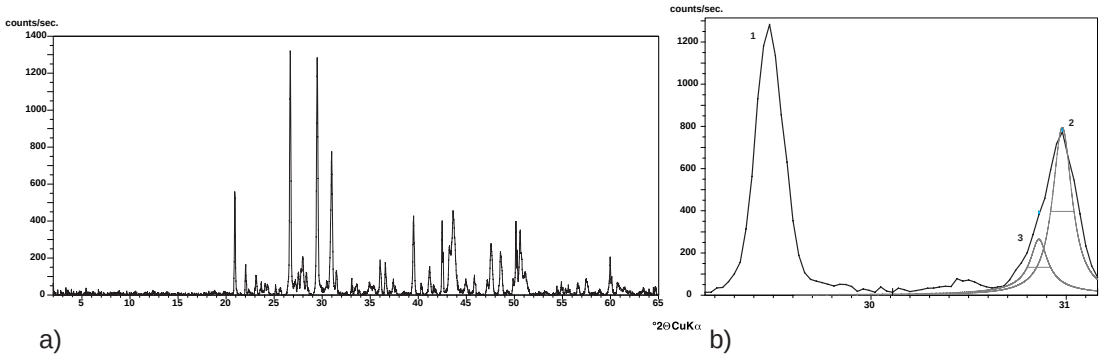

Fig. 2: a) Diffractogram of sample SU 153.5. b) Example of the deconvolution function (Pearson VII), used to separate the 104 (hkl) peak of dolomite (peak 2) from the 104 peak of ankerite (peak 3). Peak 1 represents the 104 peak of calcite.

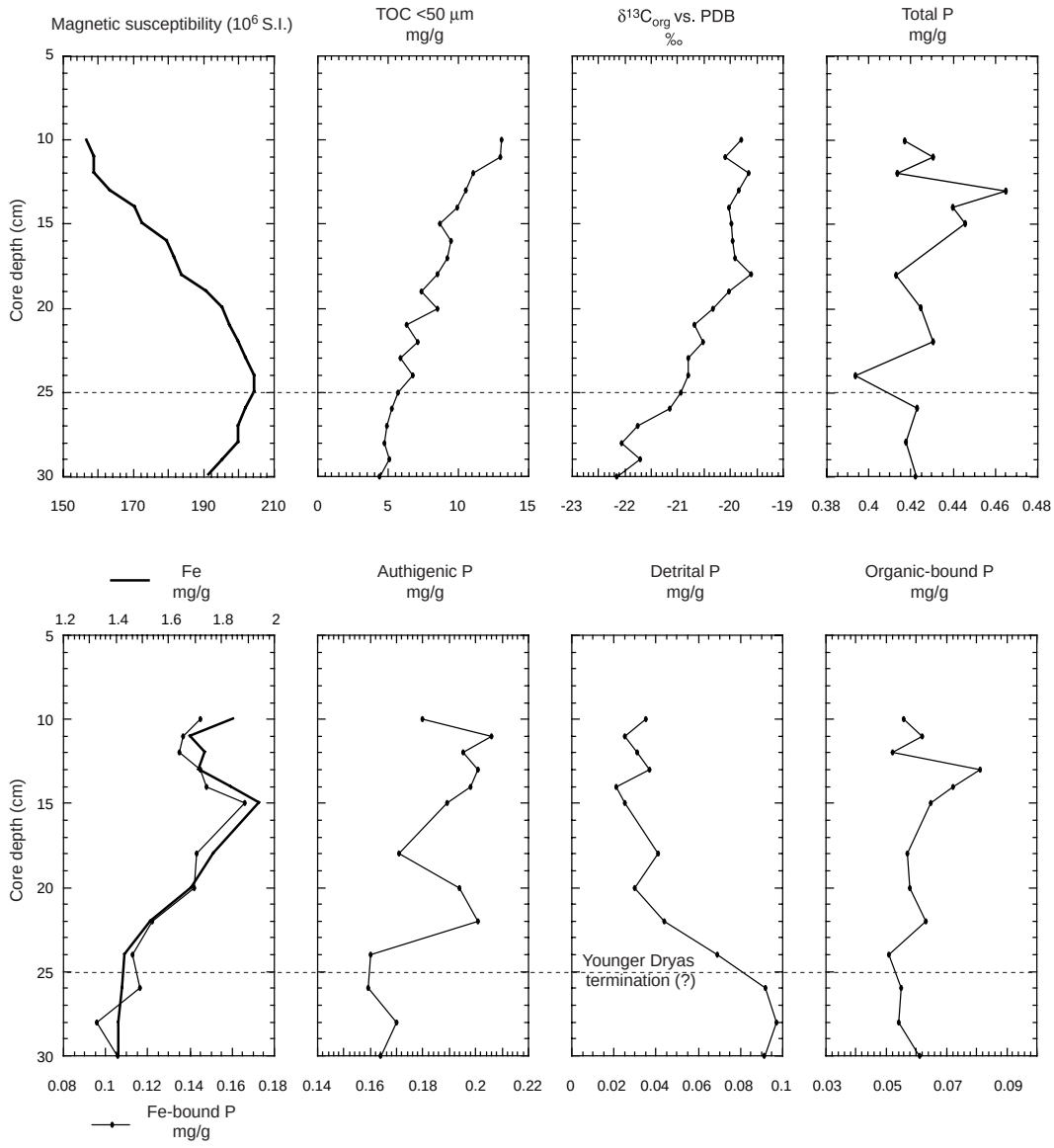

Fig. 3: Plots of down-core variations of a) Magnetic susceptibility (GROUSSET et al., 2001); b) TOC content and c) $\delta^{13}C$ of organic carbon of the <50 µm fraction (HUON et al., in press); d) total phosphorus, e) ferric Fe and Fe-bound P, f) authigenic P, g) detrital P and h) organic-bound P for the fine-sized fraction of Holocene samples from core SU 90-09. The dotted line represents the inferred Younger Drays termination (HUON et al., in press).

size fractions of the same samples (HUON et al., in press).

Bulk sediment mineralogy was determined by XRD (2θ CuKa, SCINTAG XRD 2000 Diffractometer), using a semi-quantitative estimation based on external standards (KÜBLER, 1987). Calcite, dolomite and ankerite form a solid solution, where Ca^{2+} may be replaced by Fe^{2+} and/or Mg^{2+}. Dolomite and ankerite have overlapping d-spacings and it is commonly difficult to distinguish between them. Therefore, we separated the major 104 peaks of these two minerals at around 31° 2θ CuKa, using a peak profile Pearson VI deconvolution function (SCINTAG, 1987; KÜBLER et al., 1990; Fig. 2). The relative error on mineralogical percentages is about 5%.

3. RESULTS

The down-core variations in the concentrations of different P phases within the fine-grained fraction for the Holocene and glacial

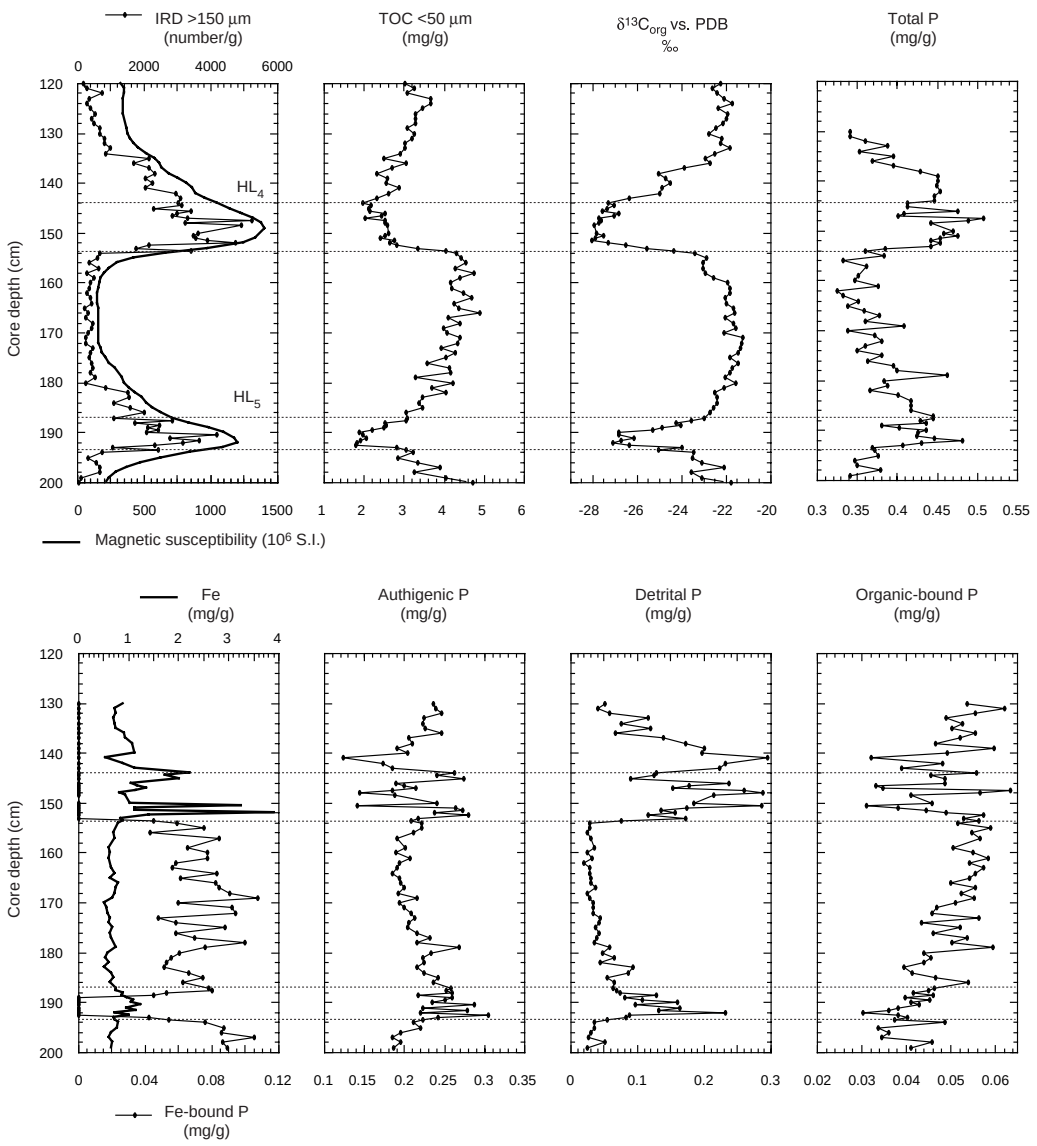

Fig. 4: Plots of down-core variations of a) Magnetic susceptibility and IRD (> 150 µm) content (GROUSSET et al., 2001); b) TOC content and c) $\delta^{13}C$ of organic carbon of the <50 µm fraction (HUON et al., in press); d) total phosphorus, e) ferric Fe and Fe-bound P, f) authigenic P, g) detrital P and h) organic-bound P for the fine-sized fraction of samples from core SU 90-09 (130 – 200 cm depth). The 144.0 - 153.5 cm and 187.0 - 193.5 cm intervals represent the Heinrich events 4 and 5, respectively (HUON et al., in press).

sediments are displayed in Figures 3 and 4, together with low-field magnetic susceptibility values (GROUSSET et al., 2001), IRD content, fine-sized TOC concentrations and $\delta^{13}C$ values (HUON et al., in press). According to the magnetic susceptibility and IRD records (Fig. 4), HL_4 is characterized by a rather broad peak shape, whereas HL_5 is narrower (GROUSSET et al., 2001). The distribution of IRD in the sediment is not only limited to the interval defined by foraminifer minima and IRD maxima (HEINRICH, 1988; BOND et al., 1992) but is more widespread due to the sequential deposition of detrital minerals, closely monitored by magnetic susceptibility values (Fig. 4).

Total P concentrations in Holocene and ambient glacial samples range between 0.33–0.46 mg/g (Figs 3, 4 and Table 2) and are comparable with total P concentrations reported for the low productivity region in the North Atlantic (< 0.5 mg/g, in BATURIN, 1988). Fe-bound, authigenic and organic-bound P concentrations are also comparable with concen-

Table 2: Phosphorus phases concentrations of fine-grained sediments from core SU 90-09 (North Atlantic, IRD belt)

Depth	Sediment	Fe	Fe-bound P	Authigenic P	Detrital P	Organic-bound P	Total P
cm	type	mgFe/g	mgP/g	mgP/g	mgP/g	mgP/g	mgP/g
SU 90-09							
130		0.894	0.000	0.236	0.051	0.054	0.341
131		0.724	0.000	0.239	0.040	0.062	0.341
132		0.739	0.000	0.246	0.059	0.056	0.360
133		0.706	0.000	0.224	0.115	0.049	0.388
134		0.718	0.000	0.224	0.076	0.053	0.352
135		0.739	0.000	0.226	0.119	0.050	0.395
136		0.908	0.000	0.246	0.067	0.056	0.369
137		0.939	0.000	0.205	0.138	0.052	0.395
138		1.084	0.000	0.209	0.173	0.047	0.428
139		1.105	0.000	0.190	0.201	0.060	0.450
140		1.129	0.000	0.205	0.197	0.049	0.451
141		0.530	0.000	0.123	0.295	0.032	0.450
142		0.881	0.000	0.173	0.232	0.048	0.453
143		1.115	0.000	0.185	0.223	0.039	0.447
144	H4	2.219	0.000	0.263	0.128	0.056	0.447
144.5	H4	1.732	0.000	0.241	0.125	0.046	0.412
145	H4	2.014	0.000	0.274	0.090	0.049	0.413
145.5	H4						
146	H4	1.056	0.000	0.189	0.237	0.049	0.475
146.5	H4	1.166	0.000	0.199	0.176	0.033	0.409
147	H4	1.348	0.000	0.214	0.152	0.035	0.402
147.5	H4	1.144	0.000	0.184	0.259	0.063	0.507
148	H4	0.818	0.000	0.144	0.288	0.057	0.488
148.5	H4	0.944	0.000	0.187	0.213	0.041	0.442
150	H4	1.023	0.000	0.240	0.185	0.046	0.470
150.5	H4	3.248	0.000	0.141	0.286	0.031	0.457
151	H4	1.126	0.000	0.264	0.173	0.038	0.476
151.5	H4	1.123	0.000	0.273	0.135	0.045	0.453
152	H4	3.900	0.000	0.237	0.156	0.049	0.443
152.5	H4	1.404	0.000	0.279	0.116	0.058	0.453
153	H4	0.850	0.000	0.216	0.172	0.053	0.442
153.5	H4	0.892	0.045	0.208	0.075	0.056	0.384
154		0.800	0.059	0.221	0.028	0.052	0.359
155		0.757	0.075	0.222	0.027	0.059	0.384
156		0.691	0.043	0.211	0.025	0.055	0.333
157		0.715	0.084	0.191	0.029	0.057	0.361
158							
159		0.603	0.065	0.200	0.036	0.050	0.352
160		0.643	0.077	0.190	0.025	0.055	0.347
161		0.614	0.077	0.207	0.032	0.058	0.375
162		0.637	0.058	0.194	0.019	0.054	0.325
163		0.651	0.056	0.190	0.028	0.057	0.332
164		0.729	0.083	0.184	0.027	0.056	0.351
165		0.631	0.061	0.193	0.030	0.054	0.338
166		0.803	0.082	0.196	0.030	0.050	0.358
167		0.738	0.084	0.200	0.037	0.055	0.377
168		0.725	0.091	0.192	0.025	0.052	0.360
169		0.677	0.108	0.216	0.029	0.055	0.408
170		0.514	0.059	0.194	0.034	0.051	0.339
171		0.573	0.092	0.199	0.033	0.047	0.371
172		0.596	0.094	0.208	0.033	0.046	0.380
173		0.644	0.047	0.212	0.044	0.056	0.360
174		0.604	0.058	0.205	0.042	0.043	0.349
175		0.684	0.088	0.203	0.037	0.052	0.380
176		0.626	0.058	0.216	0.042	0.046	0.362
177		0.666	0.069	0.232	0.039	0.054	0.394
178		0.712	0.100	0.215	0.034	0.050	0.399
179		0.756	0.076	0.269	0.058	0.059	0.462
180		0.587	0.060	0.233	0.047	0.044	0.384
181		0.546	0.055	0.223	0.064	0.046	0.388
182		0.612	0.053	0.225	0.044	0.044	0.365
183		0.520	0.051	0.216	0.093	0.040	0.400
184		0.661	0.066	0.225	0.085	0.041	0.418
185		0.710	0.074	0.241	0.055	0.047	0.417
186		0.631	0.063	0.236	0.065	0.054	0.417
187	H5	0.743	0.078	0.257	0.063	0.046	0.445
187.5	H5	0.748	0.080	0.253	0.068	0.045	0.445
188	H5	0.893	0.053	0.260	0.074	0.042	0.428
188.5	H5	0.856	0.045	0.217	0.127	0.046	0.436
189	H5	0.964	0.000	0.260	0.081	0.040	0.380
189.5	H5	1.102	0.000	0.250	0.107	0.045	0.403
190	H5	1.055	0.000	0.235	0.159	0.041	0.436
190.5	H5	1.239	0.000	0.287	0.097	0.043	0.426
191	H5	0.960	0.000	0.222	0.164	0.038	0.424
191.5	H5	1.158	0.000	0.279	0.131	0.036	0.446
192	H5	0.715	0.000	0.220	0.231	0.030	0.481
192.5	H5	1.000	0.000	0.305	0.088	0.038	0.430
193	H5	0.714	0.042	0.242	0.083	0.040	0.407
193.5	H5	0.724	0.054	0.223	0.055	0.037	0.369
194		0.787	0.076	0.212	0.035	0.049	0.371
195		0.775	0.087	0.219	0.036	0.034	0.376
196		0.666	0.086	0.195	0.030	0.036	0.347
197		0.599	0.105	0.185	0.026	0.034	0.350
198		0.670	0.086	0.196	0.051	0.046	0.378
199		0.651	0.089	0.186	0.025	0.041	0.341

Table 2 (continued): Phosphorus phases concentrations of Holocene fine-grained sediments from core SU 90-09 (North Atlantic, IRD belt)

	Depth	Fe	Fe-bound P	Authigenic P	Detrital P	Organic-bound P	Total P
	cm	mgFe/g	mgP/g	mgP/g	mgP/g	mgP/g	mgP/g
SU 90-09							
	10	1.846	0.145	0.180	0.035	0.056	0.415
	11	1.682	0.137	0.206	0.025	0.062	0.430
	12	1.739	0.135	0.195	0.031	0.052	0.413
	13	1.716	0.145	0.201	0.037	0.081	0.464
	14	1.835	0.148	0.198	0.021	0.072	0.439
	15	1.943	0.166	0.189	0.025	0.065	0.444
	18	1.769	0.143	0.171	0.041	0.057	0.412
	20	1.688	0.142	0.194	0.030	0.058	0.424
	22	1.534	0.122	0.201	0.044	0.063	0.429
	24	1.432	0.113	0.160	0.069	0.051	0.393
	26	1.423	0.116	0.159	0.092	0.055	0.423
	28	1.410	0.096	0.170	0.097	0.054	0.417
	30	1.406	0.106	0.164	0.091	0.061	0.422

trations measured in sediments of the North Atlantic (ODP site 907; TAMBURINI, unpublished data). Concentrations of most P phases in the Holocene samples are in the range of the values observed between 130 and 200 cm for ambient glacial sediments. However, Fe-bound P and reducible Fe concentrations, extracted during the first step of the SEDEX method (RUTTENBERG, 1992; SLOMP et al., 1996), exhibit higher values for Holocene samples than for ambient glacial sediments.

Detrital P concentrations in the Holocene sediments average 0.0320 ± 0.0078 mg/g above 25 cm and increase to 0.094 ± 0.003 mg/g between 25 - 30 cm. This latter depth corresponds to the termination of the Younger Dryas event (MANGERUD et al., 1974), although its position in the sedimentary column is only a rough estimation based on fine-sized organic matter TOC and $\delta^{13}C$ records (Fig. 3; see also in HUON et al., 2001). In contrast with detrital P, authigenic P, Fe-bound P

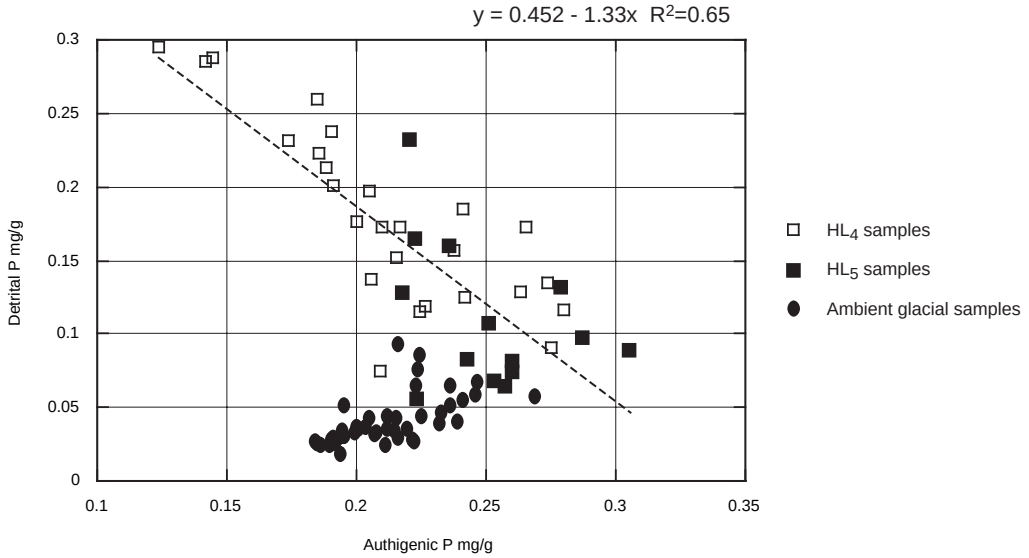

Fig. 5: Plot of authigenic P vs. detrital P concentrations for the <50 µm fraction of samples from core SU 90-09. Solid circles = ambient glacial sediment samples; empty squares = HL_4 samples and solid squares = HL_5 samples. The regression line has been calculated using a least square fit method (BEYER, 1976).

and Fe concentrations display concomitant decreasing trends toward the assumed Younger Dryas upper boundary. Heinrich layers 4 and 5 (HL_4 and HL_5) are characterized by high concentrations of detrital P, which show a 5-fold increase compared to ambient glacial sediment values (Fig. 4). The distribution of detrital P concentrations in HL_4 displays two major peaks of fine-sized detrital P supply. The first one is coeval with the maximum IRD concentration (144 - 153.5 cm, Fig. 4), while the second one (137 - 142 cm, Fig. 4) occurs immediately after HL_4 when the level of IRD supply is still high. The top and bottom of HL_4 bear lower amounts of detrital P. Despite coarse IRD contents (>150 μm) and fine-sized detrital P (<50 μm) concentrations trends parallel each other, correlation is not statistically meaningful for HLs ($r^2 = 0.26$, n = 32). In HL_4 and HL_5 authigenic P is closely linked to detrital P distribution. Detrital and authigenic P phases are roughly correlated in ambient glacial sediments ($r^2 = 0.36$, n = 44), whereas a relatively well-defined inverse correlation is observed for HL samples (Fig. 5, $r^2 = 0.65$, n = 32). Minima in detrital P concentrations correspond to intervals of high authigenic P contents (144 - 145.5 cm and 151 - 153.5 cm, Fig. 3). High amounts of Fe also characterize HLs, but, as for detrital P, the statistical correlation with IRD is rather weak (r^2=0.50, n = 32). In contrast with Holocene samples, where Fe-bound P and Fe concentrations are closely linked (Fig. 3), HLs bear no signal of Fe-bound P (Fig. 4). However, Fe ambient sedimentation levels are maintained, slightly increased or even enhanced such as for 150.5 cm and 152 cm core depths at the bottom of HL_4 (Fig. 4). Finally, Fe concentrations mirror the authigenic P concentration trends observed within HLs. The organic-bound P record is rather complex. Besides a downward decreasing trend in ambient (glacial and Holocene) sediments, no significant changes could be observed in HLs (Figs. 3 and 4).

Molar TOC/P_{org} in ambient glacial sediments (193 ± 41; Fig. 6) provide values slightly higher than the Redfield ratio estimated for marine organic matter from nutrient data analysis (117 ± 14, ANDERSON and SARMIENTO, 1994). In our samples, TOC/P_{org} generally display lower values within HLs (148 ± 30). Oxygen and hydrogen contents of organic matter, represented by OI and HI indexes, display lower and higher values in

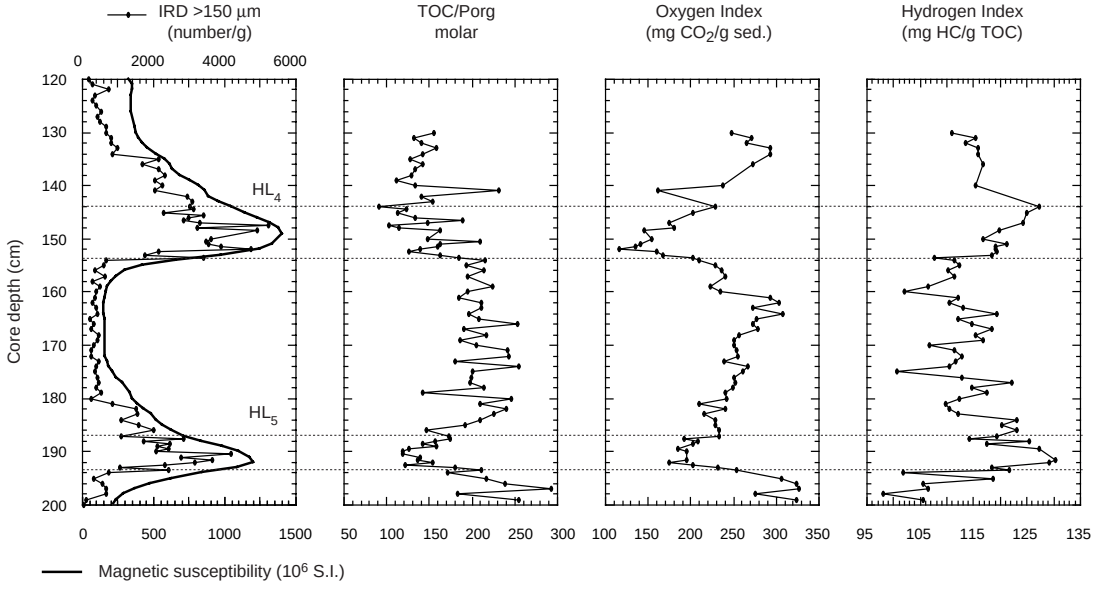

Fig. 6 – Plots of down-core variations of a) Magnetic susceptibility and IRD (>150 μm) content (GROUSSET et al., 2001); b) TOC/P of organic matter molar ratio (TOC values have been taken from HUON et al., in press); c) and d) Rock Eval oxygen (OI) and hydrogen (HI) indices.

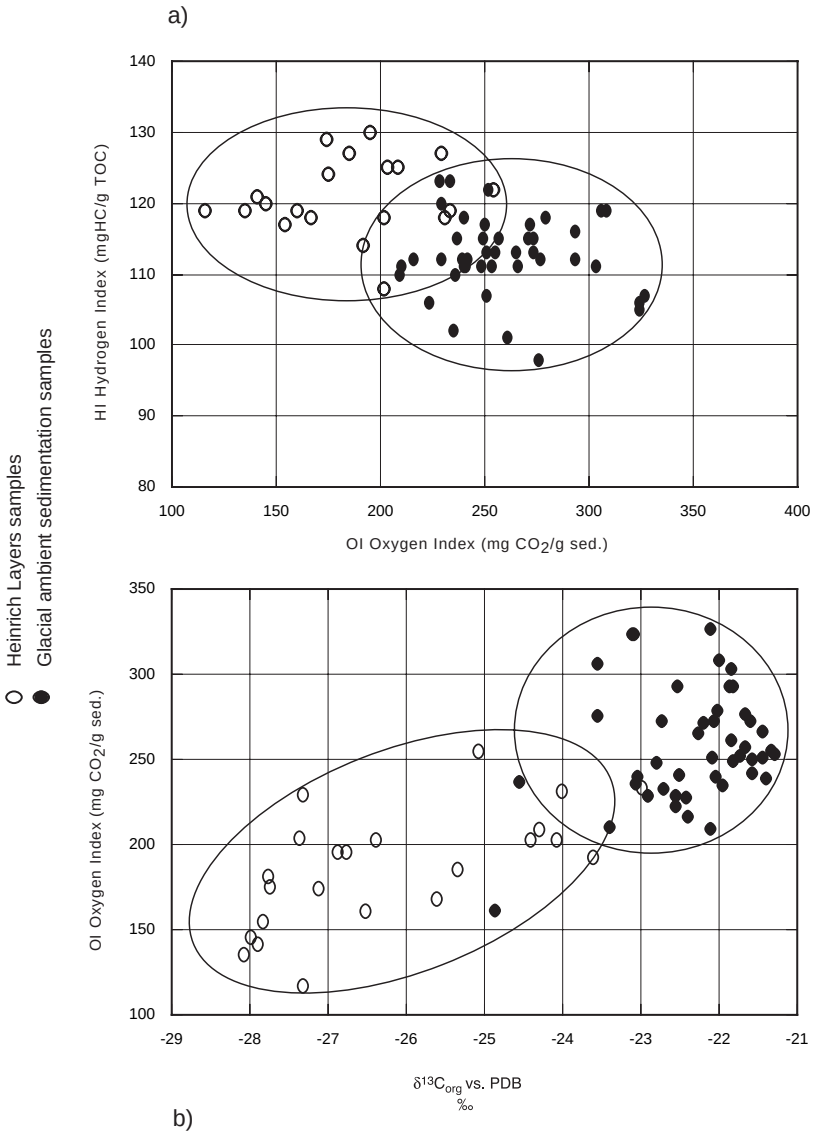

Fig. 7: a) Plot of oxygen index (OI) vs. hydrogen index (HI), and b) plot of $\delta^{13}C$ of organic carbon (HUON et al., in press) vs. oxygen index (OI) of fine-grained (<50 μm fraction) samples from core SU 90-09. Solid symbols = ambient glacial sediment samples and empty symbols = Heinrich layers 4 and 5 samples. A clear direct correlation between OI and $\delta^{13}C$ for Heinrich events samples appears.

HLs, respectively (Fig. 6). In a HI vs. OI plot, we observe two different sets of samples, corresponding to ambient glacial sediments and HLs samples, respectively (Fig. 7a). The oxygen index also covaries with organic matter $\delta^{13}C$ values: HL samples are characterized by low $\delta^{13}C$ values and OI, whereas ambient glacial sediments provide high $\delta^{13}C$ and OI (Fig. 7b).

In this study only calcite, dolomite and ankerite percentages are presented (Fig. 8). The occurrence of Heinrich events 4 and 5 is clearly brought into evidence: calcite percentages show a two-fold decrease compared to ambient glacial values, whereas dolomite and ankerite covary and increase during HL deposition (Fig. 8).

4. DISCUSSION AND INTERPRETATION

4.1 Evidence for the lack of major post-deposition diagenetic redistribution of P

Since comparable values are obtained for Holocene and ambient glacial samples, it

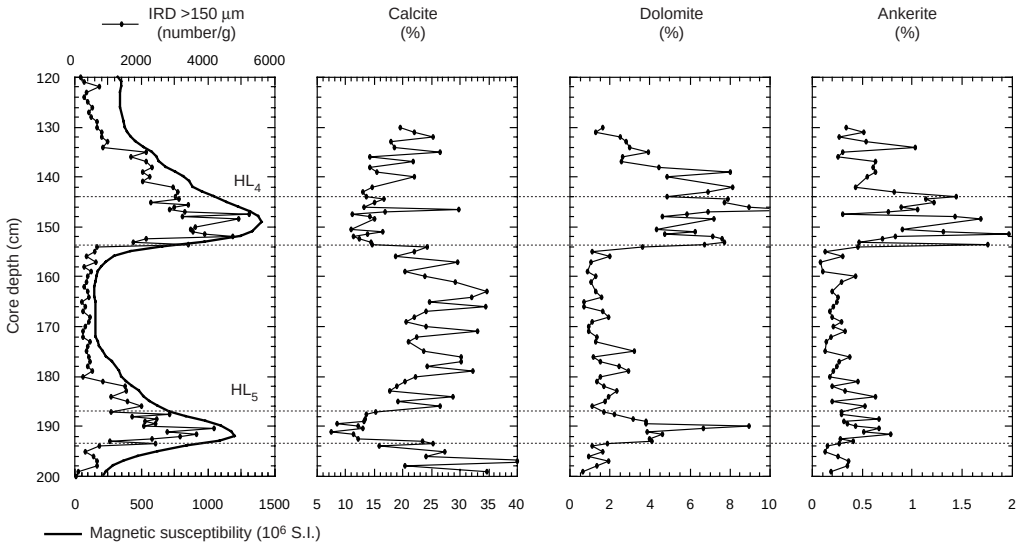

Fig. 8: Plots of down-core variations of a) Magnetic susceptibility and IRD (>150 µm) content (GROUSSET et al., 2001); b) calcite, c) dolomite and d) ankerite percentages of fine-grained samples from core SU 90-09.

appears that no major diagenetic process influenced the redistribution of authigenic and organic-bound P in sediments (Figs. 3 and 4). On the other hand, the higher Fe-bound P values displayed by Holocene sediments, hint at a diagenetic imprint with respect to this phase. P adsorbed onto Fe oxyhydroxides minerals may easily be released into pore waters once that Fe oxyhydroxides have been dissolved below the redox boundary (JARVIS et al., 1994). Thus, the observed differences between ambient glacial and Holocene samples may be the result of active adsorption-desorption processes taking place during the redox cycle in the upper section of the sediment column.

4.2 Enhanced supply of ice-rafted detrital P during Heinrich events 4 and 5

As detrital P is not involved in biological processes (DELANEY, 1998), its distribution can be regarded as mirroring detrital supply in sediments. The low point-to-point correlation between coarse IRD content and fine-grain detrital P in HLs may be explained by: 1) the different behaviour due to grain size and/or 2) the different source of detrital supply. Sr and Nd isotope analyses of IRD material indicate a succession and mixing of European and Canadian sources of detrital material for HL4 (GROUSSET et al., 1993; GROUSSET et al., 2000). Igneous and metamorphic rocks of these two geological provinces may possibly yield distinct amounts of P-bearing minerals (e.g. apatite, monazite), reflected in detrital P sedimentary records. High amounts of detrital P are observed in the central interval of HL4 (146-150.5 cm, Fig. 4), that is know to reflect enhanced supply from Canada (GROUSSET et al., 2000), while lower amounts of detrital P in the upper and bottom interval of HL_4 could reflect an European origin (Fig. 4). Detrital P shows high values also within HL_5, but no sequential deposition could be detected, probably because this layer was deposited during a weaker ice-rafted discharge event (BOND et al., 1992), as is already shown by the low IRD content (Fig. 4).

In contrast to Holocene sediments, where a positive correlation exists (Fig. 3), Fe and Fe-bound P are decoupled within HL_4 and HL_5 (Fig. 4). In fact, HLs bear no signal of Fe-bound P. This behaviour can be related either to the nature of Fe phases and/or to changing environmental conditions. Accumulation of well-crystallized detrital iron-bearing minerals (e.g. hematite coated grains; see in BOND et

al., 1992), could have taken place during HL deposition. Since these minerals constitute a less efficient sink for dissolved P than, for instance, neo-formed and amorphous Fe oxides (SLOMP et al., 1996), Fe-bound P formation was limited. On the other hand, fine-sized ankerite and dolomite peaks, coeval with Fe maxima have been identified by XRD within HLs (Fig. 8). If dolomite and ankerite were supplied to the sediments only by detrital input, they should covary with calcite during HL deposition. The lack of such correlation may point to a possible diagenetic origin of fine-sized dolomite and ankerite, although detrital input is not to excluded. Moreover, idiomorphic crystals of dolomite have been observed within HL sediments (JANTSCHIK, 1991). If neo-formed by direct precipitation into the sediments, both carbonate minerals, especially ankerite, reflect reducing and oxygen-poor conditions in bottom water (GLENN et al., 1994; MALONE et al., 1994), which are not favourable to Fe-bound P phases formation (JARVIS et al., 1994; SLOMP et al., 1996). These aspects are addressed more precisely in the following section.

4.3 Bottom water conditions during HL deposition inferred from P phases distribution

The inverse correlation between authigenic and detrital P concentrations inside HLs and the tight behavior of Fe-bound and detrital P throughout the sediments provide evidence of changing bottom water conditions. These relations are not the result of a dilution effect between the three phases as they are measured independently. Authigenic apatite and Fe-bound P are precipitated in sediments only under specific chemical and physical conditions (e.g. relatively high oxygen content, low alkalinity, high fluoride pore water content). Beyond these limiting conditions, dissolved P is released from the sediment back into the water column (INGALL and JAHNKE, 1994; JARVIS et al., 1994). It has been shown that massive discharge of icebergs during Heinrich events produced a fresh water lid, which possibly caused a temporary stratification of the water column, hampering or even shutting down North Atlantic Deep Water (NADW) formation (BROECKER, 1994; SARNTHEIN et al., 1994; MASLIN et al., 1995; VIDAL et al., 1997; CHAPMAN and SHACKLETON, 1999; MARCHAL et al., 1999). Low-oxygen levels, caused by reduced bottom water ventilation may have led to dysaerobic conditions that may in turn have reduced or even inhibited authigenic P and Fe-bound P phases formation (JARVIS et al., 1994). Each pulse of enhanced supply of detrital P may have led to a reduction in the occurrence of authigenic P and may have inhibited Fe-bound P formation in HLs. The drop of Fe-bound P and partially of authigenic P concentrations within HLs, may therefore indicate a loss of dissolved P from the sediments to the water column. As the phosphate content of bottom water is calculated using Cd/Ca ratio and $\delta^{13}C$ of benthic foraminifers (i.e. BERTRAM et al., 1995), the release of dissolved P from sediments may have consequences on the reliability and interpretation of these bottom water mass tracers.

Since sediment accumulation rates strongly increased during Heinrich events (ELLIOT et al., 1998; HUON et al., in press), the phosphorus concentrations may not reflect the amplitude of phosphorus supply to sediments. However, based on the assumption of limited post-depositional diagenesis and on the observed synchronous P phases variations, we may assume that authigenic P formation is taking place at a similar rate as detrital P input. We have not calculated phosphorus mass accumulation rates (MAR), because of the lack of high resolution age control. Simple assumptions on sedimentation rates (ELLIOT et al., 1998; HUON et al., in press) suggest that authigenic P MAR would be higher during Heinrich events than during ambient glacial sedimentation. However, the relation between detrital and authigenic P would not change

because MAR of both are calculated using the same parameters.

The authigenic P concentration increases at the beginning and at the end of HL_4 and to a lesser extent within HL_5, possibly documenting: 1) enhanced P release due to organic matter degradation; 2) increased input of nutrients (particulate and dissolved) supplied by ice-rafting from the surrounding land masses or 3) northward penetration of nutrient-rich South Atlantic waters (CHARLES and FAIRBANKS, 1992). An argument against enhanced P regeneration from organic matter source is that TOC/P_{org} decreases within HLs (Fig. 6), pointing to a relative enrichment of organic P with respect to organic carbon. The last two hypotheses can better account for the authigenic P behaviour. In fact, higher nutrient levels during iceberg discharges, enhancing primary productivity, have already been suggested (SANCETTA, 1992). However, we have no micropaleontological evidence for such an increase, at least for core SU 90-09 (GROUSSET et al., 2001; HUON et al., in press).

4.4 Selective preservation or change in the source of organic matter in HLs

During prominent Heinrich events (HL_1, HL_2, HL_4 and HL_5), the supply of terrestrial organic matter is clearly enhanced, as is shown by carbon and nitrogen stable isotopic studies of the organic matter (HUON et al., in press). Along with ambient marine organic matter, several continental sources have been postulated, including ancient soils from periglacial regions and organic matter-bearing rocks from the geological basement (e.g. carbonate rocks; BOND et al., 1992; ROSELL-MELÉ et al., 1997).

Although TOC/P_{org} values measured in this study are close to the Redfield ratio of 117 ± 14, they do not necessarily reflect a dominant marine signature in HLs, with respect to the high values usually expected for continental sources (RUTTENBERG and GÕNI, 1997). Low values for continental organic matter can possibly reflect either 1) a grain size effect (RUTTENBERG and GÕNI, 1997), as is also shown by TOC/TN (KEIL et al., 1994); 2) the degree of organic mineralization in the source area and 3) the selective preservation of organic matter in sediments.

HI and OI provide contrasting results for ambient glacial sediments and HLs, and their interpretation remains ambiguous. Low HI values are generally consistent with the signature of refractory organic matter (ESPITALIÉ et al., 1986), as is often observed in deep-sea environments (ZEGOAUGH et al., 1999). Huon and co-authors (in press) interpreted the low $\delta^{13}C$ values in HLs as reflecting a dominant terrestrial origin for OM. The positive correlation between low OI and low $\delta^{13}C$ would therefore suggest that continental organic matter has a oxygen-depleted composition. The relatively low OI of HL samples may also indicate that organic matter has been better preserved from bacterial degradation during the phases of enhanced ice-rafting supply, in contrast to more intense oxydation during ambient glacial sedimentation. This latter assumption is consistent with low oxygen bottom water conditions during Heinrich events shown by Fe-bound P and authigenic P depletions. On the whole, selective preservation as well as changing organic matter composition may both explain the observed OI and HI variations.

5. CONCLUSIONS

1. Using a sequential extraction of fine-grained phosphorus phases (detrital, authigenic, Fe-bound and organic-bound), we show that their down-core distribution in North Atlantic deep-sea sediments reflects rapidly changing environmental conditions. Millenial-time scale episodes such as Heinrich events are recorded by changes in P phases abundance.

2. During the phases of enhanced ice-rafting supply corresponding to Heinrich layers 4 and 5, dissolved P is lost from sediments because the conditions leading to Fe-bound P and authigenic P formation are no longer completely fulfilled. Stratification of the water column as well as oxygen-depleted bottom waters related to massive iceberg discharges account for these temporary suboxic-anoxic conditions. As fine-grained ankerite and dolomite may crystallize under the oxygen-depleted conditions prevailing during Heinrich events, their higher occurrences support this conclusion.

3. Detrital P, authigenic P and Fe concentrations in Heinrich layers 4 and 5 reflect sequential depositions of ice-rafted detrital material that are closely tight to the bottom water oxic/ dysaerobic conditions.

4. Total organic carbon versus organic-bound P ratios and Rock Eval pyrolysis indices provide evidence for enhanced preservation of fine-grained sedimentary organic matter during Heinrich events. However, these parameters may also reflect the presence of refractory organic matter originating from continental sources, contrasting with the marine and terrigenous inputs prevailing during ambient glacial sedimentation.

Acknowledgements. The samples used in this study were taken from core SU90-09, recovered by R/V Le Suroit (IFREMER, France). The french CNRS program VARIENTE is acknowledged for providing all the samples. We are indebted to D. Burdloff, M. Lafosse and R. Pouvreau (DGO, Université de Bordeaux I) for technical assistance. We gratefully aknowledge J. Ondrus of the "Département de la gestion du territoire" of Neuchâtel for ICP-AES analyses.

REFERENCES

Anderson L. A. and Sarmiento J. L. (1994) Redfield ratios of remineralization determined by nutrient data analysis. Global Biogeochemical Cycles 8(1), 65-80.

Anderson L. D. and Delaney M. L. (2000) Sequential extraction and analysis of phosphorus in marine sediments: Streamlining of the SEDEX procedure. Limnol. Oceanogr. 45(2), 509-515.

Andrews J. T. (1998) Abrupt changes (Heinrich events) in late Quaternary North Atlantic marine environments: a history and review of data and concepts. Journ. Quaternary Science 13, 3-16.

Baturin G. N. (1988) Disseminated phosphorus in oceanic sediments - a review. Marine Geology 84, 95-104.

Benson L. V., Burdett J. W., Kashgarian M., Lund S. P., Phillips F. M., and Rye R. O. (1996) Climatic and hydrological oscillations in the Owens lake basin and adjacent Sierra Nevada, California. Science 274, 746-751.

Bertram C. J., Elderfield H., Shackleton N. J., and MacDonald J. A. (1995) Cadmium/calcium and carbon isotope reconstruction of the glacial northeast Atlantic Ocean. Paleoceanography 10(3), 563-578.

Beyer W. H. (1976) Standard mathematical tables. CRC Press.

Bond G. C., Heinrich H., Broecker W., Labeyrie L., McManus J., Andrews J., Huon S., Jantschik R., Clasen S., Simet C., Tedesco K., Kals M., Bonani G., and Ivy S. (1992) Evidence for massive discharges of icebergs into the North Atlantic ocean during the last glacial period. Nature 360, 245-249.

Bond G. C., Broecker W., Johnsen S., McManus J., Labeyrie L., Jouzel J., and Bonani G. (1993) Correlations between climate records from North Atlantic sediments and Greenland ice. Nature 365, 143-147.

Broecker W. S. (1994) Massive iceberg discharges as triggers for global change. Nature 372, 421-424.

Broecker W. S., Bond G. C., Klas M., Clark E., and McManus J. (1992) Origin of the Northern Atlantic's Heinrich events. Climate Dyn. 6, 265-273.

Chapman M. R. and Shackleton N. J. (1999) Global ice-volume fluctuations, North Atlantic ice-rafting events, and deep-ocean circulation changes between

130 and 70 ka. Geology 27(9), 795-798.

Charles C. D. and Fairbanks R. G. (1992) Evidence from Southern Ocean sediments for the effect of North Atlantic deep-water flux on climate. Nature 355, 416-419.

Colman A. S. and Holland H. D. (2000) The global diagenetic flux of phosphorus from marine sediments to the oceans: redox sensitivity and the control of atmospheric oxygen levels. In Marine authigenesis: from global to microbial, Vol. 66, pp. 53-75. SEPM.

Cortijo E., Yiou P., Labeyrie L., and Cremer M. (1995) Sedimentary record of rapid climatic variability in the North Atlantic Ocean during the last glacial cycle. Paleoceanography 10, 911-926.

Delaney M. L. (1998) Phosphorus accumulation in marine sediments and the oceanic phosphorus cycle. Global Biogeochemical Cycles 12(4), 563-572.

Eaton A. D., Clesceri L. S., and Greenberg A. E. (1995) Standard methods for the examination of water and wastewater.

Elliot M., Labeyrie L., Bond G. C., Cortijo E., Turon J.-L., Tisnerat N., and Duplessy J. C. (1998) Millennial-scale iceberg discharges in the Irminger Basin during the last glacial period: relationship with the Heinrich events and environmental settings. Paleoceanography 13(5), 433-446.

Espitalié J., Deroo G., and Marquis F. (1986) La pyrolyse Rock-Eval et ses applications - III partie. Rev. Inst. Fr. Pet. 41(1), 73-89.

Filippelli G. M. and Delaney M. L. (1996) Phosphorus geochemistry of equatorial Pacific sediments. Geochimica et Cosmochimica Acta 60(9), 1479-1495.

Föllmi K. B. (1996) The phosphorus cycle, phosphogenesis and marine phosphate-rich deposits. Earth-Science Reviews 40, 55-124.

Glenn C. G., Föllmi K. B., Riggs S. R., Baturin G. N., Grimm K. A., Trappe J., Abed A. M., Galli-Olivier C., Garrison R. E., Ilyin A. V., Jehl. C., Rohrlich V., Sadaqah R. M. Y., Schidlowski M., Sheldon R. E., and Siegmund H. (1994) Phosphorus and phosphorites: sedimentology and environments of formation. Eclogae geol. Helv. 87(3), 747-788.

Grimm E. C., Jacobson G. L., Watts W. A., Hansen B. C. S., and Maasche K. A. (1993) A 50,000-year record of climate oscillations from Florida and its temporal correlation with the Heinrich events. Science 261, 198-200.

Grousset F. E., Labeyrie L., Sinko J. A., Cremer M., Bond G. C., Duprat J., Cortijo E., and Huon S. (1993) Patterns of ice-rafted detritus in the glacial North Atlantic. Paleoceanography 8(2), 175-192.

Grousset F. E., Pujol C., Labeyrie L., Auffret G., and Boelaert A. (2000) Were the North Atlantic Heinrich events triggered by the behavior of the European ice sheets? Geology 28(2), 123-126.

Grousset F. E., Cortijo E., Huon S., Hervé L., Richter T., Burdloff D., Duprat J., and Weber O. (2001) Zooming in on Heirich layers. Paleoceanography 16(3), 240-259.

Heinrich H. (1988) Origin and consequences of cyclic ice rafting in the Northeast Atlantic Ocean during the past 130,000 years. Quaternary Res. 29, 142-152.

Huon S. and Jantschik. R. (1993) Detrital silicates in Northeast Atlantic deep-sea sediments during the Late Quaternary: major elements, REE and Rb-Sr isotopic data. Eclogae geol. Helv. 86(1), 195-218.

Huon S. and Ruch P. (1992) Mineralogical, K-Ar and 87Sr/86Sr isotope studies of Holocene and Late Glacial sediments in a deep core from the northeast Atlantic Ocean. Marine Geology 107, 275-282.

Huon S., Grousset F. E., Burdloff D., Bardoux G., and Mariotti A. (in press) Sources of fine-sized organic matter in North Atlantic Heinrich Layers: $\delta^{13}C$ and $\delta^{15}N$ tracers. Geochimica et Cosmochimica Acta.

Ingall E. and Jahnke R. (1994) Evidence for enhanced phosphorus regeneration from marine sediments overlain by oxygen depleted waters. Geochimica et Cosmochimica Acta 58(11), 2571-275.

Jantschik R. (1991) Mineralogische und geochemische Untersuchungen spätquartärer Tiefseesedimente aus dem Westeuropäischen Becken (bei 47°30' N und 19°30' W). Ph.D. Thesis, University of Neuchâtel, Switzerland.

Jantschik R. and Huon S. (1992) Detrital silicates in northeast Atlantic deep-sea sediments during the late Quaternary: mineralogical and K-Ar data. Eclogae geol. Helv. 85, 195-212.

Jarvis I., Burnett W. C., Nathan Y., Almbaydin F. S. M., Attia A. K. M., Castro L. N., Flicoteaux R., Hilmy M. E., Husain V., Qutawnah A. A., Serjani A., and Zanin Y. N. (1994) Phosphorite geochemistry: state-of-art and

environmental concerns. Eclogae geol. Helv. 87(3), 643-700.

Keil R. G., Tsamakis E., Fuh C. B., Giddins J. C., and Hedges J. I. (1994) Mineralogical and textural controls on the organic composition of coastal marine sediments: hydrodynamic separation using SPITT-fractionation. Geochimica et Cosmochimica Acta 58(2), 879-893.

Krajewski K. P., Van Cappellen P., Trichet J., Kuhn O., Lucas J., Martin-Algarra A., Prévot L., Tewari V. C., Gaspar L., Knight R. I., and Lamboy M. (1994) Biological processes and apatite formation in sedimentary environments. Eclogae Geol. Helv. 87(3), 701-745.

Kübler B. (1987) Dosage quantitatif des minéraux majeurs des roches sédimentaires par diffraction X. Cahier de l'Institut de Géologie de Neuchâtel Série ADX.

Kübler B., Jantschik R., and Huon S. (1990) Minéralogie et granulométrie des poussières éoliennes, dites "saharienne", du 24 avril 1989 à Neuchâtel. Leur importance pour l'nevironment, les sols et les sédiments. Bulletin de la Société neuchateloise des Sciences naturelles 113, 75-98.

Lowell T. V., Heusser C. J., Andersen B. G., Moreno P. I., Hauser A., Heusser L. E., Schlüchter C., Marchant D. R., and Denton G. H. (1995) Interhemispheric correlation of Late Pleistocene glacial events. Science 269, 1541-1549.

Malone M. J., Baker P. A., and Burns S. J. (1994) Recrystallization of dolomite; evidence from the Monterey Formation (Miocene), California. Sedimentology 41(6), 1223-1239.

Mangerud J., Andersen S. T., Berglund B. E., and Donner J. J. (1974) Quaternary stratigraphy of Nordern: a proposal for terminology and classification. Boreas 3, 109-128.

Marchal O., Stocker T. F., and Joos F. (1999) Physical and biogeochemical responses to freshwater-induced thermohaline variability in a zonally averaged ocean model. In Mechanisms of global climate change at millennial time scales, Vol. 112 (ed. P. U. Clark, R. S. Webb, and L. D. Keigwin), pp. 263-284. American Geophysical Union.

Maslin M. A., Shackleton N. J., and Pflaumann U. (1995) Surface water temperature, salinity, and density changes in the northeast Atlantic during the last 45,000 years: Heinrich events, deep water formation, and climatic rebounds. Paleoceanography 10(3), 527-544.

Paillard D. and Labeyrie L. D. (1994) Role of the thernohaline circulation in the abrupt warming after Heinrich events. Nature 372, 162-164.

Rosell-Melé A., Maslin M. A., Maxwell J. R., and Schaeffer P. (1997) Biomarker evidence for "Heinrich" events. Geochimica et Cosmochima Acta 61(8), 1671-1678.

Ruddiman W. F. (1977) Late Quaternary deposition of ice-rafted sand in the subpolar North Atlantic (lat. 40° to 65°N). Geol. Soc. Am. Bull. 88, 1813-1827.

Ruttenberg K. C. (1992) Development of a sequential extraction method for different forms of phosphorus in marine sediments. Limnology Oceanography 37(7), 1460-1482.

Ruttenberg K. C. and Gõni M. A. (1997) Phosphorus distribution, C:N:P ratios, and δ^{13}Coc in artic, temperate, and tropical coastal sediments: tools for characterizing bulk sedimentary organic matter. Marine Geology 139, 123-145.

Sancetta C. (1992) Primary productivity in the glacial North Atlantic and North Pacific oceans. Nature 360, 249-251.

Sanchez-Gõni M. F., Turon J.-L., Eynaud F., and Gendreau S. (2000) European climatic response to millennial-scale changes in the atmosphere-ocean system during the Last Glacial period. Quaternary Research 54, 394-403.

Sarnthein M., Winn K., Jung S., Duplessy J. C., Labeyrie L., Erlenkeuser H., and Ganssen G. (1994) Changes in East Atlantic deep-water circulation over the last 30,000 years - an eight time slice reconstruction. Paleoceanography 9, 209-268.

Schulz H., von Rad U., and Erklenkeuser H. (1998) Correlation between Arabian Sea and Greenland climate oscillations of the past 110,000 years. Nature 393, 54-57.

SCINTAG. (1987) PAD V, Diffraction System, Users Manual.

Slomp C. P. (1997) Early diagenesis of phosphorus in continental margin sediments. Ph. D. Thesis, Instituut voor Onderzoek der Zee (NIOZ) Texel, The Netherlands.

Slomp C. P., Van der Gaast S. J., and Van Raaphorst W. (1996) Phosphorus binding by poorly crystalline

iron oxides in North Sea sediments. Marine Chemistry 52, 55-73.

Tyrrell T. (1999) The relative influences of nitrogen and phosphorus on oceanic primary production. Nature 400, 525-531.

Van Cappellen P. and Ingall E. D. (1994) Benthic phosphorus regeneration, net primary production, and ocean anoxia: a model of the coupled marine biogeochemical cycles and phosphorus. Paleoceanography 9(5), 677-698.

Vidal L., Labeyrie L. D., Cortijo E., Arnold M., Duplessy J. C., Michel E., Becque S., and Van Weering T. C. E. (1997) Evidence for changes in the North Atlantic deep water linked to meltwater surges during the Heinrich events. Earth and Planetary Science Letters 146, 13-27.

Wang L., Sarnthein M., Erlenkeuser H., Grimalt J., Grootes P., Heilig S., Ivanova E., Kienast M., and Pflaumann U. (1999) East Asian Monsoon climate during the Late Pleistocene: high-resolution sediment records from the South China Sea. Marine Geology 156, 245-284.

Zahn R., Schönfeld J., Kudrass H. R., Park M. H., Erlenkeuser H., and Grootes P. (1997) Thernohaline instability in the North Atlantic during meltwater events: stable isotope and ice-rafted detritus records from core SO75 26KL, Portuguese margin. Paleoceanography 12(5), 696-710.

Zegoaugh Y., Derenne S., Largeau C., Bertrand P., Sicre M.-A., Saliot A., and Rousseau B. (1999) Refractory organic matter in sediments from the Aorthwest african upwelling system: abundance, chemical structure and origin. Organic Geochemistry 30, 101-117.

CHAPTER 5

ODP Leg 184 Sedimentologists. From left to right: Anchun Li, Wolfgang Kuhnt, Federica Tamburini, Eve Arnold, Peter Clift, Luejiang Wang, Alain Trentesaux and Conrado Miranda (1999).

*Origin and nature of green clay layers, ODP Leg 184, South China Sea**

ABSTRACT

Green clay layers are reported from the Plio-Pleistocene interval in five of the six drilled sites in the South China Sea during Leg 184. Centimeter-scale discrete, discontinuous as well as bioturbated layers, constituted by stiff and porous green clays, were observed, sometimes associated with iron sulfides and pyrite. Detailed mineralogical and geochemical analyses indicate that they differentiate from the host sediments in their higher content of iron, smectite and mixed-layered clays and lower amounts of calcite, authigenic phosphorus, quartz and organic matter. Although no glauconite has been observed, green clay layers mineralogy and geochemistry, along with their geometrical relationship to background sediments suggest that they most likely represent the result of the first steps of glauconitization. No evident correlation between these green layers and volcanic ash layers has been found, as was suggested for green laminae observed elsewhere in Pacific sediments. Statistic analysis of their temporal distribution during the last million years suggests the presence of a temporal trend, with intervals between green layers events shortening since 600 ka and green clay layers becoming more frequent toward the top of the studied sequence. Only at site 1148 the record shows a statistically significant cyclicity which may be related to eccentricity. A possible influence of sea level variations, related both to climatic changes and tectonism, is postulated.

INTRODUCTION

During ODP Leg 184 in the South China Sea (SCS) characteristic lithological features, called green clay layers (Wang, Prell et al., 2000), were mainly observed in the Pliocene-Pleistocene interval of five of the six drilled sites (Fig. 1 and Table 1). It is not the first time that such features are found in marine sediments. Green and purple-colored bands were noted in sediments from Leg 130 in the Ontong-Java plateau (Lind, Janececk et al., 1993), and similar layers were observed in deposits from the Rio Grande Rise and the Lord Howe Rise (Gardner, Nelson et al., 1986). Inside the SCS, green clay granules and foraminifer tests infilled with green clays were reported from Holocene and Pleistocene sediments in the Vietnam inner and outer shelf (Markov, Mozherovskii et al., 1996).

Several hypotheses were taken into account in order to explain the nature and the origin of these layers: i) presence of glauconite, ii) alteration of volcanic material and iii) alteration of the original clay, but the question remained open. A total of 22 samples (11 of green clay and 11 of background sediment, Fig. 2) were collected from ODP Sites 1147 and 1148 in the SCS. Here we present the results of a multiproxy investigation, which comprises bulk and clay mineralogy, granulometry, organic matter and phosphorus sedimentary phases characterization, bulk inorganic geochemistry (by XRF), and statistical analysis of the temporal distribution of the green clay layers. The main goals of this study are to determine the nature of the green clay layers, understand their genesis and establish any possible correlation with external factors, such as sea level changes, climate variations, and tectonism.

* This chapter by Federica Tamburini, Thierry Adatte and Karl B. Föllmi has been submitted for publication in the *Proceedings of the Ocean Drilling Program, Scientific Results*, Vol. 184 (South China Sea).

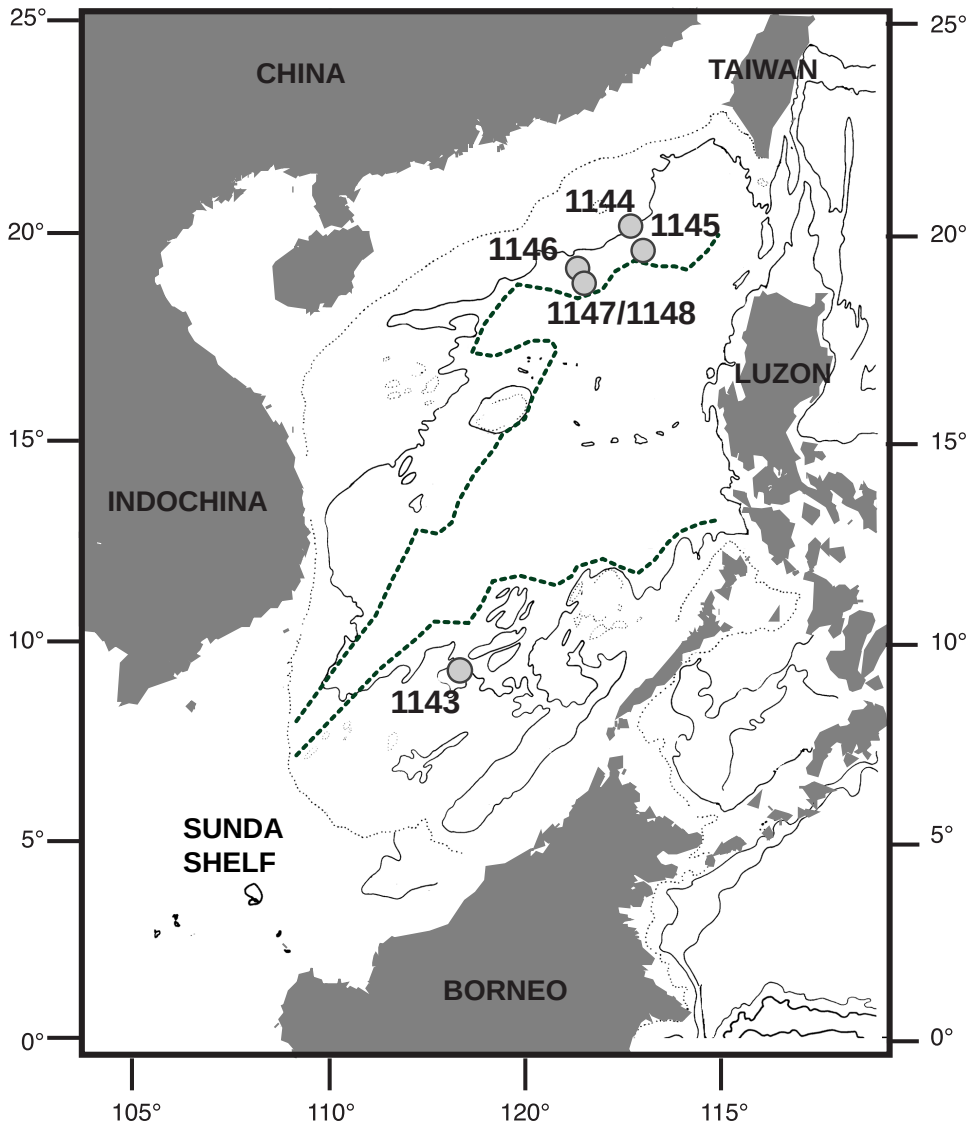

Fig. 1: Map of the South China Sea and location of the six sites drilled during ODP Leg 184. The thick dotted line indicates the continental/oceanic crust boundary, while the thin dotted line indicates the shelf limit.

Table 1: Location of the studied sites. Water depth is in meter below sea level (mbsl).

Table 1

Site	Latitude	Longitude	Water Depth mbsl
1143	9°21.72' N	113°17.11' E	2772
1145	19°35.04' N	117°37.86' E	3175
1146	19°27.40' N	116°16.37' E	2092
1147	18°50.11' N	116°33.28' E	3246
1148	18°50.17' N	116°33.94' E	3294

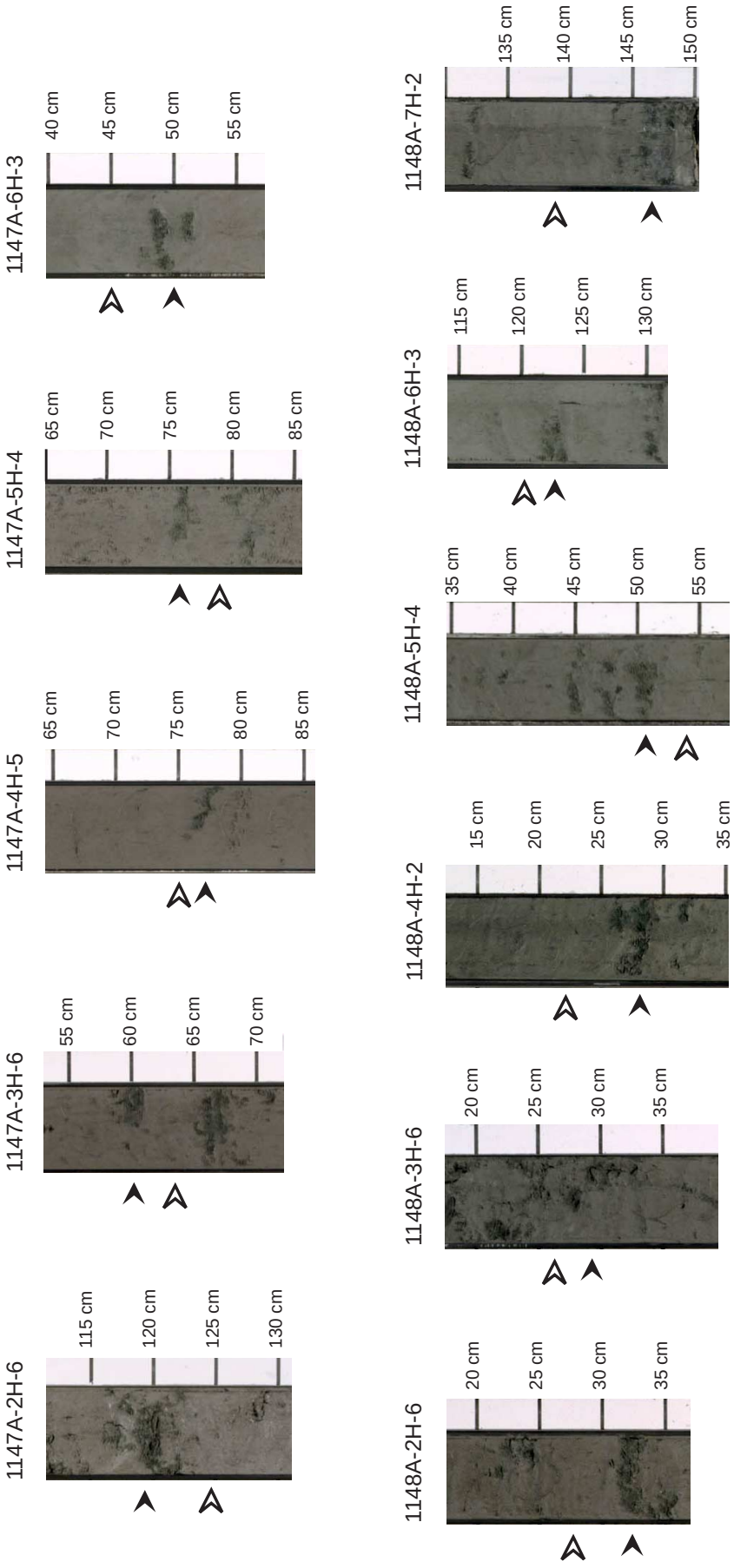

Fig. 2: Samples used for this study. The solid arrow represents the green clay layers (GCL) samples, while the open arrow the background sediment samples. It is evident from this figure that not all the GCL sampled are continuous.

METHODS

All samples were oven-dried at 50°C and divided in sub samples. Bulk sediment mineralogy was determined by XRD (SCINTAG XRD 2000 Diffractometer) based on a semi-quantitative estimation, and using external standards (Kübler, 1987). The relative error of the bulk rock mineralogy is about 5%. Clay mineral analyses were based on methods by Kübler (1987). An aliquot of the sample was mixed with de-ionized water (pH 7-8) and the carbonate fraction was removed by the addition of HCl 10% (1.25 N). XRD analyses of oriented clay samples were made after air drying at room temperature and ethylene-glycol solvated conditions. Clay minerals for each fraction are given in relative percent abundance without correction factors. Content in smectite is estimated by using the method of Moore and Reynolds (1997). The relative error does not exceed 10% of raw intensity. Granulometry analyses were performed on the insoluble and carbonate-free residues prepared for the clay mineralogy analyses using a Granulometry Laser Oriel CIS. The relative error is 10% (Jantschik, Nyffeler et al., 1992).

The characterization of organic matter was performed on 100 mg of dried and ground sediment, with a Rock-Eval 6, and using a standard whole rock pyrolysis method (Espitalié, Deroo et al., 1986; Lafargue, Espitalié et al., 1996). The distribution of sedimentary phosphorus phases was determined using a 4-step sequential extraction technique, adapted from the SEDEX method (Anderson and Delaney, 2000; Ruttenberg, 1992). For all the steps other than the iron-bound P, the ascorbic acid molybdate blue technique was employed to develop color (Eaton, Clesceri et al., 1995). A Perkin-Elmer UV/Vis spectrophotometer Lambda 10 was used to determine absorbencies and P concentrations. All samples were diluted 10:1 for determination. Concentrations of the iron-bound P phase and ferric Fe, extracted during the first step of the procedure, were determined using an OPTIMA 3000 Perkin Elmer ICP-AES, at the "Environmental laboratory" in Neuchâtel. Typical mean errors for each phase were calculated as the relative standard deviation of the consistency standards and range from 2-7% for authigenic P, 3-5% for detrital P, 2-5% for organic P, and 3-6% for iron-bound P. XRF were performed only on four selected samples, due to material limitation, at the Geological Institute of Fribourg, using a Sequential X-Ray Spectrometer PW2400.

The depth of the green clay layers was recorded during the shipboard description of the sediments directly on the AppleCore sheets. The depth in meters below sea floor (mbsf) of each GCL occurrence in Sites 1143, 1145, 1146, 1147 and 1148 has been extracted from the barrel sheets, and depths in meters composite depth (mcd) and ages (k.y.) were calculated using the splices and the age models provided in Wang, Prell et al. (2000). Test for randomness, as well as autocorrelation and spectral analysis were performed to investigate their temporal distribution over the last million year. All the records were resampled at even intervals and detrended before being analyzed. The Arand and MatLab® packages were used for statistical analyses.

DESCRIPTION AND RESULTS

Green clay layers (GCL) are mainly concentrated in the uppermost Plio-Pleistocene section and in the lower Miocene section, for Site 1148 (Wang, Prell et al., 2000). These centimeter-scale layers, consisting of generally coarser and stiffer material than background sediments, which are composed of nannofossil ooze and detrital clays, can be as thick as 3 cm and occur in high number, up to hundreds per core. Generally GCL bear low water quantities and physical properties analysis indicates that they are characterized by faster P-wave velocities (Wang, Prell et al., 2000). Discrete layers as well as discontinuous and bioturbated green

intervals were observed (Fig. 2), and in many occurrences a clear association with "iron sulfide" minerals and pyrite nodules was found (Wang, Prell et al., 2000). Smear slide analysis performed during visual inspection of the cores indicates that these layers are relatively poor in carbonate. A green mineral was recognized on smear slides and interpreted as being glauconite, but XRD analysis performed onboard did not validate this observation. After opening of the plastic bags containing the sampled sediments, about two months after sampling, the green color characteristic of GCL had disappeared and the distinction between the green clay and the host sediment samples was not so straightforward.

Granulometry, bulk and clay mineralogy

The studied sediments, both GCL and host material, are fine-grained, with material <8 μm averaging 82%. Samples are composed of phyllosilicates, which average 17%, and quartz which represents about 12% of GCL and 13% of the host sediments. Other minor constituents are K-feldspar, plagioclase, and calcite, which represent together not more than 13% of bulk mineral composition. Small amounts of pyrite have been detected in both GCL and normal sediments (Table 2). Micas (s.l.) and chlorite constitute the most abundant clay minerals. Micas averages 52% and 49% of the <2 μm and 2-16 μm fractions, respectively, while chlorite represents 40% and 23% of the same fractions. Kaolinite is present in lower percentages. Smectite, detected in the <2 μm fraction treated with glycol, makes up about 18% of the fraction. Generally, micas are of detrital origin, as it is shown by their sharp peaks (Fig. 3).

Background sediments are richer in calcite than GCL, while no consequential difference in pyrite percentages has been observed. GCL are generally coarser than background sediments, with material > 8 μm averaging 19.3%, and contain phyllosilicates, K-feldspar, plagioclase, and phyllosilicates, mainly chlorite, smectite (Table 2).

It is difficult to detect glauconite, a Fe-rich muscovite, by XRD, and there is no evidence of its presence in our samples. But a detailed analysis of clay minerals shows that mixed-layered clays are present in the GCL (Fig. 3), though in small amounts. These mixed-layered clays consist mainly of glauconite-smectite (GS) and chlorite-smectite (CS). We are able to estimate the content of Fe-rich mica at about 80-85% and of chlorite at 75-80% in GS and CS respectively (Moore and Reynolds, 1997).

Bulk inorganic and organic geochemistry

Concentration of the different phosphorus sedimentary phases and of ferric iron are reported in Table 2. Fe-bound P and authigenic P are the most abundant phases, and their concentrations average 0.11 and 0.3 mg/g, respectively. The samples contain only few amounts of detrital P and organic-bound P (Table 2). Ferric iron is present in relatively high quantities, averaging 2 mg/g. XRF results are shown in Table 3 and only few analyzed elements display important variations between normal sediments and GCL. On the whole, GCL bear higher concentrations of iron and nickel compared to host sediments, while the latter are characterized by slightly more considerable amounts of authigenic P, CaO, barium and strontium (Tables 2 and 3). Rock-Eval data indicate that GCL contain less amounts of organic matter, which averages 0.26 % in GCL and 0.34 % in host sediments.

Spatial and temporal distribution of GCL: statistical analysis

We have calculated the depth in mcd of each GCL using the splices produced onboard, in order to have a complete and theoretically continuous records of GCL for all the studied sites. Their occurrences in time are represent-

Table 2

Leg	Site	Hole	Core	Sect	Top cm	Bottom cm	Color	<8 µm %	>8 µm %	Micas 2-16 µm %	Kaol %	Chl %	Micas <2 µm %	Kaol %	Chl %	Sm %
184	1147	A	2	H 6	124	126	Normal	92.48	7.52	50.91	4.66	44.43	40.46	5.51	27.48	26.55
184	1147	A	2	H 6	118	120	Green	96.42	3.58	48.46	7.88	43.66	37.60	11.86	20.08	30.46
184	1147	A	3	H 6	63	64	Normal	89.33	10.67	55.53	4.70	39.78	58.62	10.41	24.34	6.63
184	1147	A	3	H 6	60	61	Green	85.96	14.04	51.22	6.25	42.53	49.44	9.96	24.14	16.46
184	1147	A	4	H 5	75	76	Normal	94.98	5.02	57.02	4.25	38.72	63.22	11.68	25.10	miss
184	1147	A	4	H 5	77	78	Green	90.88	9.12	58.01	4.42	37.57	59.25	10.46	28.91	1.38
184	1147	A	5	H 4	78	79	Normal	88.85	11.15	54.26	8.50	37.23	65.79	9.82	23.30	1.08
184	1147	A	5	H 4	76	77	Green	12.32	87.68	55.87	6.14	37.99	66.42	10.73	20.55	2.30
184	1147	A	6	H 3	45	46	Normal	93.48	6.52	54.61	5.40	39.99	51.32	11.00	19.04	18.64
184	1147	A	6	H 3	50	51	Green	82.10	17.90	53.40	5.85	40.76	34.05	9.70	30.81	25.43
184	1148	A	2	H 6	26	28	Normal	92.56	7.44	51.08	2.34	46.58	46.90	11.40	21.15	20.55
184	1148	A	2	H 6	31	33	Green	90.87	9.13	49.43	2.15	48.42	43.85	4.05	32.26	19.83
184	1148	A	3	H 6	25	27	Normal	94.83	5.17	50.92	6.84	42.24	49.31	13.22	24.34	13.13
184	1148	A	3	H 6	28	30	Green	91.63	8.37	50.07	7.18	42.75	50.04	5.95	22.80	21.21
184	1148	A	4	H 2	22	24	Normal	92.43	7.57	49.10	4.46	46.44	miss	miss	miss	miss
184	1148	A	4	H 2	27	29	Green	83.88	16.12	47.91	5.76	46.33	48.24	8.42	24.04	19.30
184	1148	A	5	H 4	52	54	Normal	45.93	54.07	53.33	8.66	38.01	48.12	5.72	22.09	24.07
184	1148	A	5	H 4	49	51	Green	89.27	10.73	52.35	7.17	40.49	47.32	7.43	22.98	22.28
184	1148	A	6	H 3	119	121	Normal	75.81	24.19	52.35	11.34	36.32	40.60	9.92	20.91	28.57
184	1148	A	6	H 3	121	123	Green	75.53	24.47	54.52	10.81	34.67	46.06	6.67	21.48	25.78
184	1148	A	7	H 2	137	139	Normal	90.78	9.22	53.88	8.29	37.83	44.09	10.05	20.93	24.93
184	1148	A	7	H 2	145	147	Green	89.06	10.94	53.69	7.76	38.55	58.01	13.59	23.82	4.57

	Color	<8 µm %	>8 µm %	MIcas 2-16 µm %	Kaol %	Chl %	Micas <2 µm %	Kaol %	Chl %	Sm %
AVERAGE	Green	80.72	19.28	52.27	6.49	41.25	49.12	8.98	24.72	18.44
	Normal	84.89	15.11	52.99	6.75	40.27	49.47	9.67	22.62	18.24

Table 2: Granulometry, clay (for the 2-16 µm and <2 µm fractions) and bulk mineralogy, Fe (ferric) and phosphorus sedimentary phases of selected samples. On the bottom, average values for the same parameters.

Table 2 (continued)

Leg	Site	Hole	Core	Sect	Top cm	Bottom cm	Color	Phyllosilicates %	Quartz %	K-feldspar %	Plagioclase %	Calcite %	Pyrite %	Fe mg/g	Fe-bound P mg/g	Authigenic P mg/g	Detrital P mg/g	Organic-bound P mg/g
184	1147	A	2 H	6	124	126	Normal	20.03	9.67	1.06	2.82	15.31	1.01	1.23	0.13	0.31	0.03	0.07
184	1147	A	2 H	6	118	120	Green	25.49	11.42	2.10	2.96	9.94	0.87	4.39	0.28	0.22	0.03	0.08
184	1147	A	3 H	6	63	64	Normal	25.26	17.06	1.71	5.06	3.20	0.56	2.38	0.28	0.52	0.04	0.07
184	1147	A	3 H	6	60	61	Green	11.81	9.42	1.00	2.27	0.62	0.43	6.93	0.06	0.24	0.06	0.09
184	1147	A	4 H	5	75	76	Normal	15.07	15.92	1.53	4.04	6.03	0.77	2.63	0.05	0.21	0.04	0.08
184	1147	A	4 H	5	77	78	Green	15.22	15.92	1.17	4.30	6.11	0.84	3.54	0.03	0.25	0.04	0.07
184	1147	A	5 H	4	78	79	Normal	16.79	13.29	1.09	2.40	15.04	0.81	1.78	0.06	0.34	0.04	0.06
184	1147	A	5 H	4	76	77	Green	18.23	13.29	1.64	3.00	12.23	0.81	3.44	0.07	0.21	0.05	0.07
184	1147	A	6 H	3	45	46	Normal	13.17	12.01	1.03	3.12	10.94	0.57	1.18	0.11	0.37	0.04	0.06
184	1147	A	6 H	3	50	51	Green	14.19	14.07	1.22	3.80	10.27	0.69	3.23	0.11	0.2	0.05	0.07
184	1148	A	2 H	6	26	28	Normal	14.49	8.31	1.61	3.05	1.66	0.50	1.34	0.06	0.2	0.04	0.07
184	1148	A	2 H	6	31	33	Green	19.25	11.68	0.96	3.35	1.70	0.63	2.37	0.07	0.24	0.04	0.07
184	1148	A	3 H	6	25	27	Normal	16.01	16.38	1.36	3.21	1.06	0.45	2.63	0.04	0.29	0.04	0.08
184	1148	A	3 H	6	28	30	Green	16.76	11.30	1.46	5.51	1.19	0.62	2.14	0.04	0.2	0.04	0.07
184	1148	A	4 H	2	22	24	Normal	19.98	17.82	1.32	4.42	4.44	0.80	1.76	0.04	0.57	0.04	0.07
184	1148	A	4 H	2	27	29	Green	23.02	11.51	1.74	3.42	0.97	0.48	4.46	0.37	0.35	0.04	0.07
184	1148	A	5 H	4	52	54	Normal	19.42	14.95	0.99	4.54	4.65	0.64	1.6	0.09	0.42	0.04	0.07
184	1148	A	5 H	4	49	51	Green	17.46	15.49	1.34	4.76	1.92	0.59	2.28	0.18	0.33	0.04	0.06
184	1148	A	6 H	3	119	121	Normal	12.98	10.27	0.74	2.32	9.61	0.56	1.36	0.1	0.58	0.04	0.06
184	1148	A	6 H	3	121	123	Green	13.55	10.43	2.29	2.75	11.04	0.50	1.44	0.08	0.21	0.07	0.06
184	1148	A	7 H	2	137	139	Normal	12.93	11.80	0.80	2.97	3.56	0.36	1.44	0.05	0.39	0.04	0.07
184	1148	A	7 H	2	145	147	Green	17.02	9.95	1.02	2.72	1.74	0.45	3.24	0.06	0.23	0.05	0.09

	Color	Phyllosilicates %	Quartz %	K-feldspar %	Plagioclase %	Calcite %	Pyrite %	Fe mg/g	Fe-bound P mg/g	Authigenic P mg/g	Detrital P mg/g	Organic-bound P mg/g
AVERAGE	Green	17.455	12.226	1.449	3.530	5.249	0.628	3.405	0.124	0.244	0.047	0.074
	Normal	16.920	13.407	1.201	3.450	6.863	0.639	1.661	0.101	0.379	0.040	0.067

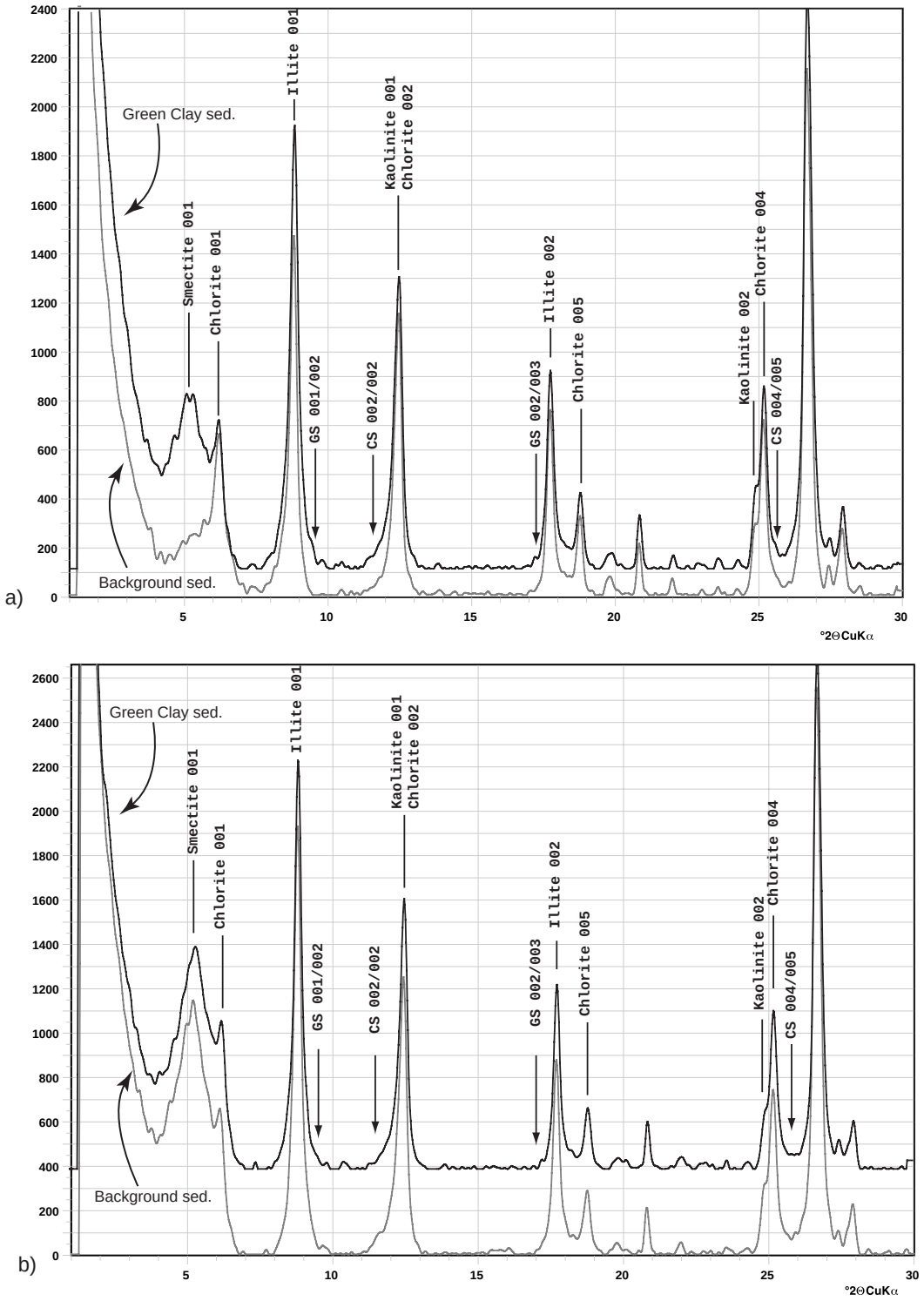

Fig. 3: a) Difractograms of samples 184-1148A-3H-6 (25-27 cm, background sediment, gray line) and 184-1148A-3H-6 (28-30 cm, GCL, black line), <2 μm glycolated fraction.
b) Difractograms of samples 184-1148A-5H-4 (52-54 cm, background sediment, gray line) and 184-1148A-5H-4 (49-51 cm, GCL, black line), <2 μm glycolated fraction. GS = glauconite/smectite, with 80-85% of Fe-rich muscovite; CS = chlorite/smectite, with 75-80% of chlorite. Mixed-layered clays estimated as described in Moore and Reynolds (1997). In both plots, the y-axes represent counts per second.

Table 3

		184-1148A 2H-6 (26-28 cm) Normal	184-1148A 2H-6 (31-33 cm) Green	184-1148A 6H-3 (119-121 cm) Normal	184-1148A 6H-3 (121-123 cm) Green
Channel	Unit				
SiO_2	%	56.76	56.04	47.10	47.15
TiO_2	%	0.66	0.68	0.66	0.64
Al_2O_3	%	16.66	16.50	15.09	14.84
Fe_2O_3	%	**3.11**	**4.48**	**4.19**	**4.38**
FeO	%	**2.22**	**2.09**	**1.86**	**1.87**
MnO	%	0.14	0.17	0.29	0.28
MgO	%	**2.72**	**2.87**	**2.90**	**2.91**
CaO	%	**2.54**	**2.08**	**9.36**	**9.28**
Na_2O	%	3.32	3.28	2.15	2.12
K_2O	%	3.25	3.28	2.65	2.68
P_2O_5	%	0.12	0.11	0.16	0.14
L O I	%	8.15	8.12	13.70	13.61
SUM %	%	99.65	99.71	100.11	99.90
Ba	ppm	**890**	**864**	**553**	**528**
Cr	ppm	74	77	78	81
Cu	ppm	96	74	18	16
Nb	ppm	12	13	12	12
Ni	ppm	**69**	**80**	**58**	**63**
Pb	ppm	<7	<7	<7	<7
Rb	ppm	140	143	113	118
Sr	ppm	**215**	**191**	**389**	**385**
V	ppm	134	130	124	124
Y	ppm	26	27	26	25
Zn	ppm	113	123	100	98
Zr	ppm	141	141	133	133
SUM ppm	%	0.19	0.19	0.16	0.16
Fe tot (Fe_2O_3)	%	**5.58**	**6.81**	**6.26**	**6.46**
TOC (RE6)	%	**0.43**	**0.29**	**0.25**	**0.24**

Table 3: Results of XRF and Rock Eval (RE6) analyses performed on four selected samples.

ed in Figure 4. No significant correlation between depths is noted (not shown). In average, 8 GCL per 20 k.y. are recorded in the studied sites, and peaks of more than 10 occurrences per 20 k.y. are observed especially at Site 1143. Generally, GCL are more recurrent in the upper part of the sequence. Sites 1143 and 1148 present the most continuous records of GCL (Fig. 4).

All records are tested for randomness in order to statistically assess if any patterns or trends in the temporal distribution of GCL exist. For all sites, except Site 1143, the results indicate that GCL are not distributed in a random way (Table 4). The lengths of the interval between two GCL events are plotted in Figure 5, and a trend in the length of the interval is observed for Sites 1143, 1145 and 1146, with intervals becoming shorter toward the upper

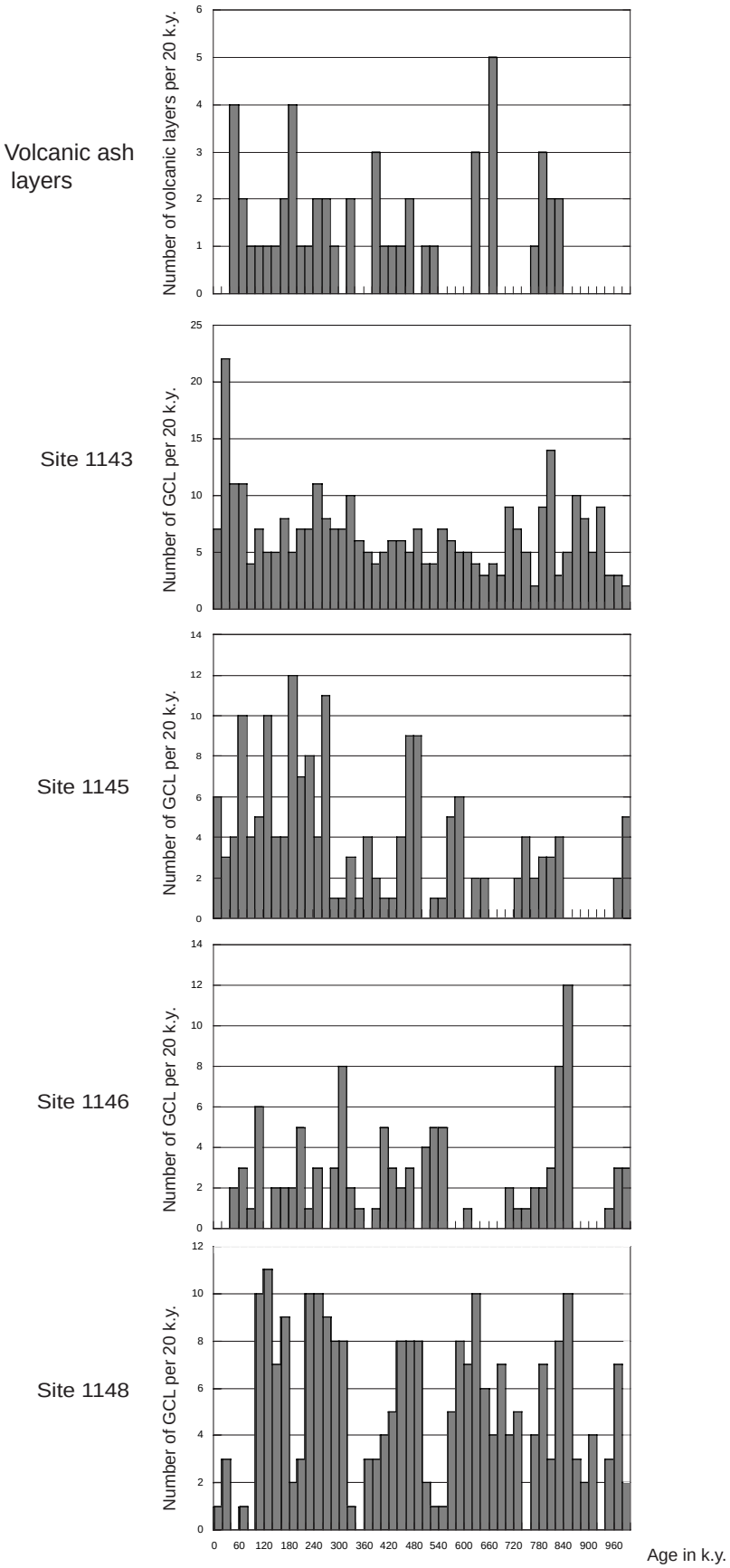

Fig. 4: Temporal distribution of volcanic ash layers and GCL in the SCS spanning the last million years. The number of volcanic layers observed in all sites drilled during Leg 184 and the number of GCL recorded for each site are reported on the y-axis. Age in k.y. is reported on the x-axis. Each bin is 20 k.y.

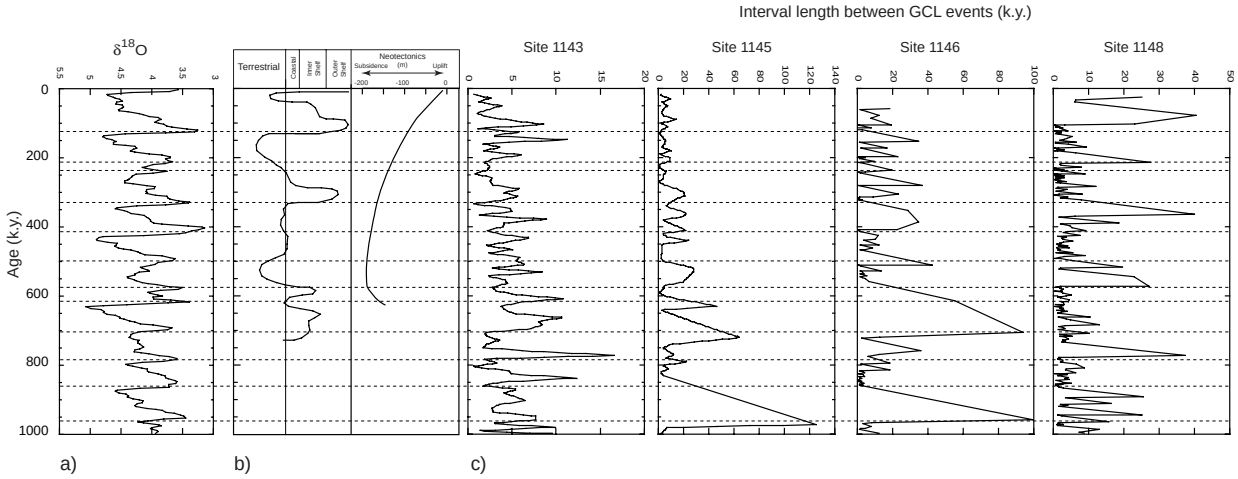

Fig. 5: From the left, a) oxygen isotopic curve of *C. wuellerstorfi* from ODP Site 849, Eastern Equatorial Pacific (Mix et al., 1995). b) Neotectonics and relative sea-level curves obtained by Lüdmann et al. (2001) from seismic data from the northern margin of the SCS. c) Interval length between GCL at the investigated Leg 184 sites vs. time, values are in k.y. The dotted lines indicate interglacial periods and in many cases correlate to longer intervals between GCL events (see text for explanation).

part of the sequence. At Site 1148, no relevant trend is noticed, while it is possible to detect a cyclicity. We execute autocorrelation analysis on the detrended records of intervals between events, and only for Site 1148 positive peaks on the autocorrelogram were statistically significant (at 80 and 90% level of confidence, Fig. 6). These peaks are located at 127, 140, 404, 270 and 477 ka.

DISCUSSION

Many theories on the origin of green colored layers have been forwarded, and the most common one is to attribute their genesis to alteration of volcanic material. Gardner and co-authors (1986) suggested that the pale green laminae found on sediment from the Lord Howe Rise east of Australia, were the product of alteration of volcanic material, as their occurrence correlated with the distribution of volcanic material and their mineralogy corresponded to bentonitic material. Lind and co-authors (1993), described colored bands from the Ontong Java Plateau sediments of Oligocene to Pleistocene age. They assigned a diagenetic origin to the laminae, as the colored bands crosscut bioturbation. No correlation between colored bands and proxies of productivity and climate was found, but their temporal distribution parallel the distribution of laminae observed at the Lord Howe Rise. Thus, Lind et al. (1993) ascribed their formation at the diagenetic alteration of volcanic material, as suggested by Gardner et al. (1986).

The origin of green granules on the Vietnam shelf was, on the other hand, attributed to diagenetic alteration of terrigenous material brought by the Mekong river onto the SCS (Markov, Mozherovskii et al., 1996). Quartz, feldspars and clay minerals, such as chlorite and micas occur in these sediments. Once settled in marine sediments, reducing conditions due to high contents of organic matter, altered the clay minerals, producing the characteristic green color.

There are few points against the volcanic origin for the GCL recovered in the SCS. The distribution of volcanic layers found in the sediments from the SCS are reported in Figure 4 and no striking similarity arises between volcanic and GCL occurrences. Several volcanic ash layers, intercalated to a number of GCL were observed onboard throughout the sediments cored during Leg 184 and, generally, no sign of green color was detected and volcanic glass was unaltered. Moreover, green layers don't crosscut pre-existent sedimentary fea-

Table 4

Leg	Site	Period k.y.	Tot. counted intervals	N. of counted green layers	Degrees of freedom	Calculated CHI square	CHI square (5% confidence)
184	1143	0-1105	221	345	4	4.553	9.488
184	1145	0-1005	201	171	3	32.967	7.815
184	1146	0-860	200	108	2	32.757	5.991
184	1148	0-1085	217	252	3	14.166	7.815

Table 4: Parameters used in testing for Poisson distribution (randomness) of green layers (Δt interval = 5 k.y.). Only for Site 1143 we fail to reject the null hypothesis (green layers follow a Poisson, so randomn distribution). For the other sites, we have to reject randomness.

tures as for the colored bands found by Lind et al. (1993). Both Lind and Gardner did not notice any remarkable distinction between the colored layers and the matrix (Gardner, Nelson et al., 1986; Lind, Janececk et al., 1993). Despite the overall variability of the measured parameters and the leveling operated by averaging (see Table 2), it is still possible to detect important differences between GCL and the host sediments: GCL are richer in iron, nickel, chlorite, smectite and mixed-layered clays, while are depleted in carbonate, authigenic P, barium and strontium (Tables 2 and 3).

We can explain these discrepancies invoking diagenetic alteration of original detrital material, thus glauconitization, as the main process influencing the genesis of GCL, so following Markov's theory (1996). Odin (1988) described the glauconitization process as being formed by three different stages, during which the original material is progressively altered (Fig. 7). SCS sediments are mainly constituted by nannofossil ooze mixed with detrital material, rich in kaolinite, micas and quartz. Relatively high content of organic mat-

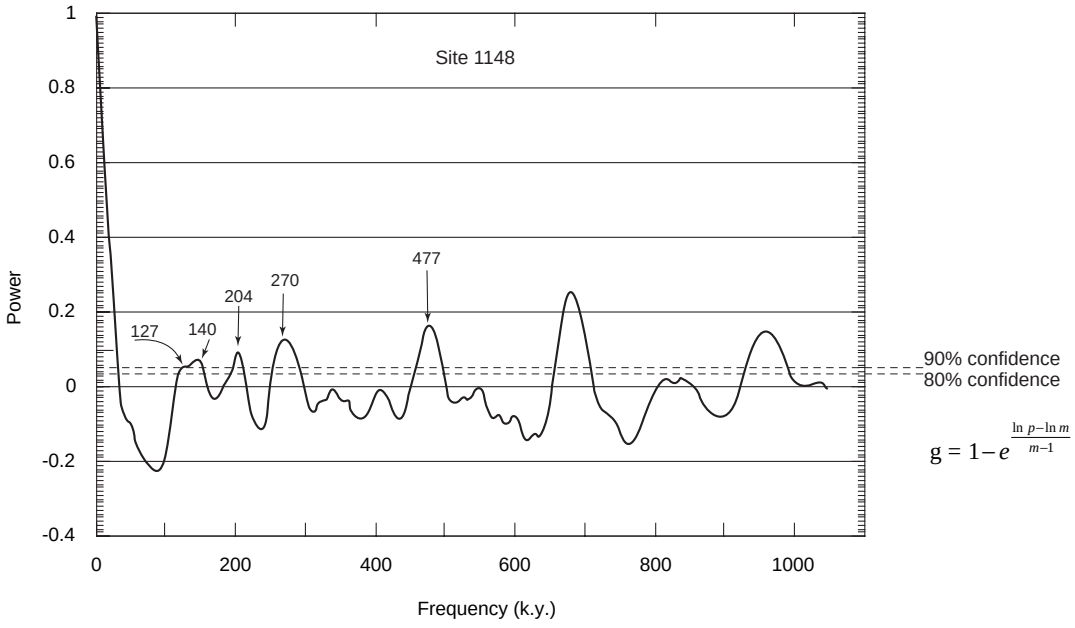

Fig. 6: Autocorrelogram of interval lengths between GCL for Site 1148. The two dotted lines represent significance levels at 80 and 90%, calculated as **g** (see formule above), where p = level of significance and m = (number of observation)/2. The choice of relatively low significance levels was determined on the consideration that during onboard observation and recording of the GCL, both continuous and bioturbated layers were counted. Signals at 127, 140, 204, 270 and 477 ka are statistically significant. Other peaks (frequencies > 500 ka) were not taken into account because statistically insignificant. Values of 127, 140, 204 and 477 ka are close to heterodynes (difference) of different eccentricity terms (Berger and Loutre, 1991).

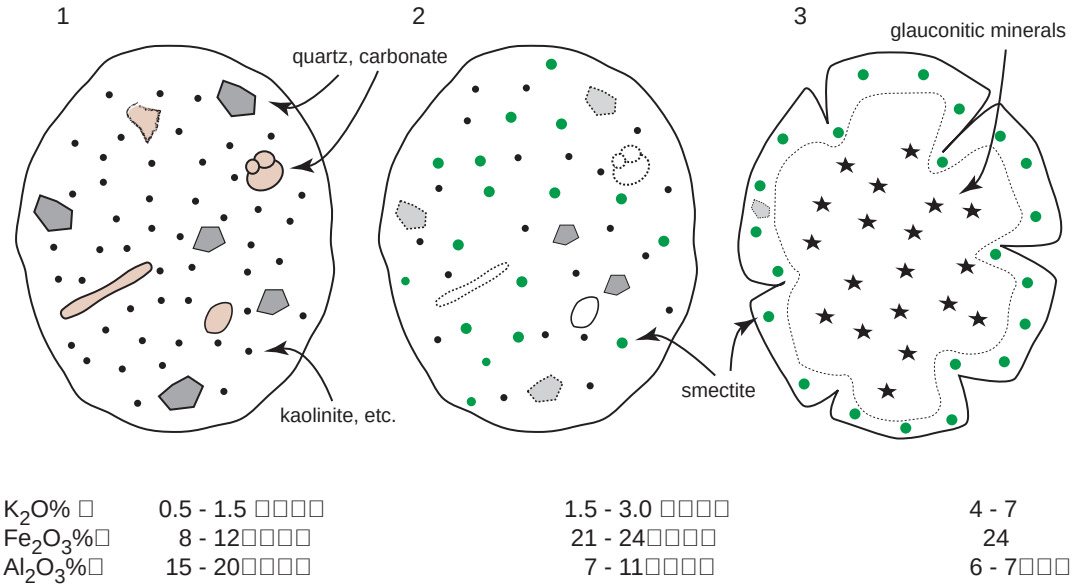

Fi. 7: Schematic evolution of green clay and glauconitic material from fecal pellets in Gulf of Guinea (Odin, 1988). GCL in the South China Sea are probably the result of the earlier diagenetic transformations between steps 1 and 2 of the above described process.

ter are reported in SCS sediments recovered during Leg 184 (Wang, Prell et al., 2000). These high concentrations could have promoted the formation of reducing micro-environments close to the water-sediment surface, which permitted an active exchange of ions from the seawater into the sediments. The few GCL observations at Site 1144 in the northern margin of the SCS, may in fact depend on the extremely high sedimentation rates that characterize this site: such sedimentation rates would fasten the burial of sediments, impeding the chemical exchange between sea and pore water, which is considered essential in the complete development of glauconitic layers (Chamley, 1989).

Increased microbial activity could have favored the degradation of organic matter, which is depleted in the GCL compared to the surrounding matrix. These conditions lead to the dissolution of carbonates which explains the observed decreases in GCL of CaO, barium and strontium, which are normally associated to carbonates in marine sediments. Clays, mainly kaolinite, are altered and decrease in abundance in the GCL, along with other detrital minerals, while authigenic Fe-rich clays, such as smectite and mixed-layered clays, increase. Iron is present at high concentrations and possibly is provided from the underlying sediments. Being in a reduced form, it is responsible for the characteristic green color that disappeared under oxygen-rich conditions. Comparable amounts of pyrite in both GCL and background sediments may be the result of oxidation of the original pyrite material in the GCL once reducing conditions have disappeared. Verdine, another authigenic green clay mineral which develops in Fe-rich and shallow environments (between 5 and 60 m, Odin, 1988), has not been found in SCS sediments.

The existence of a reducing environment during GCL formation is also attested by relatively high concentrations of nickel, that being chalcophile, tends to bind to iron sulphides. Another indication of reducing conditions is given by low amounts of authigenic phosphorus, which is mainly constituted by carbonate-fluorapatite (CFA). The precipitation in marine sediments of CFA is dependent on many factors, as pore water concentrations of dissolved phosphorus, fluorine and oxygen (Jarvis, Burnett et al., 1994). Degradation of

organic matter is a primary source of dissolved phosphorus, but under oxygen-depleted conditions and high carbonate alkalinity, CFA cannot precipitate (Jarvis, Burnett et al., 1994; Krajewski, Van Cappellen et al., 1994).

The extent of glauconitization normally depends on the nature and size of the original material, and the presence of very fine-grained particles, as it is the case for sediments from the SCS, allow glauconitization to proceed only to the very first stage of the transformation, where glauconite has not appeared yet, but already some differences between the altered material and the host sediments have become evident. Glauconitization normally occurs at shallow depths, but existence of glauconitic layers has also been reported in deeper waters (between 2000 and 3000 meter water depth), comparable to SCS sites locations (Chamley, 1989). We cannot exclude the possibility, considering the depth of the sites, the nature and geometry of the GCL, that they represent reworked material (i.e. distal turbidites) already undergone to glauconitization or whose higher porosity could have promoted glauconitization.

Many authors have used the distribution of glauconitic levels to track sea level changes during time (Chamley, 1989), as transgression and regression cycles can expose sediments located at different depth to conditions favorable to glauconitization. The study of the temporal distribution of GCL was attempted in order to asses if their formation was linked in any way to external factors, such as climatic changes, sea level variations and/or tectonism. As described in the results section, all sites except Site 1143, are characterized by non-random distribution and a trend in the length of intervals between two GCL events is evident especially for Sites 1145 and 1146 (Table 4 and Fig. 5). We have compared them to the neotectonic curve calculated for the SCS northern margin (Lüdmann, Wong et al., 2001), and it seems that since 600 ka, when the northern margin started experiencing uplift, the frequency of GCL increased and the intervals between events become shorter (Fig. 6). This observation seems to support the hypothesis of the reworked nature of the GCL, as tectonic activity and uplift may have increased the frequency of earthquakes and, thus, of turbidites.

A correlation, though poor, between interglacial periods, characterized by high sea level, and longer intervals between GCL events is brought up in Figure 5, especially for Site 1143. Only for Site 1148, the temporal distribution of GCL and the results of the autocorrelation point clearly to cyclicity, with the found frequencies really close to values of heterodynes of eccentricity frequencies. We are aware of the uncertainties in the temporal distribution of the GCL, which arise mainly from the fact that both continuous and discontinuous (e.g. bioturbated) layers were recorded during visual description of the cores. Nevertheless, we cannot exclude that changes in sea level, possibly resulting from the combination of climatic changes and tectonism, could have had any influences on the distribution and genesis of the layers. We know that during the last glaciation the shelf surrounding the SCS almost completely exposed (Pelejero, Kienast et al., 1999). Therefore, during low sea level periods the zone of active glauconitization may have moved offshore and as conditions at the sites are more favorable to diagenetic alteration, the intervals between GCL become shorter. During regression and low sea level stands, turbidites were likely to be more frequent, thus supporting the hypothesis of the possible reworked nature of the GCL.

CONCLUSIONS

Green clay layers in sediments from the South China Sea result from the diagenetic alteration of the original detrital brought in from the Asian continent. The geometric relation with the host sediments, the differences in mineralogy, granulometry and geochemistry

existing between the GCL and the background sediments favor the hypothesis that the layers represent the outcome of the initial steps of glauconitization. High organic matter content possibly set up localized reducing micro-environments which started the glauconitization process. No striking evidence exists pointing at a volcanic origin of the initial material. At present, we cannot exclude a link between GCL and turbidites. The temporal distribution of GCL, though probably biased during the recording process onboard, shows interesting correspondences with sea level and neotectonism curves, pointing at a possible influence of eustatism on the formation of these layers.

We are far from having deciphered the ultimate process responsible for the formation of green clay layers, but considered their widespread distribution in the ocean sediments and the possible amount of information they may bear, related to factors such as eustatism, climate and tectonism, the complete understanding of their nature and genesis may require further investigation.

Aknowledgements. The authors thank the captain, crew and technical staff of ODP Leg 184 for assistance and help in obtaining samples. We gratefully acknowledge the scientific party for providing the stratigraphy for all sites. The authors sincerely thank G. Galetti (University of Fribourg, Switzerland) for XRF analyses and E. Verrecchia (University of Neuchâtel, Switzerland) for help on statistical treatment of the dataset. Thanks also to J. Richard for technical assistance in preparing samples. This work was financially supported by the University of Neuchâtel (Switzerland).

REFERENCES

Anderson, L.D. and Delaney, M.L., 2000. Sequential extraction and analysis of phosphorus in marine sediments: Streamlining of the SEDEX procedure. Limnol. Oceanogr., 45(2), 509-515.

Berger, A. and Loutre, M.F., 1991. Insolation values for the climate of the last 10 million years. Quaternary Science Reviews, 10(4), 297-317.

Chamley, H., 1989. Clay sedimentology (Springler-Verlag).

Eaton, A.D., Clesceri, L.S. and Greenberg, A.E. (Eds.), 1995. Standard methods for the examination of water and wastewater

Espitalié, J., Deroo, G. and Marquis, F., 1986. La pyrolyse Rock-Eval et ses applications - III partie. Rev. Inst. Fr. Pet., 41(1), 73-89.

Gardner, J.V., Nelson, C.S. and Baker, P.A., 1986. Distribution and character of pale green laminae in sediment from Lord Howe Rise: a probable late Neogene and Quaternary tephrostratigraphic record. In: J.P. Kennett, C.C. von der Borch, P.A. Baker et al. (Eds.), Init. Repts. DSDP. 90. Washington (U.S. Govt. Printing Office), 1145-1159.

Jantschik, R., Nyffeler, F. and Donard, O.F.X., 1992. Marine particle size measurement with a stream-scanning laser system. Marine Geology, 106, 239-250.

Jarvis, I., Burnett, W.C., Nathan, Y. et al., 1994. Phosphorite geochemistry: state-of-art and environmental concerns. Eclogae geol. Helv., 87(3), 643-700.

Krajewski, K.P., Van Cappellen, P., Trichet, J. et al., 1994. Biological processes and apatite formation in sedimentary environments. Eclogae Geol. Helv., 87(3), 701-745.

Kübler, B., 1987. Dosage quantitatif des minéraux majeurs des roches sédimentaires par diffraction X. Cahier de l'Institut de Géologie de Neuchâtel, Série ADX.

Lafargue, E., Espitalié, J., Marquis, F. et al., 1996. Rock Eval 6 applications in hydrocarbon exploration, production and in soil contamination studies, Latin American Congress on Organic Geochemistry, Cancun.

Lind, I.L., Janececk, T.R., Krissek, L.A. et al., 1993. Color bands in Ontong Java Plateau carbonate oozes and chalks. In: W.H. Berger, L.W. Kroenke, T.R. Janaceck et al. (Eds.), Proc. ODP, Sci. Results. Vol. 130.

College Station, TX (Ocean Drilling Program), 453-459.

Lüdmann, T., Wong, H.K. and Wang, P., 2001. Plio-Quaternary sedimentation processes and neotectonics of the northern continental margin of the South China Sea. Marine Geology, 172, 331-358.

Markov, Y.D., Mozherovskii, A.V. and Eiberman, M.F., 1996. Origin of clay granules in the South Vietnam shelf sediments, South China Sea. Lithology and Mineral Resources, 31(4), 311-318.

Mix, A.C., N.G. Pisias, W. Rugh et al., 1995. Benthic foraminiferal stable isotope record form Site 849, 0-5 Ma: Local and global climate changes. In: N.G. Pisias, L. Mayer, T. Janecek et al. (Eds.), Proc. ODP, Scientific Results, Vol. 138. College Station TX (Ocean Drilling Program), 371-412.

Moore, D.M. and Reynolds, R.C.J., 1997. X-Ray diffraction and the identification and analysis of clay minerals (Oxford University Press).

Odin, G.G., 1988. Green marine clays. Developments in sedimentology. Amsterdam (Elsevier)

Pelejero, C., Kienast, M., Wang, L. et al., 1999. The flooding of Sundaland during the last deglaciation: imprints in hemipelagic sediments from the southern South China Sea. Earth and Planetary Science Letters, 171, 661-671.

Ruttenberg, K.C., 1992. Development of a sequential extraction method for different forms of phosphorus in marine sediments. Limnology Oceanography, 37(7), 1460-1482.

Wang, P., Prell, W.L., Blum, P. et al., 2000. Proc. ODP, Init. Repts., Vol. 184. College Station, TX (Ocean Drilling Program).

CHAPTER 6

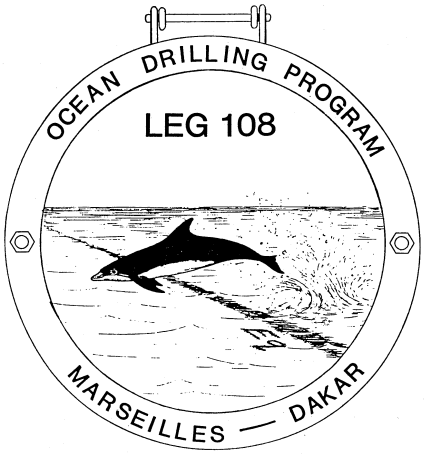

HIGH RESOLUTION

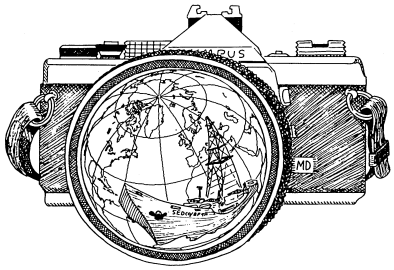

LEG 151 - Atlantic Arctic Gateways

St. John's to Reykjavik

July-September 1993

From the continent to the ocean. Phosphorus in marine sediments during the last 150,000 years: exploring relationships between continental weathering, productivity, and climate. Overview and conclusions.

1. INTRODUCTION

Phosphorus (P) is an important nutrient and is thought to limit productivity, particularly in marginal seas (Broecker, 1982; Delaney, 1998). Due to the lack of an important gaseous phase in the atmosphere, new P to the ocean is delivered principally by weathering of rocks and soils on the adjacent continents (Froelich et al., 1982). Therefore, the phosphorus record in marine sediments has been considered as a proxy to reconstruct link between continental weathering, nutrient input to the ocean and productivity (e.g. Föllmi, 1995).

As the P cycle in marine sediments is extremely complex, being driven by different chemical and physical parameters (see Chapter 1), the relationships between P records in marine sediments, continental weathering and changes in climate on short time-scales, such as glacial-interglacial timescales are still not well constrained and understood. A clear understanding of P distribution and behaviour in marine sediments through time and under different environmental conditions is essential to be achieved, in order to confidently use this tool for paleoclimatic investigations.

The data presented in this chapter are the result of the study of samples from 5 ODP sites: 108-658 (North eastern Atlantic), 112-680 (Peru margin), 128-798 (Japan Sea), 130-806 (Ontong Java plateau) and 151-907 (North Atlantic). Beside phosphorus phases, the bulk mineralogy, organic matter, and nitrogen stable isotopes of bulk sediments have been analyzed. The obtained results will be discussed along with the results coming from the study of ODP Site 724 in the Oman margin (Chapter 2), Sites 1143 and 1144 in the South China Sea (Chapter 3) and of core SU 90-09 in the North Atlantic (Chapter 4). The goal here is to decipher P sedimentary records, and better understand the link between the preserved phosphorus phases and local and global variations in weathering on continent, oceanographic conditions and climate changes, over the last glacial-interglacial cycle.

2. METHODS

All samples, of approximately 10 cc each, were dried at a temperature of 50°C and divided in subsamples for the planned analyses. All the analyses were performed at the GEA laboratory in Neuchâtel. Nearly 5 g of dried sediment was ground to obtain a homogeneous powder with particles sizes <40 μm (Kübler, 1987). Part of this powder, chosen randomly, was pressed (20 bars) in powder holders and then analyzed by XRD. Bulk sediment mineralogy was determined by XRD (SCINTAG XRD 2000 Diffractometer) based on a semi-quantitative estimation, and using external standards (Kübler, 1987). The error in the percent estimate of the bulk rock mineralogy is about 5%. The characterization of the organic matter was performed on about 100 mg of dried and ground bulk sediment, with a Vinci Technologies Rock-Eval 6, and using a standard whole rock pyrolysis method (Espitalié et al., 1986; Lafargue et al., 1996).

The distribution of different phosphorus phases in bulk sediment was determined using a 4-steps sequential extraction technique, adapted from the SEDEX method, developed

Table 1: Sequential extraction technique (SEDEX)

Step name	Treatments	P component isolated *a*	Errors *b*	Detection limits *c*
Iron-bound P *d*	10 ml CBD solution (6hr) (0.22 M sodium citrate, 0.11 M sodium bicarbonate 0.13 M sodium dithionite) 10 ml 1M MgCl2 (2hr) 10 ml H2O (2hr)	Exchangeable or loosely sorbed P Reducible or reactive iron-bound P **PLUS Ferric Fe**	3-6%	0.03
Authigenic P *e*	10 ml 1M Na-acetate buffered to pH 4 with acetic acid (5hr) 10 ml 1M MgCl2 (2hr) 10 ml 1M MgCl2 (2hr) 10 ml H2O (2hr)	Carbonate fluorapatite (CFA) biogenic hydroxyapatite	2-7%	0.025
Detrital P *e*	10 ml 1N HCl (16 hr)	Detrital fluorapatite-bound P	3-5%	0.003
Organic P *e*	1 ml 50% (w/v) MgNO3, dry in low oven, ash at 500°C (2 hr) 10 ml 1N HCl (24 hr)	Organic-bound P	2-5%	0.004

a: Concentrations of all phases are expressed in mg/g of sediment.
b: Errors for each phase determination are considered as the rel. standard deviation calculated on replicate analyses of consistency standards.
c: Detection limits are considered as 3 * rel. standard deviation calculated on replicate analyses of blank solutions.
d: Iron-bound phosphorus and ferric Fe concentrations were analyzed using an ICP-AES.
e: The other phases were analyzed using a spectrophotometer. Sample solutions were diluted in distilled water and a color developping agent was added to the solution, following the ascorbic acid method for phosphate (Eaton et al., 1995).

Table 2: ODP sites references

Site	Stratigraphy	Physical Parameters
658	*Sarnthein and Tiedemann (1989)* ODP SR Vol. 108; p. 167-185	*ODP Initial Reports (1988)* Vol 108, p. 105-219
680	*Wefer, Heinze and Suess (1990)* ODP SR Vol. 112; p. 355-367	*ODP Initial Reports (1988)* Vol 112, p. 249-303
798	*Föllmi et al. (1992)* ODP SR Vol. 127/128; p. 559-576 *Tada, Irino and Koizumi (1999)* Paleoceanography 14 (2); p. 236-247	*ODP Initial Reports (1989)* Vol 128, p. 121-236
806	*Bickert et al. (1993)* ODP SR Vol. 130; p. 411-420	*ODP Initial Reports (1991)* Vol 130, p. 291-367
907	*McManus et al. (1996)* ODP SR Vol. 151; p. 437-444	*ODP Initial Reports (1995)* Vol 151, p. 57-111

by Ruttenberg (1992) and modified by Anderson et al. (2000). This method utilizes differential dissolution of solid phases to extract P associated to well defined sedimentary components: iron and manganese oxydes-hydroxydes, authigenic minerals, detrital material and organic matter (Table 1). For all the steps other than the iron-bound P, the ascorbic acid molybdate blue technique was employed to develop color (Eaton et al., 1995). A Perkin-Elmer UV/Vis spectrophotometer Lambda 10 was used to determine absorbance and P concentrations. For the iron-bound P phase, the concentrations were detected using an ICP-AES, at the "Laboratoire des eaux et de l'environnement" in Neuchâtel, Switzerland. Reagent blanks, standards and consistency standards were used to perform calibration curves for each step and check analytical reproducibility over time (Table 1). Nitrogen stable isotopic analyses were performed on bulk sediments at the Stable Isotope Laboratory, ETH-Zentrum, Zürich, using a Carlo Erba CNS2500 CHN Elemental Analyzer coupled with a FISONS OPTIMA mass spectrometer. Mean errors, calculated as the relative standard deviation on atropine measurements are between 2 and 3% (results are reported in Annexe B). Mass accumulation rates (MAR) are here expressed in $mg/cm^2 \cdot k.y.$; sources of dry bulk density values and linear sedimentation rates values are listed in Table 2.

3. SITES DESCRIPTION AND RESULTS

In this section, we provide a schematic description of the regions, in terms of oceanography and climate, followed by a detailed description of the mineralogical and geochemical analyses.

3.1 Site 108-658: Eastern tropical Atlantic

Site 108-658 (2263.6 meters below sea level, mbsl) is situated on the continental slope west of Cape Blanc, Eastern tropical Atlantic, under an upwelling cell, which is one of the four major upwelling zones on eastern continental margins (Fig.1). Stein et al. (1989) estimated paleoproductivity at this site to vary between 150 and 190 $gC/m^2 \cdot y$. Despite the relatively high oxygen content of the bottom waters, sediments at Site 658 are rich in well-preserved organic matter (OM), probably due to rapid burial that shortened the residence time of OM in the oxic section of the sediment column (Stein et al., 1989). Based on isotopic stratigraphy, sedimentation rates at Site 658 vary between 12 and 26 cm/k.y. during the last 200 k.y. A hiatus, spanning Marine Isotope Stage (MIS) 4 and part of MIS 3, has been recognized (Sarnthein and Tiedemann, 1989).

Sediments at Site 658 are represented by a mixture of marine organism remains and of terrigenous material, coming from the African

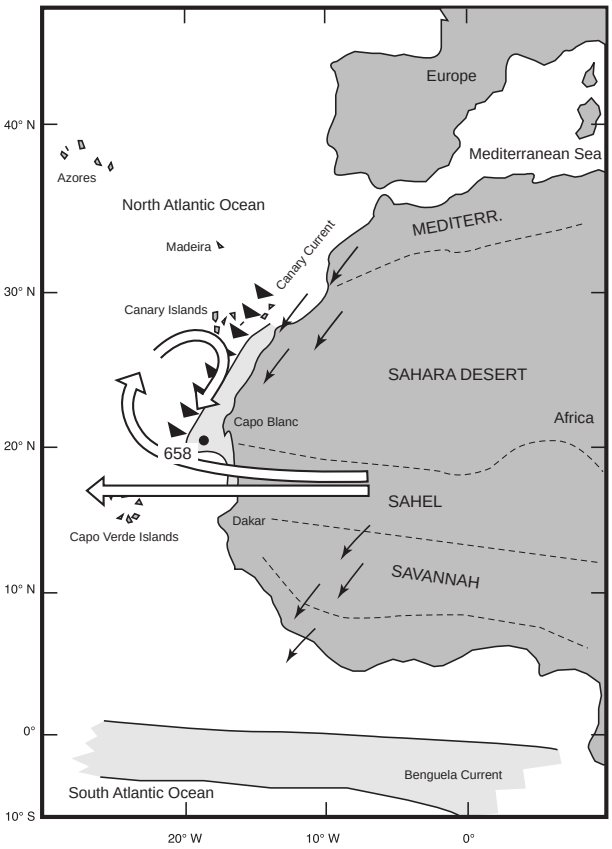

Fig. 1: Location map for ODP Site 658 (redrawn from Sarnthein and Tiedemann, 1989). Oceanic currents (solid triangles), upwelling cell (gray area), meridional winds (solid arrows) and the African Easterly Jet wind pattern (open arrows) are shown.

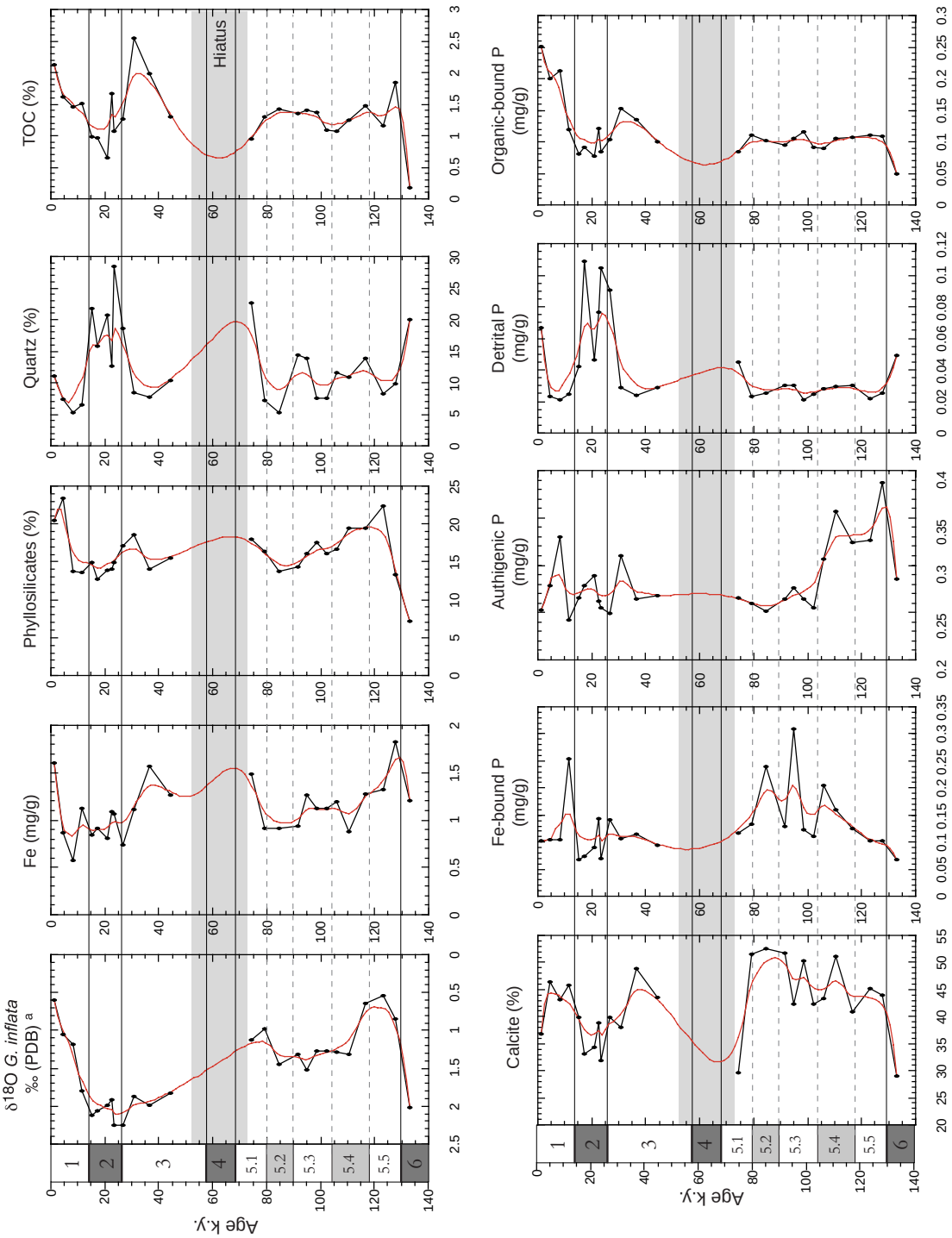

Fig. 2: Data from ODP Site 108-658. Top: $\delta^{18}O$ data of *G. Inflata*, concentration (in mg/g) of ferric Fe, percentages of phyllosilicates, quartz, and TOC. Bottom: percentage of calcite and concentrations (in mg/g) of Fe-bound, authigenic, detrital and organic-bound P. Horizontal lines represent the boundaries between isotopic stages. The gray area represents the hiatus as indicated by Sarnthein and Tiedemann (1989). a) Oxygen stable isotope data from Sarnthein and Tiedemann (1989).

continent and from the Sahara desert. According to Tiedemann and co-authors (1989) lithogenic material accumulation along the western African margin is controlled by three sources: eolian supply, linked to variations of the African Easterly Jet (AEJ) and of trade winds (Fig. 1), fluvial supply, which influenced only Site 658 among all Leg 108 sites, and turbidites, which, on the other hand, were a major contributor at Site 657.

This region is influenced by monsoon climate: during summer, a low pressure cell develops over central North Africa, promoting the inflow of humid air from the Atlantic, which brings occasional monsoon-style rains to the Saharan and sahel regions. During winter, NE trade winds are predominant and transport African dust to the ocean. Therefore, the sedimentary record recovered from Site 658 should give detailed information on changes in upwelling intensity, productivity, and in continental material input, which are related to fluctuation of the regime in trade winds and to variations in humidity and dryness over the last glacial-interglacial cycle.

Cores recovered from Holes 108-658 A and B were sampled from 0 to 17.85 meters below sea floor (mbsf), for a total of 26 samples and yielding a time resolution of about 5 k.y. Hemipelagic sediments from the sampled interval are characterized by cyclic changes between nannofossil ooze and dark silica- and detrital rich material. Calcite is the main bulk mineral component of sediments at Site 658, averaging 45%, while detrital material (the arithmetic sum between quartz, phyllosilicates, plagioclase and K-feldspar), thought present at relatively high percentages (average of 33%), is subordinate. Calcite and phyllosilicates records follow $\delta^{18}O$ curve, displaying low values during MIS 2 and high values during interglacial periods. Quartz is inversely correlated to both calcite and phyllosilicates, as higher percentages are observed during MIS 2. Fe contents average about 1.2 mg/g of sediments (Fig. 2).

Phosphorus phases constitute a small percentage of total sediments, averaging not more than 0.07 %. Fe-bound and authigenic P are the most abundant forms, with highest concentrations of about 0.3 and 0.4 mg/g, respectively. Fe-bound P reaches its highest values at around 90 ka, while authigenic P peaks at the beginning of MIS 5, during MIS 2 and the Holocene. Detrital P shows rather low concentrations, averaging 0.03 mg/g, and reaches values of about 0.1 mg/g only during glacial stage 2. No evident correlation between P phases is observed. Instead, a clear similitude in trends is noticed between authigenic P and phyllosilicates, and between detrital P and quartz. This pattern is probably caused by changes in the

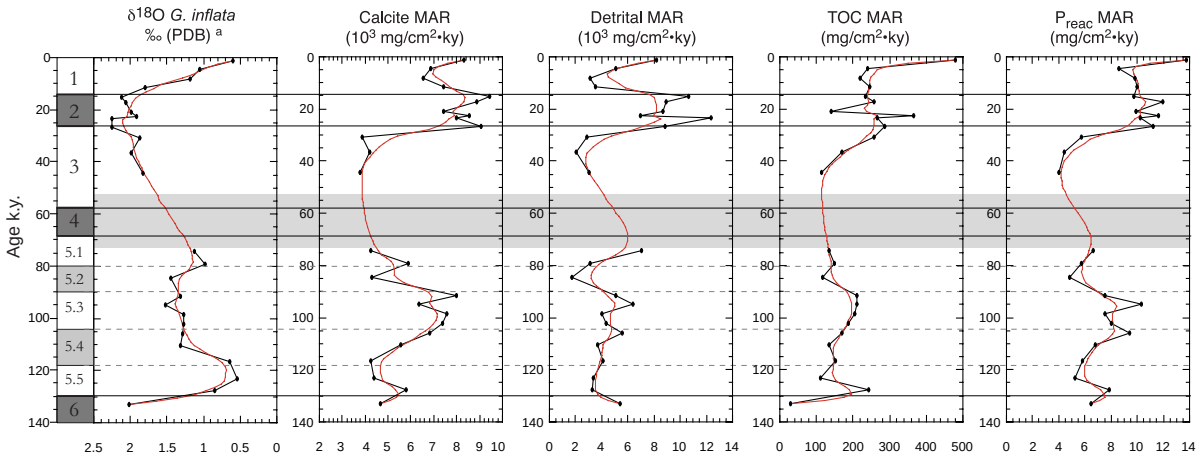

Fig. 3: Site 108-658. $\delta^{18}O$ data of *G. Inflata*, calcite, detrital silicates, TOC and reactive P Mass Accumulation Rates (MAR). Horizontal lines represent the boundaries between isotopic stages. The gray area represents the hiatus as indicated by Sarnthein and Tiedemann (1989). a) Oxygen stable isotope data from Sarnthein and Tiedemann (1989).

source of detrital material, related to variations in monsoon regime.

TOC contents are quite important and average around 1.5 %. Percentages are higher during MISs 5 and 1, and at the top of stage 3, while during glacial stage 2 they lower to about 1%. The peak in TOC at the top of stage 3 is paralleled also by other proxies, like organic-bound P, authigenic P and, to a lesser extent, Fe and calcite.

MAR of all proxies are generally higher during glacial stage 2, where both calcite detrital material MAR show values up to $9 \cdot 10^3 \cdot mg/cm^2 \cdot k.y.$ and $12 \cdot 10^3 \cdot mg/cm^2 \cdot k.y.$, respectively (Fig. 3).

3.2 Site 112-680: Peru Margin

The Peru margin upwelling area is linked to the eastern boundary currents system and is one of the five most important year-round upwelling regions in the world oceans (Fig. 4; Webster, 1987). This area is under the influence of south-easterly trade winds, which promote the upwelling of cold and nutrient-rich water parallel to the coast, fostering intense productivity. Total primary production is estimated to be higher than 500 $mgC/m^2 \cdot day$ (Reimers and Suess, 1983), and organic matter reaches more than 5 wt% of total sediment (Oberhänsli et al., 1990). The high percentage of decaying organic matter and the already low oxygen content of the Peru counter current waters contribute to the formation of an Oxygen Minimum Zone (OMZ), which extends between 100 and 600 m. Oxygen levels in the OMZ are as low as <0.2 ml/l (Resig, 1990). During the last 2-3 Ma the region has been subjected to intense tectonic subsidence (Oberhänsli et al., 1990; Resig, 1990). As a result, redeposition processes of tectonic origin have left an overprint on the climatic signal. However, micropaleontological observations permit to recognize periods of intense upwelling and development of an extensive OMZ during the upper part of MIS 5, 3 and the lower part of MIS 1 (Oberhänsli et al., 1990), allowing a paleoclimatic study of the core.

Cores from hole 112-680B (Peru margin, 252.5 mbsl) were sampled from 0 to 9.9 mbsf at a time resolution of about 5 k.y., for a total of 26 samples. The sampled interval corresponds to the Holocene and latest Pleistocene and consists of laminated and bioturbated diatomaceous clay with foraminifers, intercalated with gray, centimeter-thick clastic silt and sand layers (Suess et al., 1988). Phosphates and dolomite have been detected throughout the sequence. Laminated and diatom-rich mud is deposited preferentially during warm intervals, documented by low $\delta^{18}O$ values, while sand and silty layers repre-

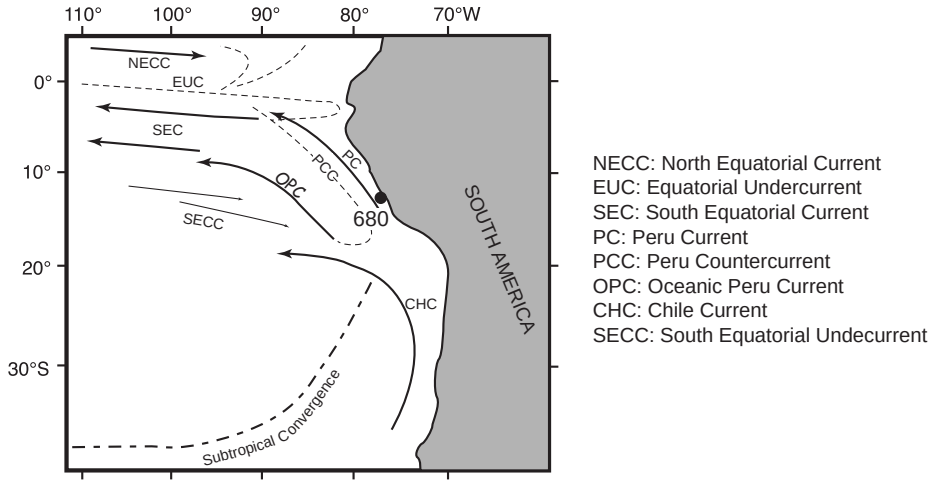

Fig. 4: Location map of ODP Site 680. The surface and subsurface current patterns are illustrated (from Oberhänsli et al., 1990).

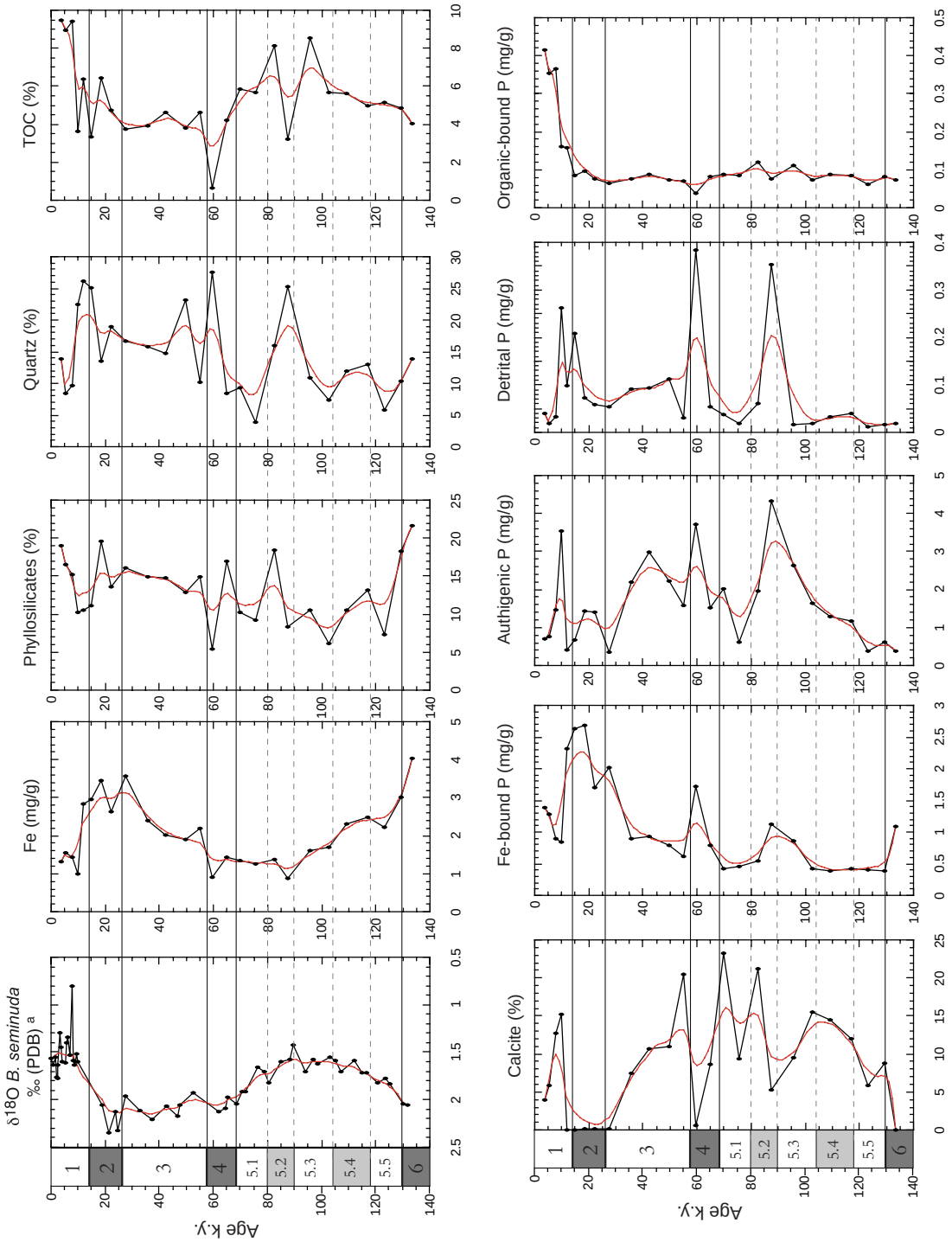

Fig. 5: Data from ODP Site 112-680. Top: $\delta^{18}O$ data of *B. seminuda*, concentration (in mg/g) of ferric Fe, percentages of phyllosilicates, quartz, and TOC. Bottom: percentage of calcite and concentrations (in mg/g) of Fe-bound, authigenic, detrital and organic-bound P. Horizontal lines represent the boundaries between isotopic stages. a) Oxygen stable isotope data from Wefer et al. (1990).

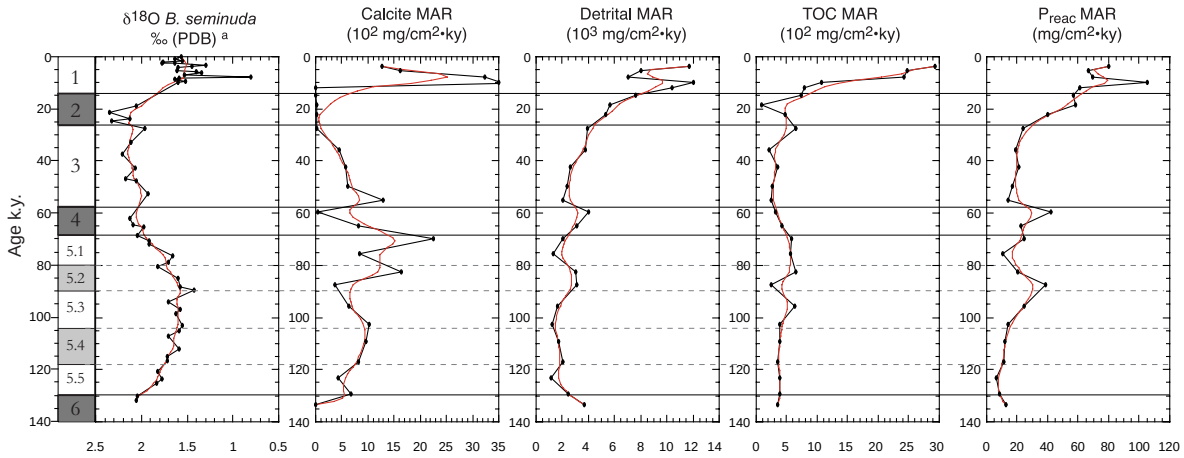

Fig. 6: Site 112-680. $\delta^{18}O$ data of *B. seminuda*, calcite, detrital silicates, TOC and reactive P Mass Accumulation Rates (MAR). Horizontal lines represent the boundaries between isotopic stages.
a) Oxygen stable isotope data from Wefer et al. (1990).

sent deposition during cold periods, as indicated by high $\delta^{18}O$ values (Wefer et al., 1990). The Pleistocene sedimentary sequence recovered at Hole 680B is characterized by relatively high sedimentation rates, ranging between 5 and 15 cm/k.y. (Oberhänsli et al., 1990).

Detrital material constitutes the principal component of the Peru margin sediments, representing in average 37 % of total sediment. Quartz and phyllosilicates are the most abundant detrital minerals, and range between 6% and 26%, and between 7.5% and 22%, respectively (Fig. 5). They most likely indicate detrital fluvial and/or eolian contributions from the continent, in relation to changes in aridity and wetness. High percentages of quartz are observed during MISs 4-2, with peaks of about 25% at the end of stages 4 and 2. Phyllosilicates roughly follow the same trend, with overall higher values in MISs 4-2. Starting from MIS 4, quartz and phyllosilicates are inversely correlated, presumably because of a different source. Calcite is present in low percentages, averaging 10%. At the end of stage 4 and during stage 2 the percentages of calcite are extremely low, indicating dissolution during glacial periods and/or dilution by detrital material.

Except for organic-bound P, all phosphorus phases show the same general trend, with higher values during glacial periods, and major peaks centred at 90, 60 and 20 ka, which coincide with peaks in quartz percentages. Fe-bound P shows a positive correlation with quartz and high values (up to 2.5 mg/g) are observed during glacial stages 4 and 2. Authigenic P reaches values up to 3-4 mg/g, while detrital P shows values not higher than 0.4 mg/g. Organic-bound P concentrations are quite low and average 0.1 mg/g, except for the youngest part of the sequence where it presents values of about 0.4 mg/g. Peru margin sediments are rich in organic matter and TOC values average 5 % for almost the entire interval, with peaks of about 10 % during the Holocene. MAR of all proxies display a consistent increase during the Holocene (Fig. 6). Detrital and reactive P MAR are quite constant throughout the interval, averaging $4 \cdot 10^3$ mg/cm^2·k.y. and 20 mg/cm^2·k.y., respectively. Moreover, a less pronounced peak is observed in both records during MIS 4. Calcite MAR are more variable, with the lowest values recorded at the end of glacial periods and a sharp increase at the beginning of stage 1.

3.3. Site 128-798: Japan Sea

The Japan Sea, one of the many back-arc basin bordering the western Pacific Ocean, began to form by continental rifting during the Tertiary, and nowadays it is undergoing the

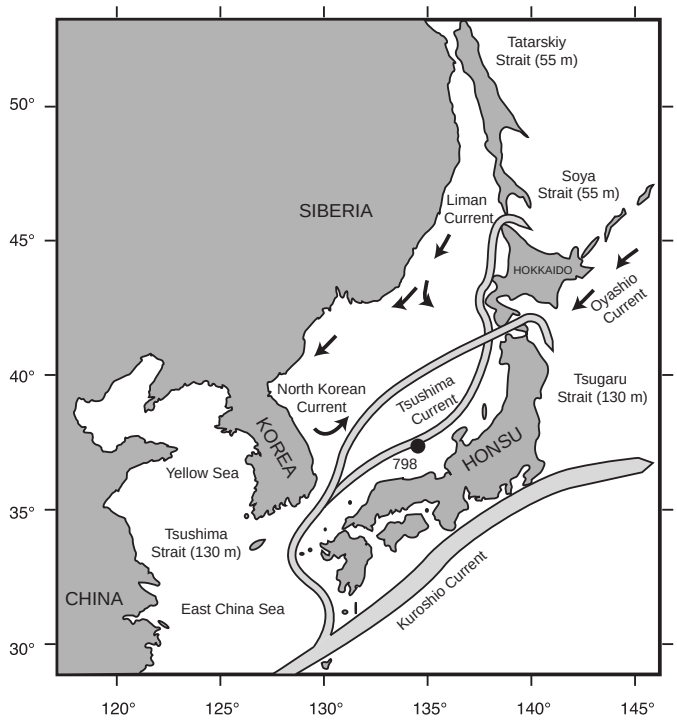

Fig. 7: Location map of ODP Site 798. The current system of the Japan Sea and of adjacent waters is represented (after Kawai, 1972). Solid black arrows indicate cold currents, while white arrows warm currents.

first stages of compressive deformation. It is connected to the Pacific Ocean through 4 straits (Tsushima, Tsugaru, Soya and Tartar straits), whose depths are ranging between 12 and 130 m (Fig. 7). The Tsushima current, a branch of the Kuroshio current bringing warm and highly saline surface water, enters the Japan sea from the south and exits from the northern straits (Fig. 7). In the northern part of the Japan sea, the production of cold and low salinity waters (the Liman current) concur in ventilating the water column and in maintaining high oxygen levels, which exceed 5 ml/l at all depths (Ingle et al., 1989). The sinking of the Liman current further south and the mixing with the Tsushima current produce a well homogenized water mass, characteristic of the Japan sea.

The particular geometry of the basin and the presence of such shallow straits, make the Japan sea extremely sensitive to sea level changes, and imply that during low sea level during glacial times, the Japan sea was most presumably a semi- if not completely isolated basin. The closing of all communications with the open ocean produced stagnant and possibly anoxic conditions, as recorded by organic-rich intervals. Moreover, the East Asian monsoon influences the climate over the region: warm and humid summers are followed by cold and dry winters, dominated by Siberian winds. Thus, the co-occurrence of tectonic, climatic and eustatic variations during the last glacial-interglacial cycle has probably left a strong and complex imprint on the sedimentological and geochemical record at Site 798.

Site 798 (902 mbsl) is located in a small depression on the Oki Ridge, in the southern part of the Japan Sea (Fig. 7). Sediments are mostly composed of diatomaceous material mixed with detrital sediments, probably of eolian origin (Ingle et al., 1989). Three superposed orders of dark-light cycles have been recognized in the sediments and interpreted as the result of winter and summer monsoons interchange, oxygen level variations in bottom waters, related to oceanic circulation and sea level changes, and balance between detrital input and organic matter production and preservation (Föllmi et al., 1992; Tada et al., 1992).

It was not possible to obtain a detailed iso-

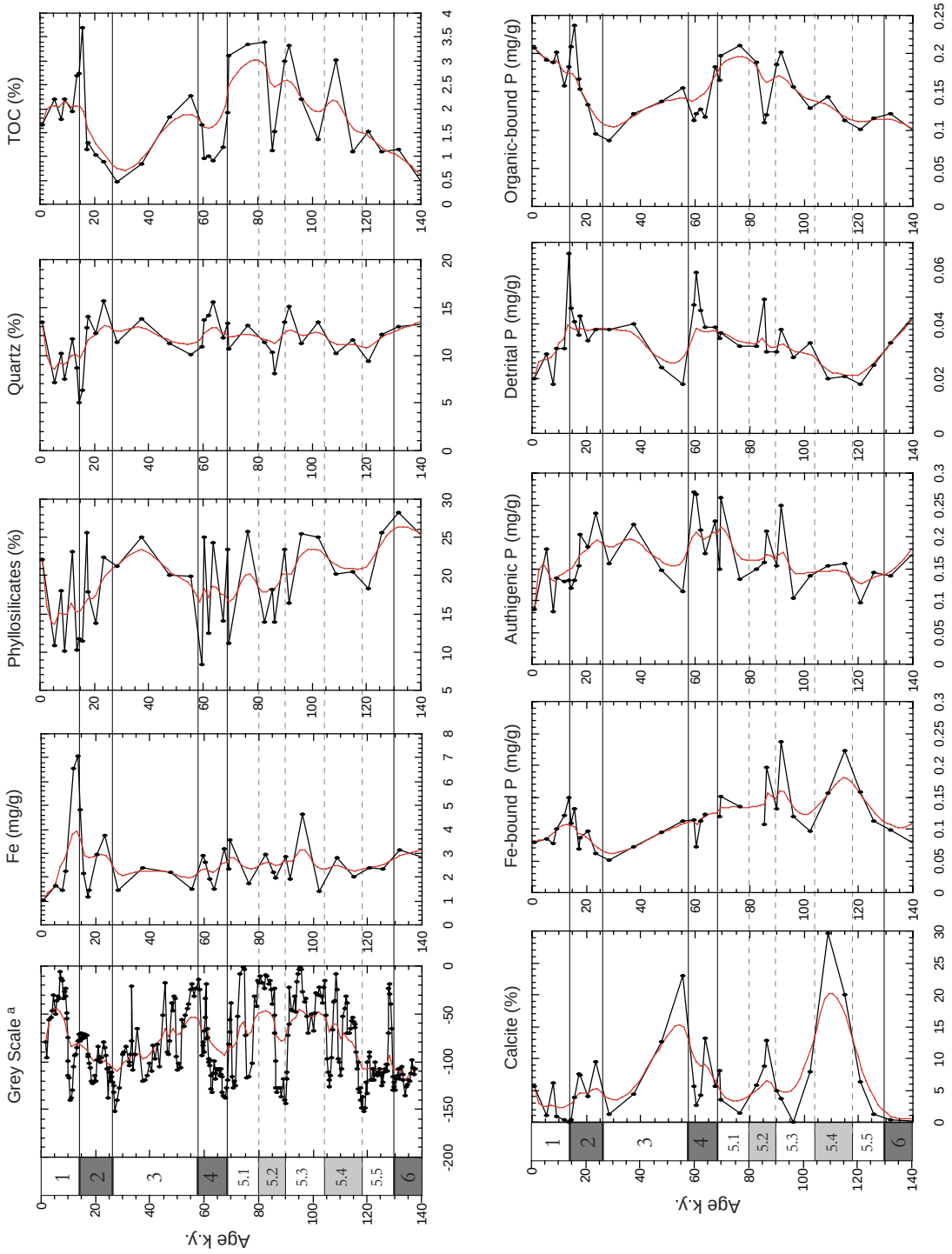

Fig. 8: Data from ODP Site 128-798. Top: Gray scale, concentration (in mg/g) of ferric Fe, percentages of phyllosilicates, quartz, and TOC. Bottom: percentage of calcite and concentrations (in mg/g) of Fe-bound, authigenic, detrital and organic-bound P. Horizontal lines represent the boundaries between isotopic stages.
a) Gray scale values are from Föllmi et al. (1992). The age model is obtained by interpolation using data from Tada et al. (1999) .

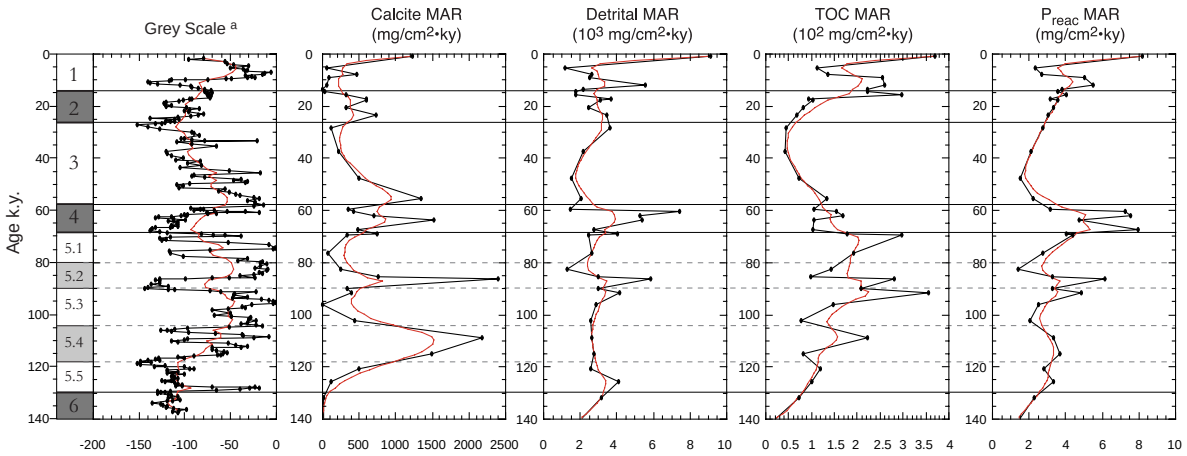

Fig. 9: Site 128-798. Gray scale, calcite, detrital silicates, TOC and reactive P Mass Accumulation Rates (MAR). Horizontal lines represent the boundaries between isotopic stages. a) Gray scale values are from Föllmi et al. (1992). The age model is obtained by interpolation using data from Tada et al. (1999).

topic stratigraphy, because of the lack of sufficient foraminifera in sediments from Site 798 (Dunbar et al., 1992). Though aware of the uncertainties arising from this procedure, we have used a graphic method and correlated spectrophotomotric grey scale values of sediments from Sites 798 and 797, for which a more precise age model has been constructed (Föllmi et al., 1992; Tada et al., 1999).

Detrital minerals average 37%, while calcite constitutes on average only 7% of bulk sediment. Phyllosilicates are the most abundant components, averaging 20%, and display a trend similar to that of quartz. Higher detrital supply is recorded during MISs 6, 3 and 2, in relation to low grey scale values. The calcite record is rather scattered. Maxima in percentage are observed during MIS 5 and at the base of MIS 3 (Fig. 8).

Phosphorus phases are low in abundance and represent not more than 0.05% of bulk sediment. Fe-bound, authigenic and organic-bound P range around comparable values of abround 0.15 mg/g. Detrital P is the less abundant P phase and its trend is similar to authigenic P (Fig. 8). Fe-bound P and Fe trends show no evident correlation. Fe concentrations are quite high, averaging 3 mg/g. Japan sea sediments are relatively rich in organic matter, which averages 1.5%. The TOC record shows a significant increase from the bottom of the sequence and highest values are observed at the top of MIS 5. Another peak is recorded at stages 2-1 boundary. Organic-bound P mirrors the TOC trend.

Probably because of the uncertainties of the age model, MAR are difficult to decipher and to correlate to known glacial-interglacial patterns. MAR values of almost all parameters increase from the base of MIS toward MIS4, and then decrease again and reach low values during MIS 3. Organic carbon and reactive P MAR show a concomitant increase at the boundary of stages 2-1 (Fig. 9).

3.4 Site 130-806: Ontong Java Plateau

The Ontong Java Plateau, a broad submarine plateau, is located in the western equatorial Pacific (Fig. 10), north of the Salomon islands. Its location inside the western Pacific warm pool (WPWP) makes surface temperatures quite stable, and, as little seasonal and interannual variations are observed, sediments are expected to record global rather than local temperature changes over glacial-interglacial cycles.

The plateau rises well above the carbonate compensation depth (CCD), allowing an important accumulation of carbonate sequences, almost not affected by dissolution. For most of the Neogene, it has been located

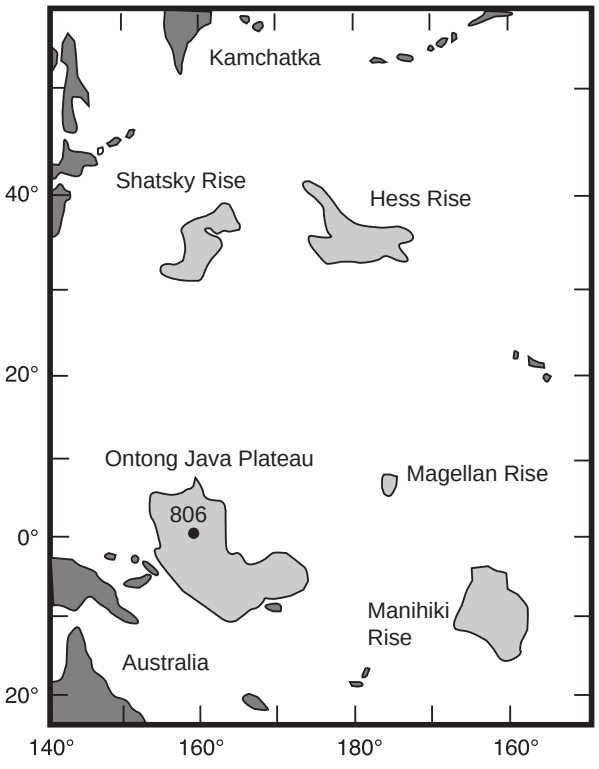

Fig. 10: Location map of ODP Site 806. Submarine plateau are represented in light gray (after Tarduno et al., 1991).

close to the equator, inside the equatorial upwelling system region that is characterized by moderately high productivity (35-60 gC/m2·yr; (Berger et al., 1989). The upwelling of cold and nutrient-rich waters has probably affected the thermocline depth, leaving an imprint on the global climatic signal. The Pacific Deep Water, characterized by low oxygen concentrations and high silica contents (Craig et al., 1972), baths the Ontong Java plateau at depths between 2000 and 3000 meters. Stable carbon isotopic records on benthic foraminifera bear indications of increased productivity during glacial periods, along with information on North Atlantic Deep Water (NADW) production (Bickert et al., 1993). Due to its location far from large continental masses, terrigenous material accumulation in Ontong Java sediments is supplied only by wind transport, provided by Northern Hemisphere westerlies, northeasterly and southeasterly trades, and local winds. As determined by mineral assemblages, the main source area of the detrital material is the Asian continent (Krissek and Janecek, 1993).

Cores from Site 806 (2520.7 mbsl) were sampled from 0 to 2.75 mbsf, for a total of 27 samples. Some of the analyzed proxies are probably biased, due to the high calcite content of the Ontong-Java site sediments. Rock Eval measurements probably underestimate TOC contents, as CO_2 produced from carbonate decomposition during pyrolysis at relatively low temperature overlaps with the CO_2 originating from organic matter. The semi-quantitative method we used to determine bulk mineralogy by XRD is valid with $CaCO_3$ % ranging 40-90, and it gives an error of 5%. With high carbonate content, as this is the case, XRD data need to be corrected and the error rises to 5-10%. On the other hand, the analytical procedure of sequential extraction of phosphorus is not concerned by the carbonate-rich nature of sediments.

Calcite constitutes the principal component of sediments at Site 806, and reaches percentages of about 97%. Detrital material averages only 6% of bulk sediment. Phyllosilicates are the most abundant detrital minerals, while quartz represents in average, only 1% of bulk sediments. No significant changes are observed in their records (Fig. 11). Measured values of all phosphorus phases are in the range of concentrations published by Filippelli and Delaney (1996) for equatorial Pacific sediments of the same age. Authigenic and Fe-bound P constitute the most abundant P phases in the Ontong-Java site sediments, and average 0.2 and 0.15 mg/g, respectively. Authigenic P increases up core from the bottom of the studied sequence to reach the highest values at the base of MIS3, and then it decreases again. Detrital P concentrations range between 0.01 and 0.03 mg/g and show no evident correlation with other detrital minerals. TOC concentrations are extremely low (0.13 - 0.26 %). Higher values, observed at the base of MIS3 and during MIS2, correlate with peaks in quartz percentages. Generally, MAR increase toward the Holocene (Fig. 12).

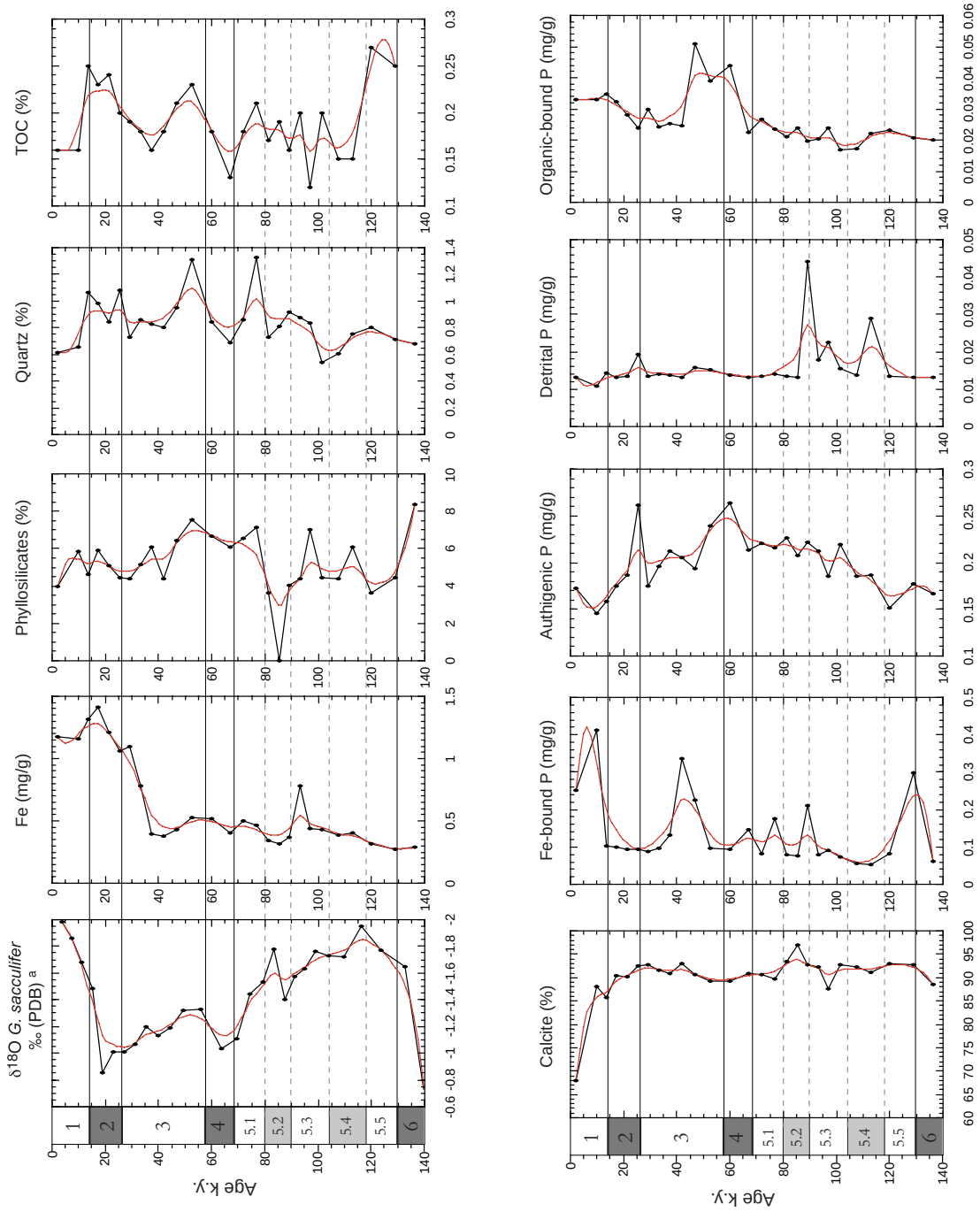

Fig. 11: Data from ODP Site 130-806. Top: $\delta^{18}O$ data of *G. sacculifer*, concentration (in mg/g) of ferric Fe, percentages of phyllosilicates, quartz, and TOC. Bottom: percentage of calcite and concentrations (in mg/g) of Fe-bound, authigenic, detrital and organic-bound P. Horizontal lines represent the boundaries between isotopic stages. a) Oxygen stable isotope data from Bickert et al. (1993).

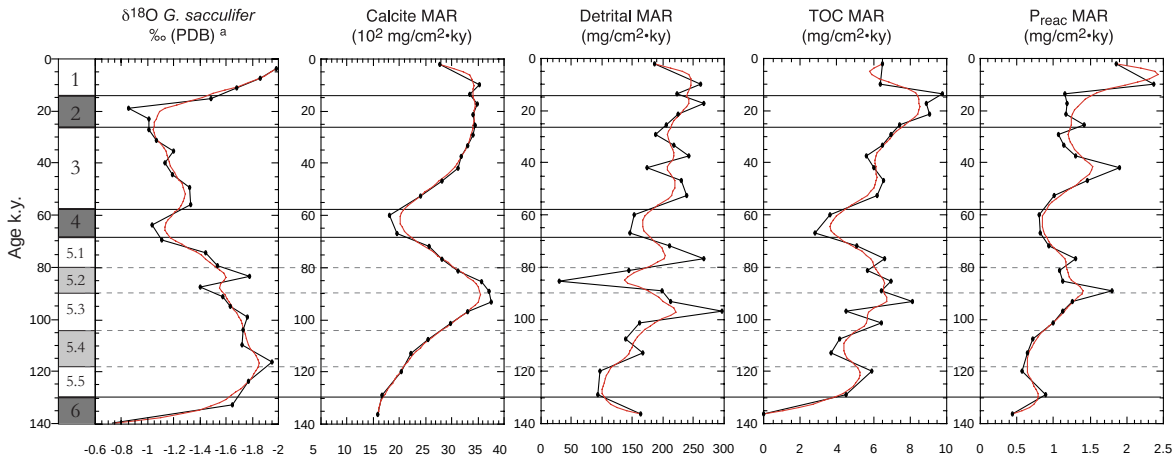

Fig. 12: Site 130-806. δ18O data of *G. sacculifer,* calcite, detrital silicates, TOC and reactive P Mass Accumulation Rates (MAR). Horizontal lines represent the boundaries between isotopic stages.
a) Oxygen stable isotope data from Bickert et al. (1993).

3.5 Site 151-907: North Atlantic Gateways

The North Atlantic Gateways are located between the North Atlantic and the Arctic oceans, in the region bordered by Greenland, Iceland, Scotland, and Norway (Fig. 13). This is a key area for climatic studies, as in this region the North Atlantic Deep Water (NADW) forms and the current system is extremely sensible to even rapid climatic changes. Surface waters are supplied by the North Atlantic Drift (NAD), which, flowing northward, brings warm and high saline waters. Once this water mass has become cold, it sinks in the Labrador Sea, northeast of Iceland, and forms the lower limb of the NADW. These waters, which fill the depth range between 1000 and 4000 meters and form the Oceanic Conveyor Belt, are characterized by high oxygen and low nutrient contents. The balance between warm Atlantic and cold polar surface water masses inputs forms in this

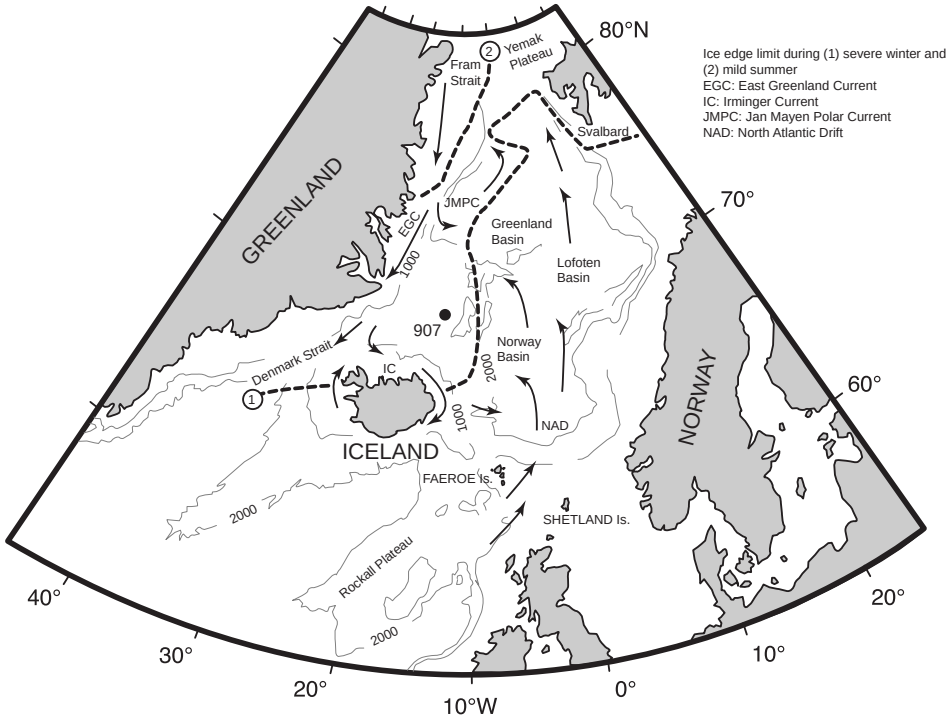

Fig. 13: Location map of ODP Site 907. Surface currents and oceanic fronts patters are from Fronval and Jansen (1996).

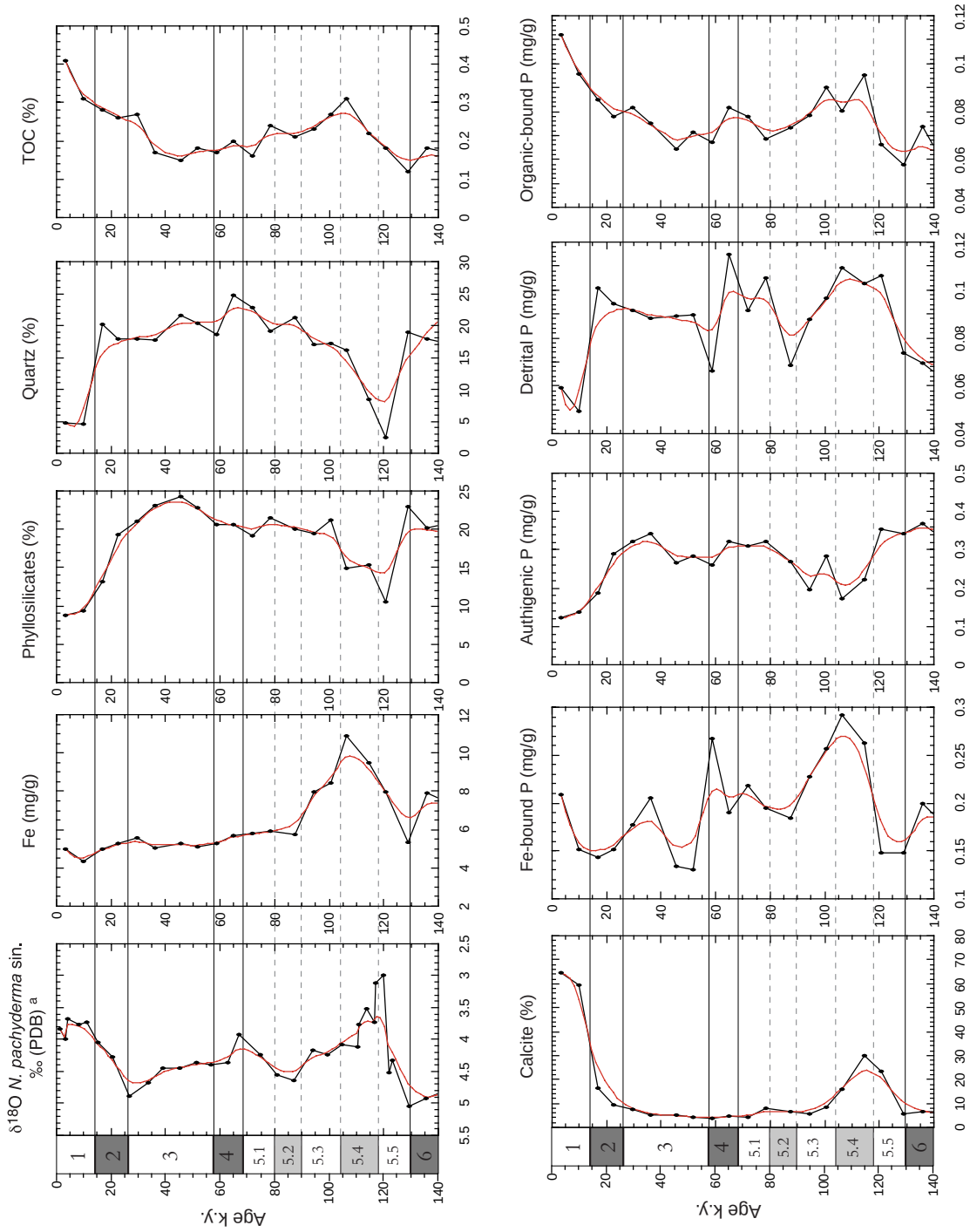

Fig. 14: Data from ODP Site 151-907. Top: $\delta^{18}O$ data of *N. pachyderma* sin., concentration (in mg/g) of ferric Fe, percentages of phyllosilicates, quartz, and TOC. Bottom: percentage of calcite and concentrations (in mg/g) of Fe-bound, authigenic, detrital and organic-bound P. Horizontal lines represent the boundaries between isotopic stages.
a) Oxygen stable isotope data from McManus et al. (1996).

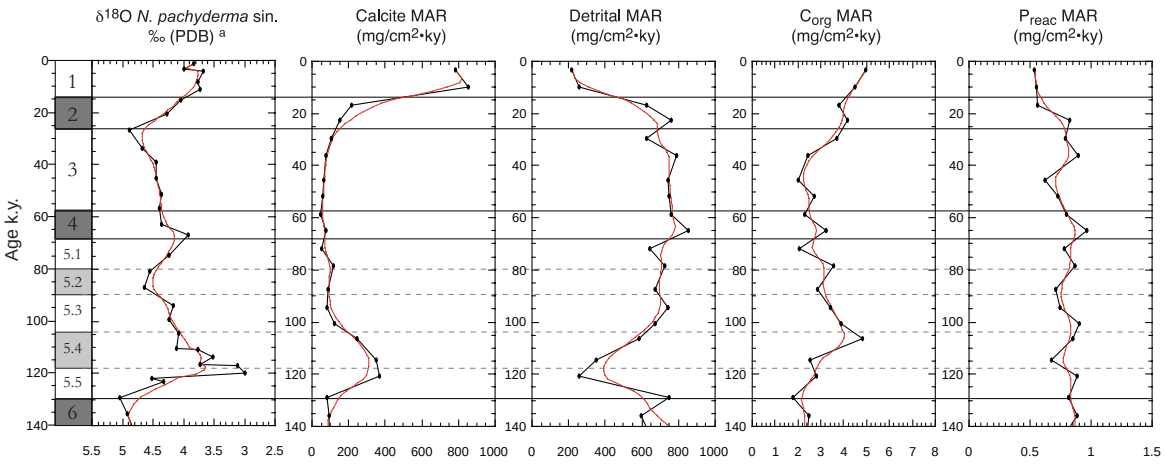

Fig. 15: Site 151-907. $\delta^{18}O$ data of *N. pachyderma* sin., calcite, detrital silicates, TOC and reactive P Mass Accumulation Rates (MAR). Horizontal lines represent the boundaries between isotopic stages.
a) Oxygen stable isotope data from McManus et al. (1996).

region distinct oceanographic boundaries. These fronts tend to migrate northward or southward following the variability of the water masses themselves (Baumann et al., 1996). Based on plankton records and abundance of ice-rafted detritus, the region north of Iceland, where Site 907 is located, was bathed by polar waters for most of the last glacial-interglacial period (Baumann et al., 1996).

Cores from Site 907 (1800.8 mbsl), located on the eastern Iceland Plateau, were sampled from 0 to 2.7 mbsf. Quaternary sediments consist of bioturbated silt and clay, with minor amounts of carbonate and siliceous bioclasts. Dropstones (>1 cm) are rare, while ice-rafted debris (IRD) are found throughout the interval (Myhre et al., 1995).

Sediments at Site 907 are rich in detrital material, which averages 46%. Quartz and phyllosilicates are the most abundant silicate minerals, and display the same temporal trend. Low values are observed only at the beginning of MIS 5 and 1. These minima in detrital minerals correspond to high values in calcite contents (Fig. 14), and this relation is probably due to a dilution effect. Dolomite is present in low percentages and behaves as quartz and phyllosilicates, indicating a probable detrital origin. Authigenic and Fe-bound P are the most abundant phosphorus phases and account together for more than 60% of total phosphorus in sediments at site 907. Fe-bound P peaks during MIS 5.4, in relation to the highest Fe concentration, and reaches values of about 0.3 mg/g. Authigenic P behaves similarly to phyllosilicates, at least during glacial period: highest values are reached during MIS 3 and both start decreasing at the beginning of MIS2. Detrital P displays high concentrations during MIS 5.4, between MIS 5.1 and 4, and it mirrors quartz variations between MIS 3 and 2.

As for sediments from Site 806, organic matter analyses by Rock Eval are probably biased. Due to the high detrital content (e.g. clays and phyllosilicates), which induces a matrix effect (Espitalié et al., 1986), as also indicated by extremely low hydrogen index (see data in Annexe B), TOC values are probably underestimated. TOC concentrations are quite low and average 0.3 %. High values are observed during MIS 5.4 and the Holocene. Organic-bound P averages 0.09 mg/g and follows the TOC trend throughout most of the studied interval (Fig. 14). MAR of detrital silicates are high except at the beginning of interglacial stages 5 and 1 (Fig. 15), where, on the contrary, calcite MAR reach highest values. P reactive MAR average 0.9 mg/cm^2·ky during the last glacial-interglacial cycle and do not display any important variations.

4. DISCUSSION

4.1. Phosphorus in sediments

In the last decades, different studies have been dedicated to the P record in marine sediments on timescales spanning millions of years (Delaney and Filippelli, 1994; Föllmi, 1995; Filippelli and Delaney, 1996; Filippelli, 1997). In these investigations, the authors tried to define long term variations in P flux to the sediments and to link them to changes in continental weathering and, ultimately, to climate. Different and sometimes contrasting conclusions were forwarded: Föllmi (1995) found a clear indication of links between phosphorus mass accumulation rates and climatic changes, while Filippelli and Delaney (1994) pointed at a discrepancy between the phosphorus mass accumulation record and other geochemical indicators of continental weathering (e.g. strontium isotopes).

The present study differs from previous works in that 1) I have investigated in high resolution a shorter time period, spanning the last glacial-interglacial cycle, also with the goal to detect short-term variations in the phosphorus record (e.g. Heinrich events, see Chapter 4); 2) I have chosen several different oceanographic settings (see Introduction and Chapter 1); and 3) using the SEDEX extraction technique (Ruttenberg, 1992), I have performed a phosphorus speciation, which allowed us to distinguish reactive from non-reactive phases of phosphorus. The use of the SEDEX extraction method had also allowed to quantify even small phosphorus concentrations in sediments (as low as 0.005 wt% or 0.05 mg/g of sediment; Ruttenberg, 1992), and, through the distinction of different phases, to recognize relationships between variations in phosphorus forms and other sedimentary proxies through time.

Phosphorus forms has been detected at all the investigated sites. Phosphorus deposition, for this reason, is not only limited to upwelling sites along the continental margins (e.g. Peru and Oman margins, Northeastern Equatorial Atlantic), but also in normal marine settings, such as dominated by terrigenous input (e.g. North Atlantic Gateways, South China Sea, Japan Sea) and deep-sea environments (e.g. Ontong-Java plateau, North Atlantic).

Two approaches have been used to study phosphorus in marine sediments: the first consists in looking at the different phosphorus phases and in defining the relationship between them, with other sedimentary proxies and also with organic carbon; the second consists in considering reactive and total phosphorus Mass Accumulation Rates (MAR) variations through time.

4.1. Relationships between phosphorus phases and other sedimentary proxies

A general picture of phosphorus distribution in marine sediments shows that the most abundant P-bearing phase at all sites is represented by authigenic P, which ranges between 36 and 78 % of total phosphorus (Fig. 16). This confirms the observation that authigenic P-bearing minerals constitute the ultimate and most stable sink for phosphorus in marine sediments (Ruttenberg and Gõni, 1997; Delaney, 1998). The relative abundance of the other phases depends on the nature of sediments and of the environmental settings (see discussion below). Fe-bound P ranges between 5% and 36% of total phosphorus, and, in many sites, it represents the second most abundant phosphorus phase (Fig. 16). It is only at few sites that organic-bound P exceeds 15% of total phosphorus. Sediments at locations characterized by relatively high primary production (e.g. upwelling sites, as the Oman and the Peru margins) generally bear low organic-bound P percentages relative to other phases. Detrital P, the non-bioavailable form of phosphorus, varies in relation to the proximity of a continental source and to transport patterns (e.g. North Atlantic versus Ontong-Java plateau;

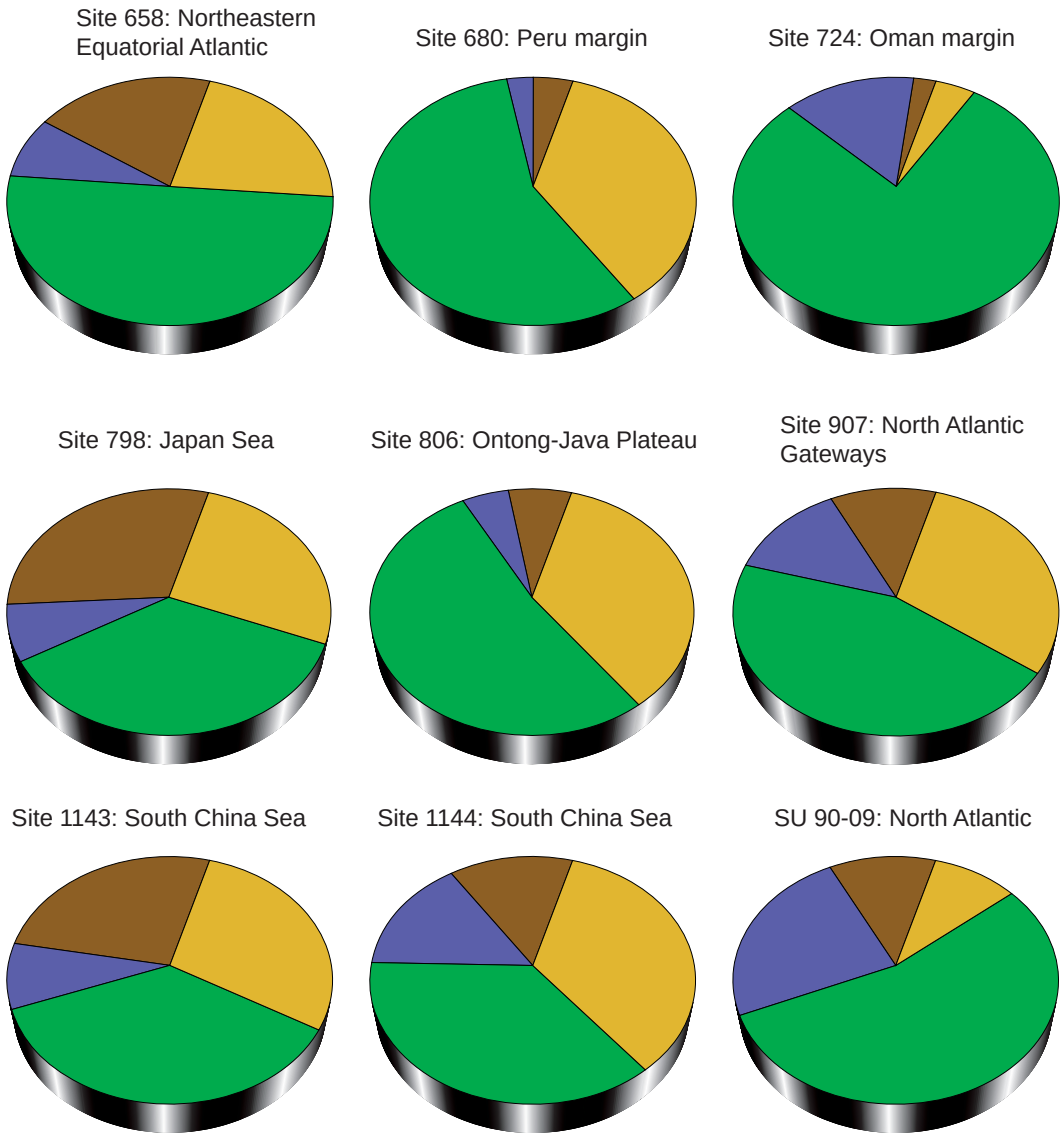

Fig. 16: Representations of relative percentages of phosphorus phases at the investigated sites. Light yellow: Fe-bound; green, authigenic; blue: detrital, and brown: organic-bound P. See Table 3 for values.

Table 3

Site	Fe-bound P %	Authigenic P %	Detrital P %	Organic-bound P %
658	21.86	50.08	8.14	19.91
680	36.07	56.57	2.95	4.42
724	4.47	78.36	14.67	2.50
798	26.58	35.65	7.40	30.37
806	35.30	52.32	5.24	7.08
907	30.67	44.05	13.36	11.92
1143	28.85	36.06	8.59	26.50
1144	34.68	36.26	15.24	13.82
SU 90-09	9.60	54.56	23.94	11.89

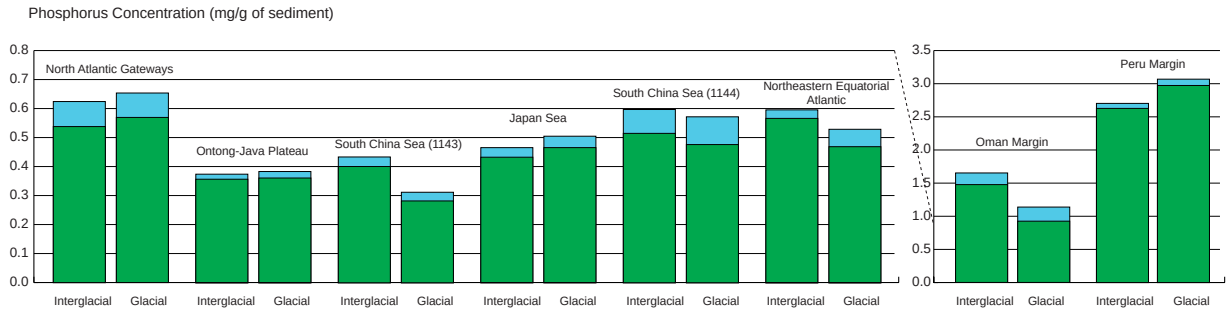

Fig. 17: Mean phosphorus concentrations at the investigated sites. Values are averaged over interglacial and glacial periods. Reactive phosphorus is represented in green, whereas detrital phosphorus in light blue.

Fig. 17). Reactive and total phosphorus concentrations, averaged for glacial and interglacial periods (Fig. 17), fall in the range of phosphorus abundance in surface marine sediments (Baturin, 1988).

As discussed in the introduction section, organic matter is the main carrier of reactive P to the sediments, but after burial, degradation of organic matter releases phosphorus and diagenetic processes lead to the loss of dissolved P from sediments and/or redistribution of P to the other sedimentary phases. Thus, the burial flux of P is not only controlled by the input of dissolved and particulate P from the continent to the oceans and the nature of the source material (e.g. labile versus refractory), but also by the environmental and diagenetic conditions in bottom waters and in the upper section of the sediment column (e.g. nature of sediments, pH, oxygen levels, alkalinity, etc.). These conditions, at their turn, are ruled by larger scale phenomena (e.g. water mass circulation, productivity and organic matter export, sea level changes). These assumptions imply that variations in phosphorus phases in sediments are likely to mirror changes in all these processes and may provide a range of important and diversified information.

Generally, organic-bound and Fe-bound P are expected to decrease with depth, as the result of the degradation of organic matter, which continues for a long time after burial (Anderson and Delaney, 2001), and desorption of dissolved P from Fe oxyhydroxides. These patterns are seen in most of the records; however, in some cases, these phosphorus phases deviate from the described behavior.

In most of the continental margin sites, where the contribution of terrestrial organic matter may be substantial, organic-bound P and its ratio to organic carbon may reflect not only the degree of the degradation, but also the nature of the organic material itself. This is the case of the Japan Sea, the South China Sea and also of the North Atlantic, where contribution at different times from different sources left a clear signal on the sedimentary record.

Fe-bound P is relatively abundant in most studied sites sediments. This may seem controversial as the redox cycle in the upper sediment column controls adsorption and desorption of phosphate from Fe oxides and hydroxides. Thus, we should expect to see a general decrease of Fe-bound-P concentrations with depth. Phosphates originally bound to Fe oxides are easily lost, regenerated, and redistributed to other phases, once that sediments are buried below the redox boundary (Jarvis et al., 1994; Slomp et al., 1996a). But changes in sedimentation rates (e.g. in the South China Sea), changes in the nature of the oxides themselves (e.g. in the North Atlantic; amorphous versus crystalline oxides; Slomp et al., 1996b), and also changes in the stratification and ventilation of the water column may decouple Fe and Fe-bound P records.

Carbonate-fluorapatite (CFA), the main P-bearing authigenic mineral in marine sediments, is considered as representing the ultimate sink of reactive dissolved P. However,

Table 4: Average phosphorus phases concentrations and MAR (in mg/m2·ky)

Site		Fe-bound P	Authigenic P	Detrital P	Organic-bound P	P reac	P tot	Preac	Ptot	Preac	Ptot
		mg/g	mg/g	mg/g	mg/g	mg/g	mg/g	MAR	MAR	MAR (µmol)	MAR (µmol)
658	intergl.	0.1514	0.2901	0.0295	0.1255	0.5670	0.5964	7.284	7.662	235.189	247.407
	glacial	0.0971	0.2728	0.0600	0.0994	0.4694	0.5294	7.454	8.407	240.676	271.456
680	intergl.	0.7533	1.7078	0.0755	0.1661	2.6273	2.7028	36.319	37.363	1172.726	1206.425
	glacial	1.3580	1.5325	0.0952	0.0825	2.9731	3.0683	30.444	31.419	983.028	1014.498
724	intergl.	0.0719	1.3668	0.1761	0.0415	1.4802	1.6563	8.363	9.358	270.045	302.172
	glacial	0.0523	0.8462	0.2134	0.0284	0.9269	1.1403	11.521	14.173	372.019	457.650
798	intergl.	0.1292	0.1520	0.0327	0.1521	0.4333	0.4660	3.973	4.273	128.290	137.980
	glacial	0.1286	0.1955	0.0393	0.1420	0.4661	0.5054	3.969	4.303	128.148	138.947
806	intergl.	0.1414	0.1924	0.0175	0.0240	0.3579	0.3753	1.074	1.126	34.667	36.357
	glacial	0.1266	0.2057	0.0224	0.0299	0.3621	0.3845	1.086	1.154	35.079	37.250
907	intergl.	0.2083	0.2483	0.0864	0.0814	0.5381	0.6244	0.852	0.989	27.520	31.938
	glacial	0.1829	0.3159	0.0842	0.0706	0.5694	0.6536	0.951	1.092	30.713	35.254
1143	intergl.	0.1190	0.1970	0.0330	0.0860	0.4020	0.4350	1.330	1.437	42.946	46.397
	glacial	0.0950	0.0840	0.0300	0.1040	0.2830	0.3130	1.272	1.407	41.062	45.416
1144	intergl.	0.2197	0.2140	0.0823	0.0816	0.5152	0.5975	33.396	37.728	1078.349	1218.227
	glacial	0.1865	0.2101	0.0957	0.0800	0.4766	0.5723	46.513	56.664	1501.881	1829.640

Table 4 (continued): Average phosphorus phases percentages on total and on reactive phosphorus

Site		Fe-bound P	Authigenic P	Detrital P	Organic-bound P	Fe-bound P	Authigenic P	Organic-bound P
		%	%	%	%	%	%	%
		% on tot P				% on reac P		
658	intergl.	25.382	48.635	4.939	21.044	26.700	51.162	22.138
	glacial	18.344	51.533	11.339	18.784	20.690	58.124	21.186
680	intergl.	27.872	63.188	2.793	6.147	28.673	65.004	6.323
	glacial	44.261	49.948	3.102	2.690	45.678	51.547	2.776
724	intergl.	4.343	82.520	10.632	2.506	4.859	92.337	2.804
	glacial	4.588	74.209	18.711	2.492	5.644	91.290	3.065
798	intergl.	27.717	32.621	7.023	32.639	29.811	35.085	35.104
	glacial	25.438	38.685	7.772	28.104	27.582	41.946	30.473
806	intergl.	37.687	51.266	4.650	6.397	39.524	53.766	6.709
	glacial	32.921	53.488	5.828	7.763	34.959	56.798	8.243
907	intergl.	33.360	39.766	13.833	13.041	38.715	46.150	15.135
	glacial	27.989	48.327	12.881	10.803	32.127	55.472	12.401
1143	intergl.	27.356	45.287	7.586	19.770	29.602	49.005	21.393
	glacial	30.351	26.837	9.585	33.227	33.569	29.682	36.749
1144	intergl.	36.774	35.808	13.768	13.649	42.646	41.526	15.828
	glacial	32.594	36.706	16.716	13.983	39.137	44.074	16.790

changes in authigenic P concentrations are not linearly linked to the variations of either Fe-bound or organic-bound P, so that we do not see a parallel increase with depth of neo-formed phosphorus minerals. The picture arising from the comparison of all the studied sites indicates that authigenic P deposition is, indeed, a rather complicated process, which responds to rapidly changing environmental conditions, both local and global.

In the Oman margin (see Chapter 2), the variations of authigenic P in sediments correlate to bottom water oxygen contents and oceanic circulation, controlled by organic matter export and sea level changes. The same factors, along with changes in fluvial input of nutrients, influenced the precipitation of authigenic P in the South China Sea sediments (see Chapter 3). At both locations, the monsoonal regime that controls wet and dry phases on the continent as well as circulation patterns, left an overprint on the records.

In the Northeastern Equatorial Atlantic, also affected by monsoon climate, authigenic P and phyllosilicates records show similarities during the investigated period. As phyllosilicates supply peaks in relation to enhanced fluvial input during wet periods on the continent,

we presume that authigenic P responds to changes in input from the continent and records at the same time wet-dry cycles linked to monsoonal variations. Sediments from core SU 90-09, in the North Atlantic, have been analyzed at high resolution, in order to characterize P geochemistry during Heinrich events (see Chapter 4). Also in this case, authigenic P varies in relation to changing inputs from the land masses and to changing oxygenation conditions, connected to iceberg discharge and consequent stratification of the water column.

As is shown by all these examples, the authigenic P record is decoupled from detrital P, which generally tends to vary along with detrital silicates minerals, as quartz and phyllosilicates. These relations clearly support the assumption of the detrital nature of this phosphorus phase, as in the case of the Oman margin, the South China Sea, the North and Equatorial Atlantic sediments. But because of the diverse content of P-bearing minerals in igneous and metamorphic rocks, P detrital record could also reflect a mix of different sources and hence move away from other detrital proxies records. This is, for example, the case of the Japan Sea. Here the presence of several detrital sources (eolian, from the interior of China, and fluvial, from China and Japan itself) and of diverse processes controlling the sedimentation (e.g. dry-wet phases linked to monsoon climate variations, changes in sea level leading to stratification of the water column and semi-isolation of the basin from the open ocean during glacial times) complicate the interpretation of the record.

At the Peru margin site, authigenic and detrital P show similarities in their trend throughout the investigated period. The process controlling the input of detrital material (e.g. continental weathering ruled by trade winds and subsequent transport) influences also the supply and recycling of dissolved P through upwelling that is controlled as well by the intensity of trade winds. However, at this particular site, tectonic-related processes, such as redeposition and reworking of particles, may influence the record.

At the Ontong-Java plateau site, almost all the analyzed parameters depict rather stable environmental conditions during the last glacial-interglacial cycle, which are reflected also by the phosphorus records. Detrital P is decoupled from the other detrital proxies, and no clear relationship between authigenic P and other parameters is found.

4.2. TOC/P molar ratios

Based on nutrient analyses, the TOC/P ratio of organic matter is extensively used to determine the origin of organic matter (OM) and the degree of degradation and preservation (Ingall et al., 1993; Anderson and Sarmiento, 1994). In the TOC vs. organic-bound P graph, the negative y axis intercept of the regression line calculated for all samples indicates that an excess of organic-bound P is present when TOC = 0 (Fig. 18). There might be several explanations for this phenomenon. 1) The analytical overestimation of the organic phosphorus fraction might explain these results. Some "resistant" inorganic phosphorus might be solubilized during the last step of the SEDEX technique, though this hypothesis is unlikely to happen as most of the inorganic phases of phosphorus have already been extracted prior to ashing (Ruttenberg, 1992). 2) The underestimation of the organic carbon content by Rock-Eval, maybe due to a high mineral matrix effect (Langford and Blanc-Valleron, 1990), could also account for the observed trend. 3) Alternatively, we may consider variations in the TOC/P_{org} ratio, which are linked to differential preservation/degradation patterns in diverse environmental conditions. The study of TOC/P_{org} in many oceanic settings has shown that organic P is preferentially regenerated compared to organic carbon, especially under oxygen-depleted bottom water conditions. During oxic degradation of the organic matter and consumption of organic

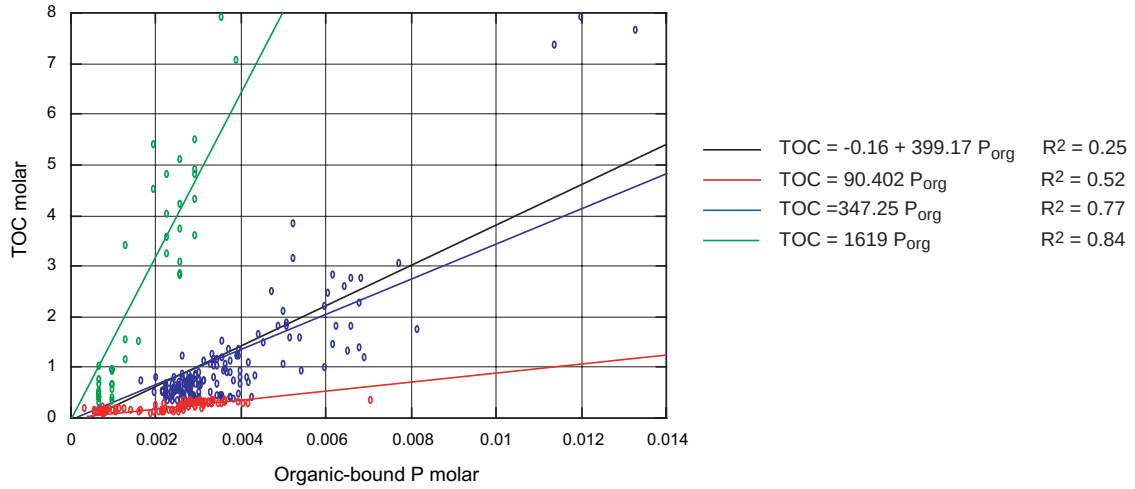

Fig. 18: TOC vs. organic-bound P. Three different populations have been separated. The black regression line has been calculated for all the analyzed samples (average TOC/P_{org} molar = 399); the red line for samples with TOC < 0.5 wt% (average TOC/P_{org} molar = 90); the green line for samples mainly from Sites 680 and 724 average TOC/P_{org} molar = 1619); and the blue line for the remaining samples (average TOC/P_{org} molar = 347).

carbon, bacteria generally store organic phosphorus, which, on the other hand, is used and released under dysaerobic/anaerobic conditions (Van Cappellen and Ingall, 1994). This behavior is expressed by the dispersion of the samples in the diagram in Fig. 18: samples from sites characterized by high organic carbon content and low oxygenation of the bottom waters, i.e. Sites 680 (Peru margin) and 724 (Oman margin), show high TOC/Porg ratios, while samples with lower TOC display relatively lower TOC/P_{org} ratios. For samples with TOC < 0.5 wt%, the calculated molar ratio is about 90, indicating organic matter enriched in organic P. This, again, is consistent with the hypothesis proposed by Van Cappellen and Ingall (1994) and discussed above.

Generally, upon degradation of OM, considered as the main carrier of dissolved P to the sediments (Delaney, 1998), a large portion of organic P turns into other sedimentary forms and/or is released from the sediments. For this reason, Anderson and Delaney (2001) demonstrate that the ratio between TOC and all potentially bioavaible forms of P (reactive P, considered as the sum of Fe-bound, authigenic and organic-bound P) is a better estimate of the molar ratio of the original OM. Using this ratio could also help in determining the presence of other significant sources of reactive P to the sediments (e.g. fish debris) than organic matter. It is for this reason that for all sampled sediments, the TOC/P_{reac} ratios have been computed, except for sediments from Sites 806 and 907 (Fig. 19). As already discussed in the result sections, Rock Eval calculations of TOC likely underestimate the "real" TOC concentrations at these sites, as the result of high carbonate and detrital contents of the sediments. At all other sites, TOC/P_{reac} ratios are generally lower than Redfield values for both marine and terrestrial organic matter (Anderson and Sarmiento, 1994). Low ratio values may indicate either the loss of part of the organic carbon from the system or an overall enrichment of phosphorus in respect to organic carbon, due to sequestration of dissolved P from pore water to mineral phases. It has been shown, for example, that dissolution of fish debris may be an additional and important source of dissolved reactive P in many oceanic settings (e.g. Oman margin sediments; Schenau et al., 2000).

On the other hand, peaks in this ratio may indicate either episodes of reduced input of reactive P to the system or P loss from the sediments. Generally, high values of the

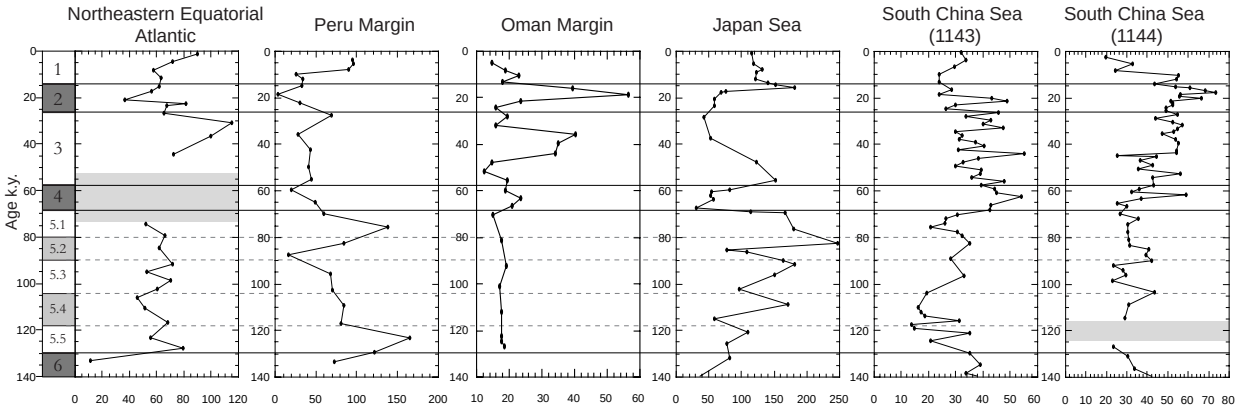

Fig. 19: TOC/P $_{reactive}$ molar ratios for some of the investigated sites. Ratios from Sites 806 (Ontong-Java Plateau) and 907 (North Atlantic Gateways) have not been calculated (see text for details).

TOC/P_{reac} ratios are observed during periods when other proxies (e.g. nitrogen stable isotopes, Fe/Fe-bound P ratios; see tables in the Annexes) indicate the presence of oxygen-depleted conditions (e.g. South China Sea, Japan Sea, Oman margin). Low ventilation of the bottom waters enhances organic carbon preservation, but inhibits phosphorus burial (Jarvis et al., 1994; Van Cappellen and Ingall, 1994). Thus, we believe that higher values of the TOC/P_{reac} point to the regeneration and loss of reactive P in respect to organic carbon, from the sediments to the water column.

4.3. Phosphorus Mass Accumulation Rates

A major problem in calculating reactive P Mass Accumulation Rates (MAR) arises from the fact that these three reactive phases do not simply represent a supply from outside the sediments, as they undergo diagenetic transformations and/or precipitate directly in the sediments. The measured reactive P, in fact, stands only for a small percentage of the original phosphorus carried to the sediments (Delaney, 1998). Some considerations need to be taken into account in order to use reactive P MAR. The first one is that all diagenetic transformations with respect to reactive P phases take place in the uppermost part of the sediment column. Petrographic and isotopic studies demonstrate that authigenic P-bearing minerals generally start developing just below the water-sediment interface (Glenn, 1990), in correspondence to high phosphate pore water concentrations. These maxima are linked to enhanced release of phosphates during organic matter degradation processes and desorption of phosphates from ferric oxides in the suboxic region of the sediments (Froelich, 1988; Glenn, 1990; Slomp, 1997). At greater depths, generally deeper than 10-20 cm, the precipitation of the authigenic P phase stops as high CO_3^{2-} levels, linked to continuing organic matter degradation, halt or hamper the process (Glenn et al., 1994; Jarvis et al., 1994). Only if dissolved carbonate is consumed by other diagenetic process (e.g. dolomite precipitation), authigenic P may precipitate deeper in the sediment column (Glenn et al., 1994).

P adsorbed on Fe oxyhydroxides undergoes diagenetic redistribution, connected to the redox cycle, but also these transformations take place in the uppermost section of the sediment column, generally just below the redox boundary (Slomp, 1997). In most marine environments, the transition from oxic to suboxic conditions, which defines the redox boundary, is located in the upper 10-15 cm (Colman and Holland, 2000). Deeper in the sediment column, all phosphate regenerated by bacterial degradation of organic matter cannot be redistributed to the other phases, as environmental conditions are generally not favorable.

In the studied cases, the linear sedimentation rates (in most cases averaging 10 cm/ky,

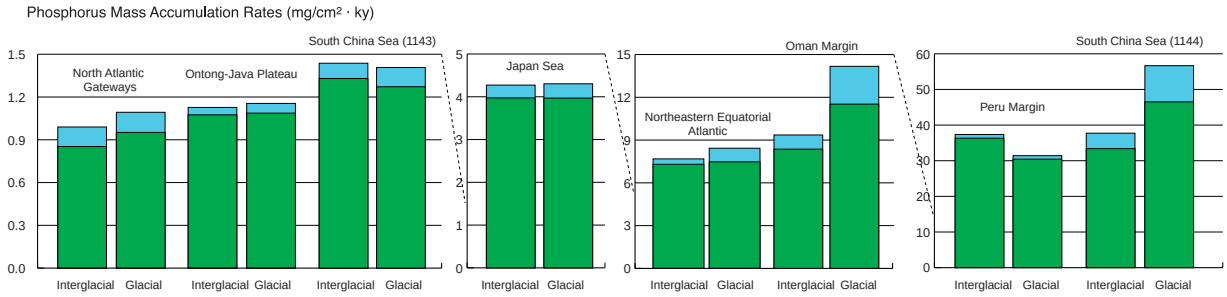

Fig. 20: Mean phosphorus Mass Accumulation Rates (MAR) at the investigated sites. Values are averaged over interglacial and glacial periods. Reactive phosphorus is represented in green, whereas detrital phosphorus in light blue.

see Table 1 in Chapter 1) and the sampling resolution (ranging between 2 and 5 ky, except for core SU 90-09) allow us to consider the processes occurring in the first 10-20 cm as "instantaneous". Moreover, phosphorus phases analyses of samples from core SU 90-09 (North Atlantic) clearly show that their concentration values measured between 10 and 30 cm are in the range of values found deeper in the core (between 130 and 200 cm), indicating that major diagenetic changes have not taken place (see Chapter 4). Therefore, though aware of the possible error, we have calculated reactive and total P MAR as the product between reactive and total phosphorus concentration, linear sedimentation rates, and dry bulk sediments density.

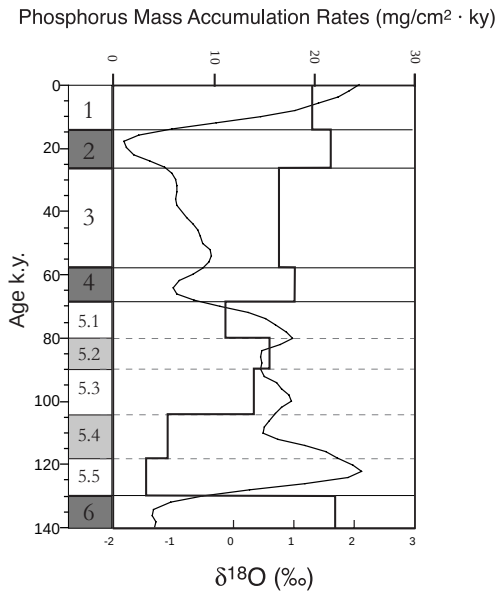

Fig. 21: Mean reactive phosphorus MAR. Values from all sites are taken into account and averaged over the different isotopic stages. The SPECMAP curve (light curve) is represented for comparison.

The main control on phosphorus accumulation rates is given by sedimentation rates (Krajewski et al., 1994; Filippelli, 1997). It is evident from Fig. 17 that average phosphorus concentrations for most of the sites are in the same range of values, spanning between 0.3 and 0.6 mg/g of sediments, regardless of the environmental settings (e.g. continental margin versus open ocean; high versus low surface primary productivity; high versus low phosphate pore water concentrations). Only the concentrations of reactive and total phosphorus from the Oman and the Peru margin sites fall outside this interval. These locations are characterized by extremely high surface productivity (Reimers and Suess, 1983; Madhupratap et al., 1996). The reason why concentrations at different locations fall in a restricted range of values is not yet known. We do not believe it to be a coincidence, as it was already observed by Filippelli (1997). We can only speculate and believe that the presence of a possible buffering mechanism, maybe related to microbial activity in the sediments, may maintain the concentrations of reactive phosphorus within certain thresholds.

Sedimentation rates are highly different between continental margins and open ocean, partly reflecting local conditions (Fig. 20). As a matter of fact, phosphorus MAR exhibit a wide range of values, from less than 1 mg/cm^2·ky (North Atlantic Gateways and Ontong-Java Plateau) to more than 100 mg/cm^2·ky (South China Sea and Peru mar-

gin). The finding that phosphorus MAR at the Peru margin (a phosphogenic site) are comparable if not lower than phosphorus MAR at Site 1144 in the South China Sea (a continental margin site characterized by extremely high sedimentation rates, see Chapter 3) undoubtedly points to the important role of sedimentation rate as a control on MAR estimates (Fig. 20). Generally, since linear sedimentation rates are higher in continental margin than in open ocean settings, we have a clear indication that sediments from the continental margins provide an important sink for reactive phosphorus, despite the small area compared to the open ocean (Filippelli, 1997).

In order to decipher the role of phosphorus as a possible "connecting proxy" between continental weathering, oceanic productivity and climate, we have calculated the reactive and total MAR averages for glacial and interglacial periods at each studied site (Fig. 20). Besides expected differences in the amount of MAR between locations, as also discussed above, we have no clear and unique indication of higher phosphorus MAR during glacial periods, as it was forwarded for the period spanning the last 165 Ma by Föllmi (1995). However, besides the fact that these are local averages, this is not an unconditional indication of lower phosphorus input from the continent during glacial periods. In fact, if averages of MAR are calculated over each isotopic stage and sub-stage taking into account MAR from all sites, a different picture is drawn: averages are higher during glacial intervals, possibly as the reflection of higher sedimentation rates compared to interglacials (Fig. 21).

If burial fluxes of reactive phosphorus are linked to large scale phenomena, as forwarded by several studies (e.g. Ruttenberg, 1993; Filippelli and Delaney, 1994; Föllmi, 1995) the comparison of a "global" reactive phosphorus MAR curve with a global climate proxy, expressed by the SPECMAP stable oxygen isotopes curve (Imbrie et al., 1989), could yield interesting information for the last glacial-interglacial cycle. However, as MAR range within a wide spectrum of values (from less than 1 to more than 100 mg/cm^2·ky), it would not be "statistically correct" to use the raw data without any previous treatment.

Studying the statistical distribution of the values, we have found that the MAR may be represented by three populations (see Fig. 22 for details): MAR lower than 4 mg/cm^2·ky (MAR from Sites 907, 1143, 806 and 798), between 4 and 18 (Sites 658, 724, and to a lesser extent 1144, 798 and 680), and higher than 18 mg/cm^2·ky (Sites 1144 and 680). The smoothed curves interpolated for the three populations show interesting relations with the SPECMAP curve, but the signals are complex (Fig. 23). Except for population 1 at the beginning of stage 5 and for populations 2 and 3 during the Holocene, that show a direct correlation with SPECMAP, reactive phosphorus MAR and SPECMAP are rather inversely correlated (Fig. 23).

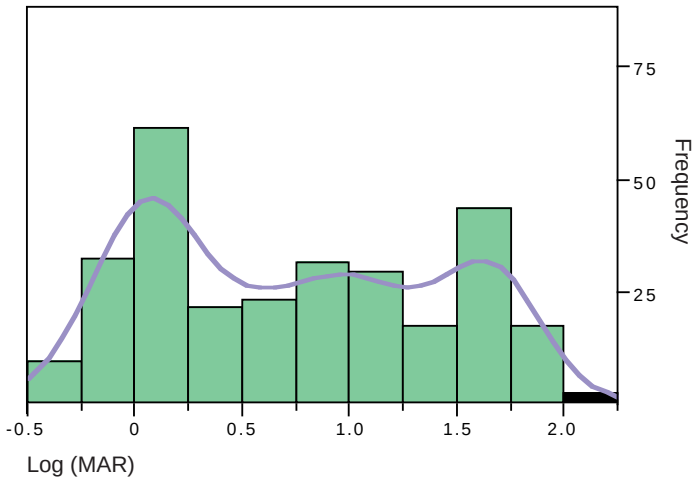

Fig. 22: Histogram showing the distribution of reactive P MAR values. The high frequency of MAR values falling between 0 and 1 has obliged to use a logaritmic scale to better represent all the values (x axis in logaritmic scale). The blue line is the approximation of the outline of the histogram. It is evident the presence of three different populations. The boundaries between populations are then recalculated using an exponential function.

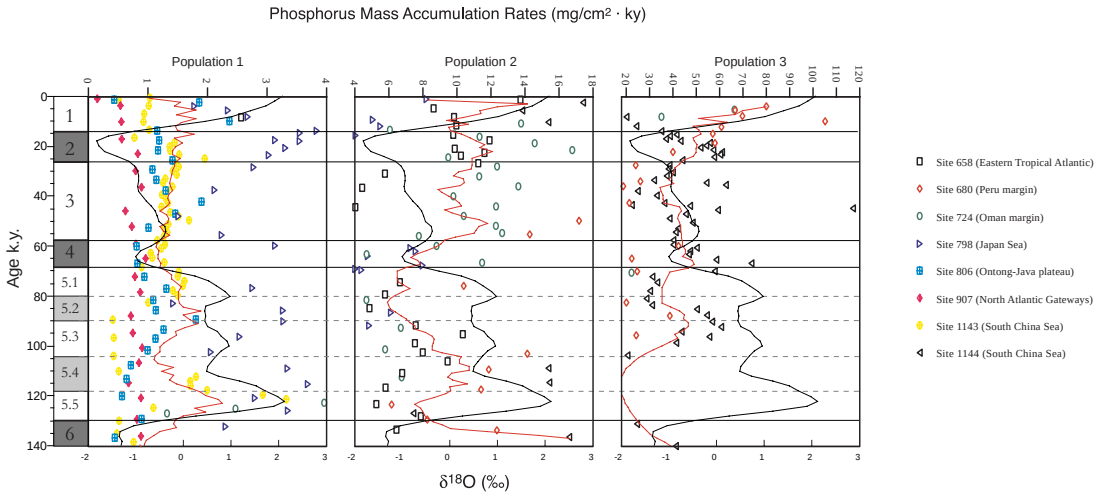

Fig. 23: Plots representing the three populations through the investigated time interval. In black is the SPECMAP curve, whereas the red line represents the smoothing curve of the data points (calculated using a least quare method). See legend on the right side for symbols explication.

We have then computed standardized MAR values, in order to compare variability of phosphorus accumulation rates between all sites (Fig. 24a, see caption for details on the calculation). The advantage of this procedure is that we eliminate the influence of the absolute MAR values, that are linked to local conditions (e.g. proximity to the continent, primary productivity), and we look only at the variability of the record at each site and at general trends. As all standardized MAR are now comparable (average= 0 and standard deviation= 1 for all sites, as well for the globality of the values), it is possible to treat them as a unique population and draw a "global" reactive P MAR curve to be compared to the SPECMAP. Of course, this approach allows only to refer to variability and trends without considering absolute values. The obtained smoothed curve shows intriguing features. First of all, the relation to the SPECMAP curve is complex, in that the two curves positively correlate during full interglacials (MISs 5 and 1), but are inversely correlated during glacial or stadial periods (Fig. 24b). This kind of relation suggests a connection with the precession cycle. In fact, the comparison with the precession curve computed for the last 140,000 years (Berger and Loutre, 1991) reveals a well-defined 23 ky cyclicity in the standardized reactive P MAR curve (Fig. 24a). As is already observed, sedimentation rates exert a relatively strong control on phosphorus MAR. At first sight, we may conclude that sedimentation rates are paced by the precession cycle and that, in turn, they control phosphorus MAR.

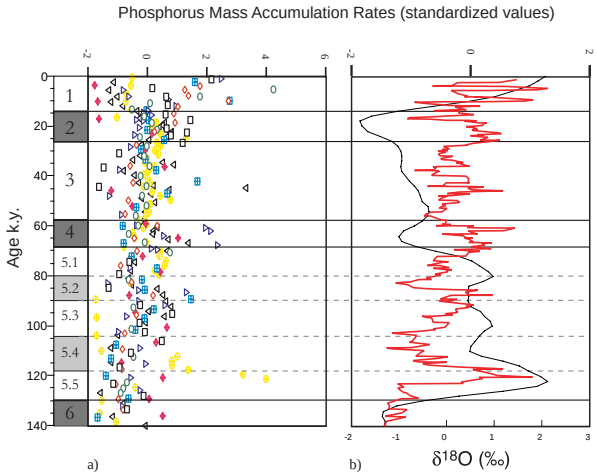

Fig. 24: a) Each point has been calculated using the formula: xs = (xi - **x**)/s, where xs is the standardized value, xi the orginal value, **x** the mean of the population (the overall MAR values at a given site), and s the standard deviation of the same population. See legend in Fig. 22 for symbols explication.
b) The red line is calculated using a 5-point average smoothing on the globality of the standardized reactive P MAR values. The black line represents the SPECMAP oxygen curve.

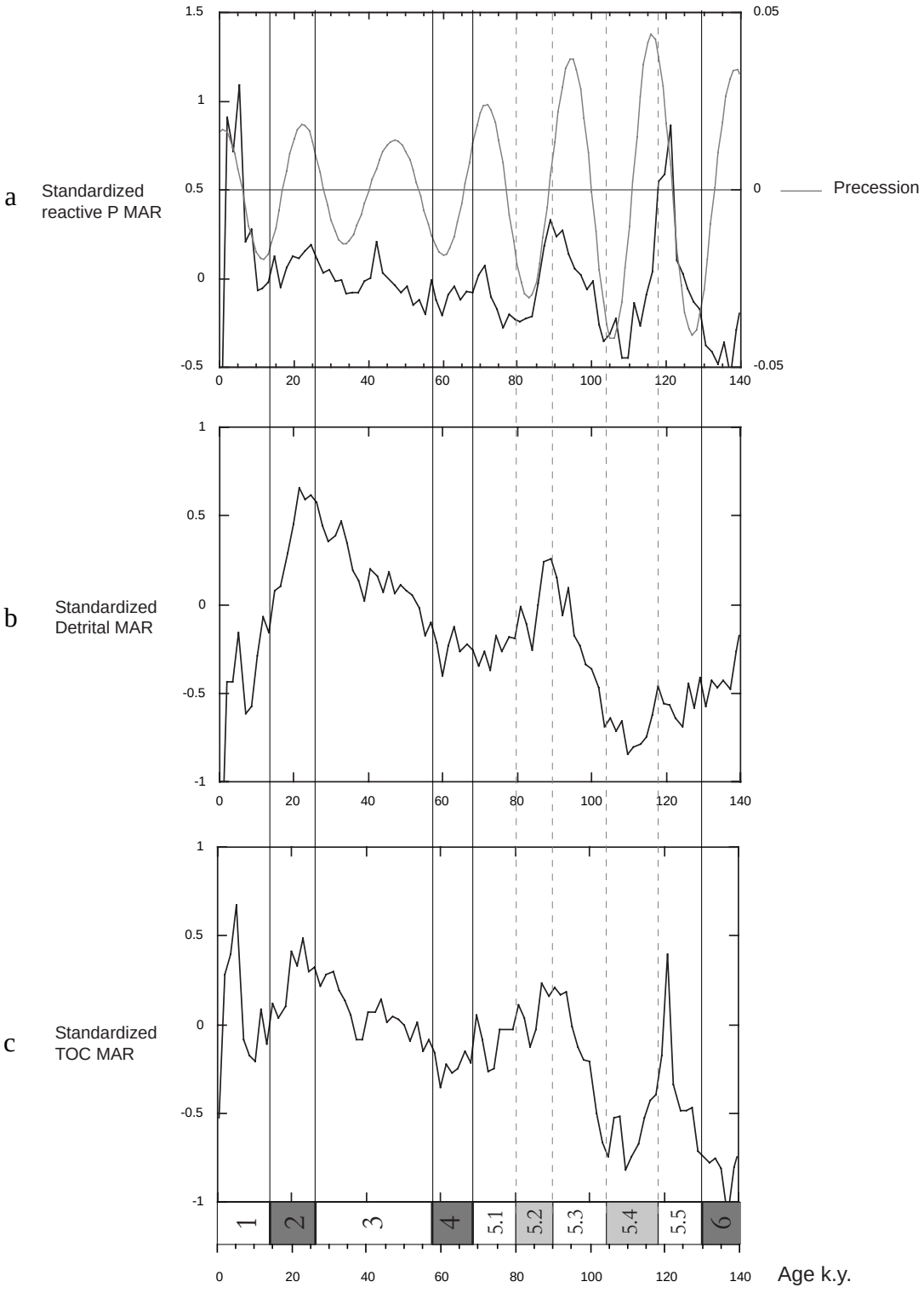

Fig. 25: a) The standardized reactive P MAR are smoothed using a least square method (black line, raw values not shown). The gray line represents the precession curve (Berger and Loutre, 1991). Smoothing of standardized detrital (b) and TOC (c) MAR values are shown for comparison. Standardized detrital and TOC MAR values were calculated using the same procedure used for reactive P MAR data (see Fig. 23 caption).

The precessional imprint on our records is not really surprising as most of the studied sites are located at low latitudes, except for Site 907 (North Atlantic). Also Site 798 (Japan Sea), though at relatively high latitudes, is under the influence of monsoon climate, which is controlled by solar radiation at the obliquity (about 41 ky) and precession (about 23 ky) periodicities (Clemens et al., 1996). To check if sedimentation rates are the only factor controlling MAR, we have calculates standardized TOC and detrital silicates MAR, following the same procedure. We have chosen these two parameters because TOC is considered as the main vector of reactive P to the sea floor and detrital silicates MAR may give an indication of continental weathering.

The 23 ky cyclicity is still recognizable, but the amplitude of the variability is different for each curve. Standardized detrital MAR show highest variability during glacial periods, in accord with the assumption of enhanced delivery of material from the continent to the ocean due to increased continental (physical) weathering (Fig. 25b). The relationship during particular time intervals (e.g. at around 90 ka and 20 ka; Fig. 25) between detrital and reactive P MAR may suggest that reactive phosphorus record in marine sediments partially mirrors weathering patterns on the continent.

Standardized TOC MAR display comparable variability both during glacial and interglacial periods (Fig. 25c). The difference in amplitude between standardized reactive P and TOC MAR may reflect 1) the influence of preferential regeneration of P in respect to organic carbon during glacial times and 2) the preferential preservation of P in respect to organic carbon along with the supply of alternative reactive phosphorus sources (e.g. fish debris) during interglacial times.

The opposite behavior of reactive P and organic carbon has been ascribed to changing oxygen levels in the sediments and in the bottom waters, which, influencing the redox boundary depth in the sediments, control early diagenetic processes (Slomp and Van Raaphorst, 1993; Van Cappellen and Ingall, 1994; Colman and Holland, 2000). Colman and Holland (2000) pointed to the existence of a direct correlation between particulate organic carbon flux, sedimentation rates and sediment redox conditions. This implies that redox conditions, ruled by the rate of organic matter degradation, are also closely tied to sedimentation rates. Therefore, we have another clear indication of regeneration of reactive phosphorus especially during glacial times, when, promoted by higher sedimentation rates, enhanced suboxic conditions are achieved in the upper part of the sediment column, and, possibly, in bottom waters.

5. CONCLUSION

Phosphorus is an essential element for life, especially in the marine realm. As its delivery to the oceans is primarily controlled by continental weathering, phosphorus is also believed to be a critical element for biogeochemical and paleoclimatic studies.

This research thesis addresses phosphorus geochemistry records in different oceanographic settings during the last glacial-interglacial cycle. The principal goals of this work have been to decipher the relationships between phosphorus sedimentary records, continental weathering and climate, and to assess the importance of global and local processes influencing the distribution of phosphorus in the sediments through time. The use of a specific sequential extraction technique (SEDEX method; Ruttenberg, 1992) has permitted to distinguish between bioavailable and refractory phosphorus forms, and to separate four sedimentary phases. The results of phosphorus analysis have been compared to the outcomes of mineralogical and geochemical investigations, in order to obtain a better and deeper understanding of phosphorus geochemistry through time. While some aspects of the phosphorus cycle in marine sediments still

remain unclear and need further investigation, this research bears important conclusions.

1) Phosphorus deposition in marine sediments is a widespread phenomenon. Phosphorus-bearing inorganic and organic forms have been detected at all locations. Authigenic P, the most important sink of reactive and formerly bioavailable phosphorus, is present at all sites. The other reactive phosphorus forms have been also detected, and their relative proportion is determined by local environmental conditions. Detrital phosphorus generally varies in relation to continental supply, but it possibly records also variations in the source and nature of detrital material.

2) The study of sediments from core SU 90-09 in the North Atlantic, sampled in order to resolve Heinrich events, has brought evidences that variations of phosphorus phases concentrations in sediments respond to rapidly changing processes. Variations in oceanic circulation, in water column ventilation, and in the organic carbon flux to the sea floor may rather swiftly influence oxygen contents in the bottom waters and hence modify environmental and diagenetic conditions. As the phosphorus cycle in the sediments is redox sensitive, its distribution is closely affected by these changes.

3) Biogeochemically available phosphorus undergoes diagenetic transformations whose rates and intensity are determined by conditions in the bottom waters and in the uppermost part of the sediment column. For this reason marine reactive phosphorus record cannot be considered as a direct indicator of dissolved phosphorus input from the continent, and thus cannot be exactly and solely linked to continental weathering and supply of nutrients from the continent. The relations with other geochemical and mineralogical proxies may help in determining the degree of transformation and the contribution of the supply from the continent.

4) Concentrations of reactive and total P are comparable between locations, regardless of the geographic, oceanographic and environmental settings. The rationale of this phenomenon is not known. Evidently, neither organic carbon flux to the sediments nor initial supply of phosphorus is the controlling factor. A possible control of microbial activity on reactive, and thus bioavailable, phosphorus concentration might be forwarded. However, at the moment we do not have enough elements to support this hypothesis. Further work that focuses on phosphorus distribution in sediments from other settings, is needed. We believe that a better understanding of the phosphorus (bio)geochemistry, will also help at finding a unique and joint process controlling phosphorus concentrations. This will be achieved also through the study of modern sediments and geochemical modeling.

5) Reactive phosphorus MAR display a relatively large range of values, depending on local conditions. Phosphorus MAR are clearly controlled by sedimentation rates. In spite of generally higher sedimentation rates during glacial periods, averages of glacial and interglacial MAR values at each site are not meaningfully different. This finding confirm that a) the supply of phosphorus from the continent has not the ultimate and leading control on the final reactive phosphorus record in the marine sediments, and that b) diagenetic transformation and regeneration of dissolved phosphorus play an important role.

The found relationship between standardized reactive P MAR and precession cycle during the last glacial-interglacial period may point to the control of monsoon climate on phosphorus delivery, diagenetic transformation and final burial at the studied sites. Further studies, focused on high latitude sites, are needed in order to verify this assumption.

6) The comparison with proxies as nitrogen stable isotopes and total organic carbon, indicates that at all investigated locations, regenerated dissolved phosphorus is lost from the sediments, especially during oxygen-depleted bottom and pore water conditions. On a glob-

al scale, this is supported by the relationship between standardized reactive P and TOC MAR, which points to a preferential loss of reactive phosphorus principally during glacial periods. This hypothesis confirms the connection between oxygen levels, preservation of organic carbon and release of reactive phosphorus from the sediments to the water column. If oceanographic conditions are favorable, regenerated dissolved P may be upwelled and/or rediffused in the upper photic zone and hence re-enter the biological cycle. This process may have critical consequences on the carbon cycle and on climate, notably during periods already characterized by high biological export. In fact, small quantities of reactive phosphorus in the system may sustain and support relatively high primary production over long time (Benitez-Nelson, 2000). Following this assumption, periods of high organic matter productivity correlate to decreasing burial rate of reactive P, as observed using standardized MAR.

Finally, a complex picture of phosphorus cycle in the ocean and in the sediments and its connections to climate arises from the present research work. As shown in the Introduction chapter of this thesis, the climate system is extremely intricate. In this network of interacting factors, weathering and productivity exert a strong control on climate. Due to its global cycle, phosphorus record in marine sediments has been considered as an essential proxy capable of tracing links between the continent and the ocean. Variations in phosphorus delivery from the continent to the oceans may have a feedback on climate. At the same time, the biophile character of phosphorus along with its sensibility to changing redox conditions may appear as an important obstacle to the use of the marine phosphorus record for paleoclimatic studies. Through the study of marine phosphorus records from different environments and its comparison with other mineralogical and geochemical proxies, I have demonstrated that it is possible to link the processes controlling phosphorus distribution to large scale phenomena. This kind of approach may be extensively used for paleoclimatic studies.

REFERENCES

Anderson, L.A. and Sarmiento, J.L., 1994. Redfield ratios of remineralization determined by nutrient data analysis. Global Biogeochemical Cycles, 8(1): 65-80.

Anderson, L.D. and Delaney, M.L., 2000. Sequential extraction and analysis of phosphorus in marine sediments: Streamlining of the SEDEX procedure. Limnol. Oceanogr., 45(2): 509-515.

Anderson, L.D. and Delaney, M.L., 2001. Carbon to phosphorus ratios in sediments: implications for nutrient cycling. Global Biogeochemical Cycles, 15(1): 65-79.

Baturin, G.N., 1988. Disseminated phosphorus in oceanic sediments - a review. Marine Geology, 84: 95-104.

Baumann, K.-H., Meggers, H. and Heinrich, R., 1996. Variations in surface water mass conditions in the Norwegian-Greenland Sea: evidence from Pliocene/Pleistocene calcareous plankton records (Sites 644, 907, 909). In: J. Thiede, A.M. Myhre, J.V. Firth, G.L. Johnson and W.F. Ruddiman (Editors), Proceedings of the Ocean Drilling Program, Scientific Results, Vol. 151. ODP, Ocean Drilling Program, College Station, TX, USA, pp. 493-514.

Benitez-Nelson, C.R., 2000. The biogeochemical cycling of phosphorus in marine systems. Earth-Science Reviews, 51: 109-135.

Berger, A. and Loutre, M.F., 1991. Insolation values for the climate of the last 10 million years. Quaternary Science Reviews, 10(4): 297-317.

Berger, W.H., Smetacek, V.S. and Wefer, G. (Editors), 1989. Productivity of the ocean; present and past. Dahlem workshop on Productivity of the ocean; present and past, 44: 471.

Bickert, T., Berger, W.H., Burcke, S., Schmidt, H. and Wefer, G., 1993. Late Quaternary stable isotope record of benthic foraminifers: Sites 805 and 806, Ontong Java Plateau. In: W.H. Berger, L.W. Kroenke and L.A. Mayer (Editors), Proceedings of the Ocean

Drilling Program, Scientific Results. Vol. 130. ODP, Ocean Drilling Program, College Station, TX, USA, 411-420.

Broecker, W.S., 1982. Ocean chemistry during glacial time. Geochimica et Cosmochimica Acta, 46: 1689-1705.

Clemens, S.C., Murray, D.W. and Prell, W.L., 1996. Non stationary Phase of the Plio-Pleistocene Asian Monsoon. Science, 274: 943-948.

Colman, A.S. and Holland, H.D., 2000. The global diagenetic flux of phosphorus from marine sediments to the oceans: redox sensitivity and the control of atmospheric oxygen levels, Marine authigenesis: from global to microbial. SEPM, pp. 53-75.

Craig, H., Chung, Y. and Fiadeiro, M., 1972. A benthic front in the South Pacific. Earth and Planetary Science Letters, 16(1): 50-65.

Delaney, M.L., 1998. Phosphorus accumulation in marine sediments and the oceanic phosphorus cycle. Global Biogeochemical Cycles, 12(4): 563-572.

Delaney, M.L. and Filippelli, G.M., 1994. An apparent contradiction in the role of phosphorus in Cenozoic chemical mass balances for the world ocean. Paleoceanography, 9(4): 513-527.

Dunbar, R.B., deMenocal, P.B. and Burckle, L.H., 1992. Late Pliocene-Quaternary biosiliceous sedimentation at Site 798, Japan Sea. In: K.A. Pisciotto, J.C.J. Ingle, M.T. von Breymann, J. Barron and e. al. (Editors), Proceedings of the Ocean Drilling Program, Scientific Results, Vol. 127/128. ODP, Ocean Drilling Program, College Station, TX, USA, 439-455.

Eaton, A.D., Clesceri, L.S. and Greenberg, A.E. (Editors), 1995. Standard methods for the examination of water and wastewater.

Espitalié, J., Deroo, G. and Marquis, F., 1986. La pyrolyse Rock-Eval et ses applications - III partie. Rev. Inst. Fr. Pet., 41(1): 73-89.

Filippelli, G.M., 1997. Controls on phosphorus concentration and accumulation in oceanic sediments. Marine Geology, 139: 231-240.

Filippelli, G.M. and Delaney, M.L., 1994. The oceanic phosphorus cycle and continental weathering during the Neogene. Paleoceanography, 9(5): 643-652.

Filippelli, G.M. and Delaney, M.L., 1996. Phosphorus geochemistry of equatorial Pacific sediments. Geochimica et Cosmochimica Acta, 60(9): 1479-1495.

Föllmi, K.B., 1995. 160 m.y. record of marine sedimentary phosphorus burial: coupling of climate and continental weathering under greenhouse and icehouse conditions. Geology, 23(6): 859-862.

Föllmi, K.B., Cramp, A., Föllmi, K.E., Alexandrovich, J.M., Brunner, C., Burckle, L.H., Casey, M., deMenocal, P., Dunbar, R.B., Grimm, K.A., Holler, P., Ingle, J.C.J., Kheradyar, T., McEvoy, J., Nobes, D.C., Stein, R., Tada, R., von Breymann, M.T. and White, L.D., 1992. Dark-light rhythms in the sediments of the Japan Sea: Preliminary results from Site 798, with some additional results from Sites 797 and 799. In: K.A. Pisciotto, J.C.J. Ingle, M.T. von Breymann, J. Barron et al. (Editors), Proceedings of the Ocean Drilling Program, Scientific Results, Vol. 127/128. ODP, Ocean Drilling Program, College Station, TX, USA, 559-576.

Froelich, P.N., 1988. Kinetic control of dissolved phosphate in natural rivers and estuaries: a primer on the phosphate buffer mechanism. Limnogeology Oceanography, 33(4, part 2): 649-668.

Froelich, P.N., Bender, M.L., Luedtke, N.A., Heath, G.R. and DeVries, T., 1982. The marine phosphorus cycle. American Journal of Science, 282(4): 474-511.

Fronval, T., and Janse, E., 1996. Late Neogene paleoclimates and paleoceanography in the Icelans-Norwegian Sea: evidence from the Iceland and Voring plateaus. In: J., Thiede, A.M., Myhre, J.V., Firth, G.L., Johnson and W.F. Ruddiman (Editors), Proceedings of the Ocean Drilling Program, Scientific Results, Vol. 151. ODP, Ocean Drilling Program, College Station, TX, USA, 455-468.

Glenn, C.G., Föllmi, K.B., Riggs, S.R., Baturin, G.N., Grimm, K.A., Trappe, J., Abed, A.M., Galli-Olivier, C., Garrison, R.E., Ilyin, A.V., Jehl., C., Rohrlich, V., Sadaqah, R.M.Y., Schidlowski, M., Sheldon, R.E. and Siegmund, H., 1994. Phosphorus and phosphorites: sedimentology and environments of formation. Eclogae geol. Helv., 87(3): 747-788.

Glenn, C.R., 1990. Pore water, petrologic and stable carbon isotopic data bearing on the origin of modern Peru margin phosphorites and associated authigenic phases. In: S.R. Riggs, Burnett, W. C. (Editor), Neogene to modern phosphorites. Phosphate deposits of the world. Cambridge Unviversity Press, New York, NY,

USA, 46-61.

Imbrie, J., McIntyre, A. and Mix, A.C., 1989. Oceanic Response to Orbital Forcing in the Late Quaternary: Observational and Experimental Strategies. In: A. Berger, S.H. Schneider and J.C. Duplessy (Editors), Climate and Geosciences, A Challenge for Science and Society in the 21st Century. Kluwer Academic Publishers, 121-165.

Ingall, E.D., Bustin, R.M. and Van cappellen, P., 1993. Influence of water column anoxia on the burial and preservation of carbon and phosphorus in marine shales. Geochimica et Cosmochimica Acta, 57: 330-316.

Ingle, J.C., Jr., Suyehiro, K., von Breymann, M.T., Bristow, J.S., Burkle, L.H., Charvet, J., Cragg, B.A., de Menocal, P., Dunbar, R.B., Follmi, K.B., Griffin, J.R., Grimm, K.A., Hamano, Y., Hirata, N., Holler, P., Isaacs, C.M., Kato, M., Kettler, R., Kheradyar, T., Krumsiek, K.A.O., Ling, H.-y., Matsumoto, R., Muza, J.P., Parkes, R.J., Pouclet, A., Scott, S.D., Stein, R. and Sturz, A.A., 1989. Site 798. In: S.K. Stewart (Editor), Proceedings of the Ocean Drilling Program, Part A: Initial Reports, Vol. 128. ODP, Ocean Drilling Program, TX, USA, 121-236.

Jarvis, I., Burnett, W.C., Nathan, Y., Almbaydin, F.S.M., Attia, A.K.M., Castro, L.N., Flicoteaux, R., Hilmy, M.E., Husain, V., Qutawnah, A.A., Serjani, A. and Zanin, Y.N., 1994. Phosphorite geochemistry: state-of-art and environmental concerns. Eclogae geol. Helv., 87(3): 643-700.

Kawai, H., 1972. Hydrography of the Kuroshio extension. In: H., Stommel, and Yoshida (Editors), Kuroshio: physical aspects of the Japan current. Seattle, Univ. Washington Press, 235-353.

Krajewski, K.P., Van Cappellen, P., Trichet, J., Kuhn, O., Lucas, J., Martin-Algarra, A., Prévot, L., Tewari, V.C., Gaspar, L., Knight, R.I. and Lamboy, M., 1994. Biological processes and apatite formation in sedimentary environments. Eclogae Geol. Helv., 87(3): 701-745.

Krissek, L.A. and Janecek, T.R., 1993. Eolian deposition on the Ontong Java Plateau since the Oligocene: unmixing a record of multiple dust sources. In: W.H. Berger, L.W. Kroenke and L.A. Mayer (Editors), Proceedings of the Ocean Drilling Program, Scientific Results, Vol. 130. ODP, Ocean Drilling Program, College Station, TX, USA, 471-490.

Kroenke, L.W. et al., 1991. Site 806 Proceedings of the Ocean Drilling Program, Ontong Java Plateau. In: E.M. Barbu (Editor), Proceedings of the Ocean Drilling Program, Part A: Initial Reports, Vol. 130. ODP, Ocean Drilling Program, College Station, TX, USA, 291-367.

Kübler, B., 1987. Dosage quantitatif des minéraux majeurs des roches sédimentaires par diffraction X. Cahier de l'Institut de Géologie de Neuchâtel, Série ADX.

Lafargue, E., Espitalié, J., Marquis, F. and Pillot, D., 1996. Rock Eval 6 applications in hydrocarbon exploration, production and in soil contamination studies, Latin American Congress on Organic Geochemistry, Cancun.

Madhupratap, M., Prasanna Kumar, S., Bhattathiri, P.M.A., Dileep Kumar, M., Raghukumar, S., Nair, K.K.C. and Ramaiah, N., 1996. Mechanism of the biological response to winter cooling in the northeastern Arabian Sea. Nature, 384: 549-552.

McManus, J.F., Major, C.O., Flower, B.P. and Fronval, T., 1996. Variability in sea-surface conditions in the North Atlantic-Arctic gateways during the last 140,000 years. In: J. Thiede, A.M. Myhre, J.V. Firth, G.L. Johnson and W.F. Ruddiman (Editors), Proceedings of the Ocean Drilling Program, Scientific Results, Vol. 151. ODP, Ocean Drilling Program, College Station, TX, USA, 437-444.

Myhre, A.M. et al., 1995. Site 907 Proceedings of the Ocean Drilling Program; initial reports; North Atlantic-Arctic gateways I. In: J.A. Marin (Editor), Proceedings of the Ocean Drilling Program, Part A: Initial Reports, Vol. 151. ODP, Ocean Drilling Program, College Station, TX, USA, 57-111.

Oberhänsli, H., Heinze, P., Diester-Haass, L. and Wefer, G., 1990. Upwelling off Peru during the last 430,000 yr and its relationship to the bottom-water environment, as deduced from coarse grain-size distributions and analyses of benthic foraminifers at Holes 679D, 680B, and 681B, Leg 112. In: E. Suess and R.e.a. von Huene (Editors), Proceedings of the Ocean Drilling Program, Scientific Results. VOl. 112. ODP, Ocean Drilling Program, College Station, TX, USA, 369-390.

Reimers, C.E. and Suess, E., 1983. Spatial and temporal patterns of organic matter accumulation on the peru continental margin. In: E. Suess, Thiede, J.

(Editor), Coastal Upwelling, Its sediment record, Part B: sedimentary records of ancient coastal upwelling. Marine Sciences. Plenum Press, New york-London, 311-345.

Resig, J., M., 1990. Benthic foraminiferal stratigraphy and paleoenvironments off Peru, Leg 112. In: E. Suess, von Huene, R. et al. (Editor), Proceedings of the Ocean Drilling Program, Scientific Results, Vol. 112. ODP, Ocean Drilling Program, College Station, TX, USA, 112263-296.

Ruddiman, W., Sarnthein, M., Baldauf, J., Backman, J., Bloemendal, J., Curry, W., Farrimond, P., Faugeres, J.C., Janacek, T., Katsura, Y., Manivit, H., Mazzullo, J., Mienert, J., Pokras, E., Raymo, M., Schultheiss, P., Stein, R., Tauxe, L., Valet, J.-P., Weaver, P. and Yasuda, H., 1988. Site 658. In: S.K. Stewart and W.D. Rose (Editors), Proceedings of the Ocean Drilling Program, Part A: Initial Reports, Vol. 108. ODP, Ocean Drilling Program, College Station, TX, USA, pp. 105-219.

Ruttenberg, K.C., 1992. Development of a sequential extraction method for different forms of phosphorus in marine sediments. Limnology Oceanography, 37(7): 1460-1482.

Ruttenberg, K.C., 1993. Reassessment of the oceanic residence time of phosphorus. Chemical Geology, 107: 407-409.

Ruttenberg, K.C. and Gõni, M.A., 1997. Phosphorus distribution, C:N:P ratios, and δ^{13}Coc in artic, temperate, and tropical coastal sediments: tools for characterizing bulk sedimentary organic matter. Marine Geology, 139: 123-145.

Sarnthein, M. and Tiedemann, R., 1989. Toward a high-resolution stable isotope stratigraphy of the last 3.4 million years: Sites 658 and 659 off Northwest Africa. In: W.F. Ruddiman, M. Sarnthein, J. Baldauf and R.G. Heath (Editors), Proceedings of the Ocean Drilling Program; Scientific Results, Vol. 108. ODP, Ocean Drilling Program, College Station, TX, USA, 167-185.

Schenau, S.J., Slomp, C.P. and De Lange, G.J., 2000. Phosphogenesis and active phosphorite formation in sediments from the Arabian Sea oxygen minimum zone. Marine Geology, 169(1-2): 1-20.

Slomp, C.P., 1997. Early diagenesis of phosphorus in continental margin sediments. Ph.D. Thesis, Den Burg, Texel, The Netherlands, 178 pp.

Slomp, C.P., Epping, E.H.G., Helder, W. and van Raaphorst, W., 1996a. A key role of iron-bound phosphorus in authigenic apatite formation in North Atlantic continental platform sediments. Journal of Marine Research, 54: 1179-1205.

Slomp, C.P., Van der Gaast, S.J. and Van Raaphorst, W., 1996b. Phosphorus binding by poorly crystalline iron oxides in North Sea sediments. Marine Chemistry, 52: 55-73.

Slomp, C.P. and Van Raaphorst, W., 1993. Phosphate adsorption in oxidized marine sediments. Chemical Geology, 107: 477-480.

Stein, R., ten Haven, H.L., Littke, R., Rullkötter, J. and Welte, D.H., 1989. Accumulation of marine and terrigenous organic carbon at upwelling Site 658 and nonupwelling Sites 657 and 659: implications for the reconstruction of paleoenvironments in the Eastern subtropical Altantic through late Cenozoic times. In: W.F. Ruddiman, M. Sarnthein, J. Baldauf and R.G. Heath (Editors), Proceedings of the Ocean Drilling Program, Scientific Results, Vol. 108. ODP, Ocean Drilling Program, College Station, TX, USA, 361-385.

Suess, E., von Huene, R., Emeis, K.-C., Bourgois, J., Cruzado Castaneda, J.d.C., De Wever, P., Eglinton, G., Garrison, R., Greenberg, M., Paz, E.H., Hill, P.R., Ibaraki, M., Kastner, M., Kemp, A.E.S., Kvenvolden, K.A., Langridge, R., Lindsley-Griffin, N., Marsters, J., Martini, E., McCabe, R., Ocola, L., Resig, J., Sanchez Fernandez, A.W., Schrader, H.-J., Thornburg, T.M., Wefer, G. and Yamano, M., 1988. Site 680 Proceedings of the Ocean Drilling Program, Peru continental margin. In: S.K. Stewart (Editor), Proceedings of the Ocean Drilling Program, Part A: Initial Reports, Vol. 112. ODP, Ocean Drilling Program, TX, USA,. 249-303.

Tada, R., Irino, T. and Koizumi, I., 1999. Land-ocean linkages over orbital and millennial scales recorded in late Quaternary sediments of the Japan Sea. Paleoceanography, 14(2): 236-247.

Tada, R., Koizumi, I., Cramp, A. and Rahman, A., 1992. Correlation of dark and light layers, and the origin of their cyclicity in the Quaternary sediments from the Japan Sea. In: K.A. Pisciotto, J.C.J. Ingle, M.T. von Breymann, J. Barron and e. al. (Editors), Proceedings of the Ocean Drilling Program, Scientific Results, Vol. 127/128. ODP, Ocean Drilling Program, College Station, TX, USA, 577-601.

Tarduno, J.A., Sliter, W.V., Kroenker, L., Leckie,

M., Meyer, H., Mahoney, J.J., Musgrave, R., Storey, M., and Winterer, E.L., 1991. Rapid formation of Ontong Java Plateau by Aptian mantle plume volcanism. Science, 254, 399-403.

Van Cappellen, P. and Ingall, E.D., 1994. Benthic phosphorus regeneration, net primary production, and ocean anoxia: a model of the coupled marine biogeochemical cycles and phosphorus. Paleoceanography, 9(5): 677-698.

Webster, P.J., 1987. The elementary monsoon. In: J. Fien, stephens, P. (Editor), Monsoon. Wiley, New York, 3-32.

Wefer, G., Heinze, P. and Suess, E., 1990. Stratigraphy and sedimentation rates from oxygen isotope composition, organic carbon content, and grain-size distribution at the Peru upwelling region: Holes 680B and 686B. In: E. Suess, R. von Huene et al. (Editors), Proceedings of the Ocean Drilling Program, Scientific Results, Vol. 112. ODP, Ocean Drilling Program, College Station, TX, USA, 355-367.

ANNEX A

Jih-Ping Shyu and Eve Arnold sampling during Leg 184 (1999)

SEDEX - Phosphorus extraction method

I give here a complete and accurate description of the extraction technique I have used to determine the different phosphorus phases. The method was first developed for marine sediments and described by Ruttenberg (1992) and subsequently modified by Filippelli and Delaney (1996) and Anderson and Delaney (2000). I also provide the description of the analytical procedure used for phosphorus concentration determination (Eaton et al., 1995).

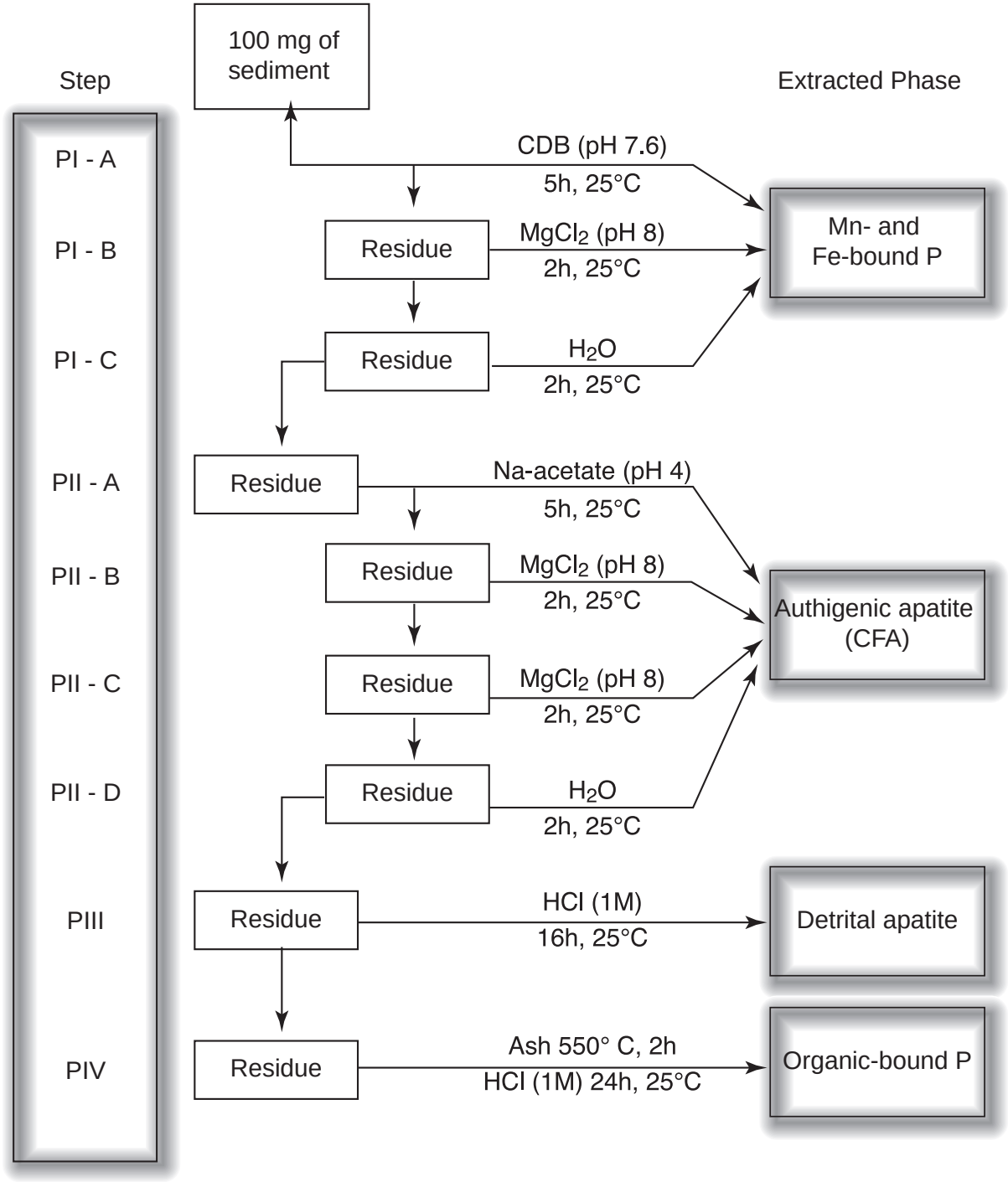

Fig. 1: Schematic representation of the SEDEX sequential extraction technique. Steps, reagents and phases are all described in the text.

MATERIAL

- Deionized water
- Mortar
- Sieve 150 μm.
- Balance
- FALCON tubes, 15 ml (n. ref. 352095); cover the label of the sample with some scotch to protect it.
- Beakers
- 3x dispenser for bottles (for water, MgCl2, HCl)
- 5x 1 liter bottles (for water, $MgCl_2$, HCl, CBD, Na-acetate)
- Pipette 1 ml, 5 ml.
- Polypropylene bottles, 30 and 60 ml (NALGENE Narrow Mouth Square Bottle PP, n. ref. 2016-0030, 2016-0060)
- Centrifuge
- pH analyzer
- 24 porcelain little cups
- Furnace (550°C) and oven

Chemicals	**Formula**
Sodium citrate	$C_6H_5Na_3O_7 \cdot 2H_2O$
Sodium bicarbonate	$NaHCO_3$
Sodium dithionite	$Na_2O_4S_2$
Magnesium chloride	$MgCl_2$
Na-acetate	$CH_3COONa \cdot 3H_2O$
Magnesium nitrate	$Mg(NO_3)_2 \cdot 6H_2O$
Acetic acid	$C_2H_4O_2$
Chloridric acid	HCl (5N)

Quantities

- 100 mg of sediment, dried at 60˚ C, ground in the mortar and sieved.
- All quantities of solutes are given for 0.5 l of solution: check Table 1 for other volumes
- 24 samples per extraction

IMPORTANT: For each step, prepare one more bottle to put the blanks to use for calibration.

CHEMISTRY

Step	**Reaction**	**Extracted Phase**
PI	Reduction of Fe by dithionite and subsequent complexation by citrate	Easily reducible + reactive ferric Fe-bound P
PII	Acid dissolution at moderately low pH and chelation of Ca by acetate	CFA + biogenic hydroxyapatite + $CaCO_3$-bound P
PIII	Acid dissolution at very low pH	Detrital apatite
PIV	Dry oxidation of organics, acid dissolution of ashed residue	Organic-bound P

Table 1

Q. of solution (l)	**Sodium Citrate**		Quantity (g)
0.05	294.1	Mol. w.	3.24
0.1	0.22	Mol. q.	6.47
0.2			12.94
0.3			19.41
0.4			25.88
0.5			**32.35**
0.6			38.82
0.7			45.29
0.8			51.76
0.9			58.23
1			64.70
	Sodium bicarbonate		
0.05	84.01	Mol. w.	0.46
0.1	0.11	Mol. q.	0.92
0.2			1.85
0.3			2.77
0.4			3.70
0.5			**4.62**
0.6			5.54
0.7			6.47
0.8			7.39
0.9			8.32
1			9.24
	Sodium dithionite		
0.05	174	Mol. w.	1.13
0.1	0.13	Mol. q.	2.26
0.2			4.52
0.3			6.79
0.4			9.05
0.5			**11.31**
0.6			13.57
0.7			15.83
0.8			18.10
0.9			20.36
1			22.62
	$MgCl_2$		
0.5	203.3	Mol. w.	101.65
0.6	1	Mol. q.	121.98
0.7			142.31
0.8			162.64
0.9			182.97
1			**203.3**
1.1			223.63
1.2			243.96
1.3			264.29
1.4			284.62
1.5			304.95
	Na-acetate		
0.1	136.08	Mol. w.	13.61
0.2	1	Mol. q.	27.22
0.3			40.82
0.4			54.43
0.5			**68.04**
0.6			81.65
0.7			95.26
0.8			108.86
0.9			122.47
1			136.08

Step PI: Reducible Phosphorus (Mn and Fe-bound P)

Solutions

• CBD solution:
  0.22 M sodium citrate
  0.11 M sodium bicarbonate
  0.13 M sodium dithionite
  0.5 l deionized water
• 1 M $MgCl_2$ solution
• Deionized water

How to prepare the CBD solution (0.5 l)
• Mix sodium citrate (32.35 g) and sodium bicarbonate (4.62 g) and then add water.
Add the sodium dithionite (11.31 g).
Important: the solution has to be prepared just before use, because the sodium dithionite oxidises.

$MgCl_2$ solution (0.5 l)
• Add $MgCl_2$ (101.65 g) to 0.5 l water, shake well.

Procedure

PI-A
• Add 10 ml of the CBD solution to the sample already set into the tube, being attentive not to lose powder during pouring; close well tight the tube, hand-shake, and, if necessary, open again to let the gas go out, close firmly.
• Put the plastic tubes in the shaker. Shake 5 to 6 hours, not longer or other phases may be attacked.
• Centrifuge the tubes for 12 minutes at 3000 turns per minute.
• Pour the solution in the 30 ml collecting bottles, trying not to lose the solid phase.

PI-B
• 1x wash with $MgCl_2$.
Pour 10 ml $MgCl_2$ solution into the tube, hand-shake well, 2 hours in the shaker, centrifuge and pour the solution in the same collecting bottle for each sample.

PI-C
• 1x wash with deionized water.
Pour 10 ml of deionized water into the tube, hand-shake well, 2 hours in the shaker, centrifuge and pour the solution in the same collecting bottle for each sample.

Step I is finished.
Bottles from step PI should contain 30 ml of final solution. Keep solid phase inside the tube.
Use the ICP-AES to analyze the solutions.

Step PII: CFA, carbonatefluorapatite.

Solutions

• Na-acetate solution
    1 M of Na-acetate anhydrous buffered to pH 4 with acetic acid.
    1 M of $MgCl_2$ solution
• Deionized water

How to prepare the Na-acetate solution (0.5 l)
• Add Na-acetate (68.04 g) to part of the water (about 0.3 l), mix well till all the solute is dissolved. Add acetic acid and adjust with the remaining water (about 80 ml for 0.5 l of final solution), controlling the pH with the pH analyzer to arrive at a pH as close as possible to 4.

Procedure

PII-A
• Pour 10 ml of the Na-acetate solution in the tubes from step PI, shake for 5 hours, centrifuge, pour the solution in a new 60 ml collecting bottle. Collect the reagent blank in a separate bottle.

PII-B, C
• 2x wash with $MgCl_2$
Pour 10 ml of the $MgCl_2$ solution in the tube, hand-shake well, 2 hours in the shaker, centrifuge and pour in the same collecting bottle. Repeat a second time.

PII-D
• 1x wash with deionized water.
Pour 10 ml of deionized water into the tube, 2 hours shaking, centrifuge and pour the solution in the collecting bottle.

• Collect all the solutions each in the corresponding collecting bottle and also the reagent blanks.

Step II is finished.
Bottles from step PII should contain 40 ml of final solution. Keep solid phase inside the tube.
Use the spectrophotometer to analyze the solutions.

Step PIII: Detrital P (Metamorphic and igneous P-bearing minerals)

Solutions

1 N HCl solution with deionized water (To obtain 1l of solution, add 200 ml of HCl (5N) to 800 ml of deionized water).

Procedure

PIII
• Add 10 ml of HCl solution to the sample in the tube from step PII, hand shake, shake for 16 hours (overnight) in the shaker, centrifuge, pour in new 30 ml collecting bottles.
• Collect the reagent blank.
No wash requested.

Step III is finished.
Bottles from step PIII should contain 10 ml of final solution. Keep solid phase inside the tube
Use the spectrophotometer to analyze the solutions.

Step PIV: Organic-bound P

Solutions

• 50% weight/volume $MgNO_3$ solution (100 g of solute in 100 ml of deionized water).
• 1 N HCl solution with deionized water

Procedure

PIV
• Transfer the all the solid from step PIII into the porcelain cups, using deionized water. Let then dry in oven at 80°C.
• Add 1 ml of the $MgNO_3$ solution. Ash in the furnace at 550˚ for 2 hours.
• Transfer ash back in the same tubes from step PIII using a plastic spatula and 1N HCl (2 ml HCl in the cup, scrap with the spatula and transfer into the tube; continue till all the material is recovered); once all the material is transfered, add 1N HCl to reach a total of 10 ml, hand shake, shake for 24 hours in shaker, centrifuge 12 minutes.
• Keep the liquid in the tube; for the analyses, take the solution at the top.

Step IV is finished
Use the spectrophotometer to analyze the solutions.

Analysis with the Spectrophotometer
Ascorbic Acid Method for Phosphate (Eaton et al., 1995)
Material

Chemicals	**Formula**
Ammonium molybdate	$(NH_4)_6Mo_7O_{24}\cdot 4H_2O$
Antimony K tartrate	$K(SbO)C_4H_4O_6\cdot 1/2H_2O$
Ascorbic acid	$C_6H_3O_6$
Sulphuric acid	H_2SO_4 (5N)

Deionized water

How to prepare the mixing reagent (0.75 l)

• 6 g of ammonium molybdate in 250 ml of deionized water.
• 0.1454 g of antimony K tartrate in 500 ml of 5N of H_2SO_4 (74 ml of H_2SO_4 in 426 ml of distilled water).
• Mix the two solutions.
Important: If stored in the fridge, this solution is stable for about 2 months.

Color developing reagent

• Add the ascorbic acid to the mixing reagent (0.053 g each 10 ml of solution).
Important: This reagent is stable for about 1 hour: prepare just before use.

Calibration of the spectrophotometer

• Before starting the analyses, prepare standards solutions to calibrate the machine.
• For each step, prepare standards using the appropriate blank for each phase.
• Follow the below described procedure for developing color.
• Make a calibration curve.

Procedure
• Dilute the solution (or standard) to analyze (1 ml of solution to analyze, 9 ml of deionized water) in a clean plastic tube.
• Add 1 ml of the color developing reagent to the diluted solution. Close tight the tubes and shake.
• Wait from 10 to 20 minutes, putting the tubes in a dark place.
• Analyze with the spectrophotometer

Errors and detection limits

Step	Method	Error (rel. Std. Dev.)	Detection Limit (3*std. Dev. Blank)
PI	ICP-AES		0.03 mg P/g sed.
PII	Ascorbic Acid	0.06	0.025 mg P/g sed.
PIII	Ascorbic Acid	0.03	0.003 mg P/g sed.
PIV	Ascorbic Acid	0.05	0.004 mg P/g sed.

A solid consistency standard (CS) was run along with solid samples. The errors given in the above table were determined as the relative standard deviations of the CS concentrations for each step.
CS average concentrations:
Fe-bound P = 0.115 mg/g;
authigenic P = 1.017 mg/g;
detrital P = 0.661 mg/g;
organic-bound P = 0.062 mg/g.

Spectrophotometer and accessories

Perkin-Elmer UV/Vis spectrophotometer Lambda 10 with computer interface.
Peristaltic Multisipper introducing samples to a 5-cm quartz cell.
UV WinLab software package for Windows.

References:

Anderson, L. D., Delaney, M. L. (2000) – Sequential extraction and analysis of phosphorus in marine sediments: Streamlining of the SEDEX procedure. Limnol. Oceanogr., 45 (2): 509 - 515.

Eaton, A. D., Clesceri, L. S., Greenberg, A. E. (1995) - Standard methods fot the examination of water and wastewater, 19th edition.

Filippelli, G. M., Delaney, M. L. (1996) – Phosphorus geochemistry of equatorial Pacific sediments. Geochimica et Cosmochimica Acta, 60 (9): 1479 - 1495.

Ruttenberg, K. C. (1992) – Development of a sequential extraction method for different forms of phosphorus in marine sediments. Limnol. Oceanogr., 37 (7): 1460 - 1482.

ANNEX B

S. Patrick's day on board of the Joides Resolution; sedimentology lab (1999)

Annexe B contains the complete dataset produced during this four-years research. Data from each site (mineralogy, inorganic and organic geochemistry) are presented in the following pages. Unless specified, the data are to be considered original.

Most of the analyses were performed at the GEA laboratories at the Geological Institute in Neuchâtel, Switzerland. Determinations of iron and iron-bound phosphorus were performed at the "Laboratoire des eaux et de l’environnement" in Peseux, Switzerland. Samples were analyzed for nitrogen stable isotopes at the ETH in Zürich, Swizterland.

Site 108-658: Eastern Tropical Atlantic
XRD results: bulk mineralogy

Hole	Core	Interval	Depth	Age*	Phyllosilicates	Quartz	K-feldspar	Plagioclase	Calcite	Detrital	Unquantified
		cm	mbsf	k.y.	%	%	%	%	%	%	%
108-658											
A	1H-1	11-15	0.23	1.13	20.51	10.98	1.54	3.00	36.80	36.02	24.36
A	1H-1	83-85	0.94	4.62	23.33	7.38	2.19	1.14	46.47	34.04	14.38
B	2H-1	104-106	1.65	8.10	13.79	5.26	0.76	0.70	43.16	20.51	15.54
A	1H-2	72-75	2.33	11.42	13.62	6.56	0.51	1.15	45.75	21.84	15.21
B	2H-2	100-102	3.11	15.18	14.96	21.73	2.65	5.67	39.91	45.00	2.05
A	1H-3	68-70	3.64	17.41	12.79	15.85	1.11	3.58	33.15	33.33	26.63
B	2H-3	93-95	4.54	20.79	13.96	20.75	3.91	1.42	34.27	40.04	18.10
A	1H-4	68-70	5.00	22.43	14.05	12.70	1.36	3.54	38.93	31.65	18.41
B	2H-4	20-22	5.31	23.57	14.87	28.38	2.28	3.87	31.83	49.41	7.95
B	2H-4	93-95	6.04	26.57	17.17	18.67	1.00	1.78	39.85	38.61	7.71
B	2H-5	17-19	6.78	30.74	18.61	8.39	0.00	1.34	38.01	28.34	18.42
B	2H-5	91-93	7.52	36.42	14.01	7.75	1.13	0.90	48.92	23.79	11.02
B	2H-6	50-52	8.31	44.17	15.56	10.41	5.99	2.48	43.52	34.44	9.58
B	2H-6	122-124	9.03	74.21	18.02	22.72	5.25	3.08	29.61	49.07	10.81
B	2H-7	36-38	9.67	79.10	16.32	7.27	2.51	1.27	51.48	27.37	7.51
B	3H-1	24-26	10.35	84.60	13.74	5.34	0.00	1.60	52.56	20.68	6.04
B	3H-1	110-112	11.21	91.49	14.40	14.47	0.00	3.74	51.70	32.61	2.16
B	3H-2	17-19	11.79	95.02	16.14	13.91	4.55	8.20	42.36	42.80	5.10
A	3H-1	13-15	12.49	98.62	17.58	7.48	0.90	0.83	50.33	26.79	13.81
A	3H-1	91-93	13.27	102.31	16.06	7.62	0.49	0.94	42.35	25.11	22.11
A	3H-2	13-15	13.99	105.90	16.63	11.51	0.60	6.64	43.30	35.38	5.73
A	3H-2	91-93	14.77	110.59	19.43	10.89	1.53	1.59	51.06	33.44	4.48
A	3H-3	13-15	15.49	116.42	19.52	13.92	1.61	4.36	40.91	39.42	15.79
A	3H-3	90-93	16.27	123.01	22.31	8.34	1.21	2.27	45.15	34.12	16.43
A	3H-4	13-15	16.99	127.88	13.33	9.86	0.78	0.71	43.91	24.67	19.35
A	3H-4	100-102	17.85	133.22	7.12	19.92	4.05	2.52	29.04	33.60	32.97

Site 108-658: Eastern Tropical Atlantic (continued)
Geochemistry: organic matter, nitrogen isotopes, iron and phosphorus phases

Depth	Age*	N	$\delta_{15}N$	TOC	HI	OI	Tmax	Fe	Fe-bound P	Authigenic P	Detrital P	Organic-bound P
mbsf	k.y.	%	‰ (air)	%			C°	mgFe/g	mgP/g	mgP/g	mgP/g	mgP/g
0.23	1.13	0.297	4.122	2.12	263.49	358.85	422	1.606	0.103	0.253	0.067	0.251
0.94	4.62	0.211	5.391	1.62	234.20	330.43	420	0.867	0.104	0.278	0.023	0.200
1.65	8.10	0.185	5.648	1.45	272.09	381.23	421	0.569	0.105	0.330	0.021	0.212
2.33	11.42	0.177	4.683	1.51	247.18	350.50	420	1.126	0.254	0.242	0.025	0.119
3.11	15.18	0.111	5.005	0.99	222.80	350.49	418	0.841	0.068	0.265	0.042	0.080
3.64	17.41	0.111	4.794	0.96	197.87	400.62	413	0.907	0.073	0.278	0.109	0.092
4.54	20.79	0.077	5.129	0.65	181.78	466.01	415	0.812	0.090	0.289	0.046	0.077
5.00	22.43	0.187	4.479	1.66	256.01	325.11	421	1.090	0.144	0.262	0.077	0.121
5.31	23.57	0.12	4.322	1.07	185.77	344.90	413	1.062	0.070	0.255	0.105	0.084
6.04	26.57	0.147	4.605	1.26	234.94	385.25	418	0.739	0.141	0.250	0.091	0.103
6.78	30.74	0.284	4.694	2.54	367.64	305.29	418	1.109	0.106	0.310	0.029	0.153
7.52	36.42	0.227	4.718	1.99	313.45	314.97	417	1.569	0.115	0.265	0.024	0.135
8.31	44.17	0.155	4.734	1.30	263.88	352.82	417	1.268	0.095	0.267	0.029	0.100
9.03	74.21	0.104	5.696	0.94	164.80	480.48	417	1.486	0.116	0.266	0.045	0.084
9.67	79.10	0.152	6.135	1.30	286.22	355.54	416	0.912	0.134	0.260	0.023	0.111
10.35	84.60	0.167	4.083	1.42	379.83	315.54	418	0.908	0.240	0.251	0.026	0.102
11.21	91.49	0.164	2.625	1.36	356.20	356.17	417	0.935	0.129	0.264	0.030	0.095
11.79	95.02	0.164	4.773	1.41	289.22	349.50	418	1.265	0.309	0.276	0.030	0.105
12.49	98.62	0.161	5.225	1.37	270.28	305.63	415	1.120	0.122	0.264	0.021	0.115
13.27	102.31	0.132	4.649	1.08	234.26	273.94	415	1.124	0.111	0.255	0.025	0.092
13.99	105.90	0.126	4.413	1.07	263.35	337.32	416	1.195	0.204	0.307	0.028	0.089
14.77	110.59	0.158	4.266	1.24	318.67	298.69	417	0.883	0.160	0.357	0.030	0.105
15.49	116.42	0.168	4.094	1.47	276.34	267.08	416	1.278	0.125	0.324	0.030	0.108
16.27	123.01	0.157	4.62	1.16	201.18	472.72	416	1.323	0.103	0.327	0.022	0.111
16.99	127.88	0.199	3.713	1.84	329.53	268.41	419	1.830	0.102	0.387	0.026	0.108
17.85	133.22	0.083	4.557	0.17	977.30	425.63	418	1.202	0.068	0.286	0.049	0.049

Site 108-658: Eastern Tropical Atlantic (continued)
Mass Accumulation Rates (MAR), molar ratios**

Depth	Age*	Calcite	TOC	Detrital	Preac.	TOC/Porg	TOC/Preac	TOC/N
mbsf	k.y.	MAR	MAR	MAR	MAR	molar	molar	molar
0.23	1.13	8328.351	479.286	8152.162	13.734	217.729	89.99	8.3127
0.94	4.62	6884.550	240.425	5043.504	8.628	209.133	71.86	8.9647
1.65	8.10	6548.258	219.504	3111.610	9.829	175.680	57.59	9.1171
2.33	11.42	7420.272	244.619	3541.279	9.966	326.303	63.30	9.9337
3.11	15.18	9441.474	235.000	10646.620	9.781	319.447	61.95	10.4310
3.64	17.41	8895.813	258.368	8945.935	11.917	269.439	55.91	10.1097
4.54	20.79	7405.994	140.455	8653.810	9.872	217.480	36.69	9.8381
5.00	22.43	8570.669	366.448	6967.780	11.618	353.487	81.33	10.3755
5.31	23.57	7972.780	267.391	12374.549	10.234	329.623	67.38	10.3709
6.04	26.57	9087.788	286.217	8805.584	11.253	314.410	65.59	9.9524
6.78	30.74	3852.990	257.255	2872.553	5.769	427.852	114.98	10.4168
7.52	36.42	4201.978	170.646	2043.752	4.429	378.465	99.36	10.2019
8.31	44.17	3784.688	113.076	2994.881	4.028	334.425	72.40	9.7793
9.03	74.21	4230.877	134.075	7012.157	6.648	289.140	52.00	10.5163
9.67	79.10	5880.531	147.920	3126.176	5.772	300.433	66.09	9.9319
10.35	84.60	4304.889	116.641	1693.937	4.860	360.383	61.88	9.9397
11.21	91.49	8011.930	210.900	5053.908	7.576	368.711	71.78	9.6723
11.79	95.02	6352.295	210.911	6418.131	10.346	346.132	52.57	9.9967
12.49	98.62	7556.406	204.997	4022.166	7.531	305.290	70.19	9.8860
13.27	102.31	7386.013	187.642	4379.966	7.992	301.190	60.54	9.5007
13.99	105.90	6818.391	168.401	5571.391	9.451	308.778	45.95	9.8939
14.77	110.59	5572.816	135.026	3649.020	6.781	303.456	51.35	9.1283
15.49	116.42	4259.891	152.907	4104.687	5.804	351.273	67.93	10.1880
16.27	123.01	4391.568	112.470	3319.357	5.262	268.065	55.12	8.5847
16.99	127.88	5785.995	242.348	3251.616	7.877	438.352	79.34	10.7726
17.85	133.22	4658.013	27.908	5390.147	6.445	92.426	11.17	2.4433

* Ages are interpolated using the age model provided in Sarnthein and Tiedemann (1989).
** Dry bulk density values are taken from ODP Initial Reports Vol. 108 (1988); sedimentation rates are taken from Sarnthein and Tiedemann (1989).

Site 112-680: Peru Continental Margin
XRD results: bulk mineralogy

Core	Interval	Depth	Age*	Phyllosilicates	Quartz	K-feldspar	Plagioclase	Calcite	Dolomite	Detrital	Unquantified
	cm	mbsf	k.y.	%	%	%	%	%	%	%	%
112-680B											
1H-1	95-97	0.95	3.82	18.99	13.92	0.00	3.87	4.01	0.00	36.79	52.76
1H-1	128-130	1.28	5.33	16.56	8.39	0.00	3.73	5.83	0.00	28.69	56.55
1H-2	25-27	1.75	7.69	15.27	9.62	0.00	2.86	12.68	0.00	27.75	53.67
1H-2	63-65	2.13	9.80	10.26	22.54	3.24	15.99	15.14	0.41	52.03	30.44
1H-2	101-103	2.51	12.11	10.48	26.10	2.79	10.09	0.00	0.53	49.46	47.06
1H-2	136-138	2.86	14.79	11.17	25.05	2.67	6.34	0.00	0.44	45.24	51.94
1H-3	36-38	3.26	18.50	19.55	13.54	2.98	4.70	0.19	0.00	40.78	55.20
1H-3	61-63	3.61	22.08	13.57	18.99	4.64	5.55	0.18	0.00	42.75	53.40
1H-3	102-104	4.02	27.38	16.11	16.72	1.68	5.55	0.16	0.00	40.07	56.78
1H-3	141-143	4.41	35.79	14.87	15.76	0.00	33.01	7.50	0.00	63.63	25.83
1H-4	19-21	4.69	42.49	14.84	14.72	15.00	5.05	10.62	0.15	49.62	36.53
1H-4	50-52	5.00	49.61	12.91	23.22	2.06	4.48	10.97	0.29	42.67	42.15
1H-4	77-79	5.27	55.07	14.88	10.25	1.49	6.42	20.42	0.00	33.03	43.30
2H-1	5-7	5.55	59.70	5.38	27.48	5.30	13.50	0.59	0.09	51.66	47.20
2H-1	42-44	5.92	64.74	16.98	8.50	3.04	5.00	8.68	0.31	33.52	53.91
2H-1	81-83	6.31	69.88	10.24	9.37	0.00	1.90	23.27	0.00	21.51	51.03
2H-1	122-124	6.72	75.69	9.19	3.84	0.00	1.59	9.38	0.00	14.62	72.13
2H-2	12-14	7.12	82.35	18.45	15.93	1.27	3.62	21.22	0.31	39.27	36.00
2H-2	41-43	7.41	87.65	8.41	25.32	1.31	9.20	5.30	0.60	44.24	47.95
2H-2	82-84	7.82	95.48	10.47	10.87	0.00	3.59	9.45	0.00	24.94	61.04
2H-2	120-122	8.20	102.84	6.18	7.39	0.00	4.74	15.47	0.00	18.31	61.79
2H-3	3-5	8.53	109.17	10.49	12.01	0.00	3.75	14.53	0.30	26.24	55.64
2H-3	46-48	8.96	117.17	13.10	12.92	0.00	4.20	12.05	0.18	30.23	54.04
2H-3	80-82	9.30	123.19	7.35	5.88	0.00	2.53	5.89	0.49	15.75	73.81
2H-3	116-118	9.66	129.20	18.26	10.38	0.00	3.38	8.84	0.00	32.01	55.81
2H-3	143-145	9.93	133.49	21.65	13.92	6.12	4.51	0.00	0.00	46.20	51.21

Site 112-680: Peru Continental Margin (continued)
Geochemistry: organic matter, nitrogen isotopes, iron and phosphorus phases

Depth	Age*	N	$\delta_{15}N$	TOC	HI	OI	Tmax	Fe	Fe-bound P	Authigenic P	Detrital P	Organic-bound P
mbsf	k.y.	%	‰	%			C°	mgFe/g	mgP/g	mgP/g	mgP/g	mgP/g
0.95	3.82	1.29	3.49	9.203	377.43	130.03	417	1.31	1.39	0.71	0.04	0.41
1.28	5.33	1.27	4.87	8.874	409.03	134.47	414	1.55	1.28	0.76	0.02	0.35
1.75	7.69	1.34	4.89	9.507	413.26	142.03	407	1.42	0.90	1.47	0.03	0.37
2.13	9.80	0.50	4.83	4.641	390.69	121.99	412	0.99	0.85	3.55	0.26	0.16
2.51	12.11	0.77	5.51	3.783	355.95	135.23	398	2.83	2.32	0.42	0.10	0.16
2.86	14.79	0.41	6.52	4.355	387.59	129.02	404	2.96	2.64	0.68	0.21	0.09
3.26	18.50	0.66	3.71	0.635	257.57	186.22	393	3.44	2.69	1.42	0.07	0.10
3.61	22.08	0.46	2.99	3.737	356.11	146.59	395	2.64	1.70	1.42	0.06	0.08
4.02	27.38	0.39	2.62	6.491	324.23	116.18	403	3.55	2.03	0.34	0.06	0.06
4.41	35.79	0.40	2.57	3.420	287.26	125.97	405	2.40	0.89	2.19	0.09	0.08
4.69	42.49	0.47	2.83	6.642	366.75	101.84	404	2.03	0.93	2.97	0.09	0.09
5.00	49.61	0.37	2.72	4.854	406.78	89.09	410	1.89	0.79	2.21	0.11	0.07
5.27	55.07	0.42	2.93	3.913	321.11	111.06	406	2.18	0.61	1.58	0.03	0.07
5.55	59.70	0.05	4.33	4.120	385.45	123.36	410	0.92	1.73	3.71	0.38	0.04
5.92	64.74	0.46	2.73	4.489	382.55	131.72	407	1.44	0.79	1.51	0.06	0.08
6.31	69.88	0.58	2.58	5.909	409.41	148.39	406	1.34	0.43	2.03	0.04	0.09
6.72	75.69	0.61	2.87	6.150	425.32	128.89	405	1.26	0.45	0.61	0.02	0.08
7.12	82.35	0.83	3.01	8.487	430.60	133.32	407	1.38	0.54	1.95	0.06	0.12
7.41	87.65	0.33	3.12	3.456	399.07	160.50	404	0.86	1.13	4.31	0.35	0.08
7.82	95.48	0.94	6.74	9.528	430.83	137.86	403	1.60	0.87	2.64	0.02	0.11
8.20	102.84	0.56	6.77	5.786	428.29	156.30	404	1.71	0.43	1.64	0.02	0.07
8.53	109.17	0.53	7.84	5.796	425.61	144.21	406	2.30	0.39	1.30	0.03	0.09
8.96	117.17	0.50	9.00	5.229	416.92	137.94	401	2.47	0.42	1.16	0.04	0.09
9.30	123.19	0.50	8.64	5.434	452.88	103.70	413	2.24	0.40	0.39	0.01	0.06
9.66	129.20	0.49	8.82	5.100	430.96	115.90	411	3.01	0.39	0.60	0.02	0.08
9.93	133.49	0.41	7.23	4.303	343.28	135.08	401	4.04	1.09	0.37	0.02	0.07

Site 112-680: Peru Continental Margin (continued)
Mass Accumulation Rates (MAR) and molar ratios**

Depth mbsf	**Age*** k.y.	**Calcite** MAR	**TOC** MAR	**Detrital** MAR	**Preac** MAR	**TOC/Porg** molar	**TOC/Preac** molar	**TOC/N** molar
0.95	3.82	1277.26	2932.32	11721.60	80.01	572.56	94.51	8.36
1.28	5.33	1626.77	2474.70	8001.10	66.61	645.15	95.80	8.15
1.75	7.69	3230.95	2423.12	7073.34	69.76	669.83	89.57	8.29
2.13	9.80	3492.72	1070.91	12006.25	105.18	747.06	26.26	10.92
2.51	12.11	0.00	794.86	10393.82	60.78	618.51	33.72	5.77
2.86	14.79	0.00	730.40	7588.22	57.06	1298.36	33.01	12.42
3.26	18.50	26.80	87.61	5621.87	58.00	167.94	3.90	1.12
3.61	22.08	22.22	467.34	5346.61	40.01	1272.46	30.12	9.44
4.02	27.38	16.22	643.35	3971.08	24.07	2588.55	68.92	19.57
4.41	35.79	444.97	203.04	3777.64	18.74	1158.20	27.93	10.03
4.69	42.49	567.48	354.99	2651.78	21.32	1929.99	42.94	16.52
5.00	49.61	611.64	270.60	2379.15	17.18	1690.91	40.62	15.43
5.27	55.07	1291.17	247.38	2088.61	14.28	1420.78	44.68	10.79
5.55	59.70	45.44	319.03	4000.68	42.38	2697.47	19.41	
5.92	64.74	816.32	422.44	3154.18	22.37	1407.60	48.70	11.41
6.31	69.88	2257.08	573.11	2086.38	24.72	1750.41	59.78	11.82
6.72	75.69	847.50	555.46	1320.53	10.40	1883.61	137.72	11.76
7.12	82.35	1631.85	652.59	3019.48	20.07	1828.75	83.85	11.92
7.41	87.65	371.65	242.31	3101.10	38.68	1176.31	16.16	12.11
7.82	95.48	633.48	638.61	1671.36	24.28	2215.68	67.81	11.78
8.20	102.84	1022.03	382.21	1209.67	14.14	2068.20	69.71	12.03
8.53	109.17	969.47	386.80	1751.30	11.87	1716.38	84.06	12.74
8.96	117.17	829.19	359.74	2079.67	11.42	1559.46	81.20	12.32
9.30	123.19	426.14	392.84	1138.53	6.16	2260.72	164.55	12.81
9.66	129.20	678.04	391.04	2454.28	8.26	1611.00	122.15	12.24
9.93	133.49	0.00	346.61	3721.58	12.35	1521.99	72.38	12.15

* Ages are interpolated using the age model provided in Wefer et al. (1990).
** Dry bulk density values are taken from ODP Initial Reports Vol. 112 (1988); sedimentation rates are taken from Wefer et al. (1990).

Site 117-724: Oman Margin
XRD results: bulk mineralogy

Core	Interval	Depth	Age*	Phyllosilicates	Quartz	K-feldspar	Plagioclase	Calcite	Dolomite	Detrital	Unquantified
	cm	mbsf	k.y.	%	%	%	%	%	%	%	%
117-724C											
1H-1	11-13	0.11	5.17	9.66	18.56	0.00	2.36	43.52	13.32	30.58	8.90
1H-1	48-50	0.48	8.00	6.79	9.21	6.05	4.41	61.16	4.91	26.45	4.57
1H-1	88-90	0.88	10.66	6.91	11.07	9.15	6.12	41.39	4.36	33.25	12.60
1H-1	127-129	1.27	13.20	7.49	14.51	0.00	8.34	29.50	6.11	30.34	30.79
1H-2	18-20	1.68	16.00	8.40	12.72	0.00	6.28	35.10	11.37	27.40	21.86
1H-2	57-59	2.07	18.57	11.00	18.03	2.14	18.70	36.39	10.38	49.87	0.20
1H-2	98-100	2.48	21.33	11.73	19.24	0.00	9.93	34.69	11.73	40.90	10.62
2H-1	12-14	2.92	24.24	10.05	15.42	1.53	13.72	35.75	6.95	40.72	13.19
2H-1	50-52	3.30	27.89	9.11	20.65	0.00	10.65	40.96	7.67	40.41	7.18
2H-1	90-92	3.70	31.86	10.52	17.87	0.00	12.16	39.62	13.58	40.55	4.20
2H-1	130-132	4.10	35.84	8.23	15.28	0.00	4.49	41.08	8.57	28.00	19.30
2H-2	20-22	4.50	39.82	7.60	13.91	0.00	12.16	40.69	12.50	33.67	10.81
2H-2	61-63	4.91	43.88	7.65	16.96	0.00	4.23	33.14	3.91	28.84	31.32
2H-2	99-101	5.29	47.68	10.08	14.61	0.73	7.49	33.43	12.33	32.91	16.98
2H-2	139-141	5.69	51.66	9.14	10.02	2.47	20.46	40.60	6.06	42.09	5.27
2H-3	30-32	6.10	55.73	9.60	11.50	1.37	18.79	37.49	9.60	41.26	5.92
2H-3	70-72	6.50	59.70	8.12	17.39	0.73	5.05	37.32	9.12	31.29	13.28
2H-3	110-112	6.90	63.01	11.75	14.36	0.61	14.41	36.00	6.36	41.13	10.12
2H-3	138-140	7.18	66.41	8.45	12.29	1.61	11.42	38.62	6.02	33.76	17.82
2H-4	28-30	7.58	70.41	6.68	14.02	0.68	7.24	47.56	3.18	28.62	15.41
2H-4	69-71	7.99	81.34	6.82	16.45	9.28	2.04	38.93	3.68	34.59	15.24
2H-4	109-111	8.39	92.47	8.39	12.63	2.10	9.18	52.04	2.92	32.30	8.68
2H-4	140-142	8.70	101.10	6.53	10.27	0.00	2.31	48.36	2.29	19.11	21.10
2H-5	30-32	9.10	112.27	7.31	6.65	0.00	8.98	43.59	3.12	22.94	22.04
2H-5	70-72	9.50	122.47	7.48	13.60	1.56	6.25	42.87	4.88	28.90	17.69
2H-5	110-112	9.90	124.84	7.97	14.75	0.47	3.44	28.86	1.74	26.63	34.98
2H-5	147-149	10.27	126.73	7.17	18.89	0.60	4.51	34.96	5.52	31.17	23.41

Site 117-724: Oman Margin (continued)
Geochemistry: organic matter, nitrogen isotopes, iron and phosphorus phases

Depth	Age*	N	$\delta_{15}N$	TOC	HI	OI	Tmax	Fe	Fe-bound P	Authigenic P	Detrital P	Organic-bound P
mbsf	k.y.	%	‰ (air)	%			C°	mgFe/g	mgP/g	mgP/g	mgP/g	mgP/g
0.11	5.17	0.31	7.620	2.21	365.5	250.2	438	0.2409	0.1826	3.582	0.190	0.15
0.48	8.00	0.19	5.122	1.50	398.5	237.4	433	0.2025	0.0912	1.904	0.129	0.08
0.88	10.66	0.10	5.000	0.72	427.4	268.3	430	0.285	0.0584	0.721	0.169	0.03
1.27	13.20	0.04		0.25	550.8	372.7	427	0.4331	0.0547	0.287	0.218	0.02
1.68	16.00	0.07	1.979					0.5616	0.0564	0.589	0.193	0.02
2.07	18.57	0.15	1.405	1.88	525.4	128.4	415	0.9084	0.0555	0.761	0.201	0.04
2.48	21.33	0.12	3.736	0.90	375.2	218.8	434	0.7621	0.0487	0.888	0.213	0.05
2.92	24.24	0.07	2.682	0.51	426.9	221.1	444	0.6096	0.0535	0.756	0.198	0.02
3.30	27.89	0.10	1.960	0.82	411.8	216.7	435	0.6216	0.0488	1.008	0.258	0.03
3.70	31.86	0.08	2.653	0.61	406.1	215.0	425	0.7922	0.0498	0.917	0.228	0.02
4.10	35.84	0.18	7.415	1.86	412.7	145.8	421	0.7298	0.0646	1.083	0.249	0.05
4.50	39.82	0.13	6.183	1.16	411.8	180.7	416	0.6583	0.0410	0.785	0.216	0.03
4.91	43.88	0.15	3.316	1.43	404.0	148.0	416	0.8263	0.0564	0.986	0.250	0.04
5.29	47.68	0.07	5.489	0.52	495.6	280.7	416	0.5182	0.0415	0.848	0.244	0.02
5.69	51.66	0.07	3.011	0.52	380.2	280.7	420	0.7427	0.0521	0.993	0.196	0.03
6.10	55.73	0.07	1.380	0.51	407.3	272.2	431	0.4771	0.0518	0.610	0.185	0.02
6.50	59.70	0.07	1.198	0.57	399.5	214.3	420	0.4874	0.0509	0.709	0.232	0.02
6.90	63.01	0.05	0.530	0.38	415.0	269.2	418	0.4274	0.0501	0.344	0.183	0.02
7.18	66.41	0.10	2.020	0.82	387.4	281.2	422	0.6712	0.0533	0.937	0.173	0.03
7.58	70.41	0.12	4.540	1.15	415.4	262.8	418	0.3484	0.0603	1.884	0.190	0.03
7.99	81.34	0.10	2.080	0.81	404.6	280.9	420	0.4045	0.0543	1.106	0.167	0.02
8.39	92.47	0.14	4.130	1.26	418.8	218.3	418	0.4576	0.0590	1.611	0.165	0.02
8.70	101.10	0.10	2.235	0.96	383.0	277.1	419	0.314	0.0654	1.373	0.139	0.02
9.10	112.27	0.12	2.490	1.16	394.6	228.8	421	0.3841	0.0639	1.619	0.180	0.03
9.50	122.47	0.07	5.927	0.68	379.0	250.9	423	0.6361	0.0478	0.938	0.205	0.02
9.90	124.84	0.05	2.284	0.43	413.3	282.9	421	0.5163	0.0505	0.539	0.194	0.03
10.27	126.73	0.03		0.24	490.4	520.7	422	0.6282	0.0462	0.275	0.223	0.01

Site 117-724: Oman Margin (continued)
Mass Accumulation Rates (MAR) and molar ratios**

Depth mbsf	Age* k.y.	Calcite MAR	TOC MAR	Detrital MAR	Preac MAR	Fe MAR	TOC/Porg molar	TOC/Preac molar	TOC/N molar	Fe/P molar
0.11	5.17	7376.64	374.60	7442.18	66.35	4.08	379.93	14.56	8.257	0.732
0.48	8.00	10366.62	254.25	5316.60	35.09	3.43	515.74	18.68	9.155	1.231
0.88	10.66	7015.61	122.04	6374.24	13.77	4.83	562.62	22.85	8.393	2.706
1.27	13.20	5000.25	42.38	6179.45	6.06	7.34	402.92	18.02	7.876	4.395
1.68	16.00	5949.45		6573.56	11.33	9.52				5.519
2.07	18.57	6168.11	318.66	10212.69	14.57	15.40	1127.42	56.40	15.010	9.069
2.48	21.33	5879.96	152.55	8920.90	16.78	12.92	437.89	23.45	9.044	8.671
2.92	24.24	4080.15	58.21	5440.75	9.49	6.96	597.79	15.82	8.144	6.320
3.30	27.89	4674.76	93.59	5488.57	12.36	7.09	813.28	19.53	9.464	7.058
3.70	31.86	4521.83	69.62	6178.49	11.31	9.04	655.42	15.88	9.481	8.828
4.10	35.84	4688.46	212.28	4173.80	13.61	8.33	1065.86	40.22	12.113	6.264
4.50	39.82	4643.95	132.39	5268.94	9.79	7.51	934.77	34.86	10.244	8.902
4.91	43.88	3782.27	163.21	3737.99	12.30	9.43	1053.58	34.23	11.039	8.120
5.29	47.68	3815.37	59.35	5162.41	10.40	5.91	609.51	14.71	8.191	6.932
5.69	51.66	4633.68	59.35	5495.37	12.29	8.48	419.04	12.45	8.785	7.900
6.10	55.73	4278.73	58.21	5804.60	7.76	5.45	730.63	19.35	8.743	5.105
6.50	59.70	4217.16	64.41	4565.66	8.80	5.51	773.61	18.87	9.917	5.310
6.90	63.01	4068.00	42.94	5366.30	4.69	4.83	466.62	23.61	8.203	4.731
7.18	66.41	4364.06	92.66	4495.39	11.48	7.58	813.28	20.81	10.062	6.986
7.58	70.41	5374.28	129.95	3592.33	22.26	3.94	1140.57	15.05	10.899	3.202
7.99	81.34	1539.68	32.04	1513.90	4.68	1.60	908.15	17.65	9.734	4.129
8.39	92.47	2058.18	49.83	1392.82	6.70	1.81	1353.81	19.18	10.880	4.299
8.70	101.10	1912.64	37.97	846.74	5.78	1.24	1125.24	16.95	10.760	2.664
9.10	112.27	1723.98	45.88	1030.51	6.75	1.52	1196.51	17.51	11.758	3.332
9.50	122.47	1695.51	26.89	1336.03	3.96	2.52	1095.94	17.50	11.324	7.383
9.90	124.84	1141.41	17.01	1121.66	2.47	2.04	326.13	17.78	10.665	5.672
10.27	126.73	1382.67	9.49	1450.93	1.32	2.48	476.06	18.52	10.119	7.541

* Ages are interpolated using the age model provided in Zahn and Pedersen (1991).
** Dry bulk density values are taken from ODP Initial Reports Vol. 117 (1989); sedimentation rates are taken from Zahn and Pedersen (1991).

Site 128-798: Japan Sea
XRD results: bulk mineralogy

Core	Interval	Depth	Age*	Phyllosilicates	Quartz	K-feldspar	Plagioclase	Calcite	Dolomite	Ankerite	Detrital	Unquantified
	cm	mbsf	k.y.	%	%	%	%	%	%	%	%	%
128-798C												
1H-1	31-33	0.31	0.912	22.12	13.42	2.27	3.52	5.56	0.00	0.00	41.33	49.20
1H-1	67-68	0.67	5.453	10.88	7.14	2.06	2.97	1.04	0.00	0.00	23.05	72.70
1H-1	97-99	0.97	8.006	18.02	10.20	1.98	3.96	6.12	0.44	0.15	34.17	55.14
1H-1	118-119	1.18	9.186	10.18	7.50	1.78	2.32	0.81	0.00	0.00	21.79	74.38
1H-2	22-24	1.72	11.800	23.11	11.68	2.65	3.77	0.39	0.32	0.08	41.21	55.30
1H-2	45-46	1.95	13.609	10.32	8.66	1.88	5.39	0.00	0.00	0.13	26.25	71.44
1H-2	56-57	2.06	14.491	11.67	5.05	1.95	2.65	0.28	0.00	0.09	21.31	76.72
1H-2	68-69	2.18	15.457	11.42	6.29	1.55	2.60	3.90	0.00	0.15	21.86	71.84
1H-2	91-93	2.41	17.315	25.62	12.87	3.11	4.19	7.53	0.88	0.00	45.79	43.32
1H-2	96-97	2.46	17.720	17.87	14.04	1.66	4.81	7.43	0.00	0.00	38.39	51.96
1H-2	130-131	2.80	20.487	13.75	12.32	0.98	3.60	4.04	0.56	0.00	30.64	63.39
1H-3	14-16	3.14	23.355	22.45	15.64	2.03	5.04	9.41	0.45	0.23	45.17	43.10
1H-3	84-86	3.84	28.210	21.28	11.40	1.69	4.09	1.30	0.00	0.00	38.46	58.70
1H-4	6-8	4.56	37.330	25.01	13.76	1.51	2.46	4.39	0.00	0.00	42.75	51.28
1H-4	70-72	5.20	47.805	20.05	11.25	1.76	4.59	12.69	2.13	0.00	37.65	45.03
1H-4	138-140	5.88	55.355	19.99	10.12	1.02	3.43	22.92	0.39	0.00	34.55	38.90
1H-cc	29-30	6.29	59.580	8.30	10.86	1.14	3.01	5.62	0.43	0.00	23.31	68.61
2H-1	23-25	6.53	60.567	25.05	13.74	2.18	5.90	2.69	0.96	0.53	46.87	47.34
2H-1	56-57	6.86	61.840	12.52	14.15	1.48	2.93	4.13	0.80	0.11	31.08	62.59
2H-1	90-92	7.20	63.762	24.30	15.58	1.57	5.59	13.24	0.70	0.20	47.04	36.74
2H-1	140-141	7.70	67.514	14.00	11.78	1.40	4.86	5.56	0.00	0.00	32.03	61.24
2H-2	10-12	7.90	68.913	23.42	13.34	1.73	4.76	7.99	0.67	0.15	43.25	46.13
2H-2	16-17	7.96	69.321	11.17	10.65	1.20	2.41	3.53	0.38	0.00	25.43	69.11
2H-2	80-82	8.60	76.550	25.74	13.07	2.32	4.53	1.37	0.59	0.26	45.65	49.52
2H-2	120-121	9.00	82.718	13.91	11.31	1.94	3.82	5.80	0.00	0.00	30.98	60.92
2H-3	8-10	9.38	85.566	18.13	10.30	1.66	4.33	8.72	0.00	0.00	34.42	55.18
2H-3	32-33	9.62	86.403	13.94	8.06	1.51	7.87	12.84	0.59	0.00	31.38	53.82
2H-3	69-71	9.99	89.875	23.37	13.49	1.67	4.39	4.84	0.45	0.00	42.93	49.70
2H-3	97-98	10.27	91.574	16.39	15.05	2.26	5.09	3.63	0.00	0.00	38.79	55.64
2H-3	143-145	10.73	96.021	25.52	11.21	2.33	4.00	0.00	0.00	0.00	43.06	55.07
2H-4	47-49	11.27	102.200	24.97	13.46	2.20	5.22	7.83	0.49	0.00	45.84	44.00
2H-4	121-123	12.01	108.750	20.20	10.24	1.33	3.79	29.64	0.00	0.00	35.55	31.91
2H-5	43-45	12.73	115.020	20.53	11.61	1.32	3.58	19.93	0.00	0.00	37.05	40.84
2H-5	110-112	13.40	120.570	18.36	9.40	1.95	2.95	6.28	0.47	0.00	32.66	56.83
2H-6	30-32	14.10	125.620	25.63	12.18	2.95	4.74	1.28	0.54	0.13	45.50	50.08
2H-6	93-95	14.73	132.000	28.30	12.95	1.91	6.39	0.33	0.00	0.16	49.55	48.03
2H-6	145-147	15.25	140.800	24.96	13.35	1.57	9.86	0.00	0.00	0.00	49.74	48.67

Site 128-798: Japan Sea (continued)
Geochemistry: organic matter, nitrogen isotopes, iron and phosphorus phases

Depth	Age*	N	$\delta^{15}N$	TOC	HI	OI	Tmax	Fe	Fe-bound P	Authigenic P	Detrital P	Organic-bound P
mbsf	k.y.	%	‰ (air)	%			C°	mgFe/g	mgP/g	mgP/g	mgP/g	mgP/g
0.31	0.912	0.278	4.645	1.67	244.00	310.00	421	1.0218	0.0787	0.086	0.020	0.208
0.67	5.453	0.242	5.579	2.19	247.10	231.42	420	1.6581	0.0836	0.180	0.029	0.191
0.97	8.006	0.288	4.305	1.78	237.00	336.00	428	1.4480	0.0777	0.083	0.018	0.189
1.18	9.186	0.221	5.341	2.21	226.90	243.31	418	2.2418	0.0996	0.135	0.031	0.202
1.72	11.800	0.320	4.397	1.94	160.00	273.00	397	6.5551	0.1217	0.130	0.031	0.158
1.95	13.609	0.278	5.154	2.68	170.60	259.67	398	7.0744	0.1500	0.131	0.066	0.183
2.06	14.491	0.299	5.113	2.74	190.00	233.23	408	4.8387	0.1096	0.119	0.046	0.209
2.18	15.457	0.384	5.066	3.69	249.00	241.77	418	2.1527	0.1320	0.132	0.041	0.237
2.41	17.315	0.184	5.790	1.15	161.00	340.00	422	1.1749	0.0692	0.155	0.036	0.166
2.46	17.720	0.122	6.196	1.28	127.70	377.60	418	1.4407	0.0866	0.203	0.043	0.153
2.80	20.487	0.109	2.579	1.03	111.70	474.46	416	2.9503	0.0973	0.184	0.034	0.133
3.14	23.355	0.120	3.032	0.89	122.00	368.00	423	3.7222	0.0608	0.237	0.038	0.095
3.84	28.210	0.091	5.226	0.48	117.00	304.00	400	1.4639	0.0503	0.158	0.038	0.087
4.56	37.330	0.151	8.289	0.84	145.00	307.00	405	2.3971	0.0716	0.219	0.040	0.122
5.20	47.805	0.254	7.672	1.82	229.00	291.00	416	2.2073	0.0940	0.148	0.024	0.138
5.88	55.355	0.332	4.379	2.26	312.00	287.00	423	1.5000	0.1131	0.114	0.018	0.155
6.29	59.580	0.165	6.752	1.66	206.30	315.09	415	2.8810	0.1137	0.271	0.047	0.113
6.53	60.567	0.159	5.003	0.97	161.00	369.00	399	2.6190	0.0717	0.267	0.059	0.122
6.86	61.840	0.113	6.134	1.00	131.20	396.06	400	1.9202	0.1115	0.211	0.045	0.127
7.20	63.762	0.162	6.280	0.92	192.00	496.00	415	1.5170	0.1237	0.173	0.039	0.117
7.70	67.514	0.138	6.104	1.20	179.00	384.00	420	3.1765	0.5147	0.224	0.039	0.183
7.90	68.913	0.284	5.078	1.92	277.00	281.00	416	2.3219	0.1186	0.150	0.035	0.165
7.96	69.321	0.303	5.759	3.12	263.10	264.82	419	3.5623	0.1516	0.261	0.037	0.198
8.60	76.550	0.469	3.885	3.35	293.00	183.00	413	1.7488	0.1346	0.134	0.032	0.210
9.00	82.718	0.325	5.407	3.40	260.50	249.84	416	2.9417	0.7194	0.149	0.032	0.189
9.38	85.566	0.187	4.706	1.13	250.00	323.00	420	2.2211	0.1072	0.160	0.049	0.110
9.62	86.403	0.179	6.205	1.51	247.60	417.79	413	1.9471	0.1973	0.209	0.030	0.120
9.99	89.875	0.397	5.690	2.99	281.00	219.00	420	2.8547	0.1310	0.155	0.030	0.186
10.27	91.574	0.319	5.135	3.32	273.20	227.85	414	1.8974	0.2361	0.250	0.038	0.202
10.73	96.021	0.293	5.226	2.21	220.00	204.00	407	4.6220	0.1191	0.103	0.028	0.156
11.27	102.200	0.202	5.183	1.35	231.00	317.00	419	1.4167	0.0968	0.138	0.033	0.128
12.01	108.750	0.388	3.106	3.03	357.00	263.00	418	2.8240	0.1566	0.155	0.020	0.144
12.73	115.020	0.177	4.359	1.11	267.00	416.00	418	2.0360	0.2236	0.158	0.021	0.112
13.40	120.570	0.228	4.526	1.52	311.00	285.00	422	2.3950	0.1585	0.096	0.018	0.101
14.10	125.620	0.189	4.616	1.11	248.00	247.00	418	2.3193	0.1129	0.144	0.025	0.115
14.73	132.000	0.186	5.169	1.14	170.00	255.00	399	3.1421	0.0989	0.138	0.033	0.122
15.25	140.800	0.141	4.137	0.39	118.00	300.00	336	2.7555	0.0756	0.177	0.044	0.097

Site 128-798: Japan Sea (continued)
Mass Accumulation Rates (MAR) and molar ratios**

Depth	Age*	Calcite	TOC	Detrital	Preac	TOC/Porg	TOC/Preac	TOC/N
mbsf	k.y.	MAR	MAR	MAR	MAR	molar	molar	molar
0.31	0.912	1227.328	368.781	9127.006	8.215	207.421	115.766	7.008
0.67	5.453	53.603	112.864	1187.966	2.343	295.321	118.090	10.036
0.97	8.006	467.508	135.958	2609.751	2.675	242.361	131.082	7.210
1.18	9.186	93.586	255.757	2521.142	5.056	281.861	123.361	11.032
1.72	11.800	52.082	260.448	5532.899	5.500	316.106	122.111	7.072
1.95	13.609		221.481	2169.527	3.833	378.087	139.952	10.561
2.06	14.491	22.580	222.120	1727.840	3.551	337.553	152.613	10.115
2.18	15.457	314.899	297.950	1765.132	4.044	401.003	181.204	10.692
2.41	17.315	605.912	92.532	3684.520	3.135	179.084	76.109	7.291
2.46	17.720	596.494	102.716	3080.522	3.548	215.901	69.489	11.394
2.80	20.487	322.426	82.266	2447.552	3.307	200.043	58.607	10.070
3.14	23.355	724.790	68.581	3480.698	3.029	241.456	58.378	8.652
3.84	28.210	121.596	44.985	3604.511	2.774	141.964	41.822	6.153
4.56	37.330	225.217	43.105	2193.613	2.119	177.452	52.456	6.489
5.20	47.805	504.054	72.279	1495.211	1.512	338.978	123.263	8.359
5.88	55.355	1341.873	132.307	2022.890	2.239	375.052	152.404	7.941
6.29	59.580	354.459	104.708	1470.301	3.135	380.432	81.462	11.099
6.53	60.567	424.632	153.313	7408.330	7.267	205.859	54.403	7.117
6.86	61.840	695.895	168.500	5237.803	7.574	203.592	52.891	9.517
7.20	63.762	1522.265	105.786	5408.988	4.762	202.410	57.288	6.625
7.70	67.514	481.564	103.945	2774.853	7.985	169.080	31.180	9.422
7.90	68.913	742.571	178.413	4019.091	4.025	300.534	114.315	7.886
7.96	69.321	337.793	298.235	2430.404	4.388	405.515	165.998	11.377
8.60	76.550	78.990	192.779	2627.004	2.754	411.383	180.524	8.332
9.00	82.718	244.471	143.320	1305.951	1.423	464.576	247.694	11.636
9.38	85.566	756.223	98.002	2985.006	3.267	265.818	77.365	7.049
9.62	86.403	2392.557	281.434	5848.324	6.122	325.235	108.217	8.983
9.99	89.875	335.033	207.113	2973.372	3.275	413.699	163.098	8.786
10.27	91.574	388.423	355.644	4155.153	4.840	423.561	181.208	11.611
10.73	96.021		148.592	2895.414	2.539	366.173	150.938	8.799
11.27	102.200	444.707	76.687	2604.193	2.057	272.441	96.133	7.796
12.01	108.750	2176.486	222.508	2610.891	3.344	544.271	171.569	9.110
12.73	115.020	1487.326	82.852	2765.427	3.685	255.961	57.973	7.316
13.40	120.570	492.632	119.272	2562.567	2.796	386.779	110.015	7.777
14.10	125.620	115.323	100.010	4099.953	3.350	249.891	76.977	6.851
14.73	132.000	21.020	73.171	3180.642	2.304	241.032	81.912	7.150
15.25	140.800		14.980	1910.654	1.341	104.113	28.801	3.227

* Ages are interpolated by graphic correlation of the gray scale values provided in Föllmi et al. (1992), and of the age model provided in Tada et al. (1999).
** Dry bulk density values are taken from ODP Initial Reports Vol. 128 (1989); sedimentation rates are calculated on the basis of the above mentioned correlation.

Site 130-806: Ontong Java Plateau
XRD results: bulk mineralogy

Core	Interval	Depth	Age *	Phyllosilicates	Quartz	Calcite	Detrital	Unquantified
	cm	mbsf	k.y.	%	%	%	%	%
130-806A								
1H-1	6-8	0.06	2.209	3.962	0.612	67.848	4.574	26.02
1H-1	26-28	0.26	9.708	5.867	0.658	88.194	6.525	2.87
1H-1	36-38	0.36	13.538	4.644	1.063	85.666	5.707	6.62
1H-1	46-48	0.46	17.422	5.914	0.980	90.492	6.895	0.48
1H-1	56-58	0.56	21.393	5.113	0.841	90.136	5.955	2.39
1H-1	66-68	0.66	25.416	4.432	1.082	92.549	5.513	0.00
1H-1	75-77	0.75	29.086	4.395	0.727	92.830	5.122	0.00
1H-1	85-87	0.85	33.238	5.147	0.859	91.531	6.006	0.22
1H-1	95-97	0.95	37.515	6.090	0.830	90.987	6.921	0.00
1H-1	105-107	1.05	41.990	4.391	0.802	92.980	5.194	0.00
1H-1	115-117	1.15	46.815	6.448	0.953	90.591	7.401	0.00
1H-1	125-127	1.25	52.388	7.564	1.307	89.197	8.871	0.00
1H-1	135-137	1.35	59.804	6.676	0.845	89.364	7.521	0.94
1H-1	145-147	1.45	66.761	6.058	0.691	90.940	6.749	0.00
1H-2	5-7	1.55	72.051	6.551	0.858	90.654	7.409	0.00
1H-2	15-17	1.65	76.816	7.159	1.325	89.670	8.484	0.00
1H-2	25-27	1.75	81.310	3.599	0.728	93.507	4.328	0.00
1H-2	35-37	1.85	85.391	0.000	0.814	96.895	0.814	0.00
1H-2	45-47	1.95	89.133	4.049	0.916	92.763	4.965	0.00
1H-2	56-57	2.06	93.191	4.364	0.873	92.174	5.237	0.59
1H-2	65-67	2.15	96.778	7.024	0.834	87.670	7.858	2.22
1H-2	75-77	2.25	101.440	4.474	0.538	92.702	5.012	0.00
1H-2	86-88	2.36	107.400	4.394	0.604	92.249	4.998	0.00
1H-2	95-97	2.45	112.930	6.064	0.754	91.065	6.818	0.00
1H-2	105-107	2.55	119.790	3.636	0.799	93.053	4.435	0.00
1H-2	116-118	2.66	128.960	4.469	0.712	92.669	5.181	0.00
1H-2	125-127	2.75	136.490	8.373	0.682	88.444	9.056	0.00

Site 130-806: Ontong Java Plateau (continued)
Geochemistry: organic matter, nitrogen isotopes, iron and phosphorus phases

Depth	Age *	N	TOC	HI	OI	Tmax	Fe	Fe-bound P	Authigenic P	Detrital P	Organic-bound P
mbsf	k.y.	%	%			C°	mgFe/g	mgP/g	mgP/g	mgP/g	mgP/g
0.06	2.209	0.015	0.16	66.1	3373.27	453	1.1729	0.2517	0.1723	0.0131	0.0330
0.26	9.708	0.013	0.16	116.2	2961.21	454	1.1546	0.4134	0.1455	0.0108	0.0331
0.36	13.538	0.022	0.25	148.9	2319.28	451	1.3162	0.1022	0.1581	0.0142	0.0347
0.46	17.422	0.021	0.23	155.3	1654.18	455	1.4095	0.1001	0.1754	0.0132	0.0322
0.56	21.393	0.019	0.24	107.1	1761.50	367	1.2094	0.0951	0.1862	0.0134	0.0281
0.66	25.416	0.014	0.2	131.3	2050.96	453	1.0625	0.0938	0.2610	0.0192	0.0239
0.75	29.086	0.017	0.19	100.4	2567.47	450	1.0993	0.0874	0.1750	0.0134	0.0299
0.85	33.238	0.014	0.18	129.3	2218.22	456	0.7839	0.0961	0.1955	0.0141	0.0242
0.95	37.515	0.012	0.16	138.4	2215.38	459	0.3958	0.1328	0.2120	0.0138	0.0253
1.05	41.990	0.013	0.18	159.2	1856.12	459	0.3783	0.3369	0.2051	0.0131	0.0244
1.15	46.815	0.017	0.21	173.7	1420.72	461	0.4286	0.2245	0.1941	0.0157	0.0508
1.25	52.388	0.018	0.23	149.8	1422.09	463	0.5270	0.0965	0.2394	0.0152	0.0391
1.35	59.804	0.012	0.18	153.3	2130.99	468	0.5172	0.0928	0.2638	0.0139	0.0438
1.45	66.761	0.011	0.13	118.3	3537.90	461	0.4021	0.1451	0.2140	0.0131	0.0225
1.55	72.051	0.016	0.18	132.2	1788.39	442	0.4995	0.0833	0.2211	0.0136	0.0267
1.65	76.816	0.013	0.21	95.8	2265.51	459	0.4624	0.1765	0.2158	0.0139	0.0235
1.75	81.310	0.012	0.17	147.5	1825.87	462	0.3450	0.0789	0.2261	0.0136	0.0212
1.85	85.391	0.012	0.19	122.4	2219.70	459	0.3131	0.0769	0.2073	0.0132	0.0238
1.95	89.133	0.008	0.16	152.2	2920.99	465	0.3724	0.2094	0.2213	0.0441	0.0195
2.06	93.191	0.011	0.2	84.4	2969.63	465	0.7829	0.0783	0.2119	0.0180	0.0202
2.15	96.778	0.01	0.12	99.3	4269.74	470	0.4390	0.0901	0.1853	0.0224	0.0239
2.25	101.440	0.009	0.2	73.8	3871.57	469	0.4311	0.0724	0.2196	0.0155	0.0169
2.36	107.400	0.006	0.15	105.3	3472.75	462	0.3829	0.0543	0.1858	0.0139	0.0174
2.45	112.930	0.009	0.15	126	1911.34	469	0.4026	0.0534	0.1868	0.0289	0.0222
2.55	119.790	0.014	0.27	78.9	2297.11	473	0.3186	0.0829	0.1517	0.0135	0.0231
2.66	128.960	0.014	0.25	102.6	1605.70	374	0.2723	0.2979	0.1776	0.0130	0.0209
2.75	136.490	0.014					0.2911	0.0608	0.1665	0.0132	0.0201

Site 130-806: Ontong Java Plateau (continued)
Mass Accumulation Rates (MAR) ** **and molar ratios**

Depth mbsf	**Age *** k.y.	**Calcite** MAR	**TOC** MAR	**Detrital** MAR	**Preac** MAR	**TOC/Porg** molar	**TOC/N** molar
0.06	2.209	186.330	6.518	2763.780	1.861	125.15	12.43
0.26	9.708	261.064	6.401	3528.375	2.368	124.70	14.35
0.36	13.538	223.513	9.791	3355.171	1.155	185.56	13.25
0.46	17.422	266.274	8.883	3494.812	1.188	184.25	12.77
0.56	21.393	224.925	9.066	3404.789	1.169	220.00	14.72
0.66	25.416	205.571	7.457	3450.734	1.412	215.63	16.65
0.75	29.086	188.420	6.989	3414.728	1.075	164.00	13.03
0.85	33.238	216.978	6.503	3306.772	1.141	191.45	14.99
0.95	37.515	242.716	5.611	3191.051	1.298	162.76	15.54
1.05	41.990	174.090	6.034	3116.637	1.899	190.06	16.14
1.15	46.815	230.085	6.528	2816.286	1.459	106.69	14.40
1.25	52.388	238.758	6.191	2400.777	1.009	151.88	14.89
1.35	59.804	152.124	3.641	1807.529	0.810	106.07	17.49
1.45	66.761	145.523	2.803	1960.759	0.823	148.90	13.78
1.55	72.051	210.095	5.104	2570.529	0.939	173.55	13.11
1.65	76.816	267.079	6.611	2822.761	1.309	230.44	18.83
1.75	81.310	144.452	5.674	3121.061	1.089	206.64	16.51
1.85	85.391	29.921	6.984	3561.435	1.132	205.74	18.46
1.95	89.133	199.009	6.414	3718.466	1.804	211.54	23.31
2.06	93.191	212.952	8.132	3747.840	1.262	255.12	21.19
2.15	96.778	295.732	4.516	3299.557	1.127	129.22	13.99
2.25	101.440	161.271	6.435	2982.689	0.994	305.98	25.90
2.36	107.400	138.374	4.153	2553.864	0.713	222.94	29.14
2.45	112.930	166.434	3.662	2223.102	0.641	174.02	19.43
2.55	119.790	96.969	5.904	2034.677	0.564	300.91	22.48
2.66	128.960	93.231	4.498	1667.440	0.893	309.03	20.82
2.75	136.490	162.354	0.000	1585.651	0.443		

* Ages are interpolated using the age model provided in Bickert et al. (1993).
** Dry bulk density values are taken from ODP Initial Reports Vol. 130 (1991); sedimentation rates are taken from Bickert et al. (1993).

Site 151-907: North Atlantic Gateways
XRD results: bulk mineralogy

Core	Interval	Depth	Age*	Phyllosilicates	Quartz	K-feldspar	Plagioclase	Calcite	Dolomite	Ankerite	Detrital	Unquantified
	cm	mbsf	k.y.	%	%	%	%	%	%	%	%	%
151-907A												
1H-1	5-7	0.05	3.505	8.84	4.68	1.02	3.25	64.72	0.54	0.00	17.79	14.84
1H-1	16-18	0.16	9.977	9.36	4.50	1.50	2.62	59.26	0.19	0.18	17.98	19.88
1H-1	27-29	0.27	16.921	13.21	20.24	5.56	7.63	16.17	0.31	0.14	46.64	35.23
1H-1	38-40	0.38	22.786	19.35	17.87	7.07	3.42	9.39	1.35	0.42	47.71	39.85
1H-1	49-51	0.49	29.640	21.11	17.94	2.45	4.19	7.68	1.45	0.43	45.69	43.35
1H-1	60-62	0.60	36.167	23.14	17.65	9.35	5.00	5.22	1.38	0.27	55.15	37.00
1H-1	75-77	0.75	45.692	24.28	21.61	2.44	7.14	5.03	0.81	0.00	55.47	37.10
1H-1	86-88	0.86	51.944	22.76	20.32	2.15	4.98	4.08	2.03	0.33	50.21	42.33
1H-1	97-99	0.97	58.908	20.67	18.68	5.24	11.92	3.62	2.06	0.46	56.50	36.46
1H-1	108-110	1.08	64.700	20.64	24.73	2.01	5.68	4.78	1.35	0.18	53.05	39.63
1H-1	119-121	1.19	71.974	19.17	22.87	1.62	6.33	4.14	0.66	0.14	50.00	44.25
1H-1	130-132	1.30	78.243	21.52	19.08	3.12	4.80	8.02	1.38	0.12	48.53	40.75
1H-1	145-147	1.45	87.637	20.04	21.29	2.67	5.73	6.42	1.68	0.00	49.73	41.24
1H-2	7-9	1.57	94.530	19.44	17.04	3.46	10.23	5.48	0.87	0.12	50.17	42.53
1H-2	17-19	1.67	100.460	21.20	17.18	2.55	6.10	8.42	0.52	0.30	47.03	42.68
1H-2	28-30	1.78	106.450	14.95	16.06	2.00	4.38	15.80	0.57	0.77	37.39	42.92
1H-2	39-41	1.89	114.520	15.29	8.49	2.07	4.49	30.18	0.42	0.20	30.34	36.78
1H-2	50-52	2.00	120.530	10.48	2.48	1.82	1.84	23.60	0.27	0.15	16.62	57.42
1H-2	65-67	2.15	129.100	22.93	18.91	1.02	7.40	5.61	0.86	0.00	50.26	42.40
1H-2	76-78	2.26	135.890	20.17	17.87	1.80	3.33	6.80	0.53	0.00	43.17	48.39
1H-2	87-89	2.37	142.610	20.98	17.07	3.72	4.50	6.26	0.64	0.13	46.28	45.71
1H-2	98-100	2.48	148.380	12.24	43.76	3.03	36.23	0.54	0.10	0.08	95.26	3.74
1H-2	109-111	2.59	154.020	18.86	15.33	4.24	3.67	9.64	1.30	0.00	42.11	45.88
1H-2	120-122	2.70	159.660	22.36	17.45	2.61	6.28	6.20	1.30	0.14	48.70	42.69

Site 151-907: North Atlantic Gateways (continued)
Geochemistry: organic matter, nitrogen isotopes, iron and phosphorus phases

Depth	Age*	N	$\delta_{15}N$	TOC	HI	OI	Tmax	Fe	Fe-bound P	Authigenic P	Detrital P	Organic-bound P
mbsf	k.y.	%	‰ (air)	%				mgFe/g	mgP/g	mgP/g	mgP/g	mgP/g
0.05	3.505	0.046	8.594	0.41	57.8	1051.0	332	5.005	0.209	0.122	0.059	0.112
0.16	9.977	0.025	4.382	0.31	48.9	882.2	341	4.341	0.151	0.137	0.049	0.096
0.27	16.921	0.03		0.28	35.8	973.5	447	4.966	0.143	0.187	0.101	0.085
0.38	22.786	0.03	1.621	0.26	38.3	829.4	446	5.299	0.151	0.291	0.094	0.078
0.49	29.640	0.039	2.409	0.27	69.0	999.0	435	5.591	0.177	0.323	0.091	0.082
0.60	36.167	0.029	1.492	0.17	55.1	860.7	327	5.065	0.205	0.343	0.088	0.075
0.75	45.692	0.026	4.734	0.15	37.0	764.5	462	5.280	0.134	0.267	0.089	0.064
0.86	51.944	0.023	2.174	0.18	25.8	940.8	446	5.091	0.131	0.285	0.090	0.071
0.97	58.908	0.023	2.640	0.17	79.9	1082.5	446	5.265	0.267	0.260	0.066	0.067
1.08	64.700	0.034	3.055	0.20	50.7	863.9	336	5.680	0.190	0.323	0.115	0.082
1.19	71.974	0.035	2.854	0.16	47.3	1073.6	433	5.827	0.218	0.311	0.092	0.078
1.30	78.243	0.025	4.645	0.24	15.9	858.9	449	5.901	0.195	0.321	0.105	0.069
1.45	87.637	0.026	3.156	0.21	18.1	916.4	452	5.732	0.185	0.268	0.068	0.073
1.57	94.530	0.034	2.602	0.23	20.3	1103.7	326	7.987	0.227	0.197	0.088	0.079
1.67	100.460	0.041	2.900	0.27	28.0	891.9	447	8.406	0.257	0.284	0.097	0.090
1.78	106.450	0.021	3.114	0.31	33.3	1198.9	448	10.898	0.291	0.172	0.109	0.080
1.89	114.520	0.031	1.798	0.22	29.8	920.4	457	9.478	0.263	0.223	0.103	0.095
2.00	120.530	0.007		0.18	16.1	1179.0	454	7.976	0.147	0.354	0.106	0.066
2.15	129.100	0.026	1.088	0.12	23.9	1276.7	443	5.359	0.148	0.342	0.074	0.058
2.26	135.890	0.036	1.790	0.18	26.9	662.5	443	7.909	0.200	0.367	0.070	0.074
2.37	142.610	0.031	0.269	0.17	16.9	720.1	427	7.468	0.180	0.331	0.064	0.060
2.48	148.380	0.025	0.706				600	8.338	0.212	0.403	0.071	0.049
2.59	154.020	0.025	3.174	0.16	23.2	759.8	450	4.892	0.180	0.318	0.077	0.066
2.70	159.660	0.032	1.293	0.18	15.6	595.1	439	5.811	0.209	0.408	0.078	0.066

Site 151-907: North Atlantic Gateways (continued)
Mass Accumulation Rates (MAR) and molar ratios**

Depth mbsf	**Age*** k.y.	**Calcite** MAR **	**TOC** MAR	**Detrital** MAR	**Reac P** MAR	**TOC/P_{org}** molar	**TOC/N** molar
0.05	3.505	784.817	4.972	215.719	0.538	94.317	10.390
0.16	9.977	856.004	4.478	259.772	0.554	83.611	14.455
0.27	16.921	217.673	3.770	627.994	0.559	84.992	10.880
0.38	22.786	149.752	4.145	760.602	0.829	86.162	10.103
0.49	29.640	104.774	3.683	623.266	0.793	85.237	8.070
0.60	36.167	74.759	2.435	789.991	0.892	58.495	6.833
0.75	45.692	67.391	2.008	742.481	0.622	60.295	6.725
0.86	51.944	61.034	2.692	750.868	0.729	64.926	9.123
0.97	58.908	48.626	2.282	758.632	0.797	65.346	8.616
1.08	64.700	77.182	3.229	856.453	0.961	63.062	6.857
1.19	71.974	53.188	2.057	642.661	0.781	52.860	5.329
1.30	78.243	119.545	3.580	723.772	0.871	90.219	11.191
1.45	87.637	87.203	2.850	674.932	0.713	73.983	9.415
1.57	94.530	81.132	3.403	742.446	0.745	75.482	7.886
1.67	100.460	120.670	3.870	674.149	0.904	77.172	7.677
1.78	106.450	246.563	4.839	583.664	0.849	99.771	17.208
1.89	114.520	349.617	2.549	351.518	0.674	59.658	8.273
2.00	120.530	367.204	2.800	258.582	0.883	69.952	29.975
2.15	129.100	83.510	1.785	747.741	0.814	53.460	5.380
2.26	135.890	93.692	2.479	594.457	0.883	62.871	5.828
2.37	142.610	87.047	2.365	643.860	0.794	73.141	6.393
2.48	148.380	8.707	1.458	1543.694	1.075		
2.59	154.020	159.841	2.652	698.025	0.935	62.747	7.460
2.70	159.660	102.862	2.984	807.331	1.132	70.678	6.557

* Ages are interpolated using the age model provided in McManus et al. (1996).
** Dry bulk density values are taken from ODP Initial Reports Vol. 151 (1995); sedimentation rates are taken from McManus et al. (1996).

Site 184-1143: South China Sea
XRD results: bulk mineralogy

Hole	Core	Interval	Depth	Depth	Age*	Phyllosilicates	Quartz	K-feldspar	Plagioclase	Calcite	Dolomite	Unquantified
		cm	mbsf	mcd	k.y.	%	%	%	%	%	%	%
184-1143												
B	1H-1	2-4	0.02	0.02	0.420	8.683	4.083	0.722	1.563	18.532	0.000	64.227
B	1H-1	7-19	0.17	0.17	3.577	10.876	4.993	0.684	0.322	23.440	0.000	57.578
B	1H-1	32-34	0.32	0.32	6.764	10.383	3.818	0.864	0.678	17.178	0.000	65.623
B	1H-1	47-49	0.47	0.47	9.981	11.314	3.436	0.578	0.910	12.153	0.000	70.534
B	1H-1	62-64	0.62	0.62	13.228	12.167	8.864	1.099	1.031	23.788	0.000	50.734
B	1H-1	77-79	0.77	0.77	16.354	15.196	7.468	1.159	0.904	16.081	0.000	56.335
B	1H-1	92-94	0.92	0.92	18.317	17.157	9.329	1.358	1.063	10.237	0.172	58.195
B	1H-1	107-109	1.07	1.07	19.935	21.249	8.761	0.943	1.562	6.890	0.000	58.552
B	1H-1	122-124	1.22	1.22	21.544	17.178	10.414	0.957	1.046	7.796	0.000	59.862
B	1H-1	137-139	1.37	1.37	23.147	9.600	3.311	1.035	0.724	3.025	0.000	81.182
B	1H-2	2-4	1.52	1.52	24.745	19.919	9.516	1.243	1.520	8.683	0.086	56.724
B	1H-2	7-19	1.67	1.67	26.372	14.847	6.105	0.797	1.504	8.554	0.000	66.803
B	1H-2	32-34	1.82	1.82	27.926	11.928	3.797	0.947	0.816	3.230	0.000	78.179
B	1H-2	47-49	1.97	1.97	29.575	26.047	11.190	1.334	1.238	8.155	0.000	49.548
B	1H-2	62-64	2.12	2.12	31.158	17.934	8.381	1.283	0.909	5.858	0.000	63.625
B	1H-2	77-79	2.27	2.27	32.770	15.080	8.032	0.798	1.055	6.833	0.000	65.842
B	1H-2	92-94	2.42	2.42	34.389	18.494	9.443	1.111	1.182	8.957	0.142	58.319
B	1H-2	107-109	2.57	2.57	35.970	16.409	6.803	0.936	1.164	10.251	0.000	62.705
B	1H-2	122-124	2.72	2.72	37.620	15.944	6.202	2.115	1.269	7.174	0.000	65.119
B	1H-2	137-139	2.87	2.87	39.209	16.398	11.156	1.273	1.423	9.393	0.000	57.526
B	1H-3	2-4	3.02	3.02	40.820	16.689	12.090	1.162	1.558	11.708	0.000	53.995
B	1H-3	7-19	3.17	3.17	42.470	13.372	5.121	1.201	1.174	5.610	0.000	71.756
B	1H-3	32-34	3.32	3.32	44.026	19.046	9.667	1.297	1.608	6.867	0.000	58.038
C	1H-1	32-34	0.32	3.52	46.185	12.999	5.610	0.771	1.063	5.337	0.000	72.512
C	1H-1	47-49	0.47	3.67	47.770	14.938	9.174	1.031	1.459	8.335	0.195	62.022
C	1H-1	62-64	0.62	3.82	49.420	14.468	7.577	0.897	1.369	9.851	0.106	63.693
C	1H-1	77-79	0.77	3.97	51.011	17.239	7.005	1.243	0.999	6.112	0.168	65.088
C	1H-1	92-94	0.92	4.12	52.620	14.110	5.618	1.067	0.984	5.612	0.000	70.872
C	1H-1	107-109	1.07	4.27	54.262	20.886	6.842	0.841	0.999	7.781	0.148	60.670
C	1H-1	122-124	1.22	4.42	55.820	20.474	6.581	1.138	1.074	4.774	0.000	63.885
C	1H-1	137-139	1.37	4.57	57.470	18.006	8.992	1.754	1.598	2.482	0.185	64.366
C	1H-2	2-4	1.52	4.72	59.097	18.043	10.295	0.872	2.085	5.664	0.151	60.504
C	1H-2	7-19	1.67	4.87	60.667	14.163	6.478	0.746	1.140	1.240	0.079	74.289
C	1H-2	32-34	1.82	5.02	62.509	15.644	6.639	1.151	1.597	0.636	0.200	72.223
C	1H-2	47-49	1.97	5.17	64.431	14.075	6.127	1.216	1.603	1.304	0.142	73.730
C	1H-2	62-64	2.12	5.32	66.275	14.094	4.017	0.943	1.524	2.057	0.241	75.954
C	1H-2	77-79	2.27	5.47	68.150	12.624	5.574	1.022	1.654	3.129	0.180	74.029
C	1H-2	92-94	2.42	5.62	70.032	21.936	8.572	0.965	2.160	3.129	0.338	61.186
C	1H-2	107-109	2.57	5.77	71.899	14.121	7.555	0.770	1.829	6.393	0.408	67.477
C	1H-2	122-124	2.72	5.92	73.756	20.490	7.772	1.081	1.666	8.929	0.344	58.405
C	1H-2	137-139	2.87	6.07	75.687	6.549	2.188	0.677	0.879	2.827	0.000	86.361
C	1H-3	2-4	3.02	6.22	77.540	12.527	4.829	1.086	1.343	2.272	0.000	76.940
C	1H-3	7-19	3.17	6.37	79.414	13.243	5.694	1.079	1.510	5.450	0.000	71.884
C	1H-3	32-34	3.32	6.52	82.336	13.795	5.798	0.808	1.635	9.191	0.391	66.877
C	1H-3	47-49	3.47	6.67	89.234	13.038	7.252	1.249	2.126	9.769	0.000	65.003
C	1H-3	62-64	3.62	6.82	96.460	7.494	3.047	0.788	0.938	6.684	0.000	80.285
C	1H-3	77-79	3.77	6.97	103.730	13.108	6.225	0.920	1.331	12.122	0.000	64.751
C	1H-3	92-94	3.92	7.12	109.840	16.478	9.016	1.211	2.186	12.376	0.208	56.710
C	1H-3	107-109	4.07	7.27	112.040	12.015	5.643	0.798	1.612	7.259	0.000	71.466
C	1H-3	122-124	4.22	7.42	113.840	15.666	7.080	0.962	2.063	7.128	0.000	65.402
C	1H-3	137-139	4.37	7.57	115.640	10.673	4.561	0.724	1.351	9.319	0.000	71.911
C	1H-4	2-4	4.52	7.72	117.440	16.290	3.920	1.057	1.141	10.885	0.000	64.928
C	1H-4	7-19	4.67	7.87	119.240	12.817	5.023	1.469	0.843	20.291	0.090	57.376
C	1H-4	32-34	4.82	8.02	121.040	9.134	5.991	0.516	1.024	28.827	0.297	51.895
C	1H-4	47-49	4.97	8.17	124.460	10.415	4.411	0.478	0.522	15.898	0.000	67.057
C	1H-4	62-64	5.12	8.32	129.700	13.300	5.724	0.807	0.980	21.237	0.000	56.115
C	1H-4	77-79	5.27	8.47	134.830	14.127	5.475	0.853	0.776	15.529	0.000	61.349
C	1H-4	92-94	5.42	8.62	138.200	17.733	6.107	0.865	1.046	12.112	0.000	59.920
C	1H-4	107-109	5.57	8.77	140.780	14.553	5.874	1.131	0.754	8.061	0.000	67.398
C	1H-4	122-124	5.72	8.92	143.390	19.989	8.850	0.905	1.530	7.631	0.000	58.454
C	1H-4	137-139	5.87	9.07	146.230	27.078	9.190	1.084	1.130	5.972	0.000	53.371

Site 184-1143: South China Sea (continued)
Geochemistry: organic matter, nitrogen isotopes, iron and phosphorus phases

Depth	Age*	N	$\delta_{15}N$	TOC	HI	OI	S2	Fe	Fe-bound P	Authigenic P	Detrital P	Organic-bound P
mcd	k.y.	%	‰ (air)	%				mgFe/g	mgP/g	mgP/g	mgP/g	mgP/g
0.02	0.420	0.052	6.816	0.521	72.683	1296.663	0.369	3.790	0.155	0.136	0.021	0.130
0.17	3.577	0.041	4.407	0.543	77.720	1108.012	0.412	3.070	0.149	0.159	0.022	0.107
0.32	6.764	0.038	4.714	0.441	60.994	1236.362	0.269	3.506	0.157	0.131	0.021	0.099
0.47	9.981	0.038	4.833	0.357	139.832	736.489	0.478	3.608	0.168	0.116	0.023	0.102
0.62	13.228	0.025	4.961	0.398	110.505	712.959	0.429	4.139	0.225	0.105	0.020	0.098
0.77	16.354	0.043	4.675	0.346	107.451	921.728	0.362	3.938	0.134	0.093	0.033	0.086
0.92	18.317	0.044	2.869	0.338	108.593	936.369	0.347	4.529	0.155	0.083	0.031	0.129
1.07	19.935	0.045	4.859	0.479	88.254	687.154	0.382	3.642	0.086	0.083	0.028	0.117
1.22	21.544	0.033	4.661	0.540	84.453	643.137	0.407	4.599	0.101	0.081	0.028	0.105
1.37	23.147	0.044	4.939	0.366	115.004	1135.147	0.381	4.290	0.122	0.088	0.043	0.107
1.52	24.745	0.046	5.742	0.415	95.328	1028.339	0.366	3.481	0.100	0.086	0.033	0.218
1.67	26.372	0.031	4.450	0.541	82.637	725.475	0.437	2.890	0.107	0.092	0.023	0.108
1.82	27.926	0.052	5.121	0.401	79.318	987.327	0.290	4.251	0.118	0.065	0.027	0.122
1.97	29.575	0.033	5.284	0.502	73.794	861.044	0.342	3.639	0.123	0.065	0.024	0.115
2.12	31.158	0.039	5.421	0.470	82.923	850.352	0.334	4.272	0.108	0.078	0.024	0.118
2.27	32.770	0.044	4.758	0.495	82.827	1024.865	0.373	3.690	0.107	0.055	0.027	0.108
2.42	34.389	0.035	4.730	0.305	104.200	1431.335	0.290	4.209	0.107	0.060	0.023	0.096
2.57	35.970	0.040	5.301	0.363	98.150	1394.539	0.347	3.000	0.114	0.073	0.025	0.102
2.72	37.620	0.027	5.362	0.342	93.564	1458.546	0.291	3.308	0.109	0.064	0.027	0.110
2.87	39.209	0.033	5.023	0.366	97.932	1374.321	0.321	3.382	0.096	0.059	0.024	0.100
3.02	40.820	0.030	4.639	0.425	91.274	1357.580	0.350	2.979	0.090	0.070	0.027	0.112
3.17	42.470	0.039	5.341	0.342	67.561			2.862	0.092	0.069	0.025	0.125
3.32	44.026		5.007	0.529	73.839	884.711	0.358	3.816	0.090	0.044	0.029	0.114
3.52	46.185	0.043	4.657	0.426	77.106	971.946	0.299	2.947	0.095	0.081	0.042	0.112
3.67	47.770	0.051	4.532	0.392	78.649	1220.885	0.279	3.196	0.105	0.093	0.034	0.112
3.82	49.420	0.043	4.583	0.418	64.309	1104.575	0.269	2.587	0.161	0.097	0.030	0.104
3.97	51.011	0.033	5.091	0.422	56.765	1334.904	0.211	3.036	0.094	0.089	0.025	0.094
4.12	52.620	0.047	4.639	0.401	66.640	1470.910	0.258	3.462	0.091	0.086	0.033	0.088
4.27	54.262	0.039	4.730	0.393	50.914	1386.391	0.190	3.009	0.104	0.087	0.032	0.091
4.42	55.820	0.050	5.210	0.473	58.194	1405.774	0.228	4.448	0.082	0.078	0.032	0.096
4.57	57.470	0.051	5.332	0.379	123.933	1350.950	0.256	4.133	0.063	0.085	0.038	0.100
4.72	59.097	0.052	4.441	0.463	61.157	1124.515	0.264	2.651	0.068	0.091	0.033	0.112
4.87	60.667	0.051	4.898	0.434	122.766			3.578	0.051	0.097	0.040	0.102
5.02	62.509	0.051	4.327	0.524	151.582			2.774	0.049	0.110	0.037	0.091
5.17	64.431	0.063	3.692					2.342	0.051	0.118	0.034	0.098
5.32	66.275	0.054	4.667	0.465	69.228	1376.180	0.274	2.448	0.064	0.124	0.039	0.092
5.47	68.150		2.801	0.330	79.923			1.274	0.042	0.096	0.035	0.062
5.62	70.032	0.055	5.203	0.404	51.637	1010.018	0.199	2.135	0.074	0.174	0.055	0.094
5.77	71.899	0.055	4.586	0.340	52.993	1488.030	0.180	1.911	0.088	0.157	0.057	0.089
5.92	73.756	0.042	4.680	0.359	39.673	1659.889	0.143	2.417	0.098	0.173	0.050	0.087
6.07	75.687	0.031	4.636	0.293	39.011	1607.710	0.114	1.778	0.110	0.171	0.040	0.085
6.22	77.540	0.043	4.668	0.372	53.748	1158.880	0.172	2.232	0.082	0.147	0.029	0.085
6.37	79.414	0.042	3.342	0.422	54.260	1118.016	0.229	1.731	0.097	0.152	0.028	0.087
6.52	82.336	0.049	4.087	0.480	82.398	923.622	0.386	1.663	0.101	0.164	0.031	0.086
6.67	89.234	0.048	4.649	0.368	118.853	1165.307	0.399	1.474	0.096	0.154	0.054	0.087
6.82	96.460	0.042	5.123	0.469	89.880	910.465	0.403	1.168	0.100	0.190	0.036	0.078
6.97	103.730	0.029	7.853	0.277	94.168	1430.573	0.525	1.342	0.102	0.185	0.064	0.081
7.12	109.840	0.036	5.664	0.233	104.597	1536.069	0.234	1.784	0.088	0.203	0.027	0.080
7.27	112.040	0.047		0.315	106.443	1189.164	0.325	1.548	0.102	0.290	0.036	0.083
7.42	113.840	0.047		0.263	113.484	1315.502	0.288	1.929	0.113	0.165	0.031	0.090
7.57	115.640	0.042		0.449	91.547	911.273	0.401	1.347	0.103	0.190	0.027	0.076
7.72	117.440	0.042		0.229	141.566	1742.846	0.314	1.494	0.113	0.237	0.025	0.078
7.87	119.240	0.028		0.362	84.556	1122.507	0.306	1.218	0.133	0.430	0.022	0.067
8.02	121.040	0.024		0.972	86.161	1105.298	0.316	1.183	0.137	0.516	0.027	0.060
8.17	124.460	0.035		0.357	65.168	1316.728	0.222	1.311	0.142	0.235	0.026	0.068
8.32	129.700	0.030	3.577	0.440	59.190	1093.556	0.250	1.706	0.120	0.134	0.021	0.069
8.47	134.830	0.031		0.443	69.435	1035.166	0.980	1.997	0.106	0.116	0.019	0.072
8.62	138.200	0.036		0.398	81.560	1107.399	0.324	2.352	0.111	0.101	0.023	0.093
8.77	140.780	0.036		0.428	70.531	1169.844	0.282	2.652	0.082	0.094	0.023	0.082
8.92	143.390	0.041		0.439	68.107	889.906	0.280	3.100	0.077	0.070	0.025	0.087
9.07	146.230	0.037		0.446	70.731	1022.498	0.277	3.930	0.060	0.095	0.028	0.082

Site 184-1143: South China Sea (continued)
Clay mineralogy

Depth	Age*	Illite	Kaolinite	Chlorite	Illite/Kaol.	Kaol./Chl.	Fk/Plagio	Smectite	Illite	Kaolinite	Chlorite
mcd	k.y.	% (2-16µm)	% (2-16µm)	% (2-16µm)	(2-16µm)	(2-16µm)	(2-16µm)	% (< 2µm)	% (< 2µm)	% (< 2µm)	% (< 2µm)
0.02	0.420	53.526	17.110	29.364	3.128	0.583	0.354	19.260	37.437	26.638	16.665
0.17	3.577	58.526	16.699	24.775	3.505	0.674	0.434	16.611	43.846	20.406	19.136
0.32	6.764	52.009	19.699	28.291	2.640	0.696	0.332	21.890	36.467	21.050	20.593
0.47	9.981	54.469	28.437	17.094	1.915	1.664	1.156	2.858	50.235	22.990	23.917
0.62	13.228	62.499	15.331	22.169	4.077	0.692	0.509	21.139	45.388	17.664	15.809
0.77	16.354	65.382	11.766	22.852	5.557	0.515	0.557	11.053	58.007	16.162	14.777
0.92	18.317	60.269	25.779	13.952	2.338	1.848	0.650	22.860	43.759	14.733	18.649
1.07	19.935	57.534	18.026	24.440	3.192	0.738	0.400	18.059	45.483	18.333	18.124
1.22	21.544	61.751	11.165	27.084	5.531	0.412	0.458	15.688	49.059	18.921	16.333
1.37	23.147	56.245	16.427	27.328	3.424	0.601	0.349	20.093	46.178	18.185	15.544
1.52	24.745	58.890	16.358	24.752	3.600	0.661	0.476	19.498	40.163	22.445	17.894
1.67	26.372	57.392	13.716	28.892	4.184	0.475	0.399	18.430	46.357	19.476	15.737
1.82	27.926	62.868	15.246	21.886	4.124	0.697	0.579	12.726	52.994	18.315	15.965
1.97	29.575	66.284	10.842	22.874	6.113	0.474	0.653	6.758	59.242	18.667	15.334
2.12	31.158	58.874	12.875	28.252	4.573	0.456	0.374	4.130	60.377	18.585	16.908
2.27	32.770	60.954	14.880	24.165	4.096	0.616	0.377	0.000	55.490	24.959	19.551
2.42	34.389	68.076	15.470	16.455	4.401	0.940	1.356	12.833	53.740	16.546	16.880
2.57	35.970	61.285	15.534	23.181	3.945	0.670	0.377	11.299	51.937	21.727	15.037
2.72	37.620	56.564	26.968	16.469	2.097	1.638	0.529	24.090	38.242	23.051	14.617
2.87	39.209	60.806	27.872	11.322	2.182	2.462	0.379	16.549	42.586	23.998	16.867
3.02	40.820	55.881	16.904	27.215	3.306	0.621	0.491	26.068	38.296	17.985	17.650
3.17	42.470	56.615	14.795	28.590	3.827	0.517	0.426	15.259	49.243	19.303	16.195
3.32	44.026	56.084	15.744	28.172	3.562	0.559	0.379	25.894	40.955	18.110	15.041
3.52	46.185	54.168	17.705	28.127	3.060	0.629	0.590	17.244	47.413	16.085	19.258
3.67	47.770	60.781	10.206	29.013	5.955	0.352	0.442	15.255	43.728	22.437	18.580
3.82	49.420	58.041	13.738	28.221	4.225	0.487	0.389	20.987	38.635	21.554	18.825
3.97	51.011	63.362	11.672	24.966	5.429	0.468	0.415	11.224	52.582	18.605	17.590
4.12	52.620	55.746	17.715	26.539	3.147	0.668	0.632	23.381	45.828	17.269	13.522
4.27	54.262	62.862	10.843	26.295	5.797	0.412	0.479	14.346	53.137	16.997	15.519
4.42	55.820	64.357	11.047	24.596	5.826	0.449	0.506	14.452	50.178	18.236	17.134
4.57	57.470	56.440	16.609	26.952	3.398	0.616	0.400	27.307	38.504	20.711	13.478
4.72	59.097	54.414	16.448	29.138	3.308	0.565	0.436	8.164	53.324	20.768	17.744
4.87	60.667	58.092	22.609	19.299	2.569	1.172	0.928	10.763	53.531	18.774	16.932
5.02	62.509	58.920	10.446	30.634	5.640	0.341	0.386	17.709	46.377	18.116	17.797
5.17	64.431	54.895	10.017	35.087	5.480	0.285	0.374	17.290	46.358	16.151	20.200
5.32	66.275	57.073	9.875	33.052	5.780	0.299	0.384	8.600	49.898	17.954	23.549
5.47	68.150	56.258	12.438	31.305	4.523	0.397	0.333	15.989	49.200	16.644	18.168
5.62	70.032	56.945	6.845	36.210	8.320	0.189	0.309	0.000	59.325	15.486	25.189
5.77	71.899	56.825	10.289	32.886	5.523	0.313	0.304	9.000	54.856	13.913	22.231
5.92	73.756	61.715	6.950	31.335	8.880	0.222	0.396	15.054	54.896	13.641	16.410
6.07	75.687	57.334	11.328	31.338	5.061	0.361	0.379	22.877	46.471	14.656	15.996
6.22	77.540	51.387	15.196	33.416	3.382	0.455	0.264	22.466	44.470	15.930	17.134
6.37	79.414	54.392	11.403	34.205	4.770	0.333	0.430	31.642	38.801	14.401	15.156
6.52	82.336	54.167	15.252	30.581	3.551	0.499	0.251	26.547	42.409	15.324	15.720
6.67	89.234	53.910	12.398	33.691	4.348	0.368	0.369	13.121	51.075	14.495	21.309
6.82	96.460	58.074	13.318	28.608	4.361	0.466	0.347	24.218	42.049	15.806	17.927
6.97	103.730	55.777	12.272	31.951	4.545	0.384	0.297	11.244	56.284	13.751	18.721
7.12	109.840	58.415	9.657	31.928	6.049	0.302	0.334	11.891	55.088	14.497	18.523
7.27	112.040	57.116	13.802	29.082	4.138	0.475	0.452	16.184	46.206	16.848	20.762
7.42	113.840	50.036	19.358	30.606	2.585	0.633	0.356	14.653	51.058	17.680	16.608
7.57	115.640	57.950	11.268	30.783	5.143	0.366	0.400	11.512	53.193	12.431	22.865
7.72	117.440	54.751	16.313	28.936	3.356	0.564	0.466	22.760	46.117	14.079	17.045
7.87	119.240	66.086	12.207	21.707	5.414	0.562	0.523	13.466	54.947	15.251	16.335
8.02	121.040	61.582	15.878	22.540	3.878	0.704	0.336	18.537	47.489	17.263	16.711
8.17	124.460	58.116	16.594	25.290	3.502	0.656	0.418	22.760	47.291	15.498	14.451
8.32	129.700	60.978	15.091	23.931	4.041	0.631	0.585	18.907	43.168	21.816	16.109
8.47	134.830	61.974	13.993	24.033	4.429	0.582	0.471	12.694	53.480	17.699	16.127
8.62	138.200	58.286	16.706	25.007	3.489	0.668	0.335	18.147	44.551	25.915	11.386
8.77	140.780	58.179	15.043	26.778	3.867	0.562	0.331	21.029	42.612	21.499	14.860
8.92	143.390	59.843	16.437	23.720	3.641	0.693	0.428	20.522	42.733	22.785	13.959
9.07	146.230	60.316	15.717	23.967	3.838	0.656	0.397	26.062	39.912	17.341	16.685

Site 184-1143: South China Sea (continued)
Clay ratios and granulometry

Depth mcd	Age* k.y.	Kaol./Ill.+Chl. (< 2µm)	Kaol./Sm. (< 2µm)	Sm./Ill.+Chl. (< 2µm)	Illite Crystallinity	Grain size <6 µm	6-63 µm	Median	Silt mode
0.02	0.420	0.442	1.241	0.356	0.304	71.12	28.88	2.78	10.93
0.17	3.577	0.343	1.300	0.264	0.321	95.31	4.69	1.61	11.59
0.32	6.764	0.419	1.093	0.384	0.372	64.82	35.18	3.95	14.25
0.47	9.981	0.364	9.439	0.039	0.175	91.46	8.54	2.66	18.56
0.62	13.228	0.343	0.993	0.345	0.282	95.88	4.12	1.84	11.75
0.77	16.354	0.208	1.371	0.152	0.187	44.57	55.43	6.50	24.04
0.92	18.317	0.265	0.724	0.366	0.198	49.61	50.39	5.95	27.15
1.07	19.935	0.322	1.133	0.284	0.413	83.25	16.75	3.34	7.89
1.22	21.544	0.302	1.259	0.240	0.330	58.80	41.20	3.92	7.06
1.37	23.147	0.274	0.843	0.326	0.516	81.86	18.14	3.19	10.82
1.52	24.745	0.416	1.238	0.336	0.473	84.00	16.00	2.83	16.02
1.67	26.372	0.345	1.161	0.297	0.380	93.18	6.82	2.72	19.53
1.82	27.926	0.271	1.467	0.185	0.308	97.60	2.40	1.86	
1.97	29.575	0.221	2.444	0.091	0.289	96.20	3.80	1.85	11.31
2.12	31.158	0.237	4.441	0.053	0.286	83.49	16.51	2.86	10.37
2.27	32.770	0.392		0.000	0.304	95.64	4.36	2.30	15.62
2.42	34.389	0.281	1.544	0.182	0.264	82.84	17.16	2.00	16.23
2.57	35.970	0.317	1.877	0.169	0.326	100.00	0.00	1.34	
2.72	37.620	0.519	1.138	0.456	0.400	99.19	0.81	1.44	8.59
2.87	39.209	0.353	1.266	0.278	0.435	99.37	0.63	1.41	9.87
3.02	40.820	0.404	0.866	0.466	0.500	99.04	0.96	1.54	
3.17	42.470	0.331	1.418	0.233	0.351	99.49	0.51	1.48	10.20
3.32	44.026	0.390	0.843	0.462	0.516	95.77	4.23	1.86	10.54
3.52	46.185	0.282	1.090	0.259	0.315	92.17	7.83	2.73	18.83
3.67	47.770	0.334	1.362	0.245	0.429	90.25	9.75	2.97	31.05
3.82	49.420	0.366	1.002	0.365	0.440	90.32	9.68	2.82	12.79
3.97	51.011	0.243	1.522	0.160	0.319	91.48	8.52	3.09	17.25
4.12	52.620	0.286	0.725	0.394	0.315	66.48	33.52	3.96	22.70
4.27	54.262	0.227	1.089	0.209	0.219	74.40	25.60	2.90	12.63
4.42	55.820	0.253	1.178	0.215	0.319	94.74	5.26	2.18	20.79
4.57	57.470	0.471	0.896	0.525	0.615	77.94	22.06	3.17	15.25
4.72	59.097	0.258	2.246	0.115	0.304	89.46	10.54	2.44	13.99
4.87	60.667	0.275	1.798	0.153	0.407	71.95	28.05	3.94	31.85
5.02	62.509	0.281	1.019	0.276	0.418	94.10	5.90	2.13	13.89
5.17	64.431	0.249	0.957	0.260	0.406	100.00	0.00	1.09	
5.32	66.275	0.210	1.798	0.117	0.250	84.66	15.34	2.45	8.07
5.47	68.150	0.237	0.999	0.237	0.473	98.35	1.65	1.73	10.38
5.62	70.032	0.152		0.000	0.271	100.00	0.00	1.08	
5.77	71.899	0.173	1.485	0.117	0.319	97.36	2.64	1.94	12.21
5.92	73.756	0.194	0.918	0.211	0.198	69.77	30.23	3.78	15.20
6.07	75.687	0.210	0.572	0.366	0.275	81.78	18.22	3.03	34.71
6.22	77.540	0.266	0.728	0.365	0.462	90.32	9.68	2.78	21.71
6.37	79.414	0.271	0.462	0.586	0.538	79.42	20.58	3.45	18.36
6.52	82.336	0.318	0.695	0.457	0.527	75.75	24.25	3.74	15.34
6.67	89.234	0.179	0.985	0.181	0.363	94.21	5.79	2.49	7.95
6.82	96.460	0.287	0.710	0.404	0.429	86.02	13.98	3.31	18.15
6.97	103.730	0.169	1.129	0.150	0.229	57.67	42.33	5.15	20.87
7.12	109.840	0.215	1.328	0.162	0.286	89.10	10.90	3.03	27.13
7.27	112.040	0.254	1.050	0.242	0.302	94.42	5.58	2.85	8.99
7.42	113.840	0.310	1.430	0.217	0.333	81.58	18.42	3.30	19.64
7.57	115.640	0.170	1.125	0.151	0.302	88.91	11.09	2.65	25.58
7.72	117.440	0.212	0.589	0.360	0.242	83.72	16.28	3.03	12.16
7.87	119.240	0.242	1.282	0.189	0.188	89.37	10.63	3.13	33.69
8.02	121.040	0.295	1.021	0.289	0.242	89.92	10.08	2.90	18.62
8.17	124.460	0.232	0.631	0.369	0.260	88.32	11.68	2.74	15.25
8.32	129.700	0.380	1.193	0.319	0.352	92.99	7.01	2.01	17.08
8.47	134.830	0.238	1.308	0.182	0.250	64.88	35.12	4.59	11.43
8.62	138.200	0.432	1.331	0.324	0.330	70.31	29.69	4.24	12.21
8.77	140.780	0.331	0.905	0.366	0.385	100.00	0.00	1.07	
8.92	143.390	0.417	1.152	0.362	0.352				
9.07	146.230	0.313	0.679	0.460	0.198				

Site 184-1143: South China Sea (continued)
Mass Accumulation Rates (MAR) and molar ratios**

Depth	Age*	Calcite	TOC	Detrital	Preac	Fe	TOC/Porg	TOC/Preac	TOC/N
mcd	k.y.	MAR	MAR	MAR	MAR	MAR	molar	molar	molar
0.02	0.42	454.2524	12.7706	368.9214	1.0329	9.2909	103.659	31.883	11.679
0.17	3.577	573.2243	13.2789	412.7026	1.0129	7.5080	131.036	33.805	15.438
0.32	6.764	416.1110	10.6828	381.3344	0.9366	8.4923	115.078	29.413	13.528
0.47	9.981	291.6738	8.5681	389.7000	0.9247	8.6583	90.523	23.894	10.951
0.62	13.228	565.5807	9.4630	550.6646	1.0198	9.8408	104.370	23.928	18.558
0.77	16.354	397.1530	8.5453	610.6929	0.7728	9.7246	103.590	28.513	9.380
0.92	18.317	402.6015	13.2934	1136.8947	1.4456	17.8141	67.379	23.714	8.955
1.07	19.935	328.7441	22.8559	1551.4501	1.3657	17.3805	105.667	43.156	12.408
1.22	21.544	374.0616	25.9107	1420.0722	1.3740	22.0692	132.929	48.629	19.075
1.37	23.147	145.6753	17.6274	706.5024	1.5243	20.6612	88.266	29.821	9.696
1.52	24.745	419.4972	20.0499	1555.5521	1.9526	16.8169	49.094	26.479	10.517
1.67	26.372	405.9147	25.6715	1103.3848	1.4560	13.7132	129.189	45.467	20.343
1.82	27.926	160.4939	19.9221	868.7922	1.5170	21.1178	84.803	33.865	8.989
1.97	29.575	381.8196	23.5031	1863.8290	1.4192	17.0369	112.354	42.706	17.733
2.12	31.158	285.6848	22.9223	1390.3200	1.4829	20.8366	102.385	39.860	14.048
2.27	32.77	327.2458	23.7073	1195.6821	1.2922	17.6712	118.107	47.310	13.114
2.42	34.389	427.1377	14.5443	1441.5401	1.2522	20.0690	82.041	29.952	10.158
2.57	35.97	500.5815	17.7262	1236.0207	1.4102	14.6498	91.653	32.414	10.579
2.72	37.62	335.6737	16.0023	1194.5267	1.3197	15.4792	80.442	31.269	14.765
2.87	39.209	456.3637	17.7827	1469.7238	1.2349	16.4296	94.452	37.133	12.929
3.02	40.82	561.0883	20.3674	1509.5146	1.3015	14.2768	98.187	40.355	16.514
3.17	42.47	262.4951	16.0023	976.4317	1.3376	13.3911	70.827	30.850	10.222
3.32	44.026	340.7069	26.2475	1568.8354	1.2282	18.9316	120.180	55.109	
3.52	46.185	254.4406	20.3113	974.7643	1.3749	14.0528	97.750	38.094	11.549
3.67	47.77	405.9934	19.0940	1295.7696	1.5108	15.5664	90.435	32.590	8.960
3.82	49.42	460.9479	19.5584	1137.5579	1.6902	12.1048	104.134	29.840	11.332
3.97	51.011	296.5937	20.4778	1285.2190	1.3424	14.7302	115.870	39.338	14.907
4.12	52.62	269.2857	19.2411	1044.9611	1.2745	16.6094	117.139	38.930	9.946
4.27	54.262	365.8592	18.4782	1390.2636	1.3251	14.1456	111.816	35.959	11.747
4.42	55.82	236.5453	23.4388	1450.3095	1.2689	22.0398	127.220	47.634	11.027
4.57	57.47	116.1396	17.7336	1420.0858	1.1583	19.3383	98.120	39.479	8.663
4.72	59.097	268.7838	21.9702	1484.9575	1.2857	12.5780	106.147	44.063	10.379
4.87	60.667	60.9788	21.3418	1107.7379	1.2262	17.5933	110.207	44.880	9.920
5.02	62.509	26.6621	21.9626	1049.1304	1.0464	11.6259	149.215	54.123	11.977
5.17	64.431	52.3918		924.7408	1.0733	9.4075			
5.32	66.275	93.4360	21.1172	934.4943	1.2754	11.1192	130.406	42.696	10.038
5.47	68.15	139.7457	14.7386	932.2733	0.8935	5.6911	137.621	42.537	
5.62	70.032	139.2313	17.9765	1496.5038	1.5169	9.4992	111.124	30.559	8.563
5.77	71.899	286.7719	15.2503	1088.8350	1.5012	8.5725	98.681	26.195	7.206
5.92	73.756	402.6632	16.1892	1398.3816	1.6122	10.9010	106.100	25.894	9.964
6.07	75.687	122.6173	12.7066	446.3571	1.5871	7.7111	89.401	20.645	11.018
6.22	77.54	102.6613	16.8117	894.1365	1.4170	10.0866	113.312	30.595	10.085
6.37	79.414	243.5523	18.8576	961.9212	1.4978	7.7332	125.542	32.465	11.712
6.52	82.336	263.3947	13.7564	631.5264	1.0071	4.7656	144.217	35.224	11.419
6.67	89.234	118.5991	4.4675	287.2910	0.4097	1.7890	109.486	28.121	8.937
6.82	96.46	77.4578	5.4352	142.1565	0.4264	1.3532	155.317	32.873	13.017
6.97	103.73	139.6359	3.1907	248.6206	0.4242	1.5463	87.742	19.394	11.134
7.12	109.84	169.6185	3.1934	395.9889	0.5093	2.4450	75.127	16.170	7.545
7.27	112.04	276.3147	11.9903	763.8795	1.8070	5.8939	97.710	17.111	7.813
7.42	113.84	331.6415	12.2356	1198.9854	1.7097	8.9744	75.332	18.455	6.523
7.57	115.64	433.5635	20.8890	805.3030	1.7156	6.2670	152.299	31.398	12.462
7.72	117.44	506.3856	10.6538	1042.5035	1.9934	6.9508	75.898	13.782	6.356
7.87	119.24	944.0221	16.8414	937.5692	2.9302	5.6645	139.874	14.821	15.071
8.02	121.04	1341.1456	45.2207	775.2832	3.3233	5.5032	414.880	35.088	18.408
8.17	124.46	389.2686	8.7415	387.4845	1.0909	3.2093	136.140	20.664	11.890
8.32	129.7	339.3907	7.0318	332.5820	0.5152	2.7260	164.577	35.195	17.097
8.47	134.83	253.4975	7.2315	346.5738	0.4784	3.2600	159.616	38.981	16.658
8.62	138.2	300.9690	9.8900	639.8749	0.7586	5.8445	110.803	33.621	12.887
8.77	140.78	261.6501	13.8921	724.2010	0.8405	8.6078	134.289	42.622	13.859
8.92	143.39	244.8536	14.0853	1003.4421	0.7528	9.9448	129.420	48.248	12.481
9.07	146.23	176.0829	13.1510	1134.7195	0.6999	11.5897	140.527	48.453	14.051

* Ages are interpolated using the age model provided by Tian and Wang (Marine Geology special volume, submitted). ** Dry bulk density values are taken from ODP Initial Reports Vol. 184 (2000); sedimentation rates are taken from Tian and Wang (Marine Geology special volume, submitted).

Site 184-1144: South China Sea
XRD results: bulk mineralogy

Hole	Core	Interval	Depth	Depth	Age *	Phyllosilicates	Quartz	K-feldspar	Plagioclase	Calcite	Dolomite	Pyrite	Unquantified
			mbsf	mcd	k.y.	%	%	%	%	%	%	%	%
184-1144													
C	1H-1	98-100	0.98	0.94	1.132	12.346	17.894	1.406	4.263	8.699	0.000	0.000	53.121
C	1H-2	98-100	2.48	2.39	3.089	11.864	11.689	1.040	4.603	8.860	0.897	0.000	59.352
C	1H-3	98-100	3.98	3.84	5.418	17.732	16.816	1.370	3.322	9.242	0.242	0.000	48.943
C	1H-4	98-100	5.48	5.30	8.189	11.693	11.201	1.494	3.506	4.525	0.508	0.000	65.421
C	1H-5	98-100	6.98	6.77	11.474	8.716	7.005	0.991	2.601	4.353	0.458	0.000	74.973
B	2H-4	98-100	5.58	9.21	13.536	13.175	15.474	1.908	3.434	9.551	0.000	0.000	54.619
A	2H-2	98-100	9.38	11.11	14.869	15.849	17.975	1.185	3.607	8.722	0.272	0.234	50.169
A	2H-3	98-100	10.38	12.09	15.530	14.279	14.738	1.001	2.270	7.598	0.000	0.456	58.119
A	2H-4	98-100	12.38	14.04	16.784	12.949	21.306	1.924	4.028	9.131	0.427	0.419	48.017
A	2H-5	98-100	13.88	15.51	17.677	13.593	12.766	0.885	4.562	5.651	0.802	0.446	59.878
A	2H-6	98-100	15.38	16.97	18.531	11.792	15.498	1.476	3.467	6.039	0.449	0.236	59.577
A	3H-1	98-100	17.38	18.93	19.629	9.333	13.815	1.548	3.686	5.246	0.394	0.592	64.257
A	3H-2	98-100	18.88	20.39	20.422	16.936	22.403	1.973	2.182	6.994	0.212	0.550	47.064
B	4H-1	98-100	20.08	22.08	21.307	9.750	16.837	1.459	5.188	6.587	0.271	0.000	58.493
B	4H-2	98-100	21.58	23.81	22.157	9.423	14.657	1.277	3.615	4.714	0.410	0.000	64.809
B	4H-3	98-100	23.08	25.54	22.975	9.350	12.837	1.758	5.206	4.579	0.000	0.000	65.261
B	4H-4	98-100	24.58	27.27	24.181	12.168	18.680	1.025	5.635	5.521	0.360	0.000	55.419
B	4H-5	98-100	26.08	29.00	26.333	13.605	18.302	1.555	4.631	5.693	0.495	0.000	54.580
A	4H-3	98-100	29.92	31.26	29.387	9.448	14.761	1.169	4.257	5.774	0.310	0.100	62.961
B	5H-1	98-100	29.58	33.03	31.179	12.485	22.826	1.322	6.898	7.467	0.478	0.000	47.162
B	5H-2	98-100	31.08	34.75	32.670	14.735	21.885	1.641	5.784	6.549	0.329	0.000	47.536
B	5H-3	98-100	32.58	36.48	34.039	11.082	15.405	1.084	4.319	5.433	0.482	0.000	60.877
B	5H-4	98-100	34.08	38.20	35.343	11.140	24.322	1.271	3.537	7.468	0.421	0.251	50.069
B	5H-5	98-100	35.58	39.92	36.610	14.799	14.998	2.315	3.114	5.987	0.465	0.181	56.893
A	5H-3	98-100	39.38	41.68	37.876	11.035	20.973	1.819	6.393	8.172	0.310	0.000	50.187
A	5H-4	98-100	40.88	43.49	39.155	16.103	12.667	1.528	2.887	6.564	0.244	0.000	58.946
A	5H-5	98-100	42.38	45.30	40.339	9.145	13.693	1.040	3.196	5.110	0.272	0.204	66.484
B	6H-4	98-100	43.58	48.73	42.407	11.619	16.627	1.190	5.728	6.897	0.000	0.000	56.801
B	6H-5	98-100	45.08	50.32	43.362	13.077	13.934	0.000	4.778	6.866	0.390	0.109	59.553
B	6H-6	98-100	46.58	51.95	44.389	13.995	18.015	1.227	4.250	6.920	0.825	0.000	53.586
A	6H-3	98-100	48.88	53.10	45.178	12.243	13.667	1.318	3.280	7.536	0.199	0.148	60.720
A	6H-4	98-100	50.38	54.89	46.615	10.686	15.669	0.937	3.903	6.351	0.160	0.000	61.430
A	6H-5	98-100	51.88	56.68	48.269	12.700	16.089	2.095	4.138	7.119	0.573	0.000	56.268
A	6H-6	98-100	53.38	58.46	50.059	11.716	17.209	0.807	4.014	8.065	0.587	0.000	56.538
C	6H-3	98-100	55.68	61.00	52.682	7.690	11.255	1.366	6.901	4.701	0.366	0.000	67.087
A	7H-2	98-100	56.88	62.57	54.262	14.411	12.234	1.142	3.116	6.311	0.568	0.106	61.026
A	7H-4	98-100	59.57	65.71	57.224	12.326	14.922	1.944	4.040	8.051	0.691	0.000	56.845
A	7H-5	98-100	61.07	67.45	58.682	10.466	12.725	0.960	3.511	5.494	0.494	0.000	65.496
B	8H-3	98-100	61.08	68.77	59.715	12.939	18.151	3.851	5.258	8.426	0.515	0.000	49.710
B	8H-4	98-100	62.58	70.20	60.768	10.392	11.187	2.507	4.496	5.479	0.595	0.000	64.563
B	8H-5	98-100	64.08	71.66	61.777	9.567	13.842	2.316	3.910	5.259	0.746	0.000	63.589
C	7H-4	98-100	66.68	74.09	63.362	14.004	19.172	1.431	4.616	8.105	1.217	0.000	50.445
C	7H-5	98-100	68.18	75.76	64.421	11.880	12.927	0.944	3.096	4.203	0.510	0.000	65.830
B	9H-4	98-100	70.79	78.90	66.579	11.386	13.391	1.911	6.049	5.412	0.779	0.000	60.095
B	9H-5	98-100	72.29	80.60	68.117	19.475	11.329	1.364	6.038	4.016	0.546	0.000	56.539
B	9H-6	98-100	73.79	82.29	69.927	13.675	14.381	0.806	4.398	8.016	0.276	0.000	57.537
A	9H-3	98-100	77.38	84.51	72.652	10.252	11.895	0.729	3.143	5.158	0.164	0.153	67.775
A	9H-4	98-100	78.88	86.40	75.357	9.553	12.153	0.000	3.372	5.808	0.677	0.000	67.719
A	9H-5	98-100	80.38	88.25	78.541	16.258	13.530	1.526	3.692	5.337	0.317	0.000	58.509
C	9H-1	98-100	81.18	89.90	82.620	14.147	11.508	0.995	3.207	4.089	0.521	0.247	64.535
C	9H-3	98-100	84.18	92.88	90.983	14.836	13.917	1.460	3.634	4.380	0.701	0.000	60.354
C	9H-5	98-100	87.18	95.76	94.948	10.087	14.737	1.229	3.370	6.401	0.753	0.000	62.658
B	11H-2	98-100	88.08	97.86	96.796	12.511	12.171	0.954	3.717	7.259	0.326	0.000	62.288
B	11H-3	98-100	89.58	99.52	98.112	13.653	11.369	1.145	3.107	6.274	0.319	0.000	63.450
B	11H-4	98-100	91.08	101.18	99.631	11.179	15.795	0.564	2.908	8.275	0.736	1.365	58.214
B	11H-5	98-100	92.58	102.85	101.780	16.301	16.678	1.361	3.261	8.698	0.387	0.213	52.274
C	10H-4	98-100	95.18	105.18	106.660	13.826	13.040	0.956	3.964	6.452	0.597	0.571	59.871
B	12H-1	98-100	96.08	107.04	111.090	18.242	14.933	1.167	4.114	7.225	0.519	0.000	52.999
B	12H-2	98-100	97.58	109.13	113.280	17.487	16.213	1.195	4.372	7.383	0.543	0.000	51.916
B	12H-3	98-100	99.08	111.34	122.450	8.930	6.007	1.006	1.690	3.502	0.271	0.000	78.156
B	12H-4	98-100	100.58	113.62	130.470	13.393	10.330	0.941	3.060	6.822	0.000	0.238	64.363
B	12H-5	98-100	102.08	115.87	137.660	19.447	14.819	1.253	3.366	7.233	0.503	0.000	52.521
A	12H-3	98-100	105.88	117.95	141.960	9.433	13.819	0.987	2.915	6.501	0.000	0.342	64.989
A	12H-5	98-100	108.88	120.81	149.850	15.351	19.378	1.161	4.138	8.081	0.367	0.226	50.207
B	13H-3	98-100	108.58	123.33	155.380	12.040	18.763	1.249	4.342	7.018	0.161	0.000	55.650
B	13H-5	98-100	111.58	126.28	160.360	9.782	13.633	1.214	2.842	5.075	0.535	0.140	66.102
B	14H-1	98-100	115.08	129.70	164.930	11.416	19.781	1.790	5.227	7.251	0.418	0.141	53.236
B	14H-3	98-100	118.08	132.59	167.940	12.065	13.134	1.331	3.270	4.867	0.485	0.000	63.969
B	14H-4	98-100	119.58	134.03	169.500	9.304	10.680	0.968	3.671	4.339	0.559	0.141	69.745
B	14H-6	98-100	122.58	136.86	173.400	11.440	15.163	1.207	3.304	5.561	0.539	0.000	62.151

Site 184-1144: South China Sea (continued)
Geochemistry: organic matter, nitrogen isotopes, iron and phosphorus phases

Depth	Age *	N	$\delta_{15}N$	TOC	Tmax	HI	OI	S2	Fe	Fe-bound P	Authigenic P	Detrital P	Organic-bound P
mcd	k.y.	%	‰ (air)	%	C°				mgFe/g	mgP/g	mgP/g	mgP/g	mgP/g
0.94	1.132	0.124	4.333	0.571	441	91.313	517.048	0.515	4.034	0.356	0.271	0.120	0.120
2.39	3.089	0.104	4.734	0.666	431	53.928	422.067	0.354	2.828	0.207	0.234	0.065	0.084
3.84	5.418		4.673	0.592	439	77.177	469.245	0.452	3.237	0.336	0.214	0.062	0.080
5.30	8.189		4.704	0.804	446	77.740	425.752	0.608	3.782	0.122	0.162	0.059	0.091
6.77	11.474		5.286	0.939	439	104.156	332.843	0.970	1.615	0.149	0.210	0.064	0.087
9.21	13.536	0.146	4.254	0.818	418	157.889	264.981	1.291	1.374	0.196	0.204	0.066	0.087
11.11	14.869	0.150	5.212	0.987	417	122.827	364.142	1.196	1.759	0.164	0.208	0.052	0.102
12.09	15.530	0.144	4.976	0.893	430	122.329	378.227	1.092	2.461	0.083	0.202	0.045	0.092
14.04	16.784	0.144	5.245	0.912	432	138.283	305.031	1.245	1.523	0.071	0.189	0.055	0.083
15.51	17.677	0.148	5.279	1.023	416	110.668	332.422	1.116	2.412	0.078	0.191	0.054	0.089
16.97	18.531	0.161	5.643	0.996	417	138.378	279.585	1.362	2.405	0.095	0.276	0.058	0.086
18.93	19.629	0.151	6.010	0.950	428	122.014	312.190	1.143	4.156	0.140	0.217	0.091	0.084
20.39	20.422	0.149	5.720	0.977	425	109.327	299.822	1.051	4.104	0.099	0.200	0.068	0.080
22.08	21.307	0.149	5.728	0.835	422	127.680	251.637	1.067	3.031	0.138	0.194	0.110	0.086
23.81	22.157	0.154	5.876	0.904	411	118.742	266.815	1.073	3.473	0.146	0.202	0.102	0.095
25.54	22.975	0.142	5.756	0.846	421	119.847	263.087	1.014	3.306	0.147	0.189	0.111	0.082
27.27	24.181	0.143	6.364	0.802	412	125.830	284.048	1.009	3.672	0.137	0.201	0.117	0.084
29.00	26.333	0.137	5.854	0.792	420	85.405	345.058	0.677	3.953	0.142	0.198	0.117	0.077
31.26	29.387	0.151	5.765	0.882	414	119.712	336.292	1.040	4.051	0.111	0.220	0.084	0.086
33.03	31.179	0.132	6.064	0.726	405	86.014	367.690	0.625	4.235	0.150	0.200	0.122	0.077
34.75	32.670	0.147	6.608	0.812	420	89.653	364.654	0.728	4.013	0.114	0.203	0.119	0.083
36.48	34.039	0.149	6.405	0.849	417	99.732	342.813	0.847	3.754	0.117	0.190	0.113	0.077
38.20	35.343	0.148	5.974	0.835	418	105.764	349.054	0.883	3.780	0.105	0.208	0.108	0.083
39.92	36.610	0.151	6.346	0.844	414	100.636	372.787	0.849	3.948	0.111	0.196	0.112	0.105
41.68	37.876	0.128	5.724	0.691	414	104.017	338.662	0.702	3.158	0.080	0.213	0.080	0.083
43.49	39.155	0.152	5.686	0.855	417	109.419	327.585	0.919	3.103	0.096	0.185	0.068	0.128
45.30	40.339	0.148	6.143	0.828	417	113.517	296.536	0.923	3.269	0.088	0.217	0.105	0.081
48.73	42.407	0.147	6.204	0.793	370	96.766	420.247	0.768	3.375	0.103	0.193	0.258	0.083
50.32	43.362	0.143	5.890	0.815	409	118.817	333.062	0.918	3.650	0.107	0.190	0.103	0.089
51.95	44.389	0.149	6.289	0.810	414	108.194	327.391	0.859	4.094	0.541	0.212	0.093	0.068
53.10	45.178	0.133	5.764	0.684	417	109.011	312.955	0.729	3.116	0.089	0.234	0.117	0.075
54.89	46.615	0.133	5.644	0.664	419	125.310	319.126	0.832	3.337	0.164	0.221	0.091	0.085
56.68	48.269	0.141	5.988	0.722	411	120.465	303.721	0.869	3.156	0.165	0.203	0.081	0.070
58.46	50.059	0.140	5.663	0.729	416	125.547	354.129	0.904	2.982	0.232	0.223	0.080	0.074
61.00	52.682		5.937	0.971	451	79.644	277.861	0.766	3.137	0.149	0.224	0.084	0.074
62.57	54.262	0.144	6.207	0.723	388	124.297	357.559	0.888	3.433	0.170	0.192	0.096	0.076
65.71	57.224	0.149	6.495	0.760	417	113.132	326.884	0.860	3.437	0.171	0.200	0.081	0.086
67.45	58.682	0.137	6.182	0.639	415	101.163	344.944	0.646	3.446	0.162	0.220	0.089	0.074
68.77	59.715	0.125	5.891	0.643	414	96.329	366.522	0.619	3.213	0.185	0.264	0.104	0.067
70.20	60.768	0.130	5.795	1.057	451	70.899	243.746	0.718	3.805	0.165	0.218	0.116	0.080
71.66	61.777	0.138	6.030	0.648	409	109.368	515.863	0.692	3.735	0.164	0.210	0.115	0.080
74.09	63.362		5.602	0.545	450	101.583	444.761	0.549	3.375	0.239	0.245	0.099	0.068
75.76	64.421		6.175	0.770	439	53.229	344.485	0.404	4.191	0.317	0.274	0.095	0.077
78.90	66.579	0.140	6.464	0.629	402	92.865	488.051	0.576	3.914	0.312	0.203	0.102	0.091
80.60	68.117	0.127	6.601	0.578	401	93.738	537.775	0.509	3.945	0.129	0.208	0.098	0.085
82.29	69.927	0.135	6.706	0.552	400	117.450	486.821	0.615	3.706	0.188	0.203	0.074	0.081
84.51	72.652	0.136	6.432	0.566	406	97.266	404.912	0.551	3.092	0.184	0.206	0.082	0.088
86.40	75.357	0.146	6.341	0.562	420	96.570	404.466	0.543	3.245	0.194	0.199	0.078	0.080
88.25	78.541	0.130	6.760	0.546	348	71.365	480.494	0.390	3.301	0.164	0.202	0.081	0.087
89.90	82.620	0.121	5.593	0.804	426	61.338	682.744	0.481	3.447	0.195	0.223	0.095	0.093
92.88	90.983	0.115	6.869	0.687	430	68.270	378.441	0.458	3.661	0.149	0.220	0.085	0.081
95.76	94.948	0.129	5.249	0.840	444	76.109	410.703	0.624	4.038	0.213	0.232	0.075	0.072
97.86	96.796	0.138	6.162	0.570	400	109.352	489.560	0.607	3.103	0.331	0.218	0.070	0.085
99.52	98.112	0.139	6.125	0.552	403	105.236	492.404	0.573	3.372	0.202	0.220	0.109	0.081
101.18	99.631	0.151	4.014	0.812	525	59.381	387.089	0.462	7.895	0.477	0.163	0.107	0.068
102.85	101.780	0.136	6.483	0.546	400	87.664	537.167	0.470	3.259	0.323	0.228	0.075	0.067
105.18	106.660	0.129	4.994	0.769	436	61.830	364.833	0.464	4.325	0.175	0.206	0.093	0.075
107.04	111.090	0.134	6.284	0.524	449	96.459	426.286	0.500	2.931	0.147	0.220	0.079	0.071
109.13	113.280	0.128	6.815	0.494	392	90.189	533.632	0.437	3.223	0.138	0.232	0.073	0.067
111.34	122.450	0.113	8.056	0.401	374	81.801	646.791	0.319	2.602	0.144	0.233	0.065	0.062
113.62	130.470	0.144	6.345	0.570	397	94.549	461.385	0.539	2.924	0.215	0.204	0.057	0.068
115.87	137.660	0.139	7.199	0.544	399	94.011	432.017	0.502	2.478	0.137	0.208	0.060	0.072
117.95	141.960	0.143	6.619	0.776	417	102.515	261.893	0.795	2.933	0.183	0.186	0.060	0.068
120.81	149.850	0.133	6.591	0.750	416	133.731	266.766	1.003	2.196	0.171	0.203	0.080	0.084
123.33	155.380	0.126	6.774	0.636	414	116.979	286.762	0.734	2.589	0.083	0.243	0.086	0.059
126.28	160.360	0.132	6.889	0.659	455	106.033	348.876	0.694	2.105	0.239	0.205	0.125	0.065
129.70	164.930	0.127	6.768	0.633	414	123.528	268.069	0.772	1.105	0.127	0.197	0.104	0.065
132.59	167.940	0.134	6.666	0.634	415	131.953	257.255	0.827	0.911	1.552	0.193	0.123	0.071
134.03	169.500	0.131	6.740	0.688	452	94.248	351.141	0.644	3.942	0.324	0.210	0.117	0.067
136.86	173.400	0.132	6.905	0.729	448	96.520	467.999	0.697	3.149	0.189	0.208	0.121	0.067

Site 184-1144: South China Sea (continued)
Clay mineralogy

Depth	Age *	Illite	Kaolinite	Chlorite	Illite/Kaol.	Kaol./Chl.	Fk/Plagio	Smectite	Illite	Kaolinite	Chlorite
mcd	k.y.	% (2-16µm)	% (2-16µm)	% (2-16µm)	(2-16µm)	(2-16µm)	(2-16µm)	% (< 2µm)	% (< 2µm)	% (< 2µm)	% (< 2µm)
0.94	1.132	46.676	3.425	49.899	13.627	0.069	0.176	4.575	51.871	6.894	36.660
2.39	3.089	47.760	4.956	47.284	9.636	0.105	0.355	0.000	61.400	5.244	33.356
3.84	5.418	44.801	3.194	52.005	14.026	0.061	0.295	1.608	57.937	8.467	31.988
5.30	8.189	47.850	5.833	46.317	8.204	0.126	0.272	0.000	53.122	8.046	38.832
6.77	11.474	46.564	5.777	47.659	8.060	0.121	0.234	5.956	50.344	6.936	36.765
9.21	13.536	46.919	6.177	46.904	7.596	0.132	0.177	8.890	48.876	8.856	33.378
11.11	14.869	44.381	7.430	48.189	5.973	0.154	0.176	15.197	42.765	9.997	32.040
12.09	15.530	43.785	8.508	47.706	5.146	0.178	0.299	6.408	45.181	14.222	34.190
14.04	16.784	40.311	7.406	52.283	5.443	0.142	0.233	12.599	46.311	11.618	29.471
15.51	17.677	44.397	5.861	49.742	7.575	0.118	0.275				
16.97	18.531	45.490	6.834	47.677	6.657	0.143	0.390	9.820	52.550	9.495	28.136
18.93	19.629	45.865	7.340	46.795	6.248	0.157	0.283	8.277	45.550	12.283	33.890
20.39	20.422	42.511	4.950	52.539	8.589	0.094	0.287	10.442	47.438	9.134	32.986
22.08	21.307	45.859	4.629	49.512	9.907	0.093	0.235	14.257	40.888	11.354	33.502
23.81	22.157	41.512	10.038	48.449	4.135	0.207	0.311	15.388	44.615	9.232	30.764
25.54	22.975	39.083	6.001	54.917	6.513	0.109	0.271	15.113	40.673	11.060	33.154
27.27	24.181	46.397	6.310	47.293	7.353	0.133	0.208	15.190	44.263	9.060	31.487
29.00	26.333	44.457	4.570	50.973	9.729	0.090	0.406	6.426	45.110	13.233	35.230
31.26	29.387	42.971	5.960	51.070	7.210	0.117	0.297	13.354	46.346	9.720	30.580
33.03	31.179	42.162	6.194	51.644	6.807	0.120	0.223	9.749	46.612	7.476	36.163
34.75	32.670	42.551	5.590	51.859	7.612	0.108	0.291	6.518	52.710	7.431	33.340
36.48	34.039	45.942	5.290	48.768	8.685	0.108	0.356	10.365	44.932	10.002	34.700
38.20	35.343	45.745	4.823	49.432	9.485	0.098	0.375	9.549	46.769	10.128	33.554
39.92	36.610	40.091	5.140	54.768	7.800	0.094	0.319	14.521	44.393	8.006	33.080
41.68	37.876	42.736	7.698	49.566	5.551	0.155	0.237	15.935	44.172	9.112	30.780
43.49	39.155	39.630	5.360	55.010	7.394	0.097	0.267	12.893	46.002	10.121	30.985
45.30	40.339	46.958	5.628	47.414	8.344	0.119	0.364	11.801	47.825	13.232	27.143
48.73	42.407	45.830	7.642	46.528	5.997	0.164	0.360	12.945	45.897	7.955	33.203
50.32	43.362	44.065	6.224	49.711	7.080	0.125	0.282	11.769	46.052	8.985	33.194
51.95	44.389	44.189	4.155	51.656	10.636	0.080	0.275	6.325	52.335	7.409	33.931
53.10	45.178	50.904	3.444	45.653	14.782	0.075	0.300	5.850	54.633	9.905	29.612
54.89	46.615	47.601	5.102	47.297	9.330	0.108	0.470	7.067	48.395	9.441	35.097
56.68	48.269	44.655	7.939	47.406	5.625	0.167	0.262	17.596	47.488	5.916	29.000
58.46	50.059	45.699	8.813	45.487	5.185	0.194	0.364	16.822	46.245	8.584	28.348
61.00	52.682	45.500	6.274	48.226	7.252	0.130	0.330	7.164	49.411	10.692	32.733
62.57	54.262	49.755	7.906	42.340	6.294	0.187	0.306	20.993	42.677	10.469	25.861
65.71	57.224	45.192	9.103	45.705	4.965	0.199	0.272	18.145	45.599	9.283	26.973
67.45	58.682	46.553	7.258	46.189	6.414	0.157	0.268	16.489	44.675	10.874	27.962
68.77	59.715	44.049	7.110	48.841	6.195	0.146	0.288	19.987	44.711	10.514	24.787
70.20	60.768	46.373	8.586	45.041	5.401	0.191	0.315	16.874	47.321	9.428	26.376
71.66	61.777	48.591	7.405	44.004	6.562	0.168	0.376	14.378	50.999	12.453	22.170
74.09	63.362	47.556	9.016	43.428	5.275	0.208	0.240	13.000	46.925	11.513	28.563
75.76	64.421	49.746	6.314	43.940	7.878	0.144	0.238	6.119	49.493	11.432	32.955
78.90	66.579	50.190	8.870	40.939	5.658	0.217	0.399	15.290	48.133	11.689	24.888
80.60	68.117	47.458	9.995	42.547	4.748	0.235	0.326	18.585	49.419	10.652	21.344
82.29	69.927	47.614	6.392	45.994	7.448	0.139	0.227	0.000	57.951	7.552	34.496
84.51	72.652	48.059	6.192	45.749	7.761	0.135	0.311	15.404	49.112	5.720	29.765
86.40	75.357	45.863	6.499	47.638	7.057	0.136	0.267	11.934	49.201	10.311	28.554
88.25	78.541	49.126	6.469	44.404	7.594	0.146	0.290	15.969	48.700	8.093	27.238
89.90	82.620	49.418	8.190	42.393	6.034	0.193	0.309	0.000	55.739	9.985	34.276
92.88	90.983	53.642	9.241	37.117	5.805	0.249	0.385	10.435	49.686	13.342	26.537
95.76	94.948	48.704	8.354	42.942	5.830	0.195	0.354	13.975	49.418	10.943	25.664
97.86	96.796	43.615	5.423	50.963	8.043	0.106	0.257	12.700	48.581	7.963	30.757
99.52	98.112	48.858	6.944	44.198	7.036	0.157	0.283	8.130	50.751	9.149	31.970
101.18	99.631	51.113	5.855	43.031	8.729	0.136	0.700	12.188	48.688	8.805	30.320
102.85	101.780	47.980	6.860	45.159	6.994	0.152	0.331	11.221	50.755	10.621	27.402
105.18	106.660	58.003	11.244	30.752	5.158	0.366	0.844	8.949	51.321	9.684	30.046
107.04	111.090	47.918	7.749	44.333	6.184	0.175	0.306	13.313	47.550	9.540	29.597
109.13	113.280	48.140	6.811	45.048	7.068	0.151	0.290	10.025	48.999	10.122	30.853
111.34	122.450	57.631	12.730	29.639	4.527	0.430	1.000	15.262	45.952	10.541	28.244
113.62	130.470	54.791	12.182	33.027	4.498	0.369	0.872	12.087	47.713	6.988	33.212
115.87	137.660	50.806	8.619	40.575	5.894	0.212	0.305	8.763	48.745	11.111	31.381
117.95	141.960	46.386	8.366	45.248	5.545	0.185	0.271	16.987	46.332	13.173	23.509
120.81	149.850	44.925	7.441	47.634	6.037	0.156	0.323	12.681	49.276	9.204	28.839
123.33	155.380	45.452	6.514	48.035	6.978	0.136	0.377	12.632	44.218	10.984	32.166
126.28	160.360	47.099	6.656	46.244	7.076	0.144	0.284	1.927	59.745	10.124	28.204
129.70	164.930	41.522	6.692	51.786	6.205	0.129	0.269	13.880	44.384	8.156	33.581
132.59	167.940	46.058	5.553	48.389	8.294	0.115	0.243				
134.03	169.500	43.239	8.155	48.606	5.302	0.168	0.297	17.170	44.878	11.222	26.730
136.86	173.400	43.010	9.221	47.769	4.664	0.193	0.301	10.862	49.622	11.986	27.530

Site 184-1144: South China Sea (continued)
Clay ratios and granulometry

Depth mcd	Age * k.y.	Kaol./Ill.+Chl. (< 2µm)	Kaol./Sm. (< 2µm)	Sm./Ill.+Chl. (< 2µm)	Illite Crystallinity	Grain size <6 µm	6-63 µm	Median	Silt mode
0.94	1.132	0.059	1.138	0.052	0.217	71.81	28.19	4.54	6.84
2.39	3.089	0.034		0.000	0.185	63.51	36.49	4.87	12.40
3.84	5.418	0.070	3.911	0.018	0.143	59.23	40.77	5.09	7.89
5.30	8.189	0.064		0.000	0.206	63.4	36.6	4.74	8.99
6.77	11.474	0.056	0.819	0.068	0.209	66.08	33.92	4.61	6.84
9.21	13.536	0.089	0.820	0.108	0.187	73.57	26.43	4.38	7.06
11.11	14.869	0.112	0.552	0.203	0.352	76.74	23.26	4.20	7.82
12.09	15.530	0.136	1.685	0.081	0.209	74.83	25.17	4.30	9.92
14.04	16.784	0.165	0.995	0.166	0.293	71.76	28.24	4.40	8.22
15.51	17.677				0.385	76.24	23.76	4.15	8.99
16.97	18.531	0.105	0.866	0.122	0.272	64.73	35.27	4.52	6.84
18.93	19.629	0.101	0.966	0.104	0.245	71.77	28.23	4.42	9.92
20.39	20.422	0.081	0.626	0.130	0.198	66.76	33.24	4.70	14.66
22.08	21.307	0.104	0.541	0.192	0.275	66.74	33.26	4.56	14.80
23.81	22.157	0.113	0.554	0.204	0.278	72.98	27.02	4.42	14.69
25.54	22.975	0.145	0.710	0.205	0.337	78.63	21.37	4.19	11.20
27.27	24.181	0.105	0.525	0.201	0.308	66.91	33.09	4.59	8.59
29.00	26.333	0.124	1.550	0.080	0.174	63.47	36.53	4.79	7.06
31.26	29.387	0.113	0.653	0.174	0.315	65.55	34.45	4.55	8.22
33.03	31.179	0.078	0.660	0.118	0.264	64.99	35.01	4.79	10.82
34.75	32.670	0.057	0.750	0.076	0.196	54.89	45.11	5.50	13.00
36.48	34.039	0.080	0.616	0.130	0.185	58.22	41.78	5.19	16.13
38.20	35.343	0.116	0.978	0.119	0.255	61.93	38.07	4.79	19.32
39.92	36.610	0.099	0.530	0.187	0.319	77.4	22.6	4.25	7.89
41.68	37.876	0.106	0.500	0.213	0.297	66.39	33.61	4.58	8.59
43.49	39.155	0.139	0.831	0.167	0.304	77.75	22.25	4.03	7.59
45.30	40.339	0.233	1.477	0.157	0.451	52.04	47.96	5.82	20.40
48.73	42.407	0.077	0.468	0.164	0.359	65.21	34.79	4.75	
50.32	43.362	0.111	0.749	0.149	0.237	63.45	36.55	4.73	9.92
51.95	44.389	0.074	1.007	0.073	0.206	75.71	24.29	4.32	
53.10	45.178	0.085	1.222	0.069	0.200	72.36	27.64	4.31	8.82
54.89	46.615	0.088	1.042	0.085	0.261	77.91	22.09	4.02	9.28
56.68	48.269	0.074	0.320	0.230	0.341	69.94	30.06	4.25	
58.46	50.059	0.092	0.409	0.226	0.440	77.96	22.04	4.22	
61.00	52.682	0.101	1.154	0.087	0.268	67.16	32.84	4.40	7.82
62.57	54.262	0.158	0.516	0.306	0.418	76.27	23.73	4.02	
65.71	57.224	0.122	0.489	0.250	0.363	75.26	24.74	4.27	
67.45	58.682	0.147	0.649	0.227	0.330	40.22	59.78	5.86	16.81
68.77	59.715	0.166	0.576	0.288	0.413	69.37	30.63	4.32	7.52
70.20	60.768	0.127	0.556	0.229	0.533	47.81	52.19	6.59	10.49
71.66	61.777	0.156	0.795	0.197	0.489	63.82	36.18	4.77	
74.09	63.362	0.144	0.838	0.172	0.354	49.72	50.28	6.06	16.08
75.76	64.421	0.117	1.582	0.074	0.261	66.86	33.14	4.50	6.84
78.90	66.579	0.162	0.772	0.209	0.359	63.54	36.46	4.84	
80.60	68.117	0.152	0.580	0.263	0.582	60.41	39.59	4.98	10.97
82.29	69.927	0.073		0.000	0.242	66.7	33.3	4.57	9.28
84.51	72.652	0.064	0.329	0.195	0.319	72.23	27.77	4.51	11.04
86.40	75.357	0.104	0.676	0.153	0.451	73.33	26.67	4.08	17.90
88.25	78.541	0.099	0.471	0.210	0.385	75.97	24.03	4.25	
89.90	82.620	0.083		0.000	0.207	65.26	34.74	4.51	6.84
92.88	90.983	0.214	1.567	0.137	0.418	71.76	28.24	4.30	6.84
95.76	94.948	0.158	0.848	0.186	0.363	72.75	27.25	4.28	7.02
97.86	96.796	0.088	0.547	0.160	0.286	68.89	31.11	4.62	
99.52	98.112	0.100	1.017	0.098	0.385	62.35	37.65	4.87	
101.18	99.631	0.118	0.763	0.154	0.381	60.89	39.11	4.75	28.19
102.85	101.780	0.142	0.987	0.144	0.402	58.92	41.08	5.08	17.64
105.18	106.660	0.098	0.892	0.110	0.198	62.08	37.92	4.94	12.09
107.04	111.090	0.132	0.767	0.173	0.429	67.64	32.36	4.62	12.69
109.13	113.280	0.126	1.003	0.126	0.385	70.6	29.4	4.34	14.28
111.34	122.450	0.133	0.646	0.206	0.341	74.87	25.13	4.27	17.53
113.62	130.470	0.083	0.555	0.149	0.141	69.48	30.52	4.55	
115.87	137.660	0.138	1.262	0.109	0.319	71.01	28.99	4.39	
117.95	141.960	0.194	0.797	0.243	0.560	71.8	28.2	4.29	
120.81	149.850	0.104	0.638	0.162	0.231	74.88	25.12	4.27	
123.33	155.380	0.139	0.840	0.165	0.253	58.31	41.69	5.07	
126.28	160.360	0.096	4.365	0.022	0.165	62.63	37.37	4.86	
129.70	164.930	0.069	0.385	0.178	0.440				
132.59	167.940				0.293				
134.03	169.500	0.163	0.679	0.240	0.374				
136.86	173.400	0.147	1.048	0.141	0.275				

Site 184-1144: South China Sea (continued)
Mass Accumulation Rates (MAR) and molar ratios**

Depth	Age *	Calcite	TOC	Detrital	Preac	Fe	TOC/Porg	TOC/Preac	TOC/N
mcd	k.y.	MAR	MAR	MAR	MAR	MAR	molar	molar	molar
0.94	1.132	2030.711	133.333	8382.786	17.412	94.170	123.334	19.762	5.369
2.39	3.089	2334.228	175.370	7691.313	13.839	74.507	205.452	32.704	7.461
3.84	5.418	2948.459	188.919	12518.660	20.085	103.261	191.795	24.276	
5.30	8.189	1855.474	329.713	11437.143	15.373	155.078	229.044	55.353	
6.77	11.474	2374.833	512.496	10536.159	24.310	88.080	279.465	54.409	
9.21	13.536	6873.078	588.571	24460.939	35.025	98.844	243.385	43.369	6.530
11.11	14.869	7634.657	863.970	33802.252	41.530	153.956	249.615	53.691	7.670
12.09	15.530	7785.339	914.994	33082.554	38.681	252.128	250.332	61.049	7.229
14.04	16.784	9827.269	981.692	43274.590	36.997	163.942	283.128	68.480	7.384
15.51	17.677	6817.376	1234.037	38371.755	43.268	291.003	295.474	73.608	8.057
16.97	18.531	7377.489	1216.444	39379.977	55.823	293.779	297.639	56.240	7.209
18.93	19.629	6454.006	1168.657	34915.882	54.245	511.262	291.987	55.602	7.333
20.39	20.422	9573.639	1336.748	59539.038	51.806	561.846	315.261	66.593	7.640
22.08	21.307	9038.727	1146.334	45606.355	57.283	415.959	250.796	51.647	6.535
23.81	22.157	6483.134	1242.912	39842.994	61.018	477.656	244.418	52.571	6.841
25.54	22.975	6609.662	1220.956	42076.838	60.285	477.157	266.159	52.270	6.944
27.27	24.181	7532.563	1094.340	51171.709	57.653	500.913	247.106	48.988	6.539
29.00	26.333	6022.748	838.352	40300.293	44.069	418.263	266.638	49.097	6.743
31.26	29.387	5344.641	816.842	27430.153	38.526	374.957	266.361	54.720	6.813
33.03	31.179	6655.376	647.354	38800.558	38.100	377.487	242.284	43.850	6.414
34.75	32.670	6535.603	809.938	43955.063	39.950	400.508	252.385	52.323	6.436
36.48	34.039	5278.485	825.327	30984.576	37.314	364.721	284.493	57.084	6.645
38.20	35.343	6029.441	674.096	32513.826	31.900	305.220	260.957	54.537	6.576
39.92	36.610	7915.236	1115.375	46572.596	54.347	521.981	208.190	52.967	6.513
41.68	37.876	13636.481	1152.745	67116.824	62.657	526.980	215.631	47.481	6.291
43.49	39.155	3997.127	520.473	20207.652	24.906	188.925	171.738	53.933	6.555
45.30	40.339	4365.433	707.128	23129.281	33.055	279.287	263.128	55.210	6.520
48.73	42.407	6617.773	761.205	33741.537	36.341	323.812	246.561	54.058	6.291
50.32	43.362	8421.458	999.110	38990.495	47.328	447.671	237.333	54.482	6.640
51.95	44.389	9862.579	1153.746	53425.939	117.086	583.409	306.422	25.431	6.333
53.10	45.178	11214.061	1017.407	45399.854	59.263	463.733	234.078	44.307	5.992
54.89	46.615	6147.071	642.645	30195.083	45.504	322.964	202.180	36.449	5.819
56.68	48.269	6273.070	635.876	30862.083	38.553	278.156	267.697	42.567	5.966
58.46	50.059	7394.035	668.061	30939.324	48.443	273.406	253.651	35.592	6.067
61.00	52.682	4433.643	916.043	25665.014	42.198	295.884	339.802	56.025	
62.57	54.262	5927.950	679.045	29029.052	41.169	322.525	245.131	42.568	5.852
65.71	57.224	7072.997	667.970	29196.643	40.165	301.921	226.969	42.921	5.948
67.45	58.682	4830.066	561.478	24318.352	40.164	302.907	221.988	36.079	5.434
68.77	59.715	8199.036	625.288	39115.997	50.205	312.671	249.145	32.144	5.993
70.20	60.768	5601.175	1080.849	29220.145	47.379	389.029	342.084	58.876	9.480
71.66	61.777	5433.057	668.982	30616.879	46.813	385.912	209.561	36.881	5.470
74.09	63.362	8588.719	577.780	41564.211	58.552	357.645	205.623	25.467	
75.76	64.421	4627.564	847.964	31757.296	73.617	461.417	257.063	29.728	
78.90	66.579	5171.110	600.885	31280.189	57.884	374.013	178.206	26.791	5.236
80.60	68.117	2967.116	427.426	28230.272	31.189	291.460	175.472	35.368	5.310
82.29	69.927	5659.585	389.705	23481.564	33.273	261.649	176.830	30.228	4.766
84.51	72.652	3254.165	357.158	16414.258	30.201	195.066	165.465	30.521	4.853
86.40	75.357	3523.592	340.945	15213.200	28.677	196.882	181.617	30.684	4.487
88.25	78.541	3662.764	374.907	24023.333	31.053	226.507	162.291	31.159	4.899
89.90	82.620	4022.152	790.542	29367.704	50.263	339.079	222.546	40.592	7.743
92.88	90.983	5312.148	832.774	41045.419	54.535	444.018	218.247	39.411	6.961
95.76	94.948	7030.760	922.869	32318.270	56.774	443.509	302.161	41.952	7.593
97.86	96.796	6945.744	545.116	28087.196	60.643	296.958	173.384	23.199	4.812
99.52	98.112	5440.773	479.065	25387.892	43.701	292.476	175.516	28.292	4.633
101.18	99.631	6505.775	638.315	23936.609	55.582	620.680	309.214	29.639	6.268
102.85	101.780	5823.808	365.595	25176.071	41.396	218.214	209.960	22.793	4.680
105.18	106.660	2903.030	346.056	14303.401	20.527	194.616	263.354	43.509	6.950
107.04	111.090	2541.031	184.240	13525.212	15.377	103.100	191.559	30.922	4.557
109.13	113.280	2604.550	174.383	13851.933	15.428	113.682	190.447	29.171	4.502
111.34	122.450	592.207	67.744	2982.231	7.438	44.002	166.041	23.506	4.132
113.62	130.470	3450.566	288.120	14022.240	24.617	147.883	216.838	30.206	4.611
115.87	137.660	2872.587	216.064	15444.157	16.598	98.409	193.876	33.596	4.562
117.95	141.960	2697.981	321.992	11269.559	18.140	121.737	295.190	45.812	6.324
120.81	149.850						230.766	42.248	6.571
123.33	155.380						279.509	42.639	5.880
126.28	160.360						262.864	33.440	5.819
129.70	164.930						250.615	41.937	5.810
132.59	167.940						230.738	9.015	5.519
134.03	169.500						264.709	29.535	6.120
136.86	173.400						281.877	40.584	6.438

* Ages are interpolated using the age model provided by Bühring and Sarnthein (Marine Geology special volume, submitted). ** Dry bulk density values are taken from ODP Initial Reports Vol. 184 (2000); sedimentation rates are taken from Bühring and Sarnthein (Marine Geology special volume, submitted).

Phosphorus geochemistry from ODP Sites 184-1143 and 1144
Phosphorus sedimentary phases

Core	Interval (cm)	Depth (mbsf)	Depth (mcd)	Fe (mgFe/g)	Fe-bound P (mgP/g)	Authigenic P (mgP/g)	Detrital P (mgP/g)	Organic-bound P (mgP/g)
184-1143A								
1H-1	145-150	1.48	1.50	3.218	0.095	0.065	0.085	0.10
2H-3	145-150	7.38	7.80	1.147	0.093	0.187	0.024	0.08
3H-3	145-150	16.88	17.98	1.911	0.049	0.081	0.033	0.08
4H-3	145-150	26.38	28.52	1.383	0.077	0.114	0.025	0.07
5H-3	145-150	35.88	38.42	1.357	0.108	0.165	0.029	0.07
6H-3	145-150	45.38	48.14	1.368	0.064	0.065	0.026	0.06
9H-3	145-150	73.88	77.98	1.164	0.053	0.255	0.029	0.09
184-1144A								
1H-4	145-150	5.98	6.44	2.169	0.080	0.344	0.049	0.07
2H-3	145-150	11.38	13.17	1.482	0.095	0.336	0.057	0.07
3H-3	145-150	20.88	22.45	3.057	0.100	0.359	0.088	0.07
4H-3	145-150	30.42	31.77	2.701	0.099	0.196	0.085	0.06
5H-3	145-150	39.88	41.37	2.428	0.090	0.204	0.080	0.06
6H-3	145-150	49.38	52.81	2.470	0.094	0.189	0.073	0.07
8H-3	145-150	68.38	75.11	3.321	0.091	0.215	0.086	0.06
9H-3	145-150	77.88	84.27	2.317	0.126	0.216	0.065	0.10
12H-2	145-150	104.88	116.68	1.643	0.140	0.193	0.049	0.07
15H-2	145-150	133.38	145.04	1.756	0.085	0.197	0.106	0.05
18H-2	145-150	161.88	176.05	1.500	0.072	0.172	0.076	0.04
20H-2	145-150	180.88	197.69	1.823	0.101	0.195	0.059	0.05
26X-2	145-150	237.88	263.13	1.905	0.071	0.181	0.116	0.05
30X-2	145-150	273.05	303.44	1.830	0.086	0.152	0.053	0.08
33X-2	145-150	301.95	336.17	1.419	0.114	0.206	0.064	0.05
39X-2	145-150	359.65	404.40	1.560	0.082	0.257	0.077	0.05
45X-2	145-150	417.35	474.53	1.986	0.060	0.275	0.076	0.06

Phosphorus geochemistry from ODP Sites 184-1143 and 1144 (continued)
Pore water (data from Wang et al., 2000)

Depth (mcd)	pH	Alkalinity (mM)	Salinity	Cl^- (mM)	Na^+ (mM)	K^+ (mM)	Mg^{2+} (mM)	Ca^{2+} (mM)	SO_4^{2-} (mM)	HPO_4^{2-} (mM)	NH_4^+ (mM)	H_4SiO_4 (mM)	Li^+ (mM)	Sr^{2+} (mM)
1.50	7.78	4.26	35.0	549	472	12.4	51.5	10.3	27.6	15.6	0.2	476	29	93
7.80	7.74	5.35	35.0	555	476	11.9	51.2	9.9	25.5	33.7	0.4	651	27	100
17.98	7.74	6.82	34.0	558	484	12.2	49.3	8.8	24.0	16.6	0.5	693	33	107
28.52	7.83	7.79	34.0	558	484	12.2	48.5	8.5	22.9	12.0	0.6	689	38	118
38.42	7.86	8.05	35.0	561	482	11.4	47.3	8.0	17.9	6.9	0.6	579	46	128
48.14	7.84	8.00	34.0	559	487	11.1	46.1	7.2	19.2	3.6	0.7	501	52	139
77.98	7.86	7.93	33.5	559	486	9.9	44.1	6.0	15.1	1.6	0.9	355	63	186
6.44	7.73	5.68	34.5	552	472	12.50	51.5	9.40	25.18	21.7	0.8	628.6	24	92
13.17	8.20	34.94	34.0	555	452	11.20	47.3	4.80	0.00	191.1	3.7	717.4	11	75
22.45	7.86	32.29	33.5	555	457	11.40	44.9	3.40	0.00	260.7	7.1	814.9	13	68
31.77	7.87	31.95	34.0	557	457	11.40	44.2	3.20	0.00	254.3	7.8	793.2	12	72
41.37	7.84	30.36	34.0	559	455	11.30	44.0	3.30		219.2	8.0	804.1	15	74
52.81	7.84	29.3	33.0	558	458	11.20	43.4	3.20	0.00	175.1	7.3	780.2	15	71
75.11	7.87	22.88	32.0	556	454	10.80	38.7	3.40	0.00	197.4	7.7	754.3	12	70
84.27	7.89	21.75	32.0	556	454	10.80	38.8	3.40		165.5	7.6	767.3	13	69
116.68	7.84	27.3	32.0	552	452	10.50	40.9	3.80		228.8	8.0	771.6	17	73
145.04				556	452	10.00	36.9	3.90	0.00	176.7	8.3	804.1	15	74
176.05	7.68	21.44	32.0	554	457	9.70	36.7	3.90	0.00	157.5	8.4	743.4	17	77
197.69	7.54	22.82	32.0	550	456	10.20	36.0	3.90	0.00	108	7.8		19	82
263.13	7.87		32.0	550	453	9.50	34.8	4.30		66.5	7.5		19	90
303.44	7.84	17.16	32.0	552	451	9.20	34.2	4.90	0.16	61.7		767.3	21	95
336.17	7.87	17.12	32.0	549	449	8.90	34.9	5.00	0.00	36.1	7.4	810.6	27	104
404.40	7.77	12.47	31.0	555	452	8.20	33.8	5.71	0.00	16.2		851.7	28	114
474.53	7.48	8.53	31.0	553	473	6.90	33.7	6.10	0.00	6.6	3.1	414.2	27	143

Core SU 90-09: North Atlantic, IRD belt
Geochemistry: Fe, phosphorus phases, organic matter

Depth	Sediment	Fe	Fe-bound P	Authigenic P	Detrital P	Organic-bound P	Total P	TOC <50 µm *	TOC/P	TOC/Preac	Fe/P	OI	HI
cm	type	mgFe/g	mgP/g	mgP/g	mgP/g	mgP/g	mgP/g	mg/g	molar	molar	molar		
SU 90-09													
130		0.894	0.000	0.236	0.051	0.054	0.341	3.23	154.95	28.76		247.529	110.90
131		0.724	0.000	0.239	0.040	0.062	0.341	3.17	131.65	27.13		271.191	115.35
132		0.739	0.000	0.246	0.059	0.056	0.360	3.03	140.45	25.92		265.048	113.50
133		0.706	0.000	0.224	0.115	0.049	0.388	3.01	158.90	28.45		293.260	115.73
134		0.718	0.000	0.224	0.076	0.053	0.352	2.91	142.50	27.16		293.033	115.73
135		0.739	0.000	0.226	0.119	0.050	0.395	2.48	127.28	23.15			
136		0.908	0.000	0.246	0.067	0.056	0.369	3.06	141.93	26.14		272.328	116.84
137		0.939	0.000	0.205	0.138	0.052	0.395	2.71	133.85	27.19			
138		1.084	0.000	0.209	0.173	0.047	0.428	2.32	128.49	23.39			
139		1.105	0.000	0.190	0.201	0.060	0.450	2.57	111.05	26.53			
140		1.129	0.000	0.205	0.197	0.049	0.451	2.54	133.25	25.82		237.290	115.35
141		0.530	0.000	0.123	0.295	0.032	0.450	2.87	231.31	47.70		161.071	
142		0.881	0.000	0.173	0.232	0.048	0.453	2.62	140.28	30.52			
143		1.115	0.000	0.185	0.223	0.039	0.447	2.31	153.31	26.64			
144	H4	2.219	0.000	0.263	0.128	0.056	0.447	1.98	91.67	16.04		228.645	127.23
144.5	H4	1.732	0.000	0.241	0.125	0.046	0.412	2.17	122.92	19.54			
145	H4	2.014	0.000	0.274	0.090	0.049	0.413	2.12	112.42	16.94		202.707	125.01
145.5	H4							2.13					
146	H4	1.056	0.000	0.189	0.237	0.049	0.475	2.53	134.08	27.42			
146.5	H4	1.166	0.000	0.199	0.176	0.033	0.409	2.43	189.35	26.98			
147	H4	1.348	0.000	0.214	0.152	0.035	0.402	2.01	148.65	20.79		175.405	124.26
147.5	H4	1.144	0.000	0.184	0.259	0.063	0.507	2.51	102.01	26.13			
148	H4	0.818	0.000	0.144	0.288	0.057	0.488	2.52	114.95	32.41		181.320	84.17
148.5	H4	0.944	0.000	0.187	0.213	0.041	0.442	2.58	162.12	29.13		145.145	119.81
150	H4	1.023	0.000	0.240	0.185	0.046	0.470	2.61	147.36	23.55		153.790	116.84
150.5	H4	3.248	0.000	0.141	0.286	0.031	0.457	2.51	209.05	37.71			
151	H4	1.126	0.000	0.264	0.173	0.038	0.476	2.41	162.28	20.53		140.594	121.29
151.5	H4	1.123	0.000	0.273	0.135	0.045	0.453	2.77	160.13	22.47		135.361	119.07
152	H4	3.900	0.000	0.237	0.156	0.049	0.443	2.64	138.90	23.79		116.022	119.07
152.5	H4	1.404	0.000	0.279	0.116	0.058	0.453	2.81	126.00	21.51		159.933	119.44
153	H4	0.850	0.000	0.216	0.172	0.053	0.442	3.35	162.97	32.07		166.759	118.32
153.5	H4	0.892	0.045	0.208	0.075	0.056	0.384	4.03	184.12	33.57	10.99	201.797	107.56
154		0.800	0.059	0.221	0.028	0.052	0.359	4.30	214.97	33.45	7.56	209.760	111.27
155		0.757	0.075	0.222	0.027	0.059	0.384	4.41	192.85	31.90	5.57	229.327	112.38
156		0.691	0.043	0.211	0.025	0.055	0.333	4.53	213.27	37.90	8.99	236.153	110.16
157		0.715	0.084	0.191	0.029	0.057	0.361	4.29	195.16	33.33	4.70	240.021	111.27
158								4.73					
159		0.603	0.065	0.200	0.036	0.050	0.352	4.39	224.19	35.80	5.12	223.412	106.45
160		0.643	0.077	0.190	0.025	0.055	0.347	4.15	194.14	33.24	4.63	235.470	101.99
161		0.614	0.077	0.207	0.032	0.058	0.375	4.20	185.24	31.56	4.40	293.260	112.01
162		0.637	0.058	0.194	0.019	0.054	0.325	4.45	211.58	37.44	6.07	303.499	110.53
163		0.651	0.056	0.190	0.028	0.057	0.332	4.70	210.87	39.84	6.40	273.466	113.13
164		0.729	0.083	0.184	0.027	0.056	0.351	4.24	196.79	33.85	4.87	308.049	119.44
165		0.631	0.061	0.193	0.030	0.054	0.338	4.37	207.70	36.54	5.75	276.879	112.01
166		0.803	0.082	0.196	0.030	0.050	0.358	4.90	253.14		5.40	273.011	114.61
167		0.738	0.084	0.200	0.037	0.055	0.377	4.10	190.60	31.14	4.86	278.926	118.32
168		0.725	0.091	0.192	0.025	0.052	0.360	4.40	216.51	33.86	4.43	257.312	115.35
169		0.677	0.108	0.216	0.029	0.055	0.408	3.98	186.10	27.08	3.48	249.804	116.84
170		0.514	0.059	0.194	0.034	0.051	0.339	4.06	205.55	34.37	4.80	250.941	106.82
171		0.573	0.092	0.199	0.033	0.047	0.371	4.40	241.89		3.46	252.989	111.27
172		0.596	0.094	0.208	0.033	0.046	0.380	4.32	243.54	32.07	3.52	254.582	112.76
173		0.644	0.047	0.212	0.044	0.056	0.360	3.93	180.19	32.10	7.52	239.338	111.64
174		0.604	0.058	0.205	0.042	0.043	0.349	4.29	254.65	36.07	5.74	265.503	110.53
175		0.684	0.088	0.203	0.037	0.052	0.380	4.04	200.38	30.37	4.33	261.180	100.51
176		0.626	0.058	0.216	0.042	0.046	0.362	3.56	198.78	28.69	5.97	251.397	112.76
177		0.666	0.069	0.232	0.039	0.054	0.394	4.13	198.22	29.99	5.34	252.307	122.04
178		0.712	0.100	0.215	0.034	0.050	0.399	4.15	213.26	29.32	3.95	248.666	114.61
179		0.756	0.076	0.269	0.058	0.059	0.462	3.27	141.97	20.87	5.52	239.793	117.58
180		0.587	0.060	0.233	0.047	0.044	0.384	4.21	246.45	32.22	5.40	242.068	112.38
181		0.546	0.055	0.223	0.064	0.046	0.388	3.70	209.13	29.47	5.46	209.078	109.79
182		0.612	0.053	0.225	0.044	0.044	0.365	4.10	240.49		6.45	240.931	110.53
183		0.520	0.051	0.216	0.093	0.040	0.400	3.46	225.32	29.03	5.61	216.131	112.01
184		0.661	0.066	0.225	0.085	0.041	0.418	3.37	209.91	26.16	5.55	228.417	123.15
185		0.710	0.074	0.241	0.055	0.047	0.417	3.47	192.04	24.71	5.30	228.872	120.18
186		0.631	0.063	0.236	0.065	0.054	0.417	3.05	145.82	22.32	5.60	232.740	123.15
187	H5	0.743	0.078	0.257	0.063	0.046	0.445	3.09	172.22		5.30	233.195	119.44
187.5	H5	0.748	0.080	0.253	0.068	0.045	0.445	3.04	174.49	20.78	5.20	191.786	114.24
188	H5	0.893	0.053	0.260	0.074	0.042	0.428	2.53	156.97	18.41	9.36	207.940	125.38
188.5	H5	0.856	0.045	0.217	0.127	0.046	0.436	2.55	142.81	21.30	10.51	201.797	117.58
189	H5	0.964	0.000	0.260	0.081	0.040	0.380	2.45	158.72	21.09			
189.5	H5	1.102	0.000	0.250	0.107	0.045	0.403	2.21	126.11	19.28		185.188	127.23
190	H5	1.055	0.000	0.235	0.159	0.041	0.436	1.88	118.18	17.55		194.744	
190.5	H5	1.239	0.000	0.287	0.097	0.043	0.426	1.98	119.13	15.49			
191	H5	0.960	0.000	0.222	0.164	0.038	0.424	2.05	138.80	20.30			
191.5	H5	1.158	0.000	0.279	0.131	0.036	0.446	1.90	135.67	15.56		195.107	130.37
192	H5	0.715	0.000	0.220	0.231	0.030	0.481	1.81	154.28	18.66		174.267	129.09
192.5	H5	1.000	0.000	0.305	0.088	0.038	0.430	1.80	121.84	13.54		202.401	
193	H5	0.714	0.042	0.242	0.083	0.040	0.407	2.80	179.74	22.26	9.41	230.692	118.32
193.5	H5	0.724	0.054	0.223	0.055	0.037	0.369	3.06	210.88	25.11	7.41	254.331	121.63
194		0.787	0.076	0.212	0.035	0.049	0.371	3.23	171.36	24.80	5.78	619.532	101.74
195		0.775	0.087	0.219	0.036	0.034	0.376	2.83	216.41	21.45	4.93	306.445	118.65
196		0.666	0.086	0.195	0.030	0.036	0.347	3.34	238.36	27.15	4.29	323.683	105.64
197		0.599	0.105	0.185	0.026	0.034	0.350	3.91	292.79	31.10	3.16	326.830	106.55
198		0.670	0.086	0.196	0.051	0.046	0.378	3.25	182.75	25.59	4.32	276.203	98.01
199		0.651	0.089	0.186	0.025	0.041	0.341	4.04	254.51	32.93	4.05	324.387	105.47

* TOC values are from Huon et al. (in press).

Core SU 90-09: North Atlantic, IRD belt (continued)
XRD results: bulk mineralogy

Depth cm	Phyllosilicates %	Quartz %	K-feldspar %	Plagioclase %	Calcite %	Dolomite %	Goethite %	Ankerite %	Unquantified %
130	3.293	4.786	0.453	2.094	19.630	1.640	0.000	0.341	67.317
131	4.778	8.328	0.670	4.768	21.939	1.310	0.000	0.515	57.314
132	5.257	5.853	0.950	2.257	25.321	2.536	0.224	0.271	56.960
133	2.702	14.716	1.924	3.145	17.948	2.802	0.000	0.538	55.851
134	4.105	3.615	1.815	1.554	18.418	2.993	0.496	1.029	65.655
135	4.013	12.049	1.536	3.762	26.413	3.925	0.219	0.308	47.367
136	3.652	4.081	0.650	1.343	14.239	2.635	0.414	0.258	72.541
137	3.740	8.169	2.180	2.362	21.870	2.581	0.000	0.636	58.136
138	3.004	7.888	1.034	2.174	14.161	4.454	0.000	0.605	66.309
139	3.040	8.338	1.935	4.122	15.474	8.014	0.000	0.634	58.085
140	5.642	9.498	1.661	3.230	22.009	4.880	0.646	0.551	51.559
141									
142	2.408	8.737	1.426	2.281	14.628	8.110	0.205	0.428	61.534
143	3.188	10.433	1.659	2.158	12.909	6.915	0.081	0.824	61.610
144	5.535	10.478	3.624	4.215	13.631	4.832	0.205	1.441	55.835
144.5	4.620	15.247	1.902	4.490	16.612	7.881	0.000	1.134	47.806
145	4.392	14.646	2.619	2.911	15.065	7.748	0.289	1.219	50.761
145.5									
146	1.815	9.796	7.581	3.888	13.107	8.966	0.163	0.891	53.550
146.5	3.102	11.256	3.311	5.113	29.742	10.033	0.357	1.053	35.236
147	4.818	8.308	2.003	10.771	16.868	6.913	0.082	0.766	49.181
147.5	1.407	10.492	1.152	24.429	11.154	5.840	0.152	0.299	44.794
148	3.144	12.871	2.650	5.967	14.159	4.642	0.245	1.429	54.503
148.5	2.274	16.740	1.825	5.974	15.119	7.191	0.286	1.686	48.644
150									
150.5	1.706	7.952	1.875	2.920	10.924	4.329	0.311	0.903	68.870
151	1.768	14.661	1.592	8.445	16.413	6.268	0.000	1.314	49.248
151.5	1.511	9.910	1.073	6.933	13.815	4.765	0.000	1.964	59.821
152	2.184	9.161	2.348	3.354	11.414	7.161	0.000	0.832	63.398
152.5	2.604	5.453	2.075	3.766	12.341	7.616	0.000	0.705	65.248
153	1.061	8.046	3.606	3.488	14.384	7.720	0.303	0.463	60.721
153.5	1.785	8.821	2.793	3.301	14.613	6.720	0.000	1.755	60.142
154	1.651	6.059	3.009	2.859	24.324	3.607	0.435	0.459	57.125
155	2.387	4.049	1.352	2.041	22.042	1.119	0.171	0.132	66.247
156	3.934	4.139	0.280	1.565	18.739	1.998	0.486	0.307	68.191
157	5.815	4.728	1.064	2.712	29.481	1.031	0.133	0.087	54.503
158									
159	2.792	4.475	1.477	1.059	20.447	0.884	0.299	0.106	68.031
160	0.978	4.803	1.169	1.843	23.758	1.261	0.752	0.428	64.510
161	2.388	7.170	1.213	1.219	29.116	1.046	0.178	0.288	56.680
162									
163	4.757	3.903	1.398	2.327	34.692	1.292	0.000	0.205	50.458
164	4.455	4.005	0.908	3.886	31.965	1.563	0.000	0.257	52.403
165	5.496	3.938	1.568	0.918	24.665	0.694	0.000	0.251	62.008
166	3.389	5.289	1.722	4.593	34.412	0.723	0.535	0.207	48.455
167	4.004	3.483	1.029	1.290	24.028	1.647	0.218	0.177	63.755
168	2.856	3.077	0.445	1.028	22.005	1.938	0.289	0.205	67.775
169	1.022	5.729	0.935	1.458	20.576	1.127	0.000	0.298	68.452
170	5.822	3.130	1.366	1.008	24.132	0.958	0.130	0.216	62.807
171	1.825	5.082	0.830	1.260	32.985	0.912	0.275	0.324	55.879
172	1.523	3.514	0.964	1.995	22.449	1.321	0.204	0.193	67.293
173	2.109	2.962	1.887	1.522	20.965	1.293	0.128	0.139	68.553
174									
175	0.912	6.796	0.947	1.635	23.638	3.207	0.000	0.133	62.307
176	3.070	4.573	1.188	1.927	30.178	1.178	0.000	0.369	56.977
177	4.787	5.458	0.969	1.705	30.138	1.497	0.179	0.264	54.611
178	1.296	5.955	0.467	3.130	24.230	2.476	0.216	0.242	61.589
179	1.519	12.634	2.424	7.578	32.292	2.955	0.575	0.211	39.303
180	3.331	3.275	1.516	1.197	22.204	1.525	0.000	0.177	66.473
181	4.478	3.388	1.637	6.735	20.304	1.352	0.180	0.456	61.100
182	2.098	2.589	1.586	5.068	18.836	1.708	0.168	0.204	67.447
183	1.319	4.197	1.596	2.764	17.763	2.326	0.252	0.323	69.176
184	2.714	6.425	2.554	3.116	28.658	1.958	0.088	0.633	53.520
185	3.244	4.004	2.870	4.282	19.199	1.731	0.042	0.204	64.070
186	2.173	11.774	4.151	3.030	26.452	1.138	0.087	0.531	50.276
187	0.782	3.100	0.622	4.353	15.235	1.723	0.457	0.298	73.074
187.5	4.202	3.133	2.388	4.836	13.511	2.215	0.328	0.293	68.891
188									
188.5	5.085	5.399	2.393	4.236	13.378	3.184	0.205	0.663	65.169
189	1.685	6.409	1.468	3.915	13.110	3.776	0.122	0.320	68.923
189.5	1.457	4.337	1.750	2.953	8.456	3.828	0.522	0.349	76.176
190	3.948	14.336	3.641	3.890	12.133	8.951	0.160	0.437	52.290
190.5	2.476	14.178	1.310	7.434	12.911	6.650	0.159	0.666	54.065
191	1.033	7.320	1.256	2.605	7.435	3.838	0.622	0.513	75.220
191.5	4.457	8.771	4.060	5.206	11.301	4.601	0.282	0.786	60.301
192									
192.5	1.100	9.072	3.690	4.686	12.080	3.972	0.404	0.281	64.520
193	1.473	7.350	5.673	5.861	23.443	4.077	0.043	0.405	51.314
193.5	2.238	4.902	2.519	2.383	25.222	1.870	0.087	0.269	60.189
194	1.000	1.612	0.901	1.311	15.872	1.095	0.000	0.154	77.733
195	2.107	3.881	0.563	1.654	27.411	1.616	0.379	0.130	61.838
196	1.938	2.309	0.707	0.882	24.020	0.931	0.000	0.254	68.593
197	1.620	3.820	1.310	1.651	39.978	1.943	0.000	0.363	48.803
198	1.315	2.617	1.277	1.567	20.322	1.329	0.085	0.346	70.719
199	1.333	2.998	2.194	1.509	34.763	0.652	0.183	0.188	55.754

Core SU 90-09: North Atlantic, IRD belt (continued)
Phosphorus geochemistry

Depth	Fe	Fe-bound P	Authigenic P	Detrital P	Organic-bound P	Total P
cm	mgFe/g	mgP/g	mgP/g	mgP/g	mgP/g	mgP/g
SU 90-09						
10	1.846	0.145	0.180	0.035	0.056	0.415
11	1.682	0.137	0.206	0.025	0.062	0.430
12	1.739	0.135	0.195	0.031	0.052	0.413
13	1.716	0.145	0.201	0.037	0.081	0.464
14	1.835	0.148	0.198	0.021	0.072	0.439
15	1.943	0.166	0.189	0.025	0.065	0.444
18	1.769	0.143	0.171	0.041	0.057	0.412
20	1.688	0.142	0.194	0.030	0.058	0.424
22	1.534	0.122	0.201	0.044	0.063	0.429
24	1.432	0.113	0.160	0.069	0.051	0.393
26	1.423	0.116	0.159	0.092	0.055	0.423
28	1.410	0.096	0.170	0.097	0.054	0.417
30	1.406	0.106	0.164	0.091	0.061	0.422

Core SU 90-09: North Atlantic, IRD belt (continued)
Bulk mineralogy

Depth	Phyllosilicates	Quartz	K-feldspar	Plagioclase	Calcite	Dolomite	Ankerite	Unquantified
cm	%	%	%	%	%	%	%	%
10	1.079	1.066	0.364	0.308	55.005	0.379	0.055	40.792
11	0.910	4.075	0.358	0.948	50.416	0.000	0.000	42.350
12	1.023	0.893	0.000	0.306	37.442	0.349	0.029	59.274
13	0.000	1.160	0.191	0.308	40.295	0.724	0.062	56.453
14	1.596	1.092	1.651	0.979	52.363	1.227	0.253	39.989
15	0.883	1.545	0.202	0.378	43.241	0.365	0.125	52.675
18	0.827	1.447	0.000	0.940	50.271	0.640	0.091	45.017
20	0.000	1.151	0.529	0.567	34.506	0.451	0.133	62.040
22	1.764	2.041	0.783	1.064	43.159	0.842	0.088	49.626
24	0.000	2.782	0.729	1.057	39.871	1.283	0.131	53.471
26	0.619	2.738	0.826	0.912	32.273	1.542	0.238	60.353
28	1.250	5.951	1.392	1.283	40.439	2.292	0.240	46.488
30	1.134	3.509	0.312	0.836	35.647	2.480	0.237	55.327

REFERENCES

Bickert, T., Berger, W.H., Burcke, S., Schmidt, H. and Wefer, G., 1993. Late Quaternary stable isotope record of benthic foraminifers: sites 805 and 806, Ontong Java Plateau. In: W.H. Berger, L.W. Kroenke and L.A. Mayer (Editors), Proceedings of the Ocean Drilling Program, Scientific Results. Vol. 130. ODP, Ocean Drilling Program, College Station, TX, USA, 411-420.

Föllmi, K.B., Cramp, A., Föllmi, K.E., Alexandrovich, J.M., Brunner, C., Burckle, L.H., Casey, M., deMenocal, P., Dunbar, R.B., Grimm, K.A., Holler, P., Ingle, J.C.J., Kheradyar, T., McEvoy, J., Nobes, D.C., Stein, R., Tada, R., von Breymann, M.T. and White, L.D., 1992. Dark-light rhythms in the sediments of the Japan Sea: Preliminary results from site 798, with some additional results from sites 797 and 799. In: K.A. Pisciotto, J.C.J. Ingle, M.T. von Breymann, J. Barron et al. (Editors), Proceedings of the Ocean Drilling Program, Scientific Results, Vol. 127/128. ODP, Ocean Drilling Program, College Station, TX, USA, 559-576.

Huon S., Grousset F. E., Burdloff D., Bardoux G., and Mariotti A. (in press) Sources of fine-sized organic matter in North Atlantic Heinrich Layers: $\delta^{13}C$ and $\delta^{15}N$ tracers. Geochimica et Cosmochimica Acta.

Ingle, J.C., Jr., Suyehiro, K., et al., 1989. Site 798. In: S.K. Stewart (Editor), Proceedings of the Ocean Drilling Program, Part A: Initial Reports, Vol. 128. ODP, Ocean Drilling Program, TX, USA, 121-236.

Kroenke, L.W. et al., 1991. Site 806. In: E.M. Barbu (Editor), Proceedings of the Ocean Drilling Program, Part A: Initial Reports, Vol. 130. ODP, Ocean Drilling Program, College Station, TX, USA, 291-367.

McManus, J.F., Major, C.O., Flower, B.P. and Fronval, T., 1996. Variability in sea-surface conditions in the North Atlantic-Arctic gateways during the last 140,000 years. In: J. Thiede, A.M. Myhre, J.V. Firth, G.L. Johnson and W.F. Ruddiman (Editors), Proceedings of the Ocean Drilling Program, Scientific Results, Vol. 151. ODP, Ocean Drilling Program, College Station, TX, USA, 437-444.

Myhre, A.M. et al., 1995. Site 907. In: J.A. Marin (Editor), Proceedings of the Ocean Drilling Program, Part A: Initial Reports, Vol. 151. ODP, Ocean Drilling Program, College Station, TX, USA, 57-111.

Prell, W.L., Niitsuma, N., et al., 1989. Site 724. In: N.J. Steward (Editor), Proceedings of the Ocean Drilling Program, Part A: Initial Reports, Vol. 117. ODP, Ocean Drilling Program, TX, USA, 385-417.

Ruddiman, W., Sarnthein, M., et al., 1988. Site 658. In: S.K. Stewart and W.D. Rose (Editors), Proceedings of the Ocean Drilling Program, Part A: Initial Reports, Vol. 108. ODP, Ocean Drilling Program, College Station, TX, USA, pp. 105-219.

Sarnthein, M. and Tiedemann, R., 1989. Toward a high-resolution stable isotope stratigraphy of the last 3.4 million years: sites 658 and 659 off Northwest Africa. In: W.F. Ruddiman, M. Sarnthein, J. Baldauf and R.G. Heath (Editors), Proceedings of the Ocean Drilling Program; Scientific Results, Vol. 108. ODP, Ocean Drilling Program, College Station, TX, USA, 167-185.

Suess, E., von Huene, et al., 1988. Site 680. In: S.K. Stewart (Editor), Proceedings of the Ocean Drilling Program, Part A: Initial Reports, Vol. 112. ODP, Ocean Drilling Program, TX, USA,. 249-303.

Tada, R., Irino, T. and Koizumi, I., 1999. Land-ocean linkages over orbital and millennial scales recorded in late Quaternary sediments of the Japan Sea. Paleoceanography, 14(2): 236-247.

Wang, P., and Prell, W.L., et al., (2000). Site 1143 and site 1144. In: S. Nessler (Editor), Proceedings of the Ocean Drilling Program, Part A: Initial Reports, Vol. 184. ODP, Ocean Drilling Program, TX, USA.

Wefer, G., Heinze, P. and Suess, E., 1990. Stratigraphy and sedimentation rates from oxygen isotope composition, organic carbon content, and grain-size distribution at the Peru upwelling region: Holes 680B and 686B. In: E. Suess, R. von Huene et al. (Editors), Proceedings of the Ocean Drilling Program, Scientific Results, Vol. 112. ODP, Ocean Drilling Program, College Station, TX, USA, 355-367.

Zahn, R., and Pedersen, T.F., 1991. Late Pleistocene evolution of surface and mid-depth hydrography at the Oman margin: planktonic and benthic isotope records at Site 724. In W.L. Prell., Niitsuma, N., et al. (Editors), Proceedings of the Ocean Drilling Program, Scientific Results, Vol. 117, ODP, Ocean Drilling Program, College Station, TX, USA, 291-308.

ANNEX C

Coffee supplies in the sedimentology lab during Leg 184 (1999)

7th Meeting of Swiss Sedimentologists, Fribourg, Switzerland. January 1999.
Oral Presentation

Changes in mineralogy, phosphate and nitrogen stable isotopes from marine records of the last 150,000 years: preliminary results from ODP Sites 658, 680, 724, 798, 806, 907

Federica Tamburini, Thierry Adatte, Stefano Bernasconi, Philipp Steinmann, Karl B. Föllmi

In the last few decades, our knowledge of the Pleistocene climate has substantially increased, and several factors have been forwarded as important controls on glacial-interglacial cyclicity, such as changes in deep-water formation and ocean circulation, events of fresh water input into the North Atlantic, changes in atmospheric CO_2, and Milankovitch cyclicity. Much of the progress achieved is based on research on marine sediment and continental ice cores, whereas other continental records have been integrated to a lesser extent, mainly because of their incomplete character.

In this project, we propose to trace continent-ocean links in marine Pleistocene sediment records by means of phosphorus (P) sequential analysis, stable nitrogen isotope analysis, and XRD-mineral characterization. Targeted sites are ODP Sites 658, East equatorial Atlantic (Leg 108); 680, offshore Peru (Leg 112); 724, Arabian Sea, offshore Oman (Leg 117); 798, Japan Sea; 806 (Ontong-Java Plateau (Leg 130); 8907, North Atlantic Gateways (Leg 151), which are characterized by different oceanographic and climatic conditions, and well calibrated by stable oxygen isotopes.

We use P as a proxy of continental weathering and marine productivity, because 1) the primary source of P is continental weathering, and 2) P is an essential nutrient with limiting capacities in marginal marine settings. N is equally an essential nutrient and nitrogen isotopes fractionation is mainly caused by phytoplankton nutrient uptake and denitrification, and stable nitrogen isotopic composition of sediment is for this reason, an useful indicator of nutrient utilization and productivity (Farrell et al., 1995). Mineralogical analyses are used to constrain and characterize detrital flux rate.

The first series of data seta measured shows variations which are mostly consistent with the climate record, as is also confirmed by time series analyses and cross-spectra correlations with the SPECMAP oxygen stable isotope curve.

With regards to bulk mineralogy, the detrital records (phyllosilicates and quartz) are among the most interesting features which emerged from the initial phase of this study.

The detrital content from Sites 680, 724 and 798 increased during glaciations, with highest values of phyllosilicates occurring during the beginning of glacial stages, whereas quartz peaks are recognizable at the end of glacial stages. This is probably related to an enhanced continental weathering and/or eolian, due to more arid conditions during glacial times and to lowered sea level, increasing the area of continental margin exposed to erosion (Wefer et al., 1990).

A different situation is present at Site 658, where the phyllosilicates and quartz show an opposite trend: the phyllosilicates are higher during interglacial than during glacial stages, while quartz is consistent with trends shown by the detrital records of the other sites. This trend can be explained by means of different wind intensity in the equatorial region during interglacial and glacial times, as is also confirmed by pollen data (Dupont et al., 1989).

Site 806, situated on the Ontong Java plateau, is mainly characterized by carbonate deposition (up to 90% of the bulk rock) and the small quantities of quartz are probably related to eolian influx from Asia (Krissek and Janecek, 1993). These records show little correlation to the oxygen isotope record, except for a slight increase of quartz during glacial stage 4.

The detrital record from Site 907 is quite complex. The high percentage of quartz and phyllosilicates, along with K-feldspar and plagioclase, can be related to continuous input of ice rafted debris. Stable nitrogen isotopes at Site 724, measured on non-decarbonatized samples, vary between 2 and 4 for isotopes stage 5, decrease to a value of almost 0 during stage 4, increase to a values of almost 8 during stage 3, go back to values between 2 and 4 for stage 2, and return to a maximum values of 8 during stage 1. The trend in the nitrogen stable isotopes is probably the result of increased nutrient utilization during interglacial periods, with possible denitrification. due to the development of an oxygen minimum zone, especially during stage 3. Further nitrogen stable isotope analyses on samples from the other sites are in progress.

Phosphate analyses are underway and will presumably be presented during the meeting.

REFERENCES

Dupont, L.M., Beug, H.-L., Stalling, H. and Tiedemann, R., 1989. First palynological results from site 658 at 21° N off northwest Africa: pollen as climate indicators. In: W.F. Ruddiman, M. Sarnthein, J. Baldauf and R.G. Heath (Editors), Proceedings of the Ocean Drilling ProgramScientific Results, Vol. 108. Ocean Drilling Program, College Station, TX, pp. 93-112.

Farrell, J.W., Pedersen, T.F., Calvert, S.E. and Nielsen, B., 1995. Glacial-interglacial changes in nutrient utilization in the equatorial Pacific Ocean. Nature, 377: 514-517.

Krissek, L.A. and Janecek, T.R., 1993. Eolian deposition on the Ontong Java Plateau since the Oligocene: unmixing a record of multiple dust sources. In: W.H. Berger, L.W. Kroenke and L.A. Mayer (Editors), Proceedings of the Ocean Drilling Program, Scientific Results, Vol. 130. Ocean Drilling Program, College Station, TX, pp. 471-490.

Wefer, G., Heinze, P. and Suess, E., 1990. Stratigraphy and sedimentation rates from oxygen isotope composition, organic carbon content, and grain-size distribution at the Peru upwelling region: Holes 680B and 686B. In: E. Suess, R. von Huene et al. (Editors), Proceedings of the Ocean Drilling Program, Scientific Results, Vol. 112. Ocean Drilling Program, College Station, TX, pp. 355-367.

X EUG, Strasbourg (France). April 1999.
Poster presentation.

Pleistocene glaciation-deglaciation cycles: mineralogy, phosphate and stable nitrogen isotopes from marine records (ODP Sites 658, 680, 724, 798, 806, 907)

Federica Tamburini, Thierry Adatte, Stefano Bernasconi, Karl B. Föllmi

---

In the last few decades, our knowledge of the Pleistocene climate has substantially increased, and several factors have been forwarded as important controls on glacial-interglacial cyclicity, such as changes in deep-water formation and ocean circulation, events of fresh-water input into the North Atlantic, changes in atmospheric CO_2, and Milankovitch cyclicity. Much of the progress achieved is based on research on marine sediment cores and continental ice cores, whereas other continental records have been integrated to a lesser extent, mainly because of their incomplete character.

In our project, we propose to trace continent-ocean links in marine Pleistocene sediment records by means of P-sequential analysis, stable nitrogen isotope analysis, and XRD-mineral characterization. Targeted sites are ODP Sites 658, East equatorial Atlantic; 680, offshore Peru; 724, Arabian Sea, offshore Oman; 798, Japan Sea; 806, Ontong-Java Plateau; 907, North Atlantic Gateways; sites which are characterized by different oceanographic and climatic conditions, and well calibrated by stable oxygen isotopes.

We use P as a proxy of continental weathering and marine productivity, because 1) the primary source of P is continental weathering, and 2) P is an essential nutrient with limiting capacities in marginal marine settings. N is equally an essential nutrient and nitrogen isotope fractionation is mainly caused by phytoplankton nutrient uptake and denitrification, and stable nitrogen isotopic composition of sediment is for this reason, an useful indicator of nutrient utilization and productivity. Mineralogical analyses are used to constrain and characterize detrital flux rate.

In a first approach, we concentrated on ODP Sites 680B and 724C (offshore Peru and Oman). The first series of data sets measured and to be presented during the meeting shows variations, which are consistent with the climate record, as time-series analyses confirm.

These data suggest that productivity and carbon storage diminished in the two upwelling centers offshore Peru and Oman during glacial periods, as has been shown in previous studies.

XV INQUA International Congress, Durban (South Africa). August 1999.
Poster Presentation.

Continent-ocean interactions and their influence on marine productivity records during the last 150'000 years

Federica Tamburini, Philipp Steinmann, Thierry Adatte, Karl Föllmi, Stefano Bernasconi

---

Our knowledge of changes in marine productivity records during the last 150'000 years is based on a selection of criteria which include barite contents, Ca/Cd ratios, stable carbon and nitrogen isotopes, composition of preserved planktic and benthic organisms, and organic carbon contents. For the last glacial maximum, shifts in marine productivity trends towards higher values have been proposed for low and middle-latitude parts of the open oceans, whereas decreased productivity rates have been proposed for the southern Ocean, as well as in coastal upwelling centers.

In our group, we are tracing these climate-related changes in marine productivity and exploring eventual links between them and changes in the intensity of continental weathering (as an important source of biophile elements). We study a selection of ODP sites, which are characterized by different oceanographic and climatic conditions, and well calibrated by stable oxygen isotopes (Sites 658, east equatorial Atlantic; 680, offshore Peru; 724, Arabian Sea; 798, Japan Sea; 806 Ontong-Java; and 907, North Atlantic). Samples were selected with a resolution of approximately 3000 to 5000 years; they are submitted to an analysis of different phosphate phases, $\delta^{15}N$ isotopes, mineralogy (by XRD), and organic matter (by Rock-Eval).

We use P as a proxy of continental weathering and marine productivity, because 1) the primary source of P is continental weathering, and 2) P is an essential nutrient with limiting capacities in marginal marine settings. N is equally an essential nutrient and nitrogen isotope fractionation is mainly caused by phytoplankton nutrient uptake and denitrification of organic matter; $\delta^{15}N$ is, for this reason, an useful indicator of nutrient utilization and productivity. Mineralogical analyses are used to constrain and characterize detrital flux rates. Rock-Eval analyses of organic matter serves to determine the quality and origin of organic matter.

The first series of data sets measured and to be presented during the meeting shows variations, which are consistent with the climate record (as is confirmed by time-series analyses). In a first and preliminary approach, and thereby confirming earlier interpretations, variations in productivity patterns during the last 150'000 years appear to be determined by the intensity of upwelling and the importance of continental-ocean fluxes of nutrients.

7th ECOD Workshop, Amsterdam (Holland). September 1999.
Oral Presentation.

ODP Leg 184: exploring the Asian monsoon through drilling in the South China Sea

Federica Tamburini and Leg 184 Scientific Party

The Asian monsoon system is a major component of both regional and global climate, its evolution is linked with the uplift of the Himalayan-Tibetan orogen, the opening and closing of marginal seas and with changes in global climate.

ODP Leg 184, which represents the first Ocean Drilling Project campaign to the South China Sea, recovered an almost complete sequence of hemipelagic sediments recording the last 32 Ma, from lower Oligocene to Holocene.

The location of the South China Sea (SCS) between the Asian continent and the Pacific Ocean makes it an ideal region to record the paleoceangraphic responses to winter and summer monsoons.

The broad scientific themes of Leg 184 are:

-To document the Cenozoic history of the South China Sea

-To reconstruct the evolution and variability of the east Asian Monsoon during the Late Cenozoic on different time scales

-To identify and understand the links between tectonic uplift, weathering and erosion, marine deposition, and climate change, with particular regard to the Asian Monsoon evolution and the Neogene global cooling.

Leg 184 cored 17 holes at six sites, one located on the southern margin and five on the northern margin of the South China Sea. All the shipboard analyses were performed to acquire “high resolution” records, that allowed to evaluate the completeness of the stratigraphic section and splice a complete, representative record for each site.

Sediments recovered during Leg 184 consist in a mixing of nannofossil ooze and detrital material, mostly clay, derived from the Asian continent and from Borneo, and representing deep water sedimentation.

All the measured properties of the recovered sequences show significant trends and cyclicity, clearly related to environmental and climatic changes and monsoonal climate.

These cores provide for the first time in the low-latitude Western Pacific, a high resolution record of hemipelagic. The sedimentary sequences recovered by Leg 184 provide high quality material for further studies, with the goals of decipher the variability and role of the Monsoon system in the evolution of the Earth’s climatic system.

8th Meeting of Swiss Sedimentologists, Fribourg, Switzerland. January 2000.
Poster Presentation.

Dark-light rhythms in Pleistocene sediments of the Japan Sea: a high-resolution record of east Asian monsoon activity during the last 1.25 million years

Federica Tamburini and Karl B. Föllmi

During Ocean Drilling Program Legs 128 and 129 in the Japan Sea, the existence of dark-light rhythms of remarkable consistency was revealed in sediments of Pleistocene age (Föllmi et al., 1992). Light-colored units within these rhythms are massive or bioturbated, consist of diatomaceous clays, silty clays, or nannofossil-rich clays, and are generally poor in organic matter (average of 1 wt%). Dark-colored units are homogeneous, laminated or thinly bedded, and include substantial amounts of biogenic material such as well-preserved diatoms, planktonic foraminifers, calcareous nannofossils, and organic matter (maximum value measured: 7.4 wt%).

The dark-light rhythms show self-similar behavior on three different time scales: First-order rhythms consist of a cluster dominated by dark-colored units followed by a cluster dominated by light-colored units (3-5 m). Spectral analysis suggest correlation to eccentricity and obliquity cycles. The second-order dark-light rhythms include a light and a dark-colored unit (10-160 cm), which were formed in time spans of several hundred to several ten thousand years, with main perodicity centered around 10’500 years. Third-order rhythms appear as laminated or thinly bedded dark-light couplets (2-15 mm) within the dark-colored units of the second-order rhythms and may represent decennial to annual cycles.

The rhythms are interpreted as a record of changes in times dominated by summer and winther monsoon, with the dark rhythms representing periods of summer monsoon activity and the light rhythms representing periods of winter monsoon activity. The detailed record obtained shows a remarkable correlation with the GRIP oxygen isotope record for the last 250’000 years (Johnsen et al., 1997), with the Vostok oxygen-isotope record for the last 420’000 years (Petit et al., 1999), with the Specmap oxygen-isotope record for the last 780’000 years (Imbrie et al., 1993), and with the ODP Site 849 oxygen-isotope record for the last 1’275’000 years (Mix et al, 1995). The good correlations between these records and the east Asian monsoon record suggests the presence of an important connection between changes in east Asian monsoon behavior and global climate change for the last 1.25 million years.

REFERENCES

Föllmi, K.B., Cramp, A., Föllmi, K.E., Alexandrovich, J.M., Brunner, C., Burckle, L.H., Casey, M., DeMenocal, P., Dunbar, R.B., Grimm, K.A., Holler, P., Ingle, J.C., Kheradyar, T., McEvoy, J., Nobes, D.C., Stein, R., Tada, R., von Breymann, M.T., and White, L. (1992). Dark-light rhythms in the sediments of the Japan Sea: Preliminary results from Site 798, with some additional results from Site 797 and 799. In: Tamaki, K., Suyehiro, K., Allan, J., et al., Proceedings of the Ocean Drilling Program, Scientific Results, v. 127/128. College Station, Texas (Ocean Drilling Program), p. 559-576

Imbrie, J., Berger, A., Boyle, E. A., Clemens, S. C., Duffy, A., Howard, W. R., Kukla, G., Kutzbach, J., Martinson, D. G., McIntyre, A., Mix, A. C., Molfino, B., Morley, J. J., Peterson, L. C., Pisias, N. G., Prell, W. L., Raymo, M. E., Shackleton, N. J., and Toggweiler, J. R. (1993). On the structure and origin of major glaciation cycles; 2, The 100,000-year cycle. Paleoceanography, 8 (6), p. 698-735.

Mix, A. C., Pisias, N. G., Rugh, W., Wilson, J., Morey, A., and Hagelberg, T. K. (1995). Benthic foraminifer stable isotope record from site 849 (0-5 Ma): local and global climate changes. In: Pisias, A. C., Mayer, N. G., Janecek, L. A., et al., Proceedings of the Ocean Drilling Program, Scientific Results, v. 138. College Station, Texas (Ocean Drilling Program), p. 371-412

Johnsen, S. J., Clausen, H. B., Dansgaard, W., Gundestrup, N. S., Hammer, C. U., Andersen, U., Andersen, K. K., Hvidberg, C. S., Dahl-Jensen, D., Steffensen, J. P., Shoji, H., Sveinbjornsdottir, A. E., White, J. W. C., Jouzel, J., and Fisher, D. (1997). The d18O record along the Greenland Ice Core Project deep ice core and the problem of possible Eemian climatic instability. Journal of Geophysical Research, 102, p. 26397-26410.

Petit, J. R., Jouzel, J., Raynaud, D., Barkov, N. I., Barnola, J. M., Basile, I., Bender, M., Chappellaz, J., Davis, M., Delaygue, G., Delmotte, M., Kotlyakov, V. M., Legrand, M., Lipenkov, V. Y., Lorius, C., Pepin, L., Ritz, C., Saltzmann, E., and Stievenard, M. (1999) Climate and atmospheric history of the past 420,000 years from the Vostok ice core, Antarctica. Nature 399 (6735), p. 429-436.

European ODP Forum, La Grande Motte, France. April 2000.
Poster Presentation.

High-resolution record of East Asian Monsoon activity during the last 1.4 million years

Federica Tamburini and Karl B. Föllmi

Monsoon climate represents one of the basic and most important elements of global circulation and climate. During the last 20 years, several ODP cruises (Leg 116, Distal Bengal Fan, Leg 117, Oman Margin, Legs 128 and 129, Japan Sea, Leg 184, South China Sea) and studies have been carried out, aiming to decipher the mechanisms of the monsoon system, its variability, its role on global climate changes, and, recently, the possibility of a tele-connection with high latitude climate.

During Ocean Drilling Program Legs 128 and 129 in the Japan Sea, the existence of dark-light rhythms of remarkable consistency was revealed in sediments of Pleistocene age (Föllmi et al., 1992). The geochemical and mineralogical signature of dark and light sediments revealed to be significantly different; these cycles have been consequently interpreted as the oceanographic response to east Asian monsoon variability, with dark rhythms representing periods of strong summer monsoon activity and light rhythms representing periods of strong winter monsoon activity.

Three orders of cycles, with "fractal behaviour", are found and while the first- and second-order cycles correlate to millenial periodicities, the third-order cycle seems to represent annual variability. Preliminar observations of material retrieved during Leg 184 in the South China Sea, area subjected to the influence of the East Asian monsoon, revealed the presence of similar light-dark cycles in the sediments.

The high-resolution dark-light cycles record obtained from the Japan Sea shows a remarkable correlation with climatic records from different latitudes, as the GRIP oxygen isotope record (Johnsen et al., 1997), the ODP Site 849 oxygen-isotope record (Eastern Equatorial Pacific, Mix et al, 1995), and other records.

The good correlations between these records and the East Asian monsoon record suggest the presence of an important tele-connection between changes in East Asian monsoon behavior, high latitudes and global climate changes, not only for the Last Glacial period (Wang and Oba, 1998), but also for the last 1.4 million years.

REFERENCES

Föllmi, K.B., Cramp, A., Föllmi, K.E., Alexandrovich, J.M., Brunner, C., Burckle, L.H., Casey, M., DeMenocal, P., Dunbar, R.B., Grimm, K.A., Holler, P., Ingle, J.C., Kheradyar, T., McEvoy, J., Nobes, D.C., Stein, R., Tada, R., von Breymann, M.T., and White, L. (1992). Dark-light rhythms in the sediments of the Japan Sea: Preliminary results from Site 798, with some additional results from Site 797 and 799. In: Tamaki, K., Suyehiro, K., Allan, J., et al., Proceedings of the Ocean Drilling Program, Scientific Results, v. 127/128. College Station, Texas (Ocean Drilling Program), p. 559-576

Mix, A. C., Pisias, N. G., Rugh, W., Wilson, J., Morey, A., and Hagelberg, T. K. (1995). Benthic foraminifer stable isotope record from site 849 (0-5 Ma): local and global climate changes. In: Pisias, A. C., Mayer, N. G., Janecek, L. A., et al., Proceedings of the Ocean Drilling Program, Scientific Results, v. 138. College Station, Texas (Ocean Drilling Program), p. 371-412

Johnsen, S. J., Clausen, H. B., Dansgaard, W., Gundestrup, N. S., Hammer, C. U., Andersen, U., Andersen, K. K., Hvidberg, C. S., Dahl-Jensen, D., Steffensen, J. P., Shoji, H., Sveinbjornsdottir, A. E., White, J. W. C., Jouzel, J., and Fisher, D. (1997). The d18O record along the Greenland Ice Core Project deep ice core and the problem of possible Eemian climatic instability. Journal of Geophysical Research, 102, p. 26397-26410.

Wang, L., and Oba, T. (1998). Tele-connections between East Asian Monsoon and the High-latitude Climate: a comparison between the GISP2 Ice Core record and the high resolution marine records from the Japan and the South China Seas. The Quaternary Research, 37, 3, p. 211-219.

EGS 25, Nice (France). Mai 2000.
Oral Presentation.

Weathering and climate change

Karl B. Föllmi, Rachel Hosein, Kaspar Arn, Federica Tamburini, Tessa van Westrenen, Bas van de Schootbrugge, Philipp Steinmann, Thierry Adatte

---

Weathering is important in regulating the long-term carbon cycle. Temporal changes in biogeochemical weathering rates modulate the uptake of atmospheric CO_2, and lead to changes in the release rates of biophile elements (such as P, Si, Ca, Fe), which modulate transformation rates of inorganic carbon into organic carbon through photosynthesis. Variations in weathering may, therefore, exert an important control on a row of globally interlinked processes such as productivity, transformation of inorganic carbon into organic carbon, oxygen contents, as well as climate.

Presently, in the field of research on weathering, several main topics have been identified as partially unresolved: 1) Quantification of weathering rates in the geolo-gical past; 2) The degree of dependency of biogeochemical weathering rates on total weathering rates; and 3) The influence of glaciation on total and biogeochemical weathering rates. These topics are relevant to several open questions, such as 1) to what extend continental weathering did contribute to phases of enhanced marine productivity during the Neogene and Quaternary, dependent on climate change; and 2) which types of feedback mechanisms may have developed between weathering and climate change in the case glaciation events did contribute to enhanced biogeo-chemical weathering.

Goldschmidt 2000, Oxford (U.K.). September 2000.
Oral Presentation.

Phosphorus geochemistry of marine records: examples from diverse oceanographic settings.

Federica Tamburini, Thierry Adatte, Philipp Steinmann, and Karl Föllmi

In the last decades, new emphasis has been posed on the importance of nutrients in the ocean, mainly because of their control on productivity and organic carbon burial and, ultimately, on climate. But still little is known about the cycling of biophile elements, such as P, N, Fe etc., their primary source, their fate once in the ocean and in the sediment, and their response to rapid and extreme climate changes.

We concentrate on understanding the geochemistry of phosphorus in marine and non-marine environments, first because phosphorus is an essential nutrient controlling and modulating productivity on long time scales, secondly because, due to the lack of an important atmospheric phase and of a substantial input from volcanic and hydrothermal activity, its primary source comes from the continent and its variations in the sedimentary record could be directly linked to changes in continental weathering.

The oceanic P balance is therefore controlled by the input from the continent, oceanic circulation, uptake by biomass, transport and regeneration, and finally, burial in a number of different sedimentary sinks. We have started tracing continent-ocean links in marine Pleistocene sediment records from different regions of the world characterised by diverse oceanographic, climatic, productivity and geographic settings, trying at the same time to seek for feedback mechanisms between climate, productivity and continental weathering, and for glacial-interglacial changes.

Samples from ODP Sites 658, East equatorial Atlantic; 680, offshore Peru; 724, Arabian Sea, offshore Oman; 798, Japan Sea; 806, Ontong-Java Plateau; 907, North Atlantic Gateways, 1143 and 1144, South China Sea were selected to perform a multi-proxy investigation based on the SEDEX extraction of solid phases of P, mineralogy (by XRD), organic matter determination (by Rock Eval), and nitrogen stable isotopes.

The sequential P extraction allowed to differentiate between reactive and biologically available (Fe-bound P, authigenic P and organic P) and non-reactive (detrital apatite) phosphorus.

It is substantial to underline the capability of removing the detrital phase from the total phosphorus budget in the sediments because of the important implication for the calculation of the C/P ratio and estimates of phosphorus regeneration from organic matter oxidation.

Despite expected differences in the concentration and in the accumulation rates of the 4 extracted P phases between the sites, mainly related to local factors, preliminary results from these studies bring new and interesting insights on the P cycle and possible implications for productivity and climate variations for the last 150,000 years.

In most of the investigated sites detrital P covaries with other detrital indices, such as quartz and phyllosilicates, and show evident glacial-interglacial variations.

Burial of Fe- and organic-bound P, mainly regulated by sedimentation rates and oxygenation near the sediment-water interface, give important indications about chemical conditions in the uppermost part of the sediment.

Authigenic P is more and more considered as an efficient and important sink for reactive P and its presence, once thought to be limited to upwelling regions, has been demonstrated in many other sedimentary settings. The precipitation of authigenic P is controlled by many chemical and physical factors, and its variations in the records are interpreted as reflecting important changes in oceanography, input of dissolved P, and regeneration of organic matter.

Typical values are about 0.15 mg P/g of sediment for Fe-bound P, ranging between 0.2 and 1.7 mg P/g for authigenic P, with higher values in sediment from the Peru margin, between 0.02 and 0.2 mg P/g for detrital apatite, and between 0.02 and 0.16 mg P/g for organic P.

Against the difficulty of tracing global trends, due to the imprint of regional patterns, mean interglacial values of the phosphorus phases are generally significantly different from glacial values, showing that the burial of phosphorus and its delivery to the oceans are influenced by climate-induced changes.

Goldschmidt 2000, Oxford (U.K.). September 2000.
Oral Presentation.

Variations of detrital inputs to the South China Sea from 0 to 150 ky: a mirror of climate change

Federica Tamburini, Philipp Steinmann, Céline Gueguen, Thierry Adatte, and Karl Föllmi

---

Two ODP sediment cores from the South China Sea (Leg 184) sampled at about 2 ky intervals from 0 to 150 ky are investigated in order to decipher climate- and monsoon-driven signals recorded in the sediments.

Site 1143 is located northwest of the "Dangerous Ground", a region of islands and carbonate reefs on the southern continental slope of the South China Sea. Its location between carbonate reefs and the detrital deposit of the paleo-Sunda and the Mekong rivers makes the site sensitive to variations of both pelagic and terrigenous inputs. The sedimentation rate for the last 150 kyr at Site 1143 is about 6 cm/kyr. Present day water depth is 2772 m.

Site 1144 is situated on the northern continental margin of the South China Sea, at 2037 water depth and close to Pearl River mouth, the second largest water discharge of China's rivers. The sedimentation rate at this site is remarkably high, on the order of 90 cm/kyr. Its position close to the mainland makes this site extremely sensitive to changes in riverine and aeolian input, and to shift between winter and summer monsoon.

Our group is using a wide range of geochemical (major and trace elements, Rock-Eval parameters, forms of P, etc.) and mineralogical parameters (bulk mineralogy, clay minerals) as proxies to understand the modes of past climate changes and the interplay of the various active feedback mechanisms. For example: changes in detrital inputs (i.e. changes in nutrient inputs) > effects on biogeochemical cycles of the oceans > feed-back on climate > changes in detrital inputs.

The present contribution focusses on geochemical parameters (such as Si, Ti, Al, Ba, Mg, K, Zr, but also Cd, Pb, V, Cr, Cu, Zn + REE, and others), which areuseful to distinguish aeolian from riverine inputs, and to identify possible responses of autochthonous sedimentation to changes in the supply of detrital material.

9th Meeting of Swiss Sedimentologists, Fribourg, Switzerland. January 2001.
Poster Presentation.

Drawing information from phosphorus in marine sediments.

Federica Tamburini, Thierry Adatte, Philipp Steinmann, Karl Föllmi, Sylvain Huon.

We are interested in tracing continent-ocean links in marine Pleistocene sediment records from different regions of the world, trying to seek for feedback mechanisms between climate, productivity and continental weathering, and for changes at glacial-interglacial or even shorter timescales (i.e. Heinrich events). We concentrate on understanding the geochemistry of phosphorus in marine and non-marine environments, first because phosphorus is an essential nutrient controlling and modulating productivity on long time scales, secondly because its primary source comes from the continent and its variations in the sedimentary record could be directly linked to changes in continental weathering. The oceanic P balance is therefore controlled by the input from the continent, oceanic circulation, uptake by biomass, transport and regeneration, and finally, burial in a number of different sedimentary sinks.

Samples from several ODP Sites (658, East equatorial Atlantic; 680, offshore Peru; 724, offshore Oman; 798, Japan Sea; 806, Ontong-Java Plateau; 907, North Atlantic Gateways, 1143 and 1144, South China Sea) and from core SU 9009, located in the North Atlantic, inside the IRD (Ice Rafted Debris) zone, were selected to perform a multi-proxy investigation based on the SEDEX extraction of solid phases of P, mineralogy (by XRD), organic matter determination (by Rock Eval), and nitrogen stable isotopes.

The sequential P extraction allowed to differentiate between reactive and biologically available (Fe-bound P, authigenic P and organic P) and non-reactive (detrital apatite) phosphorus.

Detrital P covaries with other detrital indices, such as quartz and phyllosilicates, and show evident glacial-interglacial variations. Burial of Fe- and organic-bound P, mainly regulated by sedimentation rates and oxygenation near the sediment-water interface, give important indications about chemical conditions in the uppermost part of the sediment. The precipitation of authigenic P is controlled by many chemical and physical factors, and its variations in the records are interpreted as reflecting important changes in oceanography, input of dissolved P, and regeneration of organic matter.

Typical values are about 0.15 mg P/g of sediment for Fe-bound P, ranging between 0.2 and 1.7 mg P/g for authigenic P, with higher values in sediment from the Peru margin, between 0.02 and 0.2 mg P/g for detrital apatite, and between 0.02 and 0.16 mg P/g for organic P.

Against the difficulty of tracing global trends, due to the imprint of regional patterns, mean interglacial concentrations and mass accumulation rates of the phosphorus phases are generally significantly different from glacial values, showing that the burial of phosphorus and its delivery to the oceans are influenced by climate-induced changes.

XI EUG, Strasbourg (France). April 2001.
Poster presentation.

Changes in mineralogy and geochemistry in the South China Sea (ODP Site 1143) during the last 150,000 years: relations between the East Asian monsoon, continental weathering and productivity.

Federica Tamburini, Thierry Adatte, Karl B. Föllmi, Philipp Steinmann

---

The Asian monsoon system is a major component of both regional and global climate, its evolution is linked with the uplift of the Himalayan-Tibetan orogen, the opening and closing of marginal seas and with changes in global climate. The location of the South China Sea between the Asian continent and the Pacific Ocean makes it an ideal region to record the paleoceanographic responses to winter and summer monsoons.

ODP Site 1143 (2772 mbsl) is located on the southern continental slope of the South China Sea. The sedimentation rate for the last 150 kyr at Site 1143 is about 6 cm/kyr. This site was chosen because its location between carbonate reefs and the detrital deposit of the paleo-Sunda and the Mekong rivers makes the site sensitive to variations of both pelagic and terrigenous inputs, which vary in relation to the monsoon regime and glacial-interglacial changes in sea level.

Site 1143 (Leg 184, South China Sea) was sampled at about 2 ky intervals from 0 to 150 ky and sediments have been studied by means of a multi-proxy investigation (bulk and clay mineralogy, granulometry, phosphorus phases determination and organic matter characterization), in order to decipher climate- and monsoon-driven signals.

Sediments are mainly composed of clay over the entire studied sequence and granulometry does not show important variations. Coarser material is recorded at discrete intervals, generally correlating with peaks in magnetic susceptibility, quartz and micas. One of these maxima, located at around 10 ky, may coincide with the Younger Dryas event.

Clay minerals contents show important changes between glacial and interglacial periods, pointing at variations in sources (eolian vs. river) and in monsoon regime (winter-dry vs. summer-wet monsoon). Kaolinite, mica, smectite and detrital minerals, such as quartz, show higher values during stages 4, 3 and 2, while minima are recorded especially at the beginning of interglacial stage 5. Calcite and authigenic P show a similar trend and correlate with the oxygen isotopic record, with peaks at the beginning of stage 5 and decreasing to relatively low values during the rest of the sequence. Organic matter contents are quite low (averaging about 0.35 wt%) and the scattered values make their interpretation quite difficult at this stage of the research. Only few intervals, maily located during glacial stages, are characterized by slightly higher Corg values (0.5-0.6 wt%).

From this preliminary investigation Site 1143 appears to record changes related to variations in monsoon and continental weathering during the last 150,000 years. Notwithstanding, productivity proxies seems not to be affected by these changes: the interplay between eolian and riverine input of nutrients, modulated by both winter and summer monsoons, could have supported nonstop primary production.

ANNEX D

Derrick of the Joides Resolution.

Curriculum Vitae

FEDERICA TAMBURINI

ADDRESS

Institut de Géologie
Université de Neuchâtel
CH-2007 Neuchâtel
Switzerland
Tél.: +41 32 718 26 65
Fax: +41 32 718 26 01
E-mail: federica.tamburini@unine.ch

PRIVATE ADDRESS

Tamburini Federica
Rue des Fahys, 33
CH-2000 Neuchâtel
Switzerland
Tél.: +41 32 725 64 82

PERSONAL

Born in Pesaro, January 18th, 1971.
Nationality: Italian

PRESENT POSITION

PhD student at the Institut de Géologie, Université de Neuchâtel, Switzerland. (Prof. K. B. Föllmi)
Thesis Title: "Phosphorus in marine sediments during the last 150,000 years: exploring relationships between continental weathering, productivity, and climate"

EDUCATIONAL BACKGROUND

Laurea in Geology*, March 10th, 1995, Department of Earth Sciences of the University of Urbino, Loc. Crocicchia, 61029 Urbino, Italy. (* U.S. Master equivalent). Grading: full marks and honours.

Diploma di Maturità Scientifica*, July 1990, Liceo Marconi, Pesaro, Italy.
(* U.S. General Science Secondary Education Certificate equivalent). Grading: 52/60

Post-grade Courses

March 2000	Controls on rock weathering and continental erosion. University of Bern, Switzerland
October-November 1999	Elements of Statistics for Research. Prof. Y. Dodge, University of Neuchâtel, Switzerland

Field Work

April 1998	Western region of the U.S.A. as assistant with the Geological Institute of Neuchâtel. Field work objective: regional geology and teaching.
September 1995 - August 1996	Marchean Apennines. Field work objective: geological mapping, with in the C.N.R. (Italian National Council of Research) project 'Geodinamica del sistema Tirreno - Appennino'.
January 1994 - May 1994	Outer Marchean Apennines. Field work objective: geological mapping and paleoenvironment study.
June 17 - July 1 1993	Piobbico, Central Apennines. Field work objective: geological mapping.

GRANTS and SALARIES

January 2002 – December 2002	Swiss National Science Fondation postdoctoral fellowship
October 1197 – present	Assistant at the Institut de Géologie, Université de Neuchâtel, Switzerland
August 1999	Travel grant from the Swiss Quaternary Group to participate to the XV INQUA Congress in Durban, South Africa
January - July 1997	Scholarship from Urbino University (Italy), to study abroad (ETH-Zürich, Switzerland, under the supervision of Professor Judy A. McKenzie)
1995 - 1996	C.N.R. (Italy)

PROFESSIONAL APPOINTMENTS

Undergraduate and graduate courses (Teaching assistantship)

1997 - present	Mineralogy and Crystallography
2001 Summer Semester	BENEFRI course: Creating an Organic Geochemistry Glossary for the Internet (Resp. Dr. P. Steinmann)
January 2001	Geophysiology Lecture: The formation and the uplift of the Himalayas and its influence on life and the environment
January 2000	Geophysiology Lecture: Glacial periods, a stable mode for the biosphere?
January 1998	Geophysiology Lecture: Holocene and Pleistocene climate: glacial-interglacial cycles.

Cruise participation and ODP-related appointments

August 1999 invited to the editing meeting of the Initial Reports Volume for Leg 184 (College Station, Texas).
February – April 1999 participation to ODP Leg 184 (South China Sea) as a Sedimentologist.

RECENT SCIENTIFIC RESEARCH COLLABORATORS

Dr. D. Ariztegui, Insitut Forel, Geneva, Switzerland.
Dr. S. M. Bernasconi, ETH-Zentrum, Zürich, Switzerland.
Dr. S. Huon, Université Pierre et Marie Curie (UPMC-CNRS-INRA), Paris, France.

AFFILIATIONS and MEMBERSHIPS

European Union of Geosciences
American Geophysical Union
FROMAGE Group

ANALYTICAL EXPERTISE

Phosphorus SEDEX extraction (organisation of the extraction line in Neuchâtel)
Perkin-Elmer UV/Vis spectrophotometer Lambda 10
Nitrogen isotopes (CHN Elemental Analyzer)
SCINTAG XRD 2000 Diffractometer
Rock-Eval RE6
Granulometry Laser Oriel CIS

COMPUTER SKILLS

Very good knowledge of the Macintosh system, experience with PC. Word processing, calculation and database (Microsoft Office, FileMaker Pro). Graphic design and publishing (Adobe Illustrator, Photoshop, Acrobat, Quark Xpress). Statistics, data analyses and representation (JMP, Kaleidagraph, CricketGraph, MatLab, Analyseries, Arand). Web design and management (Adobe Golive, Flash, Webstar, Timbuktu).

LANGUAGES

Italian	mother language
English	TOEFL examination, 11 May 1996, grade: 630/660
French	fluent comprehension and speaking skills, good in writing

Cycle of P

I put some P into the sea
the biomass did swell

But settling down soon overcame
and P went down toward Hell

From Purgatory soon released
it moved up to the land

To make a perfect rose for thee
to carry in thy hand

But roses wilt and die you know
then P falls on the ground

Gobbled up as ferric P
a nasty brown compound

The world is moral still you know
and Nature's wheels do grind

Put ferric P into the sea
and a rose someday you'll find.

Robert M. Garrels